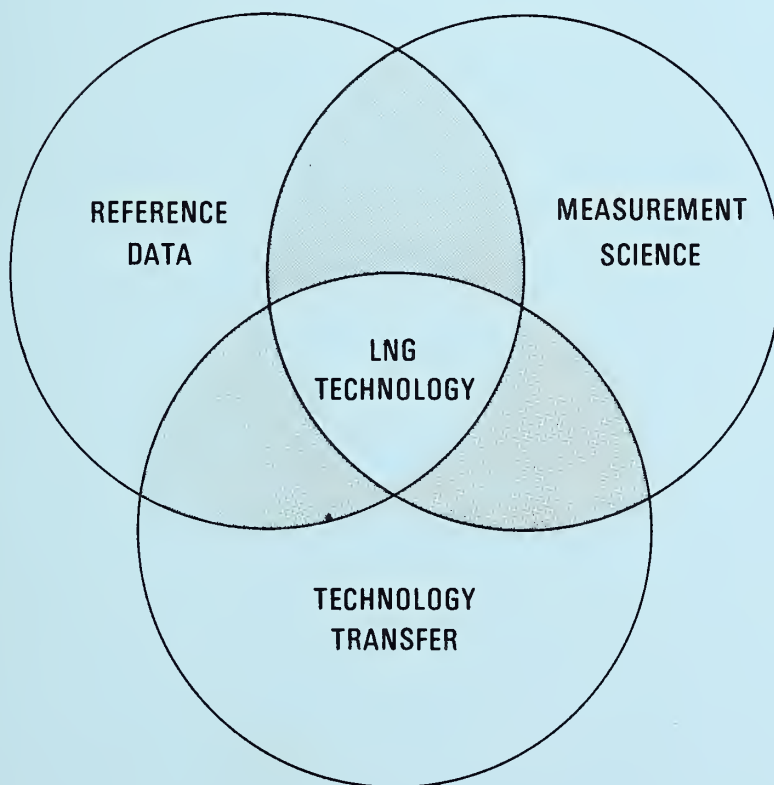


LIQUEFIED NATURAL GAS RESEARCH *at the* NATIONAL BUREAU OF STANDARDS

PROGRESS REPORT FOR THE PERIOD
1 JULY - 31 DECEMBER, 1975

4/7/76
612

D. B. Mann, Editor



NBSIR 76-831

LIQUEFIED NATURAL GAS RESEARCH
at the
NATIONAL BUREAU OF STANDARDS

D. B. Mann, Editor

Cryogenics Division
Institute for Basic Standards
National Bureau of Standards
Boulder, Colorado 80302

Progress Report for the Period

1 July - 31 December, 1975



U.S. DEPARTMENT OF COMMERCE, Rogers C. B. Morton, Secretary
James A. Baker, III, Under Secretary
Dr. Betsy Ancker-Johnson, Assistant Secretary for Science and Technology
NATIONAL BUREAU OF STANDARDS, Ernest Ambler, Acting Director

Prepared for:

American Gas Association, Incorporated - -
1515 Wilson Boulevard
Arlington, Virginia 22209

LNG Density Project Steering Committee
(in cooperation with the American Gas Association)

Pipeline Research Committee
(American Gas Association)

Federal Power Commission
Bureau of Natural Gas
Washington, DC 20426

U. S. Department of Commerce
Maritime Administration
Washington, DC 20235

U. S. Department of Commerce
National Bureau of Standards
Institute for Basic Standards
Boulder, Colorado 80302

U. S. Department of Commerce
National Bureau of Standards
Office of Standard Reference Data
Washington, DC 20234

U. S. Department of Commerce
National Bureau of Standards
Office of Energy Conservation
Washington, DC 20234

Aerospace Safety Research and Data Institute
National Aeronautics and Space Administration
Lewis Research Center
Cleveland, Ohio 44135

National Aeronautics and Space Administration
Lewis Research Center
Cleveland, Ohio 44135

ABSTRACT

Nineteen cost centers supported by six other agency sponsors in addition to NBS provide the basis for liquefied natural gas (LNG) research at NBS. During this six month reporting period the level of effort was at a 20 man-year level with funding expenditures of over \$600,000. This integrated progress report to be issued in January and July is designed to:

- 1) Provide all sponsoring agencies with a semi-annual and annual report on the activities of their individual programs.
- 2) Inform all sponsoring agencies on related research being conducted at the Cryogenics Division of NBS-IBS.
- 3) Provide a uniform reporting procedure which should maintain and improve communication while minimizing the time, effort and paperwork at the cost center level.

The contents of this report will augment the quarterly progress meetings of some sponsors, but will not necessarily replace such meetings. Distribution of this document is limited and intended primarily for the supporting agencies. Data or other information must be considered preliminary, subject to change and unpublished; and therefore not for citation in the open literature.

Key words: Cryogenic; liquefied natural gas; measurement; methane; properties; research.

CONTENTS

	Cost Center	Page
I. REFERENCE DATA		
a) SURVEY OF CURRENT LITERATURE ON LNG AND METHANE (American Gas Association, Inc.)	2759574	1
b) LNG FUELS SAFETY (NASA-Aerospace Safety and Data Institute)	2750427	3
c) THERMOPHYSICAL PROPERTIES DATA FOR PURE COMPONENTS OF LNG MIXTURES (American Gas Association, Inc.)	2750574	5
d) FLUID TRANSPORT PROPERTIES (NBS-Office of Standard Reference Data)	2750124	9
e) PROPERTIES OF CRYOGENIC FLUIDS (NBS)	2750141	11
f) PROPERTIES OF CRYOGENIC FLUID MIXTURES (NBS; NBS-Office of Standard Reference Data; NASA)	2750142, 2750145 and 2750548	13
g) DENSITIES OF LIQUEFIED NATURAL GAS MIX- TURES (LNG Density Project Steering Committee - AGA)	2751574 and 2752574	15
h) LOW TEMPERTURE MATERIAL BEHAVIOR (Maritime Administration)	2750430	17
i) PROGRAM FOR REDUCING THE COST OF LNG SHIP HULL CONSTRUCTION -- PHASE II SHIP STEEL IMPROVEMENT PROGRAM (Mari- time Administration)	2751430 2752430 2753430	19
II. MEASUREMENT SCIENCE		
a) CUSTODY TRANSFER - LNG SHIPS (Maritime Administration)	2750460	21
b) HEATING VALUE OF FLOWING LNG (Pipeline Research Committee - AGA)	2756579	25
c) LNG DENSITY REFERENCE SYSTEM (American Gas Association, Inc.)	2757574	29
III. TECHNOLOGY TRANSFER		
a) LIQUEFIED NATURAL GAS TECHNOLOGY TRANSFER (Maritime Administration)	2750401	31
b) FEDERAL POWER COMMISSION CONSULTATION (FPC)	2750404	37
IV. BIBLIOGRAPHY		39

V. APPENDICES

A.	Phase transition and melting pressures of solid ethane, G. C. Straty and R. Tsumura	A-1
B.	PVT and Vapor Pressure Measurements on Ethane, G. C. Straty and R. Tsumura	B-1
C.	Hypersonic velocities in saturated and compressed fluid methane, G. C. Straty	C-1
D.	Dielectric constant data and the derived Clausius-Mosotti function for compressed gaseous and liquid ethane, L. A. Weber	D-1
E.	Equation of state for thermodynamic properties of fluids, Robert D. Goodwin	E-1
F.	Orthobaric liquid densities of normal butane from 135 to 300 K as determined with a magnetic suspension densimeter, W. M. Haynes and M. J. Hiza	F-1
G.	On the consistency of liquid-vapor equilibria data for binary mixtures of methane with the light paraffin hydrocarbons, W. R. Parrish and M. J. Hiza	G-1
H.	Liquid-vapour phase equilibria in the N_2 - CH_4 system from 130 to 180 K, A. J. Kidnay, R. C. Miller, W. R. Parrish and M. J. Hiza	H-1
I.	Fracture mechanics and its application to cryogenic structures, H. I. McHenry	I-1
J.	Ship steel weldments for low temperature service, Harry I. McHenry	J-1
K.	The refractive index and Lorenz-Lorentz function of fluid methane, James D. Olson	K-1
L.	Thermophysical properties data research on compressed and liquefied gases at the NBS Cryogenics Division, Dwain E. Diller	L-1
M.	Equations for the viscosity and thermal conductivity coefficients of methane, H. J. M. Hanley, R. D. McCarty, and W. M. Haynes	M-1
N.	Evaluation of capacitance densitometry by examination of the relationships between density, dielectric constant, pressure and temperature for LNG mixtures, P.J. Giarratano and R. S. Collier	N-1

1. Title. SURVEY OF CURRENT LITERATURE ON LNG AND METHANE
Principal Investigator. Neil A. Olien
2. Cost Center Number. 2759574
3. Sponsor Project Identification. American Gas Association Project BR-50-10.
4. Introduction. It is important that all NBS personnel working in LNG, as well as the AGA and others, keep up with what is going on throughout the world in the LNG field. This project is designed to provide the Current Awareness and other information services to allow workers to keep abreast of new research and other developments.
5. Objectives or Goals. We will publish and distribute each April, July, October, and January a listing of all significant papers, reports, and patents relating to methane and LNG properties and technology. The references will be listed under convenient subject headings. The Quarterly will be distributed to all interested AGA member companies and be made available to the general public on a subscription basis. In addition, LNG related information will be entered into the Cryogenic Data Center's Information System for quick retrieval. A continuing awareness of the current publication scene will be maintained for any new periodicals to be reviewed cover-to-cover. Finally we will update and make available comprehensive bibliographies on the properties and technology of LNG. There are three bibliographies involved: methane properties, methane mixtures properties, and processes and equipment involving methane and LNG. These three will be updated each October.
6. Background. In 1969 we made a thorough review of the world's publications to determine which periodicals and abstracting services should be scanned cover-to-cover to adequately encompass the LNG field. The result is that we now scan over 300 primary publications and nearly 30 secondary publications. Of these, approximately one-third are directly related to LNG. In addition, within the past year we have increased our coverage of the energy field to include hydrogen as a future fuel. Much of this information is also pertinent to LNG and as such is listed in our LNG-related publications. Our Current Awareness Service has been published weekly since 1964 (beginning in 1975 the publication became biweekly) and the Liquefied Natural Gas Survey has been published quarterly since 1970.
7. Program and Results. Four issues of the LNG Quarterly are prepared each year and distributed. There are now 120 subscriptions going to AGA Member Companies and 168 to other subscribers.

The three comprehensive bibliographies mentioned in section 5 have been reviewed and shortened, and more selective bibliographies have resulted. The latest versions were completed as of January 1, 1976.

THE THERMOPHYSICAL PROPERTIES OF METHANE AND DEUTERO-METHANE IN THE SOLID, LIQUID AND GASEOUS PHASES - A SELECTED BIBLIOGRAPHY. Indexed by property, phase and author, 80 pages (Jan 1976). (\$8.00).

THE THERMOPHYSICAL PROPERTIES OF METHANE MIXTURES - A SELECTED BIBLIOGRAPHY. Indexed by property, system and author, 140 pages (Jan 1976). (\$10.00).

B-1264 PROCESSES AND EQUIPMENT INVOLVING LIQUEFIED NATURAL GAS AND METHANE - A SELECTED BIBLIOGRAPHY. Indexed by subject and author, 76 pages (Feb 1975). (\$8.00).

B-1367 Supplement to B-1264, indexed by subject and author, 40 pages (Jan 1976). (\$5.00).

These are being updated now and will be available in January 1976. Over the past five years we have distributed over 400 copies of these and the comprehensive bibliographies. A bibliography on LNG Patents was supplied to AGA in May, 1975. Two supplements to this were also completed, one in July 1975 and one in January 1976.

8. Problem Areas. None.

9. Funding. July 1 - December 31, 1976.

Labor	2.8K\$
Other Costs	1.1K\$
Total	3.9K\$
Remaining	6.1K\$

10. Future Plans. Issue 75-4 was mailed to the National Technical Information Service (NTIS) for printing and distribution on January 8, 1976. That will be the last issue which NTIS will handle. Beginning in 1976 all functions, including subscription fulfillment and distribution, will be returned to the Cryogenic Data Center. We feel that this will give us closer and more positive control over the entire operation.

1. Title. **LNG FUELS SAFETY**
Principal Investigators. Neil A. Olien and A. F. Schmidt
2. Cost Center Number. 2750427
3. Sponsor Project Identification. National Aeronautics and Space Administration, Cleveland, Ohio, Aerospace Safety Research and Data Institute. Order No. C-39327-C.
4. Introduction. The NASA-Aerospace Safety Research and Data Institute (ASRDI) was established to provide a focal point for information and research in aerospace safety. One of the areas of concern for ASRDI is Cryogenic Fluid Safety. In fact, this was the first area of effort for ASRDI. The thrust of the program is two-fold: first, to provide an automated information bank for retrieving references, and second, to publish series of state-of-the-art reviews. The information system is now operational and contains over 7000 references in cryogenic fluid safety. In addition, ASRDI has published approximately twenty reviews.

Until this time, ASRDI has focused its attention and efforts on the two primary cryogenic propellants, hydrogen and oxygen. The oxygen work was started at NBS-Boulder in 1970 and the hydrogen work in 1972. With the coming possibility of methane or LNG fueled aircraft and the close affinity of LNG safety and cryogenic safety, ASRDI felt that it was timely to begin work in that area.
5. Objectives or Goals. The following objectives are to be achieved:
 - a) Review and modify an existing Cryogenic Fluids Safety Grid and thesaurus to include and adequately cover LNG safety.
 - b) Make a thorough search of over eleven information sources for LNG information. This will include published and unpublished material.
 - c) Catalog, index, abstract and put into machine readable form all available documents located in b) above. The indexing will be done by technical personnel with demonstrated competence in cryogenic safety and related fields.
6. Background. This program was started at NBS-Boulder by ASRDI in 1970. Since then considerable skill and experience has been gained in locating, processing and, most important, detailed subject indexing of safety-related information. In addition, NBS-Boulder has been providing detailed coverage of the LNG field for the American Gas Association since early 1970. The present program, then, provides an opportunity for industry, government and the public to capitalize on the accumulated past efforts of two seemingly unrelated programs.
7. Program and Results. Under this and another ASRDI-funded program we have started a major review of the indexing and retrieval terminology which will be used in the Cryogenic fuels safety information system. This review will result in a thesaurus to be published by NASA. The review is complete and we are now in the process of editing and preparing the thesaurus in its final form. Publication has been delayed awaiting a decision as to publishing the thesaurus separately or combined with one in fire safety and one in the mechanics of structural failure. Most of the terminology unique to LNG safety is now incorporated into this thesaurus. Approximately 500 papers, reports, etc., have been carefully indexed, abstracted, cataloged and transmitted to ASRDI.

8. Problem Areas. None.

9. Funding. July 1 - December 31, 1975

Allocation (9/30/74 - 10/1/75) - 50K\$ NASA/ASRDI

Labor	0.2 MY	8.1K\$
-------	--------	--------

Other Costs		.8K\$
-------------	--	-------

Total		8.9K\$
-------	--	--------

Remaining		--
-----------	--	----

10. Future Plans. The work on this project has been completed and there are no current plans to continue the effort.

1. Title. THERMOPHYSICAL PROPERTIES DATA FOR PURE COMPONENTS OF LNG MIXTURES

Principal Investigators. R. D. Goodwin, G. C. Straty, L. A. Weber, H. M. Roder, and R. Tsumura*.

2. Cost Center Number. 2750574

3. Sponsor Project Identification. American Gas Association, Inc., Project BR-50-10.

4. Introduction. Accurate phase equilibrium, equation of state (PVT), and thermodynamic properties data are needed to design and optimize gas separation and liquefaction processes and equipment. Accurate data for the pure components of LNG mixtures will permit developing comprehensive accurate predictive calculation methods which take into account the dependence of the thermophysical properties of mixtures on the composition, temperature, and density.

This project will provide comprehensive accurate thermophysical properties data and predictive calculation methods for compressed and liquefied hydrocarbon gases to support the development of LNG technology at NBS and throughout the fuel gas industry.

5. Objectives or Goals. The objectives of our work are the determination of comprehensive accurate thermophysical properties data and predictive calculation methods for the major pure components (methane, ethane, propane, butanes, and nitrogen) of liquefied natural gas mixtures at temperatures between 90 K and 300 K and at pressures up to 350 bar (5000 psi). Our goal is to provide a range and quality of data that will be recognized as definitive or standard for all foreseeable low temperature engineering calculations.

6. Background. Liquefied natural gas is expected to supply an increasing percentage of the United States' future energy requirements. It is likely that massive quantities of liquefied natural gas will be imported during the years 1976 - 1990. Ships and importation terminals are being built for transporting, storing, and vaporizing liquefied natural gas for distribution. Accurate physical and thermodynamic properties data for compressed and liquefied natural gas mixtures are needed to support these projects. For example, accurate compressibility and thermodynamic properties data are needed to design and optimize liquefaction and transport processes; accurate data for the heating value, which for liquefied natural gas mixtures depends on the total volume, the density, and the composition, are needed to provide a basis for equitable custody transfer.

Accurate thermodynamic properties data for liquefied gas mixtures must be based on precise compressibility and calorimetric measurements; compressibility data give the dependence of thermodynamic properties on pressure and density (at fixed temperatures); calorimetric data give the dependence of thermodynamic properties on temperature (at fixed pressures and densities). It is impossible, however, to perform enough compressibility and calorimetric measurements directly on multicomponent mixtures to permit accurate interpolation of the data to arbitrary compositions, temperatures and pressures. Instead, thermodynamic properties data for multicomponent mixtures usually must be predicted (extrapolated) from a limited number of measurements on the pure components and their binary mixtures.

* Consejo Nacional de Ciencia y Tecnologia (CONACYT) Mexico City. Currently a guest worker with the Cryogenics Division, National Bureau of Standards, Institute for Basic Standards in Boulder, Colorado.

This project was initiated to provide the natural gas industry with comprehensive accurate data for pure compressed and liquefied methane, the most abundant component in LNG mixtures. We have published National Bureau of Standards Technical Note 653, "Thermophysical Properties of Methane, From 90 to 500 K at Pressures to 700 Bar," by Robert D. Goodwin (April 1974). This report contains the most comprehensive and accurate tables available for the thermophysical properties of pure gaseous and liquid methane, and provides an accurate basis for calculating thermophysical properties data for LNG mixtures. Similar data is now being obtained for compressed and liquefied ethane.

7. Program and Results.

7.1. Melting Pressures, Vapor Pressures and Equation of State (PVT) Data -- G. C. Straty and R. Tsumura

Comprehensive, accurate measurements of the melting pressures, vapor pressures and equation of state (PVT) for compressed and liquefied ethane, 90-320 K, to 35 MPa (5000 psi), have been completed. Two reports have been completed and submitted for publication:

- a) G. C. Straty and R. Tsumura, "Phase Transition and Melting Pressures of Solid Ethane." J. Chem. Phys. (in press, 1976).
- b) G. C. Straty and R. Tsumura, "PVT and Vapor Pressure Measurements on Ethane." J. Res. Nat. Bur. Stand. (in press, 1976).

Both reports are reprinted in the appendices (see Appendices A and B).

7.2. Methane, Sound Velocity Data -- G. C. Straty

A light scattering spectroscopy apparatus has been employed to obtain hypersonic (GHz) velocity data at the lower densities where measurement by ultrasonic techniques were impossible. Data have been obtained to densities as low as 1 mol/% along several isotherms. Measurements in the regions of overlap agreement with calculated sound velocity data is satisfactory. The data have been combined with previously measured PVT data to obtain the isentropic compressibility and specific heat ratio C_p/C_v . A manuscript reporting the results of the hypersound velocity measurements has been published in Cryogenics 15, 729 (1975) and is reprinted in the appendices (Appendix C).

7.3. Ethane, Dielectric Constant Data -- L. A. Weber

Dielectric constant measurements have been completed over a temperature range of 95-323 K, including the saturated liquid from triple point to near the critical point and compressed liquid and fluid states at pressures up to 390 bar. The dielectric constant data have been combined with available accurate density data to form the Clausius-Mosotti function $[1/\rho(\epsilon-1)\sqrt{\epsilon+2}]$, which has been expressed analytically as a function of density and temperature over a wide range, with an overall estimated accuracy of 0.1%. This function has been used to examine the consistency of the various sources of density and PVT data for ethane. A manuscript reporting the results has been completed, and is preprinted in the appendices (Appendix D).

7.4. Ethane, Specific Heat Data -- H. M. Roder

Specific heat data (C_v) are required to accurately define the derivatives of the equation of state (PVT), which in turn are used to calculate other thermodynamic functions such as enthalpy. Measured values of C_v are particularly valuable to cross-check thermodynamic calculations for the compressed liquid states. We have prepared for a series of C_v and C_{SAT} measurements on ethane similar to those completed on

methane under this program. Measurements of the heat capacity of the empty calorimeter have been extended from 300 to 330 K to permit C_v measurements of compressed gaseous ethane at temperatures above critical. Since the critical temperature of ethane (305.3 K) is well above room temperature, fluid of relatively high density will reside in the filling capillary part of the system, and will have to be accounted for accurately.

During the reporting period, we completed the measurements on the heat capacity of the empty calorimeter, and measured 32 C_v points for methane. Deviations between present and previous measurements on methane vary from several tenths of a percent to 0.8 percent.

We have converted the data reduction programs for methane to ethane, and have measured a total of about 200 points on 9 different isochores for ethane. Since we had planned for about 350 points, data taking is about 60% complete. Measurements of C_{SAT} and C_v have been combined; that is both are made for a single filling of the cell. Since we have measured only liquid phase isochores to date, the measurements on C_{SAT} are nearly complete. Deviations for C_{SAT} from the values calculated in NBSIR 74-398 are on the order of 0.5%. Deviations from values of other authors run up to 2% because the earlier papers do not account accurately for the amount of fluid vaporized or condensed during the measurement. Present values of C_v usually differ from NBSIR 74-398 by 1% or less, with larger deviations, i.e., up to 3%, occurring very close to the saturation boundary. We have yet to determine if this latter effect is real, or if it occurs because we have not accurately accounted for the amount of sample in the capillary.

7.5. Ethane, Sound Velocity Data -- R. Tsumura

New ultrasonic measurements of the velocity of sound in compressed and liquefied ethane (90-320 K, 35 MPa (5000 psi)) are in progress. The ultrasonic velocities of sound in pure saturated liquid ethane have been measured at MHz frequencies. Data have been obtained along the saturation boundary from near the triple point (90.35 K) to 280 K, using the pulse-echo technique, in which the imprecision is estimated to be less than 0.05%. In the temperature interval 150 K to 280 K these data appear to be consistent with other available data within the experimental error. There is, however, a systematically increasing disagreement as the triple point is approached, reaching a maximum of 0.4% near this point.

7.6. Ethane, Thermodynamic Properties Data -- R. D. Goodwin

In a previous report, NBSIR 74-398 (June 1974), "Provisional Values for the Thermodynamic Functions of Ethane," we made use of available physical properties data to derive provisional thermofunctions at the earliest possible date, including results never before available for the compressed liquid at temperatures from the normal boiling point (185 K) down to the triple point (90 K).

Our purpose during both the previous and forthcoming six months is to utilize newly available accurate physical properties data to improve the accuracy of the derived thermofunctions and to produce a final report giving these results.

For the computation of consistent and accurate thermodynamic functions, it is essential to have an accurate equation of state, describing the $P(\rho, T)$ surface in three dimensions, which is much more than merely accurate in reproducing experimental PVT data. The derivatives of this surface must be regular in their behavior and must be consistent with the known behavior of specific heats and other thermodynamic properties. See for example "Equation of State for Thermodynamic Properties of Fluids," by R. D. Goodwin, J. Res. NBS 79A (1), 71 (1975) (Appendix E).

New experimental data have become available for the vapor pressure, the orthobaric densities near the critical point, the saturated liquid densities at low temperatures, and for PVT data at densities from the critical density to the liquid triple point density. Forthcoming new dielectric constants, specific heats, and speeds of sound will permit further indirect checks on thermodynamic computations via the equation of state.

Our new form of equation of state is so highly constrained for self-consistency (e.g., between orthobaric densities and the PVT surface) and for consistency with the behavior of specific heats, that the use of experimental PVT data from different sources, which are not consistent with each other, yields deviations which are quite disturbing when compared with the "good" fit of PVT data to which the reader may be accustomed. This problem has occupied much of our efforts during the past reporting period.

8. Problem Areas. None.

9. Funding. July 1 - December 31, 1975.

Man-years expended	1.0
Equipment and/or Services Purchased	4.7K\$
Total Reporting Period Cost	69.0K\$
Balance Remaining	71.0K\$

10. Future Plans.

Objectives and Schedule:	Year	
	Quarter 1	Quarter 2
Measure, analyze and report specific heat (C_{SAT} and C_v data for ethane.		
Measure, analyze and report ultrasonic velocity data for ethane.		
Calculate and report accurate thermodynamic properties data for ethane.		

1. Title. FLUID TRANSPORT PROPERTIES
Principal Investigator. Howard J. M. Hanley
2. Cost Center Number. 2750124
3. Sponsor Project Identification. NBS-Office of Standard Reference Data
4. Introduction. Methods for predicting the transport properties of fluid mixtures are unreliable and data are scarce. Prediction methods are needed, however, to supply the necessary design data needed to increase efficiency and reduce costs.
5. Objectives or Goals. The long range or continuing goal of the program is to perform a systematic study of the theories and experimental measurements relating to transport properties, specifically the viscosity and thermal conductivity coefficients, of simple mixtures over a wide range of experimental conditions. The specific objectives of the program include: 1) the systematic correlation of the transport properties of simple binary mixtures and the development of prediction techniques, 2) development of a mixture theory for the dilute gas region and the dense gas and liquid regions, 3) extension of the theory and prediction techniques to multicomponent systems, and 4) suggested guidelines for future areas of experimental work.
6. Background. A continuing program has successfully expanded the state-of-the-art of transport phenomena for pure fluids. Information for pure fluids is required as a prerequisite for mixture studies. The theory of transport phenomena has been developed and applied to produce practical numerical tables of the viscosity, thermal conductivity and diffusion coefficients of simple fluids: Ar, Kr, Xe, N₂, O₂, F₂, He, H₂, CH₄. Recent work has extended this approach to ethane. It is felt that a successful mixture program will emerge from combining the results for pure fluids with equation of state studies. The equation of state work is being carried out by other investigators in this laboratory.
7. Program and Results. Statistical mechanics has been applied to predict and correlate the dilute and moderately dense thermophysical properties of carbon dioxide.¹ Carbon dioxide was selected as a typical polyatomic molecule. The self-diffusion coefficients of methane have been correlated and tabulated.² Results for the dilute gas transport properties of oxygen and nitrogen have been published.³ The well-known critical point anomaly in the thermal conductivity can now be predicted to within experimental error.⁴ An equation to calculate the dense gas and liquid transport properties of several simple fluids has been reported.⁵ Preliminary work on the transport properties of mixtures has been very promising. Theoretical studies on transport theory have been reported.⁶
8. Problem Areas. The lack of suitable mixture transport experimental data for comparison purposes is the main problem.
9. Funding. July 1 - December 31, 1975.

Allocation	59.0K\$	OSRD
Labor	0.5 MY	31.1K\$
Other Costs		3.0K\$
Total		<u>34.1K\$</u>

10. Future Plans. The transport properties of methane and ethane have been tabulated and will be published. Propane is being investigated. A preliminary procedure to calculate the transport properties of mixtures will be reported.

References

1. J. F. Ely and H. J. M. Hanley, Mol. Phys. 30, 565 (1975).
2. K. R. Harris, H. J. M. Hanley, et al., "The Self-Diffusion of Simple Fluids," Australian National Univ. Press., DRU-RR 2 (1974).
3. H. J. M. Hanley and J. F. Ely, J. Chem. Phys. Ref. Data 2, 735 (1973).
4. H. J. M. Hanley, J. V. Sengers and J. F. Ely, Proc. 14th Int. Conf. Thermal Conductivity (Pergamon Press, 1975).
5. H. J. M. Hanley, W. M. Haynes and R. D. McCarty, Cryogenics 15, 413 (1975); J. Chem. Phys. Ref. Data 3, 979 (1974).
6. For example, H. J. M. Hanley and W. M. Haynes, J. Chem. Phys. 63, 358 (1975); H. J. M. Hanley and R. O. Watts, Physica 79A, 351 (1975).

1. Title. PROPERTIES OF CRYOGENIC FLUIDS
Principal Investigators. G. C. Straty, B. J. Ackerson, and D. E. Diller
2. Cost Center Number. 2750141
3. Sponsor Project Identification. NBS
4. Introduction. Accurate thermophysical properties data and predictive calculation methods for cryogenic fluids are needed to support advanced cryogenic technology projects. For example, liquefied natural gas is expected to supply an increasing percentage of the United States' energy requirements through 1990. Liquefaction plants, ships and receiving terminals are being constructed to transport and store natural gas in the liquid state (LNG). Accurate thermophysical properties data for LNG are needed to design low temperature processes and equipment. Accurate data will benefit the energy industries and the consumer by providing for safe and efficient operations and reduced costs.
5. Objectives or Goals. The objectives of this project are to provide comprehensive accurate thermodynamic, electromagnetic and transport properties data and calculation methods for technically important compressed and liquefied gases (helium, hydrogen, oxygen, nitrogen, methane, ethane, etc.) at low temperatures. Precise compressibility, calorimetric and other physical property measurements will be performed to fill gaps and reconcile inconsistencies. Definitive interpolation functions, computer programs and tables will be prepared for engineering calculations. The immediate goals of this work are to obtain accurate sound velocity and thermal diffusivity data for compressed and liquefied gases by using laser light scattering spectroscopy techniques. Sound velocity data are useful for testing the consistency of volumetric, calorimetric and thermodynamic properties data, and are potentially useful for density gauging applications. Thermal diffusivity data are required for performing thermodynamic and heat transfer calculations.
6. Background. When light is incident on a perfectly homogeneous fluid, the reradiated (scattered) light field sums to zero in all but the exact forward direction. For a "real" fluid, however, fluctuations, arising through various mechanism, destroy the perfect homogeneity and results in the scattering of light in other directions as well. For example, thermally activated density fluctuations (phonons), propagating with the characteristic velocity of sound, give rise to scattered light which is Doppler shifted in frequency from the incident light frequency and whose spectrum contains information on the sound velocity and attenuation. Local non-propagating temperature fluctuations, which decay diffusively, give rise to scattered light in a narrow frequency band about the incident light frequency and whose spectrum contains information on the lifetime of the fluctuations (thermal diffusivity). Since the frequency shifts are generally very small, it was not until the advent of the lasers with their extremely well defined frequency, that practical experiments using these phenomena were possible.

The application of laser light scattering techniques to obtaining thermophysical properties data was initiated to complement and check other measurement methods and to solve measurement problems inherent in more conventional methods. For example, laser light scattering techniques permit measurements of sound velocities for fluids under conditions for which sound absorption is too large to perform ultrasonic measurements; laser light scattering techniques permit measurements of thermal diffusivities under conditions for which convection interferes with measurements of thermal conduction. The feasibility of light scattering experiments to obtain data on binary diffusion coefficients has also been demonstrated.

7. Program and Results. An apparatus has been assembled for laser light scattering spectroscopy on compressed and liquefied gases (76-300 K, 350 bars). The apparatus consists of a high pressure optical cell, a cryostat refrigerated by means of liquid nitrogen, an argon ion laser and low-level light detection equipment.

The light scattered from fluctuations in the fluid can be analyzed with either digital autocorrelation techniques for the examination of the very narrow lines associated with scattering from temperature fluctuations (Rayleigh scattering) or with a pressure scanned Fabry Perot interferometer for the measurement of the Doppler frequency shifts associated with the scattering from propagating density (pressure) fluctuations (Brillouin scattering).

Data on the hypersound velocities in pure methane have been obtained by Brillouin scattering techniques at low densities ($< 14 \text{ mol/l}$) where the large sound absorption in methane prohibits more conventional ultrasonic measurements. Data have been obtained along several isotherms from 210 K to 300 K at densities down to 1 mol/l . Agreement with previously measured ultrasonic velocities in the regions of overlapping data is good. The data have been combined with previously measured PVT data to obtain the isentropic compressibility and ratio of the specific heats. A manuscript reporting the results of these measurements has been published in Cryogenics 15, 729 (1975) and is reprinted in the appendices (Appendix C).

Equipment modifications have been made which should permit the determination of the thermal diffusivity, $\lambda/\rho C_p$, of pure methane. The most accurate method of doing this is to use photon-counting and digital autocorrelation techniques to measure the temporal behavior of the spontaneous temperature fluctuations occurring in the fluid which is governed by the bulk fluid thermal diffusivity. This is equivalent to measuring the very narrow Rayleigh line width and requires a resolution of about one part in 10^{12} .

Preliminary checks of the modified apparatus on a well-characterized test fluid appear to have been satisfactory. Further testing with methane is planned.

Current work involves the interfacing of mini-computer systems with the scattering apparatus to permit more rapid data accumulation and accurate on-line computer analysis of the data.

8. Problem Areas. None.

9. Funding. July 1 - December 31, 1975

Man-years expended	0.3
Equipment and/or Services Purchased	3.9K\$
Total Reporting Period Cost	20.0K\$
Balance Remaining	17.5K\$

10. Future Plans.

		Year	
Objectives and Schedule:	Quarter	1	2
Measure, analyze and report thermal diffusivity coefficient data for methane.			

1. Title. PROPERTIES OF CRYOGENIC FLUID MIXTURES
Principal Investigator(s). M. J. Hiza, A. J. Kidnay (part-time), R. C. Miller (part-time), and W. R. Parrish (part-time).
2. Cost Center Numbers. 2750142, 2750145 and 2750548
3. Sponsor Project Identification. NBS, NBS (OSRD), NASA
4. Introduction. Accurate thermodynamic properties data and predictive calculation methods for mixtures of cryogenic fluids are needed to design and optimize low temperature processes and equipment. This project provides new experimental measurements on equilibrium properties and compilations of evaluated equilibrium properties data which are suitable for direct technological use or for the evaluation of predictive calculation methods.
5. Objectives or Goals. The overall objectives of this project are to provide critically evaluated data, original and from other sources, on the phase equilibria and thermodynamic properties of cryogenic fluid mixtures. The program has been divided into the following elements:
 - a) Preparation of a comprehensive bibliography on experimental measurements of equilibrium properties for mixtures of selected molecular species of principal interest in cryogenic technology.
 - b) Selection and/or development of methods for correlation, evaluation and prediction of equilibrium properties data.
 - c) Retrieval and evaluation of experimental data for specific mixture systems selected on the basis of theoretical and/or technological importance.
 - d) Preparation of guidelines for future research based on the deficiencies noted in (a), (b), and (c).
 - e) Performing experimental research to alleviate deficiencies and provide a basis for improvement of prediction methods.
6. Background. A physical equilibria of mixtures research project was established in the Cryogenics Division in 1959. The initial effort, based on a bibliographic search and other considerations, was directed toward the acquisition of new experimental data on the solid-vapor and liquid-vapor equilibria and physical adsorption properties for a limited number of binary and ternary mixtures of components with widely separated critical temperatures. Most of the systems studied included one of the light hydrocarbon species -- methane, ethane, or ethylene (ethene) -- with one of the quantum gases -- helium, hydrogen, or neon. The data for these systems led to significant improvements in the predictions of physical adsorption equilibrium and a correlation for the prediction of deviations from the geometric mean rule for combining characteristic energy parameters. In addition, significant new information was obtained for interaction third virial coefficients which was used in a correlation by one of our consultants, J. M. Prausnitz. The approach taken in this work has been as fundamental as possible with the intention of having an impact on a broad range of mixture problems.

Recent efforts have been directed toward problems associated with systems containing components with overlapping liquid temperature ranges, such as the nitrogen + methane system.

7. Program and Results. The recent progress of this program is summarized as follows:

- a) The comprehensive bibliography of fluid mixtures data entitled "Equilibrium Properties of Fluid Mixtures: A Bibliography of Cryogenic Data" has been published (IFI/Plenum Press, 1975).
- b) Work is continuing on the compilation of liquid-vapor equilibrium data and derivation of the excess Gibbs functions and Henry's constants for binary systems containing methane with the light hydrocarbons, argon and nitrogen. A paper, "On the Consistency of Liquid-Vapor Equilibria Data for Binary Mixtures of Methane with the Light Paraffin Hydrocarbons," which covers a portion of this work, was presented at the 1975 Cryogenic Engineering Conference. This paper is reprinted in the appendices (Appendix G).
- c) A paper entitled "Liquid-Vapor Phase Equilibria in the System $N_2 + CH_4$ from 130.00 K to 180.00 K," has been published, Cryogenics 15, 531 (1975). This paper includes an evaluation of available data for this system, as discussed in (b), as well as the new measurements. This paper is reprinted in the appendices (Appendix H).
- d) New liquid-vapor equilibrium composition measurements at selected conditions for the methane + ethane system have been obtained and are being analyzed.
- e) Funds have been received to initiate research on PVTx (equation of state) data for mixtures of compressed and liquefied gases.

8. Problem Areas. None.

9. Funding. July 1 - December 31, 1975

Man-years expended	0.7
Equipment and/or Services Purchased	2.6K\$
Total Reporting Period Cost	37.1K\$
Balance Remaining	83.8K\$

10. Future Plans.

Objectives and Schedule: Quarter	Year	
	1	2
Compile, evaluate, correlate and report liquid-vapor equilibrium data for methane-ethane mixtures.		
Initiate evaluation of promising predictive equation of state calculation methods using available data.		
Measure, analyze and report liquid-vapor equilibrium data for methane-ethane mixtures.		

1. Title. DENSITIES OF LIQUEFIED NATURAL GAS MIXTURES

Principal Investigators. M. J. Hiza, W. M. Haynes, R. D. McCarty and
W. R. Parrish

2. Cost Center Numbers. 2751574, 2752574

3. Sponsor Project Identification. LNG Density Project Steering Committee;
American Gas Association, Inc., Project BR-50-11.

4. Introduction. Accurate density measurements and calculation methods for liquefied natural gas mixtures are needed to provide a basis for custody transfer agreements and for mass, density, and heating value gauging throughout the fuel gas industry.

The basis for the custody transfer of natural gas is its heating value. It is difficult to determine and agree on the heating value of extremely large volumes of natural gas in the liquid state. For example, methods for calculating the heating value of a liquefied natural gas mixture require knowing its density, which in turn depends on its composition, temperature, and pressure. As the compositions of LNG mixtures vary considerably, depending on the sources of the gas and the processing conditions, accurate methods are needed for calculating liquid densities at arbitrary compositions, temperatures and pressures. The accuracy is important because of the extremely large volumes of liquid involved.

5. Objectives or Goals. The objectives of this work are to perform accurate (0.1%) and precise (0.02%) measurements of the densities of saturated liquid methane, ethane, propane, butanes, nitrogen and their mixtures mainly in the temperature range 105-140 K, and to test and optimize methods for calculating the densities of LNG mixtures at arbitrary compositions and temperatures.

6. Background. This project is being carried out at NBS because of the realization that equitable custody transfer agreements could be reached more readily if the density measurements and the evaluation and development of calculation methods were performed by independent professionals of established reputation.

Prior to this reporting period an apparatus incorporating a magnetic suspension technique has been developed for absolute density measurements on liquids and liquid mixtures, particularly at saturation, for temperatures between 90 and 300 K. The repeatability and estimated precision of measurement are better than 0.02% while the accuracy is better than 0.1%.

7. Program and Results. Density measurements on mixtures of LNG components are in progress. Saturated liquid density measurements have been carried out for the following mixtures:

- a) $0.30 \text{ N}_2 + 0.70 \text{ CH}_4$ (105-130 K)
- b) $0.67 \text{ C}_2\text{H}_6 + 0.33 \text{ nC}_4\text{H}_{10}$ (110-140 K)
- c) $0.65 \text{ C}_2\text{H}_6 + 0.35 \text{ nC}_4\text{H}_{10}$ (115, 120 K)
- d) $0.47 \text{ iC}_4\text{H}_{10} + 0.53 \text{ nC}_4\text{H}_{10}$ (125-140 K)
- e) $0.49 \text{ C}_3\text{H}_8 + 0.51 \text{ iC}_4\text{H}_{10}$ (105-130 K)
- f) $0.50 \text{ C}_3\text{H}_8 + 0.50 \text{ iC}_4\text{H}_{10}$ (125, 130 K)
- g) $0.72 \text{ C}_2\text{H}_6 + 0.28 \text{ iC}_4\text{H}_{10}$ (105-130 K)
- h) $0.69 \text{ C}_2\text{H}_6 + 0.31 \text{ iC}_4\text{H}_{10}$ (115, 120 K)

- i) $0.68 \text{ CH}_4 + 0.32 \text{ C}_2\text{H}_6$ (105-130 K)
- j) $0.35 \text{ CH}_4 + 0.65 \text{ C}_2\text{H}_6$ (105-130 K)
- k) $0.75 \text{ CH}_4 + 0.25 \text{ C}_3\text{H}_8$ (105-130 K)
- l) $0.90 \text{ CH}_4 + 0.10 \text{ C}_3\text{H}_9$ (105-140 K)
- m) $0.34 \text{ CH}_4 + 0.31 \text{ C}_2\text{H}_6 + 0.34 \text{ C}_3\text{H}_8$ (110-125 K)
- n) $0.85 \text{ CH}_4 + 0.05 \text{ C}_2\text{H}_6 + 0.04 \text{ C}_3\text{H}_8 + 0.03 \text{ iC}_4\text{H}_{10} + 0.03 \text{ nC}_4\text{H}_{10}$
(105, 110 K)
- o) $0.34 \text{ N}_2 + 0.34 \text{ CH}_4 + 0.32 \text{ C}_2\text{H}_6$ (105-115 K)

The new experimental data for the binary mixtures have been used as input data to several equations of state, which have been then used to predict the densities of the multicomponent systems. Most of these predictions agree with direct measurements to about 0.05% in density.

A paper "Orthobaric Liquid Densities of Normal Butane from 135 to 300 K as Determined with a Magnetic Suspension Densitometer," was presented at the 1975 Cryogenic Engineering Conference. This paper is included in the appendices (Appendix F).

8. Problem Areas. None

9. Funding. July 1 - December 31, 1975

2751574 (measurements)

Man-years expended	0.8
Equipment and/or Services Purchased	3.0K\$
Total Reporting Period Cost	52.2K\$
Balance Remaining	68.2K\$

2752574 (calculation methods)

Man-years expended	0.25
Equipment and/or Services Purchased	0.5K\$
Total Reporting Period Cost	8.3K\$
Balance Remaining	25.6K\$

10. Future Plans.

Objectives and Schedule: Quarter	Year	
	1	2
Measure orthobaric liquid densities of mixtures containing methane, ethane, propane, butanes and nitrogen.		
Evaluate and optimize several available accurate density calculation methods.		

1. Title. LOW TEMPERATURE MATERIAL BEHAVIOR
Principal Investigators. H. I. McHenry and R. P. Reed
2. Cost Center Number. 2750430
3. Sponsor Project Identification. Maritime Administration Misc. P.O. #400-58074.
4. Introduction. For cryogenic applications, the ASME Boiler and Pressure Vessel Code and the API Standard 620 Appendix Q Code specify the same design allowable stress level for 5Ni steel as for 9Ni steel. Since 5Ni steel costs approximately 20% less than 9Ni steel, significant cost savings could be achieved by using this material for LNG applications. At the present time, 5Ni steel cannot be used in place of 9Ni steel for marine applications because the U. S. Coast Guard has not approved it. The principal reasons that the USCG has delayed approval are lack of service experience in land based tankage and concern that the fracture resistance of the weld heat affected-zone (HAZ) is inadequate.
5. Objectives. This program is being conducted to evaluate the fracture resistance of the heat affected zone of 5Ni steel weldments at room temperature, 111 K and 76 K.
6. Background. This program is a continuation of the program conducted by Reed, et al. to determine the mechanical properties of candidate materials for LNG tankage. The work demonstrated that 5Ni steel plate has adequate mechanical properties for LNG applications. Further work was recommended to verify that the plate properties would be retained in the weld heat affected zone.
7. Program and Results. The program to evaluate 5% Ni steel weldments consists of evaluating the weldment toughness in accordance with the USCG requirements for weld procedure qualification and determining the fatigue crack growth and fracture toughness properties of the weldment.

Weld procedure qualification involves testing three Charpy impact specimens at five locations within the weld zone: at the weld centerline, the fusion line, and the heat affect zone at 1, 3 and 5 mm beyond the fusion line. The tests were conducted in accordance with ASTM Standard Method E-23 at 76 K. The results exceeded the USCG requirements in all weldment locations.

Fatigue crack growth tests are being conducted using three-thickness bend specimens to enable definition of the part of the HAZ most susceptible to crack growth. To date, tests have been conducted on the base metal at room temperature and 76 K and on the HAZ at room temperature. The base metal results are essentially the same as those obtained previously using compact specimens. In the HAZ test, the crack was started in the fusion line, but proceeded to propagate into the base metal -- in the direction perpendicular to maximum stress. Thus, at room temperature, HAZ embrittlement is not apparent in the crack growth tests.

Fracture toughness tests have been conducted on the base metal and the HAZ at 111 K. The results indicate that the base metal toughness is approximately 150 ksi $\sqrt{\text{in}}$. No crack extension could be detected prior to failure despite repeated efforts using heat-tinting procedures. The HAZ toughness ranged from 94 to 102 ksi $\sqrt{\text{in}}$ on the three specimens that exhibited crack extension (pop-in) prior to fracture and from 106 to 133 ksi $\sqrt{\text{in}}$ on the three specimens that failed prior to any detectable crack extension.

A paper entitled "Fracture Mechanics and its Application to Cryogenic Structures" was prepared and presented at the International Cryogenic Materials Conference in Kingston, Ontario (see Appendix I).

8. Problem Areas. The test schedule has been extended to March 31, 1976 (from December 31, 1975) and no additional problems are anticipated to completion.
9. Funding. July 1 - December 31, 1975

Expended	30K\$
Remaining	20K\$
10. Future Plans. All testing will be completed by March 31, 1976.

1. Title. PROGRAM FOR REDUCING THE COST OF LNG SHIP HULL CONSTRUCTION --
PHASE II SHIP STEEL IMPROVEMENT PROGRAM

Principal Investigators. H. I. McHenry, M. B. Kasen, and R. P. Reed

2. Cost Center Number.

2753430 - LNG Ship Hull Materials (Shipyard Contracts)
2751430 - LNG Ship Construction Materials (Metallurgical Evaluation)
2752430 - LNG Ship Hull Materials (Fracture Properties)

3. Sponsor Project Identification. Maritime Administration Misc. P. O.
400-58073.

4. Introduction. Construction of LNG tankers requires the use of fine grain normalized steels for the part of the hull structure that is cooled by the cargo to temperatures in the range of 0 to -50°F. Several ABS steels have satisfactory base plate properties but extreme care must be exercised during welding to avoid degradation of the steel adjacent to weld (the heat affected zone) to a level of toughness below U. S. Coast Guard requirements. Significant cost problems are being encountered by U. S. shipyards due to the resulting inefficient low-heat-input welding procedures that must be employed to meet the fracture requirements in the heat affected zone.

The feasibility of reducing the cost of LNG ship hull construction was investigated in Phase I of this project, leading to the Phase II program described below.

5. Objective. The objectives of the Phase II program are 1) to have the four major plate producers supply three LNG shipyards with production heats of ABS steels modified to possess improved transverse fracture properties at low temperatures, 2) to have the LNG shipyards evaluate these plates by qualifying optimum welding procedures in accordance with the USCG requirements, and 3) to provide a metallurgical evaluation of factors that influence heat affected zone toughness in the improved steels.

6. Background. Early in 1974, the Welding Panel of MarAd's Ship Production Committee recommended that a program be conducted to reduce the cost of ship hull construction. NBS was requested by MarAd to propose such a program to the LNG subcommittee of the Welding Panel at a meeting in Boulder in August. In mid-October, MarAd approved the initial phase of NBS's recommended program, i.e., to survey the problem and the technology available for its solution. On the basis of this survey and as the result of a meeting of the Welding Panel in March, 1975, a coordinated program involving the LNG shipyards, the steel suppliers, and NBS was recommended to MarAd and to the Welding Panel. This program was approved and work started in May 1975.

7. Program and Results. Contracts have been awarded to the three shipyards currently building LNG tankers: Avondale Shipyard, Inc.; General Dynamics/Quincy Shipbuilding Division; and Newport News Shipbuilding. Each of these yards has placed orders for steel as follows:

<u>Shipyard</u>	<u>Steel Co.</u>	<u>Test Temperature</u>	<u>Steel Grade*</u>
Avondale	Armco	-25°F	V-062
		-50°F	V-062 (SSC) **
General	U.S. Steel	-25°F	CS (SSC)
Dynamics	Bethlehem	-60°F	ASTM A537A-Mod.
Newport News	Bethlehem	-25°F and -50°F	V-051 (SSC)

* The steel grades V-062, V-051 and CS are American Bureau of Shipping (ABS) grades

** SSC - Sulfide Shape control employed.

Upon receipt of material, each participating shipyard will evaluate the steel plates by qualifying optimum weld procedures in accordance with USCG requirements. The welding processes being qualified are submerged arc, gas metal arc, and shielded metal arc. The test weldments will also be subjected to a metallurgical evaluation to determine the effect of microalloying and sulfide shape control on heat affected zone toughness.

A paper entitled "Ship Steel Weldments for Low Temperature Service" was prepared and presented at the Fourth Materials Technology Conference in Boston, MA (see Appendix J).

8. Problem Areas. The development work has been delayed because more time was required for contract negotiation and steel procurement than was originally anticipated.

9. Funding. July 1 - December 31, 1975

<u>Cost Center</u>	<u>Cost to 12/21/75</u>	<u>Balance</u>
2753430	\$105 K	\$105 K (obligated)
2751430	\$ 57 K*	\$ 18 K
2752430	\$ 26 K	\$ 14 K

*Includes phase I costs.

10. Future Plans. The steels should be delivered and the shipyard and metallurgical evaluations should be started during the next reporting period.

1. Title. CUSTODY TRANSFER - LNG SHIPS
Principal Investigators. R. S. Collier, P. J. Giarratano, and J. D. Siegwarth
2. Cost Center Number. 2750460
3. Sponsor Project Identification. Maritime Administration, Misc. P.O. #400-58074.
4. Introduction. In response to a request from the U.S. shipbuilding industry, NBS is conducting an independent design review of the shipboard custody transfer systems under the sponsorship of the Maritime Administration and in cooperation with the major U.S. shipbuilding companies.
5. Objectives. The objectives of this program are to 1) Identify the major technical areas relating to uncertainties in the measurement of total mass and total heating value, 2) Estimate uncertainties in the total mass and total heating value due to these identified factors, 3) Develop a proposed testing program for custody transfer system components, and 4) Investigate improved gauging techniques.
6. Background. Calendar year 1974 funding provided for the initial review of ships designated by MA Design LG8-S-102a MA Hulls 289, 290, 291. The current funding provides for an extension of this program to include ships of other designs which are being built by the major U.S. shipbuilding companies.
7. Program and Results. A. Working relationships with four major U. S. shipbuilders have been established. Most of the problem areas which are common to custody transfer systems of all types have been identified and are listed as follows:
 1. Density
 - a) accuracy
 - b) rangeability
 - c) stability
 2. Tank Strapping
 - a) thermal effects
 - b) loading factors
 - c) measurement techniques
 3. Convection (Non-Uniform Density)
 - a) density or composition stratification
 - b) possible isolation of measurement stillwells
 4. Tank Weathering
 - a) time changes in composition, stratification, etc.
 - b) composition measurement
 - c) sampling
 5. Liquid Level/Total Volume Measurement
 6. Pressure and Temperature Measurements (gradients included).
 7. Electronic Signal Conditioning, Data Reduction, Analysis and Readout

B. We have reviewed in detail the capacitance densitometer both from theoretical and experimental point of view. The theoretical analysis has shown two major effects for LNG near the saturation temperature

and pressure nominally close to atmospheric pressure (or slightly above). These two effects are:

1. The heavy hydrocarbons in the absence of nitrogen tend to partially compensate for their density as a function of molecular weight to the extent that, at saturation, the density versus dielectric constant is approximately single valued relationship (within a certain error which, for a typical range of LNG mixtures, is approximately 0.3 percent). This is a new result which is independent of the Clausius-Mosotti relationship. The Clausius-Mosotti function does not delineate the saturation curve of the LNG mixtures and includes subcooled fluids; but when the saturation curve is delineated, the unique one to one relationship between density and dielectric constant very nearly exists.
2. Nitrogen has a very pronounced effect on the density versus dielectric constant. Mole fractions of nitrogen on the order of 1 percent of the total composition can cause about 1% increase in the density for the same dielectric constant. This nitrogen effect tends to negate the usefulness of dielectric properties for density measurement except for the fact that the saturation temperatures of LNG mixtures containing nitrogen are somewhat lower. Consequently, we have found that it is possible to temperature compensate the capacitance densitometer using a bilinear relationship between density, dielectric constant, and temperature; curves for this bilinear relationship and the coefficients that go in this relationship have been obtained by the use of least squares computer programs together with the correlations using 1) the law of corresponding states as proposed by Jørgen Möllerup¹ and as modified by Bob McCarty at NBS and 2) the Clausius-Mosotti relationships as proposed by Pan, et al.². The details of this analysis are contained in the appendices of this report (see Appendix N).

C. As part of the testing program in the area of capacitance densitometers we have obtained dielectric constant data for methane binary mixtures with hydrocarbons and also some typical LNG mixtures with and without nitrogen. These measurements confirm the theoretical analysis described above to within about 3/10 of one percent. This experimental program together with the theoretical analysis gives positive and conclusive indication of the capability of the capacitance densitometers as their anticipated end use onboard ship custody transfer systems.

D. In connection with the program on the density reference systems (Cost Center 2757574) we have conducted a prototype capacitance densitometer system which although not temperature compensated for nitrogen, performs within theoretical uncertainties for the hydrocarbon mixtures and is capable of the suggested temperature compensation for nitrogen. Further testing is in progress.

E. We have calculated the difference between the corresponding states theory and the Klosek-McKinley relationship for the temperature and pressure and composition ranges envisioned by the LNG industry and found that these two agree to within 2/10 of a percent. If a temperature is measured accurately, and also composition, the density can then be obtained using the Klosek-McKinley relationship to about the same certainty as using the densitometer approach. (The Klosek-McKinley approach is to be used by the industry in the absence of a more precise correlation or an adequate densitometer.)

F. We have investigated the heating value of LNG as a function of density and dielectric constant for the saturated LNG mixtures. We find again that for mixtures without nitrogen the heating value versus saturation density is very close to unique functions and the heating value versus dielectric constant is a unique function to the same order of

magnitude that the density is a unique function of dielectric constant. Here again, however, the effect of nitrogen is pronounced. The heating value versus density and dielectric constant changes markedly with the addition of nitrogen. Further work needs to be done in the area of direct therm-metering for mixtures containing nitrogen.

G. We have begun to review in detail the ability of the ship companies to measure fluid volume which together with the density will give them a total mass. The fluid volume is a function of both the tank strapping and the liquid level measurement:

1. There are two basic techniques for tank strapping: a) the stereophotogrammetric method of measuring the inside dimension of the tank and b) tape measurements on selected circumferences of the tank. Both of these methods are under consideration by the ship companies and we are presently discussing, with the industry, possible NBS involvement concerning verification of the accuracies of either or both of these methods.
2. We have begun preliminary design (consistent with manufacturers specifications) concerning a test facility for stratification research and level testing. This facility would be capable of testing prototype level gauges on the order of 10 meters in length which seems to be adequate for observing thermogradient effects, LNG stratification effects, and also possible effects caused by condensation of heavy hydrocarbon vapor on the sensing elements. A preliminary test plan has been drawn up and distributed to MarAd, the engineering departments of the major shipyards, and some of the manufacturers. It is likely that industry will participate in these tests which would involve consignment of equipment and some financial commitment on their part to complete the tests.

H. We have been involved in pursuing advanced gauging techniques including therm-metering and RF gauging techniques. We have modeled the spherical LNG ship tanks in the laboratory, including a model of the measurement stillwell (which in the ship is a cylindrical tube 8 feet in diameter running along a 120 foot spherical diameter from the top to the bottom of the tank). We have found for the laboratory model that it is feasible to use the measurement stillwell as an RF antenna with the electrical connection being made directly to the stillwell at mid point. In this configuration the model can be resonated as an electromagnetic resonant cavity and the resonant modes have been identified; as the tank is filled with LNG the resonant frequencies decrease as the LNG fills the tank. The scaling laws for the RF cavity are under investigation and experiments are in progress for testing the scaling laws in tanks that range between the laboratory model which is 18 inches in diameter and the actual spherical LNG tank which is 120 feet in diameter.

I. We have conducted preliminary studies into the possibility of a direct reading therm-meter for LNG custody transfer. It seems worthwhile, at this point, to conduct some feasibility studies involving the electromagnetic spectroscopic properties of LNG as well as some of the thermodynamic physical properties for possible use in a direct reading therm-meter.

8. Problem Areas. One of the most difficult estimates to make is the degree of density or composition stratification within the tank; this could also include the effect of stillwells and remote access areas within the tank. It will probably not be possible to estimate these effects to the desired accuracy. It is therefore recommended that some of these ship tanks be fitted experimentally to measure density, temperature and composition at various locations within the tank during the normal course of checkout of these systems.

9. Funding. July 1 - December 1, 1975

Man-years expended	0.5
Total Cost	33.4K\$
Balance Remaining	11.7KS

10. Future Plans.

1. Complete the rangeability test of the capacitance type densitometer.
2. Continue a program of exchange of information with the U.S. ship-building companies.
3. Develop and update procedures for calculating weathering and boil-off rates for tanks containing LNG mixtures.
4. Initiate studies of stratification and detection in large systems consistent with solving problem areas as in paragraph 8 above.
5. Conduct further experiments on RF gauging in large tanks.

References

1. J. Möllerup and J. S. Rowlinson, Chemical Engineering Science 29, 1373 (1974).
2. W. P. Pan, M. H. Mady, and R. C. Miller, Dielectric constants and Clausius-Mosotti functions for simple liquid mixtures: systems containing nitrogen, argon and light hydrocarbons, AIChE Journal 21, No. 2 (March 1975).

1. Title. HEATING VALUE OF FLOWING LNG
Principal Investigators. J. A. Brennan and J. M. Arvidson
2. Cost Center Number. 2756579
3. Sponsor Project Identification. Pipeline Research Committee (American Gas Association) PR-50-48.
4. Introduction. This project will test instrumentation for making heating value measurements in actual applications of flowing LNG. Information from projects currently underway by Younglove (cost center 2757574) on densimeters and by Haynes and Hiza (cost center 2751574) on mixture densities will be utilized where appropriate to provide state of the are information.
5. Objectives. The objective of this program is to measure total heating value of LNG flowing in a pipeline by the integration of individual measurements of flow, density and specific heating value. Flow measurement requires determination of flowmeter performance in line sizes larger than presently available calibration facilities. Therefore, a secondary objective is to establish appropriate flowmeter scaling laws.
6. Background. The LNG flow facility at NBS will be utilized to evaluate the response of the individual elements in the heating value measurement. Different compositions of LNG will be prepared to provide a range of densities and temperatures sufficient to determine any dependencies. A limited amount of sampling work is included to determine the relative importance of this parameter to the overall measurement.

Flowmeter scaling is being done utilizing the cryogenic and the water flow facilities at NBS and private LNG peak shaving facilities. This portion of the program is behind schedule because of scheduling problems at the private LNG facilities. Work in this area did progress during this reporting period when a short field test at the peak shaving facility was completed. If additional testing can be completed during the current send-out season additional delays in the project will be prevented.
7. Results. Field testing of the four-inch flowmeter at the LNG peak shaving facility was completed December 16, 1975. The actual test period available was approximately 3-1/2 hours which was shorter than desirable but long enough to obtain some very useful data.

A preliminary analysis of the data indicates agreement between the liquid and gas flow measurements within about one percent. Data analysis is still proceeding and the final results must await receipt of the final gas phase measurements from the peak shaving facility. Therefore, results from this test will not be reported until the next semi-annual report.

In the last semi-annual report it was stated that a new LNG peak shaving facility had been selected for testing the eight-inch flowmeter since this new facility had a high probability of send-out during the current season. To reduce the possibility of additional delays in this phase of the program plans were made to move the flowmeter tests. These plans had to be dropped, however, because the cost involved was too high. Therefore, the eight-inch flowmeter has been installed in the same location as the four-inch meter and the smaller meter has been removed from the line.

Some component testing on the NBS flow facility was also completed during this reporting period. As previously stated it was necessary to assemble a natural gas condenser for making LNG. This condenser uses liquid nitrogen to condense low pressure natural gas and was used as the source of the LNG for the testing in the flow facility.

Figure 1 is a schematic of the NBS flow facility in which the various elements of the measuring station are being tested. During the most recent tests data were obtained on all the individual elements and cross checks are being calculated. The individual signals will be integrated into a single indication of heating value during the next years test program.

8. Problem Areas. None.

9. Funding. July 1 - December 31, 1975

Man-years Expended	0.2
Total Reporting Period Costs	70K\$
Balance Remaining	.5K\$

10. Future Plans. Flowmeter tests on the eight-inch meter will be run whenever there is a send-out. The current send-out season ends in March 1976. Additional tests on the NBS flow facility will be run after the instrumentation integration has been completed.

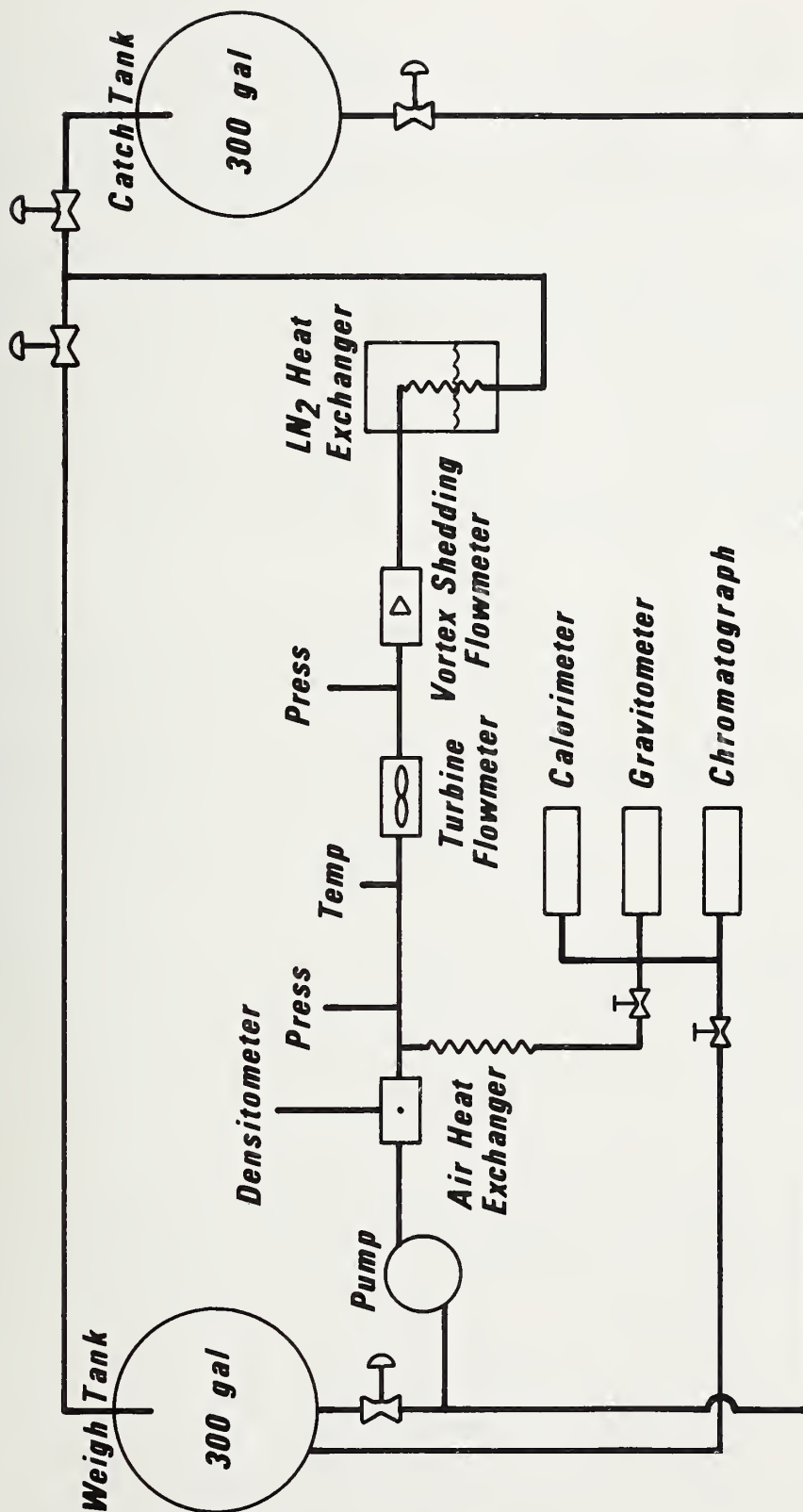


Figure 1

FLOW SCHEMATIC LNG FLOW FACILITY

1. Title. LNG DENSITY REFERENCE SYSTEM
Principal Investigator. Ben Younglove

2. Cost Center Number. 2757574

3. Sponsor Project Identification. American Gas Association, Inc.,
Project BR-50-10

4. Introduction. The emphasis of the LNG effort of NBS is in providing technical support to industry in meeting the energy needs of our economy with natural gas.

The density reference system will evaluate the ability of commercially available instruments to measure densities of LNG. Density is an essential measurement in performing total energy content determinations of natural gas reservoirs. While this effort is oriented towards metrology, the output from cost center 2751574 will provide basic reference data on pure liquids and mixtures which will serve as density standards.

5. Objectives. This research will provide a system for evaluating the density measurement capability of commercially available meters. We will evolve a density reference system capable of generating accurate densities for this evaluation. From the commercial meters we will attempt to select one capable of performance as a transfer standard in order to provide traceability of accuracy to field density measurement systems.

6. Background. The density reference system was initiated in 1973 with a proposal to the AGA for research on LNG technology. Since that time the reference system has been selected, designed, constructed, and is now in operation, evaluating density metering systems.

7. Program and Results. Data have been accumulated on performance of the vibrating cylinder, vibrating plate, and the capacitance meter in liquid methane, methane + ethane, methane + propane, methane + butane, methane + nitrogen, and two LNG type mixtures.

Pure methane runs are incorporated on a regular basis in an attempt to establish reliability limits of the density reference system over an extended time.

A second series of tests is underway to evaluate the commercial displacement type (or Archimedes type) meter. The other devices were left in the system in order to accumulate more data on them as well. We have accumulated data on pure methane and methane + nitrogen in this configuration.

John Labrecque of the NBS Statistical Engineering Laboratory has analyzed the pure methane runs of the first series. Using the model

$$\delta = \mu + \alpha\rho + \eta + \epsilon$$

where δ is density deviation from NBS densities for pure methane from vapor pressure, μ is the bias independent of density, temperature, or pressure; η error constant within an occasion (or data taken on a given run); and ϵ is an error changing randomly from occasion to occasion, he finds these results, where σ is an estimate of "one sigma" deviation:

Accuracy Affected by Density		σ_{η} kg/m ³	σ_{ϵ} kg/m ³
NBS DRS	Not Significant	0.20	0.30
Cylinder	Significant	0.49	0.57
Plate	Significant	1.55	1.16
Dielectric Cell	Significant	0.41	0.07

These results will be given in more detail in the final report.

Results taken so far for the displacement type meter show roughly a constant bias of -1 kg/m^3 and a random scatter of about half that. This latter observation is very preliminary.

8. Problem Areas. Deviations of the meters for the mixtures data show roughly the same behavior as the above with the notable exception of the capacitance (or dielectric cell) densimeter, which showed marked deviations with nitrogen composition. Two binary mixtures of nitrogen were taken, showing approximately a 1 to 1 or greater deviation of density indication to nitrogen composition (mol %).
9. Funding. July 1 - December 31, 1975

Man-years expended	0.75
Equipment and/or Services Purchased	3.0K\$
Total Project Cost	43.0K\$
Balance Remaining	2.0K\$
10. Future Plans. To complete measurements and write summary of results.

1. Title. LIQUEFIED NATURAL GAS TECHNOLOGY TRANSFER
Principal Investigator. D. B. Mann
2. Cost Center Number. 2750401
3. Sponsor Project Identification. Maritime Administration, Misc. P.O. 400-58074.
4. Introduction. The NBS support of the Maritime Administration (MarAd) LNG ship program is divided into three areas. These are a materials experimental program, LNG ship custody transfer, and cryogenic technology transfer. In addition to those objectives listed below this program provides a cohesive structure for the coordination of the NBS LNG program.
5. Objectives. Cryogenic Technology Transfer is designed to provide cryogenic technical information, data, and advice to the Maritime Administration (MarAd), its contractors and other agencies performing work of interest to, or for, MarAd in the design, development, testing, construction, and operation of LNG ships and ship components.
6. Background. The Merchant Marine Act of 1970 restructured federal maritime policies to make bulk carrier vessels, such as tankers and LNG ships, eligible for construction and operating subsidies. In December 1973 the keel was laid for a 926 foot long LNG vessel carrier at Quincy, Mass. The keel laying initiated the construction of the first LNG tanker to be built in the United States. American ship builders have orders for a total of 15 of these complicated ships. Various future projections indicate a total of from 25 to well over a 100 ships will be required to handle the LNG importation within the next 10-15 years. Recent proposals to liquefy and transport Alaskan gas to the U.S. only reinforced the importance of this new technology to providing a measure of energy self-sufficiency to the U.S.

LNG marine technology is presently foreign dominated. As a matter of fact, many of the ships being constructed in U. S. shipyards are using designs under license from foreign industrial groups or governments. LNG is a cryogenic fluid and the massive technology developed over the past 15-20 years in cryogenics, as applied to industrial gases and the aerospace effort, provides a resource which could be applied profitably to improving the U. S. competitive position in the construction and operation of LNG shipping. Because of its historical association with broad based cryogenic technology over a period of some 20 years, the NBS Cryogenics Division was requested to provide support to the MarAd LNG ships program in order to aid in the transfer of cryogenic technology where it could enhance the effectiveness of maritime LNG shipping. Therefore, on April 17, 1973 we submitted a work statement which was confirmed by the establishment of a program in May of that year.
7. Program and Results. As a result of extensive assessments of user requirements, it was found that a most effective mode for technology transfer would be a LNG Materials and Fluids Data Book. The purpose, scope, format, content and schedule were developed over a period of 10 months and involved LNG interests in the gas industry, Maritime Administration, NASA and other Division of NBS in addition to the staff of the Cryogenics Division

A description of the Data Book is as follows:

LIQUEFIED NATURAL GAS MATERIALS AND FLUIDS DATA BOOK

Purpose. To provide a method of quick dissemination of property data and related information for the effective generation, utilization, and transportation of LNG. The object is to improve technology transfer from the current NBS Cryogenics Division LNG physical measurements program to the users, including federal agencies, the states, and industry. For the purposes of this data book, Liquefied Natural Gas is defined as a cryogenic mixture (at less than ~ 150 K) of hydrocarbons, predominantly methane, with less than a total of twenty percent of the minor components ethane, propane, iso and normal butane, and nitrogen as an inert contaminant.

Scope. The data book is only one of a number of information dissemination methods used to provide workers in the Liquefied Natural Gas (LNG) industry with properties data of known quality in a format consistent with the requirements of the intended user. In the case of the LNG Data Book, the intended audience is the field engineer, plant manager, ship designer or process engineer interested in a ready reference of assessed quality for data to be used in conceptual design, process monitoring, process analysis, and inter-comparisons where precision and accuracy are secondary to specific problem solutions. The hierarchy of accuracy and precision will be defined and traceable through reference to the scientific and engineering literature.

Data is classified into three groups by NBS Cryogenics Division.

Group I. Data which has been generated experimentally by NBS or has been assessed, evaluated, and experimentally verified by NBS.

Group II. Data which has been assessed and evaluated by NBS.

Group III. Data available in the scientific and engineering literature through the NBS-Cryogenic Data Center or elsewhere. No NBS evaluation or assessment has been made at this date.

In general all data included for the LNG Data Book will be from Groups I and II. No new assessments or correlations are anticipated or required for this work.

Format. Data will be presented primarily in graphical form. Tables and analytical expressions will be used only where absolutely necessary. Graphs and charts will be in loose-leaf form for ease of updating and additions. This form will also allow immediate implementation for data already available under the NBS-LNG Program and will provide a convenient form for output of data from existing projects. The data book will not be a substitute for traditional publications in the scientific literature where measurement science, technique, precision, and accuracy are paramount, but will provide the data and references for the necessary assessment by the user.

Content.

Part 1. LNG Materials - Primarily those materials used directly or indirectly in the liquefaction, storage, transport, and measurement of LNG. This will include primary and secondary containment structure, weldments, insulations, etc. A proposed table of contents is as follows:

Section	Description
1.1.	Introduction
1.1.1.	Objective of Data Book
1.1.2.	Overview of temperature effect on materials
1.1.3.	Nomenclature

Section	Description
1.2.	Structural Metals and Alloys
1.2.1.	Alloy steels
1.2.2.	Nickel steels
1.2.3.	Stainless steels
1.2.4.	Aluminum alloys
1.2.5.	Copper alloys
1.2.6.	Nickel alloys
1.2.7.	Miscellaneous metals
1.3.	Thermal Insulations
1.3.1.	Wood products
1.3.2.	Inorganics
1.3.3.	Fiberglass
1.3.4.	Foams
1.3.5.	Mineral wools
1.3.6.	Vapor barrier systems
1.4.	Joining Materials
1.4.1.	Welding rod, filler materials
1.4.2.	Brazing consumables
1.4.3.	Soldering consumables
1.4.4.	Mechanical fasteners
1.4.5.	Adhesives
1.5.	Structural Composite Materials and Aggregates
1.5.1.	Glass reinforced plastics
1.5.2.	Concrete
1.5.3.	Reinforced concrete
1.5.4.	Wood
1.5.5.	Advance composites
1.6.	Polymeric Materials
1.6.1.	Thermalsetting plastics
1.6.2.	Thermoplastics
1.6.3.	Elastomers
1.6.4.	Silicones
1.7.	Miscellaneous Non-structural Materials
1.7.1.	Lubricants
1.7.2.	Sealants
1.7.3.	Threading compounds
1.7.4.	Gaskets and packings
1.7.5.	Paints and coatings

Data for each material or class of materials will include a general description and its primary LNG usage, availability, and chemical composition. Mechanical properties as a function of temperature (76-300 K) will be presented in graphical form. These will include:

Tension	Modulus	Static fatigue
Compression	Poisson's Ratio	Thermal fatigue
Shear	Fracture toughness	Wear resistance
Bearing	Dynamic fatigue	Impact

Design allowable performance specifications (ASME & API) will be provided for various product forms including restrictions.

Physical properties as a function of temperature (76-300 K) will be provided in graphical form including:

- Thermal conductivity
- Thermal expansion
- Density
- Magnetic properties
- Specific heat

Compatibility of the materials with LNG will be presented where possible as to:

- Flammability
- Solubility
- Adsorption and swelling
- Corrosion/Erosion
- Permeability
- Aging and effects of thermal cycling

Specifications for fabrication will be defined for:

- Welding and brazing
- Thermal treatment
- Forming
- Machining
- Forging and casting
- Environmental considerations
- Handling characteristics

Finally, the data on all materials will be extensively documented with references.

Part 2. Fluids - Primarily those fluids which compose LNG which is defined here as at least 80% methane with minor components of ethane, propane, iso and normal butane, and nitrogen.

A proposed table of contents is as follows:

Section	Description
2.1.	Introduction
2.1.1.	Objective of Data Book
2.1.2.	Overview of non-ideal behavior of pure fluids and mixtures
2.1.3.	Nomenclature
2.2.	Pure Fluids: Methane, ethane, propane, iso and normal butane, nitrogen.
2.2.1.	Physical
2.2.1.1.	Compressibility - $Z = f(P, T, \rho)$
2.2.1.2.	Pressure - $P = f(T, \rho)$
2.2.1.3.	Temperature - $T = f(P, \rho)$
2.2.1.4.	Density - $\rho = f(P, T)$
2.2.1.5.	Sound Velocity - $W = f(T, P)$
2.2.1.6.	Surface Tension - $\sigma = f(T, P)$
2.2.1.7.	Vapor Pressures = $f(T, \ln P)$
2.2.2.	Thermophysical
2.2.2.1.	Density, temperature, entropy as functions of pressure and enthalpy (Mollier chart)
2.2.2.2.	Pressure, density, enthalpy as functions of temperature and entropy (T-S chart)
2.2.2.3.	Pressure, density, temperature as functions of enthalpy and entropy (H-S chart)
2.2.2.4.	Specific heats at constant pressure as a function of temperature and pressure.
2.2.3.	Electromagnetic Properties
2.2.3.1.	Dielectric constant - $\epsilon = f(T, P)$
2.2.3.2.	Dielectric constant - $\epsilon = f(T, \rho)$
2.2.3.3.	Refractive index - $\eta = f(T, P)$
2.2.3.4.	Refractive index - $\eta = f(T, \rho)$
2.2.3.5.	Clausius-Mosotti - $CM = f(T, \rho)$
2.2.3.6.	Lorentz-Lorenz - $L-L = f(T, \rho)$
2.2.4.	Transport Properties
2.2.4.1.	Viscosity - $\eta = f(P, T)$
2.2.4.2.	Thermal conductivity - $k = f(P, T)$

- 2.3. Fluid Mixtures - Binary mixtures of methane with ethane, propane, iso and normal butane, nitrogen.
- 2.3.1. Liquid Vapor Equilibrium
- 2.3.1.1. K values
- 2.3.1.2. Vapor pressures
- 2.3.1.3. Pressure-composition
- 2.3.2. Saturated Liquid Densities
- 2.3.2.1. Density-temperature
- 2.3.2.2. Excess volumes-temperature

Ternary and higher order mixtures will be considered for graphical presentation if data and methods of graphical display are practical.

Schedule. Data now available or which, as a logical output of existing funded programs, will be available within the next 18 months can be considered in the first edition of the data book. Therefore, during calendar years 1976 and 1977, the following sections can be completed and the data book binder and data sheets printed and issued.

Section	Calendar Year		
	1976	1977	1978 +
1.1	X	-	-
1.2	X	-	-
1.3	-	X	X
1.4	-	-	X
1.5	-	-	X
1.6	-	-	X
1.7	-	-	X
2.1	X	-	-
2.2.1	methane, nitrogen	ethane	propane, butanes
2.2.2	methane, nitrogen	ethane	propane, butanes
2.2.3.1,	methane,		ethane, propane,
2.2.3.2	nitrogen		butanes
2.2.3.3,	methane	-	ethane, propane,
2.2.3.4			butanes, nitrogen
2.2.3.5	methane, nitrogen	-	ethane, propane, butanes, nitrogen
2.2.3.6	methane	-	ethane, propane, butanes, nitrogen
2.2.4	methane, nitrogen	ethane	propane, butanes
2.3.1.1, 2.3.1.2,	methane-nitrogen	-	methane, propane
2.3.1.3	methane-ethane	-	methane-butaness
2.3.2.1,	methane-nitrogen	methane-propane	-
2.3.2.2	methane-ethane	methane-butaness	

It is estimated that this should result in the production of ~ 220 charts in CY 1976 and ~ 250 charts in 1977. The balance of charts would be issued after the end of 1977 based on need and assessment of the value of the data book to the user.

It is anticipated that the binder and up to 70 charts could be issued within six months with the additional charts sent to subscribers in six month intervals thereafter. A yearly review of the program as to content and form by sponsors and users would guide NBS in the management of the long range program. Data exists now in a quantity and quality to define the two year program at a two man year per year level. The table of contents and current interest levels within the industry indicate that this level could be maintained to late 1979. A one man year per year level thereafter would provide the necessary support until such time as the original content is completed or active NBS participation is no longer necessary.

8. Problem Areas. The data book as described above is an extremely ambitious proposal. The first year effort should involve only a conversion of existing LNG Program output to graphical format. However, the continuing support will depend on the utility of this first year effort.
9. Funding. Funding for this cost center has been exhausted and future support will be directed to the generation and distribution of the data book.
- | | |
|--------------------------|--------|
| Labor | 0.2 MY |
| Cost to 31 December 1975 | 8K\$ |
10. Future Plans. Four potential sponsors of the data book have been identified. A description of the first year effort is included in section 7. A slight slippage in the schedule may occur, caused by funding transfer delay.

1. Title. FEDERAL POWER COMMISSION CONSULTATION
Principal Investigators. D. B. Chelton, A. F. Schmidt and T. R. Strobridge.
2. Cost Center Number. 2750404
3. Sponsor. Federal Power Commission - Bureau of Natural Gas -- letter agreement dated 4 June 1973.
4. Goals. The Cryogenics Division will provide consultation and advisory services to the Federal Power Commission on the cryogenic safety and the design aspects of several current applications before the FPC for authorization of LNG terminal and storage facilities. These services cover properties of cryogenic environments, insulation systems, cryogenic safety, thermodynamics, heat transfer, instrumentation, and cryogenic processes such as refrigeration and liquefaction.
5. Background. Cost Center initiated July 7, 1973.
6. Program and Results. The status of those facilities presently under the jurisdiction of the Federal Power Commission and subject to our review are outlined in the following table.

Elements of the facilities that are subject to review are the land-based cryogenic storage tank components, bounded by the tanker or barge, the inlet and distribution pipelines. These include, but are not limited to the transfer lines, the storage tanks, the vaporizers and the process piping as it interacts with the storage tanks. It is essential that the reviews cover the operation, maintenance and emergency procedural philosophies for each terminal. Based upon these studies, reports are submitted to the staff of the FPC setting forth the technical evaluations and conclusions on each proposal.

Emphasis is placed on the safety aspects of the facilities including their possible interactions with the surrounding areas. The impact of engineering design such as appropriate use of existing technology and material selection for structural integrity must be assessed. The basis of review includes various codes and standards, prior experience, precedent and engineering knowledge. Vapor cloud generation and plume dispersion is considered a subject beyond our area of expertise.
7. Funding.

FY 76	35K\$
July 1 - December 31, 1975	15K\$
Anticipated Man-years of Effort FY 76	0.5
8. Future Plans. At the present time there are several pending applications, but detailed information is not yet available. It is anticipated that additional facilities will be reviewed as applications are made to the Federal Power Commission.

FPC CONSULTATION - LNG FACILITY REVIEW

Applicant	Location	Type Facility	Storage Facility	Status	
				Site Inspection	Technical Meeting
Distrigas - New York Terminal	Staten Island, NY	Import Terminal	2-900,000 barrel	8/21/73	8/21/73
Distrigas - Everett Marine Terminal	Everett, MA	Import Terminal	1-600,000 barrel 1-374,000 barrel	8/23/73	8/23/73
Algonquin LNG, Inc.	Providence, RI	Import Terminal	1-600,000 barrel	8/24/73	8/24/73
Northern Natural Gas Co.	Carlton, MN	Peak Shaving	1-630,000 barrel 10.8 MMCFD liquefier	10/30/73 7/29/75	10/30/73
Northwest Pipeline Corp.	Plymouth, WA	Peak Shaving	1-348,000 barrel 6.0 MMCFD liquefier	10/31/73 7/31/75	10/31/73
East Tennessee Natural Gas Co.	Kingsport, TN	Peak Shaving	1-348,000 barrel 5.0 MMCFD liquefier	6/24/75	11/29/73
Transco Terminal Co.	Bridgeport, NJ	Import Terminal	3-600,000 barrel	1/23/74	1/23/74
Southern Energy Co.	Savannah, GA	Import Terminal	4-400,000 barrel	1/24/74	2/06/74
Alabama-Tennessee Natural Gas Co.	Greenbrier, AL	Peak Shaving	1-117,000 barrel 2.0 MMCFD liquefier	**	2/05/74
Trunkline LNG, Inc.	Lake Charles, LA	Import Terminal	3-600,000 barrel	2/07/74	5/14/74
Chattanooga Gas Co.	Chattanooga, TN	Peak Shaving	1-348,000 barrel 10.0 MMCFD liquefier	2/28/74	2/28/74
Tennessee Natural Gas Co.	Nashville, TN	Peak Shaving	1-290,000 barrel 5.0 MMCFD liquefier	2/27/74	2/27/74
Northern Natural Gas Co.	Hancock Co., IA	Peak Shaving	1-630,000 barrel 10.8 MMCFD liquefier	*	***
Texas Eastern Transmission Company	Staten Island, NY	Peak Shaving/ Import	*	*	In process
El Paso Alaska Co.	Gravina Pt., Alaska	Export Terminal	9.0 MMCFD liquefier	8/19/74	Pending
Pacific Alaska LNG Co.	Nikiski, Alaska	Export Terminal	4-550,000 barrel	*	Pending
Western LNG Terminal Co.	L. A. Harbor, CA Oxnard, CA	Import Terminal Import Terminal	2-550,000 barrel 2-550,000 barrel	*	Pending
	Pt. Conception, CA	Import Terminal	2-550,000 barrel	12/09/75 12/10/75	In process Pending
Northern States Power Co.	Eau Claire, WI	Peak Shaving	1- 78,000 varrel 2.0 MMCFD liquefier	*	In process
Northwest Pipeline Corp. LNG-II	Plymouth, WA	Peak Shaving	1-522,000 barrel 10.0 MMCFD liquefier	*	In process

* to be determined

** NBS visit not scheduled

*** technical meeting not scheduled.

BIBLIOGRAPHY

NBS reports and publications related to LNG technology.

1. R. D. Goodwin, "Provisional values for the thermodynamic functions of ethane," NBSIR 74-398 (1974).
2. J. F. Ely and G. C. Straty, "Dielectric constants and molar polarizabilities of saturated and compressed fluid nitrogen," J. Chem. Phys. 61, 1480 (1974).
3. G. C. Straty, "Velocity of sound in dense fluid methane," Cryogenics 14, 367 (1974).
4. H. J. M. Hanley, R. D. McCarty and W. M. Haynes, "The viscosity and thermal conductivity coefficients for dense gaseous and liquid argon, krypton, xenon, nitrogen, and oxygen," J. Phys. Chem. Ref. Data 3, 979 (1974).
- 5.* R. D. Goodwin, "Equation of state for thermodynamic properties of fluids," J. Res. NBS 79A, 71 (1975).
- 6.* J. D. Olson, "The refractive index and Lorenz-Lorentz function of fluid methane," J. Chem. Phys. 63, 474 (1975).
- 7.* D. E. Diller, "Thermophysical properties data research on compressed and liquefied gases at the NBS Cryogenics Division," talk prepared for the 1975 Cryogenic Engineering Conference, Kingston, Ontario, Canada.
- 8.* G. C. Straty, "Hypersonic sound velocities in saturated and compressed fluid methane," Cryogenics 15, 727 (1975).
9. H. J. M. Hanley and W. M. Haynes, "The density expansion of the viscosity coefficient," J. Chem. Phys. 63, 358 (1975).
- 10.* H. J. M. Hanley, R. D. McCarty and W. M. Haynes, "Equations for the viscosity and thermal conductivity coefficients of methane," Cryogenics 15, 413 (1975).
11. B. A. Younglove, "The specific heats, C_p and C_v , of compressed and liquefied methane," J. Res. NBS 78A, 401 (1974).
12. J. F. Ely and D. A. McQuarrie, "Calculation of dense fluid transport properties via equilibrium statistical mechanical perturbation theory," J. Chem. Phys. 60, 4105 (1974).
- 13.* W. M. Haynes and M. J. Hiza, "Orthobaric liquid densities of normal butane from 135 to 300 K as determined with a magnetic suspension densimeter," talk prepared for 1975 Cryogenic Engineering Conference, Kingston, Ontario, Canada.
- 14.* G. C. Straty and R. Tsumura, "Phase transition and the melting pressures of solid ethane," J. Chem. Phys. (in press, 1976).
- 15.* G. C. Straty and R. Tsumura, "PVT and vapor pressure measurements on ethane," J. Res. NBS (in press, 1976).
- 16.* L. A. Weber, "Dielectric constant and derived Clausius-Mosotti function data for ethane," Physica (to be published, 1976).

* See attached preprints or reprints in appendices.

17. H. J. M. Hanley and R. O. Watts, "Molecular dynamics of an m-6-8 fluid," *Physica* 79A, 351 (1975).
18. H. J. M. Hanley and R. O. Watts, "Molecular dynamics calculation of the thermodynamic properties of methane," *Aust. J. Phys.* 28, 315 (1975).
19. H. J. M. Hanley and R. O. Watts, "The self diffusion coefficient of liquid methane," *Mol. Phys.* 29, 1907 (1975).
20. J. F. Ely and H. J. M. Hanley, "The statistical mechanics of non-spherical polyatomic molecules," *Mol. Phys.* 30, 565 (1975).
21. Max Klein, F. J. Smith, H. J. M. Hanley, and P. M. Holland, "Tables of collision integrals and second virial coefficients for the m-6-8 potential," NBS-NSRDS Monograph 47 (1974).
22. R. D. McCarty, "Correlation of the equilibrium and transport properties of fluids," *Proc. of Eighth Int. Conf. on Properties of Steam*, Giens, France (1975).
23. W. R. Parrish and M. J. Hiza, "Liquid-vapor equilibria in the nitrogen-methane system between 95 and 120 K," *Advances in Cryogenic Engineering* 19, 300 (Plenum Press, 1974).
- 24.* A. J. Kidnay, R. C. Miller, W. R. Parrish, and M. J. Hiza, "Liquid-vapor phase equilibria in the nitrogen-methane system from 130.0 K to 180.0 K," *Cryogenics* 15, 531 (1975).
25. M. J. Hiza, A. J. Kidnay and R. C. Miller, "Equilibrium properties of fluid mixtures; a bibliography of data on fluids of cryogenic interest," (IFI, Plenum, 1975).
- 26.* W. R. Parrish and M. J. Hiza, "On the consistency of liquid-vapor equilibria data for binary mixtures of methane with the light paraffin hydrocarbons," talk prepared for 1975 Cryogenic Engineering Conference, Kingston, Ontario, Canada.
- 27.* H. I. McHenry, "Fracture mechanics and its application to cryogenic structures," Presented at International Cryogenic Materials Conference, Kingston, Ontario, Canada (August 1975).
- 28.* H. I. McHenry, "Ship steel weldments for low temperature service," Fourth Army Materials Technology Conf., Boston, MA (Sept. 1975).

* See attached preprints or reprints in appendices.

APPENDIX A

Phase transition and melting pressures of solid ethane*

G. C. Straty and R. Tsumura[†]

National Bureau of Standards, Institute for Basic Standards, Cryogenics Division, Boulder, Colorado 80302
(Received 29 September 1975)

The melting pressures of ethane at 14 temperatures from near the triple point to 95.50 K and pressures to 32.0 MPa are reported. A triple point temperature of 90.348 ± 0.005 K is obtained from the data which is in agreement with the determination of Clusius and Weigand (1940) but in substantial disagreement with other determinations. Qualitative evidence has been obtained which indicates the existence of a previously unrecognized solid phase transition along a boundary roughly parallel to the melting line at a temperature about 0.5 K below the melting temperature, suggesting that some previous melting point determinations may have been influenced by a misinterpretation of the effects of this transition.

INTRODUCTION

Although a number of melting point determinations have been reported for ethane,¹⁻⁴ there still exists considerable disagreement on the correct triple-point temperature. Furthermore, no accurate data for the melting pressures above about 4.3 MPa exist. Clusius and Weigand¹ in 1940 reported the measurement of the melting line of ethane to a maximum pressure of 4.27 MPa and obtained a triple-point temperature of 90.35 K. Other determinations of the melting temperature,²⁻⁴ however, yielded values in the vicinity of 89.9 K.

In this paper we report new measurements of the melting pressures of ethane at 14 different temperatures to a maximum pressure of 32.8 MPa at 95.5 K. The data have been represented by a Simon equation which has been used to obtain the triple-point temperature of 90.348 ± 0.005 K in excellent agreement with the earlier data of Clusius and Weigand.¹ Qualitative evidence has been obtained which indicates the existence of a solid-phase transition along a (P , T) boundary roughly parallel to the melting line at a temperature about 0.5 K below the melting temperature, suggesting that some previous determinations of the melting point may have been influenced by a misinterpretation of the effects of this transition.

EXPERIMENTAL PROCEDURES

The ethane used in these experiments was commercially available research grade with minimum purity certified by the supplier at 99.98%. This purity was verified by chromatographic analysis. Temperatures were measured with a platinum resistance thermometer calibrated by the National Bureau of Standards on the IPTS-1968. Pressures were determined by referencing, through differential pressure transducers, to oil pressures derived from a precision oil dead-weight gauge accurate to within the greater of 500 Pa or 0.015%. The apparatus and instrumentation was similar to that used previously in this laboratory⁵ with small modifications to be discussed.

Measurements of the pressure as a function of temperature along the melting line of other fluids such as H_2 , O_2 , F_2 , and CH_4 ⁶⁻⁹ have been performed routinely in this laboratory as part of programs to accurately characterize technically important cryogenic fluids. For such measurements, it has only been necessary to fill the cell with compressed liquid to the maximum

pressure, at a temperature slightly above the freezing temperature corresponding to that pressure, and to then measure the pressure as the temperature is reduced. The slope of the pressure-temperature locus changes dramatically as the liquid begins to freeze indicating that the two-phase condition exists in the cell. Measurements along the freezing line can then be made. The normal temperature gradient along the filling capillary and the small solid fraction in the cell during these measurements have been sufficient to prevent solid from plugging the capillary. Furthermore, upon solidification there is usually a sufficient change in density so that the solid-liquid boundary can be traversed over a considerable pressure range from near the filling pressure to low pressures near the triple point.

Initial attempts to use these procedures for ethane were unsuccessful because of experimental difficulties associated with the somewhat unusual properties of ethane. In attempting to obtain samples in the two-phase region by filling at higher pressures and cooling to the melting line, considerable subcooling was observed before the onset of freezing. When freezing began, a solid plug would apparently form in the filling capillary, isolating the pressure measurement system from the cell. To remedy this, the capillary was brought into the cell through a reentrant cavity machined into the stainless steel cell closure and was provided with a heater. In this configuration, a considerable temperature difference could be maintained between the massive copper cell body and the filling capillary.

Several attempts were made to obtain data with this modification. The samples were prepared by filling at moderate pressure, cooling to well below the expected triple point to ensure solidification and then taking data while warming. Data obtained in this way clustered about a line as indicated by • in Fig. 1. These data suggested a triple point temperature of about 89.9 K, consistent with some earlier determinations,²⁻⁴ and were initially interpreted incorrectly as representing the melting line. Attempts to make measurements above about 4 MPa by warming were found to be impossible, however, since this pressure corresponds to the vapor pressure of ethane at the ambient laboratory temperature and when this pressure was exceeded, considerable mass transfer out of the cell was associated with the condensation of liquid into the external portions

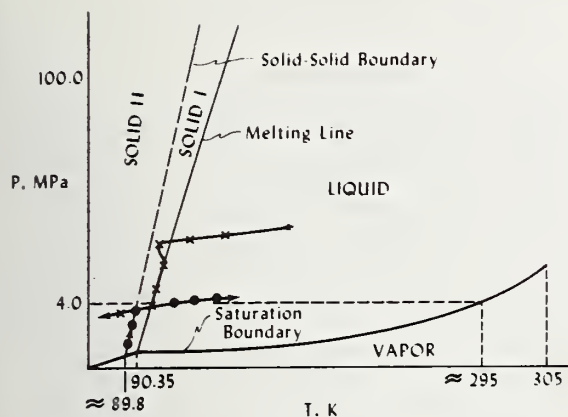


FIG. 1. Schematic phase diagram in the PT plane for ethane. The solid-solid boundary above 100.0 MPa was observed by Webster and Hoch (Ref. 11). The solid-solid boundary below 4.0 MPa from this work. Path of typical data before apparatus modifications: ● data obtained by warming, X data obtained by cooling. For a more complete explanation, see text.

of the system. Attempts to obtain data by cooling from high pressure and temperature were also unsatisfactory since the data then clustered about a second curve indicated in Fig. 1 by X. In either case, it was impossible to cross the pressure of about 4.0 MPa because of the mass transfer problem. Both sets of measurements were also unsatisfactory because of large scatter and lack of adequate reproducibility. The indications of what appeared to be segments of two separate melting curves were also difficult to explain at first.

The behavior was, however, understood upon closer examination. For measurements below the pressure of 4.0 MPa, almost all of the ethane in the system resided in the cell, resulting in a sample almost entirely in the solid phase. Heat applied to the capillary was sufficient to ensure that pressure communication with the cell was always maintained, and the data obtained were, in fact, a manifestation of a solid transition along a boundary (● Fig. 1) roughly parallel to the true melting curve but about 0.5 K lower. The higher pres-

sure line (X, Fig. 1) traversed a portion of the true melting line. The lack of reproducibility and large scatter were found to be associated with large cell temperature gradients imposed by an unnecessarily high power input to the capillary heater.

To verify this interpretation of the results, additional modification to the apparatus was made. The cell volume was increased to over 50 cm³ while the volume of the external portions of the system were minimized to less than 1 cm³. In addition, these external portions were heated to about 330 K, well above the ethane critical temperatures of 305 K.

With these modifications it was then found possible to fill the cell with liquid at the highest pressure of interest, to cool sufficiently to initiate solidification, and to then traverse the melting line in either direction without encountering the difficulty at 4 MPa as found previously. Under these conditions, the solid fraction in the cell was always small. The heat input to the capillary necessary to prevent plugging was also found to be very small or zero, consistent with the experience with other fluids. Data were highly reproducible with minimum scatter, and were found to coincide roughly with the high pressure portion of the curve observed previously and its extension to lower pressures.

THE MELTING LINE

The results of the melting line measurements were fitted to the Simon melting pressure equation,

$$P = P_t + P_0 \left[\left(T/T_t \right)^\epsilon - 1 \right], \quad (1)$$

where the subscript t refers to the triple point, and P and T are the pressure and temperature. The value of $P_t = 1.2$ Pa was taken from a vapor pressure correlation for ethane by Goodwin¹⁰ at the triple point temperature of 90.35 K. The parameters yielding the best fit were the following:

$$P_t = 1.2 \text{ Pa (Ref. 10)},$$

$$P_0 = 255.97 \text{ MPa},$$

$$T_t = 90.348 \text{ K},$$

$$\epsilon = 2.179.$$

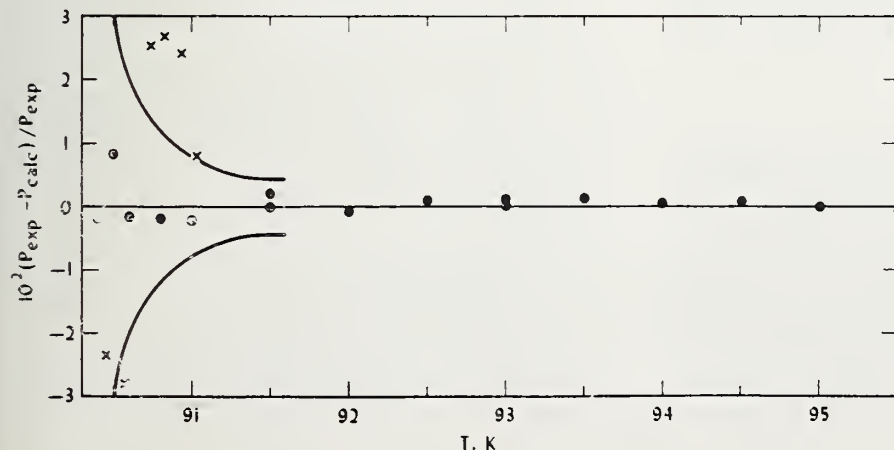


FIG. 2. Deviations of experimental melting pressures from the Simon equation, ●, this work, X, Ref. 1. The solid line corresponds to the range of pressure resulting from a difference of ± 0.005 K in temperature.

TABLE 1. Ethane melting pressures and deviations from Eq. (1).

T (K)	P (MPa)	$\frac{P_{\text{exp}} - P_{\text{calc}}}{P_{\text{exp}}} \times 10^2$
90.40	0.3231	-0.189
90.45 ^a	0.6181	-2.345
90.50	0.9496	+0.810
90.57 ^a	1.338	-2.804
90.60	1.558	-0.182
90.64 ^a	1.895	3.549
90.74 ^a	2.493	2.551
90.80	2.795	-0.219
90.83 ^a	3.070	2.690
90.93 ^a	3.698	2.411
91.00	4.035	-0.247
91.03 ^a	4.266	0.801
91.50	7.182	0.196
91.50	7.145	-0.317
92.00	10.30	-0.095
92.50	13.49	0.081
93.00	16.66	0.008
93.00	16.67	0.091
93.50	19.89	0.117
94.00	23.09	0.024
94.50	26.35	0.064
95.00	29.59	-0.026
95.50	32.85	-0.107

^aReference 1.

The experimental results and their deviations from the equation are given in Table I. These deviations are plotted in Fig. 2 along with the data of Clusius and Weigand¹ for comparison. The derived triple point temperature of 90.348 ± 0.005 K is in excellent agreement with 90.35 ± 0.03 K obtained by Clusius and Weigand.¹

It is interesting to note that experiments performed by completely freezing a solid sample and then warming through the melting transition resulted in values for the triple point of about 89.9 K^{2-4} while those of Clusius and Weigand,¹ made by cooling the liquid until freezing, resulted in a higher melting temperature. This suggests that the measurements performed by warming the solid from low temperature may have been misinterpreted and that the effect of the solid transition has been responsible for obtaining such low melting points. This would, of course, be the situation for specific heat type experiments if the heat of transition was incorrectly interpreted as a large pre-melting effect or as the heat of fusion.

SOLID-SOLID TRANSITION

When measurements were made with a small solid fraction in the cell and with very low heater power to the capillary, as was necessary for the melting line measurements, it was, of course, impossible to observe the solid transition due to the unavoidable plugging of the capillary. However, if the cell were filled to a large solid fraction, and by using fairly large heater power to the capillary, pressure communication with the cell could be maintained and the solid transition could be detected. The necessary large gradients imposed on the cell, however, introduces considerable

uncertainty in the temperature determinations and the observations can only be considered qualitative.

An additional check on the existence of the solid transition was made by observing the temperature as a function of time as the cell, filled with solid, was slowly warmed. A number of runs using various constant input powers to the cell were made and in each case distinct changes in the warming rate were observed at about 89.8 K associated with the solid transformation and at about 90.3 K corresponding to melting. Based on these qualitative results, it appears that the solid-solid boundary is roughly parallel to the melting line at a temperature about 0.5 K lower. This is not inconsistent with the measurements of Webster and Hoch¹¹ who detected a definite solid transformation above about 100.0 MPa. Experimental difficulties prevented them from making measurements below 100.0 MPa but from their data and from certain theoretical considerations, they predicted a solid-solid-liquid triple point for ethane at lower pressure. No evidence for such a triple point below our maximum pressure of 32.8 MPa was observed in this work, and the solid-solid boundary, in fact, appears to continue to low pressure.

Note: After the completion of this work, we learned of some visual observations and dilatometric measurements on solid ethane by Professor D. Eggers¹² who confirms the existence of a plastic-crystalline phase in a temperature range extending to about 0.45 K below the melting temperature. He has found this isotropic phase to be thermodynamically stable and not a metastable phase formed only under certain special conditions.¹³ We thank Dr. Eggers for discussing his work with us prior to publication.

*This work was carried out at the National Bureau of Standards under the sponsorship of the American Gas Association, Inc.
[†]Consejo Nacional De Ciencia Y Tecnologia (CONACYT) Mexico City. Currently a guest worker with the Cryogenics Division, National Bureau of Standards, Institute for Basic Standards.

¹K. Clusius and K. Weigand, Z. Phys. Chem. B 46, 1 (1940).

²R. Wiebe, K. H. Hubbard, and M. J. Brevoort, J. Am. Chem. Soc. 52, 611 (1930).

³R. K. Witt and J. D. Kemp, J. Am. Chem. Soc. 59, 273 (1937).

⁴L. J. Burnett and B. H. Muller, J. Chem. Eng. Data 15, 154 (1970).

⁵See for example G. C. Straty, and R. Prydz, Rev. Sci. Instrum. 41, 1223 (1970).

⁶R. D. Goodwin, J. Res. Nat. Bur. Stand. C 65, 231 (1961).

⁷L. A. Weber, J. Res. Nat. Bur. Stand. A 74, 1 (1970).

⁸R. Prydz and G. C. Straty, Nat. Bur. Stand. (U.S.) Tech. Note 392 (Revised 1973).

⁹R. D. Goodwin, Nat. Bur. Stand. (U.S.) Tech. Note 653 (1974).

¹⁰R. D. Goodwin, Natl. Bur. Stand. (U.S.) Interim Report, NBSIR 74-398 (1974).

¹¹D. S. Webster and M. J. R. Hoch, J. Phys. Chem Solids 32, 2663 (1971).

¹²D. F. Eggers, Jr., J. Phys. Chem. 79, 2116 (1975).

¹³For an example of metastable behavior, see for example, W. F. Glauque and J. B. Ott, J. Am. Chem. Soc. 82, 2689 (1960).

APPENDIX B

PVT AND VAPOR PRESSURE MEASUREMENTS ON ETHANE[†]

G. C. Straty and R. Tsumura*

Cryogenics Division
National Bureau of Standards
Institute for Basic Standards
Boulder, Colorado 80302

Abstract

New measurements of the vapor pressures and PVT properties of ethane are reported. PVT determinations have been made from near the triple point to 320 K at pressures to 33 MPa. The density range investigated extends to more than three times the critical density. The new measurements of the vapor pressures of ethane extend from 160 K to near the critical point.

[†]This work was carried out at the National Bureau of Standards under the sponsorship of the American Gas Association, Inc.; and it is not subject to copyright.

*Consejo Nacional De Ciencia Y Tecnologia (CONACYT) Mexico City. Currently a guest worker with the Cryogenics Division, National Bureau of Standards, Institute for Basic Standards.

G. C. Straty and R. Tsumura

Introduction

Liquefied fuel gases, such as LNG, are expected to play an increasing role in satisfying future energy requirements. Accurate thermophysical properties data for these liquefied gas mixtures are necessary for the design of liquefaction plants, transport equipment, shipping and receiving terminals, and for custody transfer. The near infinite variations in mixture compositions encountered with these fuel gases rule out completely experimental or strictly computational approaches for determining these properties. Calculation methods, based on accurate, wide range pure component data and selected mixtures data are being developed in a number of laboratories, and appear to offer the only reliable and economical approach for the generation of the necessary thermophysical properties.

This paper reports new measurements of vapor pressures and PVT properties of pure ethane. The measurements have been made as part of a comprehensive program to provide the required experimental data and to develop suitable calculation techniques for mixture properties determinations. PVT measurements have been made from near the triple point (90.348 K) [1] to 320 K at pressures up to 33 MPa. The density range extends to more than three times the critical density. The new measurements of the vapor pressures extend from 160 K to near the critical temperature (305 K).

Experimental

To measure single-phase densities, the gas expansion technique was used. A series of pressure-temperature observations are made on a nearly constant density sample of fluid confined in a cell of accurately calibrated volume. When either the maximum pressure or maximum temperature is reached, the fluid is expanded, to low pressure, into large calibrated volumes maintained at an accurately known temperature above room temperature. The density can then be determined from the cell volume and the compressibility factor (PV/RT) of the ethane at the conditions of the expansion volumes.

The ethane used was commercially available research grade with specified minimum purity of 99.98%. This purity was verified by chromatographic analysis. Temperatures were measured on the IPTS (1968) with a platinum resistance thermometer calibrated by the National Bureau of Standards. Pressures above about 3 MPa were measured by referencing to oil pressures derived from an oil dead weight gage accurate to within 0.015%. Lower pressures were measured with a precision fused quartz bourdon tube gauge which had been previously calibrated against an air dead weight gauge accurate to within 0.01%. The apparatus and procedures were similar to those used previously in this laboratory for measurements on several other cryogenic fluids [2-5] and have been described in detail [6-8]. Slight modification to existing apparatus was necessary because of the higher critical temperature of ethane. Those external parts of the system, which contained fluid during a measurement, were heated to well above the critical temperature (typically 330 K) in order to reduce the relatively density of the fluid residing in these parts, permitting a more accurate adjusted density to be computed.

Results

With the techniques used here, each experimental PVT "run" consists of a number of pressure-temperature observations lying along a near-isochoric path. About 50 such runs were made covering a density range of from about 1.5 to over 21.5 mol/l. Each run consisted of from 5 to 16 PVT points, depending on the density. Measurements were always made at fixed temperatures to permit direct analysis in terms of isotherms. A total of over 450 PVT data points was determined. These data are tabulated along isotherms in Table 1.

Although comparison with data from other sources is, in general, impossible without multiple interpolations, the agreement has been deduced by examining the density deviations of the various data sets [9,10] from densities calculated from an equation of state for ethane due to Goodwin [11]. The agreement is found to be, in general, within the combined experimental error. Maximum differences occur in the critical region where the equation of state representation is expected to be less satisfactory and where the experimental densities are subject to increasing uncertainty. Estimated uncertainty in the experimental densities in this work is typically $\pm 0.1\%$ at the lowest temperatures, increasing to $\pm 0.2\%$ at higher temperatures and lower densities, becoming as much as $\pm 1.0\%$ in the critical region.

New vapor pressure measurements also have been made at 5 K intervals from 160 to 300 K and are given in Table 2. At each temperature, the pressure was measured at least twice with some ethane being removed from the cell between measurements. Identical pressure observations indicated that the two-phase condition existed in the cell.

A vapor pressure equation of the form

$$\ln (P/P_t) = A\chi + B\chi^2 + C\chi^3 + D\chi^4 + E\chi(1-\chi)^{3/2} \quad (1)$$

was fit to all available data for ethane [12]. Here, $\chi = (1-T_t/T)/(1-T_t/T_c)$, P and T are the pressure and temperature and t and c refer to the triple and critical points. Coefficients giving the best fit were found to be the following:

$$A = 10.67324$$

$$B = 8.33782$$

$$C = -3.08489$$

$$D = -0.65857$$

$$E = 6.04955$$

$$P_t = 1.14 \times 10^{-5} \text{ bar}$$

$$T_t = 90.348 \text{ K [Ref 1]}$$

$$T_c = 305.330 \text{ K [Ref 10]}$$

Deviations of the experimental vapor pressures from those calculated from this equation for the various data sets [9, 10, 13] are shown in Fig. 1.

Summary

We have made new wide-range measurements of the vapor pressures and PVT properties of ethane. These are the only data currently available which cover the entire temperature range from the triple point to 320 K. In addition, these data are the only accurate PVT data available for the compressed liquid below about 190 K. The data are being used along with other available data to refine the calculation of thermodynamic functions for ethane and as input to, and as a check upon, new calculation methods for predicting liquefied natural (fuel) gas properties being studied in this and other laboratories.

References

1. G. C. Straty and R. Tsumura, J. Chem. Phys., to be published.
2. L. A. Weber, J. Res. Nat. Bur. Stand. 74A, 93 (1970).
3. R. Prydz and G. C. Straty, NBS Tech. Note 392 (Revised, 1973).
4. R. D. Goodwin, NBS Tech. Note 653 (1974).
5. L. A. Weber, NASA SP-3088/NBSIR 74-374 (1975).
6. R. D. Goodwin. J. Res. Nat. Bur. Stand. 65C, 231 (1961).
7. G. C. Straty and R. Prydz, Rev. Sci. Inst. 41, 1223 (1970).
8. R. D. Goodwin and R. Prydz, J. Res. NBS 76A, 81 (1972).
9. G. A. Pope (also reports vapor pressure and PVT data of A. K. Pal).
Ph.D. Thesis, Dept. of Chemical Engineering, Rice University,
Houston, Texas (July 1971).
10. D. R. Douslin and R. H. Harrison, J. Chem. Thermo 5, 491 (1973).
11. R. D. Goodwin, NBS IR 74-398 (1974). Goodwin has used a non-analytic equation of state to correlate previously available data on ethane and to calculate provisional thermodynamic functions. Experimental data from this work are being used to fill in gaps in previously published data and to refine the equation of state to permit more accurate calculations of thermodynamic properties to be made. We defer extensive comparisons between data sets and a more elaborate analysis for inclusion in a final report in preparation.
12. Further refinements in the correlation are expected which will probably alter slightly the final values of the constants. The deviation plot, however, is representative of the agreement among data sets. Coefficients for this equation will be included in the final report. See also reference 8.

13. W. T. Ziegler, B. S. Kirk, J. C. Mullins and A. R. Berquest,
Tech. Rept. No. 2, Project A-764, Eng. Expt. Sta. Georgia
Inst. Tech.; Atlanta, Georgia, December 1964.

Table 1

P (MPa)	ρ (mol/l)	P (MPa)	ρ (mol/l)
T= 92.00 K		6.4514	21.125
.7928	21.629	12.4806	21.193
T= 93.00 K		29.0045	21.412
8.7870	21.682	T=110.00 K	
T= 94.00 K		4.7101	21.034
3.5870	21.599	16.4766	21.176
10.4980	21.664	33.5810	21.403
T= 96.00 K		T=112.00 K	
6.3091	21.555	1.19	20.911
14.6217	21.641	6.84	20.990
T= 98.00 K		11.2851	21.041
8.1853	21.503	20.6898	21.163
19.1732	21.625	T=114.00 K	
T=100.00 K		3.8739	20.882
1.7991	21.348	8.8149	20.942
11.3755	21.468	24.9715	21.152
23.8694	21.613	T=116.00 K	
T=102.00 K		1.9636	20.776
4.7964	21.315	6.3156	20.841
15.4890	21.448	12.0035	20.913
28.5382	21.603	19.0660	21.009
T=104.00 K		29.2820	21.143
1.1828	21.198	T=118.00 K	
6.9564	21.269	8.0478	20.791
19.9098	21.434	15.7492	20.896
33.1959	21.594	23.2017	20.997
T=106.00 K		T=120.00 K	
9.0567	21.221	1.2747	20.621
24.4329	21.422	6.8130	20.702
T=108.00 K		10.8020	20.757
1.8227	21.065	19.6919	20.883
		27.3594	20.988
		T=122.00 K	
		3.8664	20.592
		14.2998	20.737
		23.7193	20.873

Table 1 (cont'd)

P (MPa)*	ρ (mol/l)	P (MPa)	ρ (mol/l)
31.5310	20.979	T=138.00 K	
T=124.00 K		3.7831	20.008
6.2436	20.553	12.1243	20.144
11.6827	20.627	28.2309	20.407
18.0492	20.724	T=140.00 K	
27.7606	20.863	6.0574	19.972
T=126.00 K		15.3375	20.129
7.9236	20.505	31.9091	20.400
21.9553	20.712	T=142.00 K	
31.8410	20.855	7.6559	19.926
T=128.00 K		18.7024	20.117
.6715	20.312	35.5822	20.392
10.4787	20.470	T=144.00 K	
18.8911	20.597	.9387	19.722
25.8617	20.703	9.8460	19.890
35.9026	20.847	22.1094	20.107
T=130.00 K		T=148.00 K	
2.9285	20.287	5.4489	19.667
13.7499	20.450	15.7717	19.856
29.7809	20.694	28.9678	20.091
T=132.00 K		T=152.00 K	
5.4980	20.254	1.2079	19.424
17.2765	20.436	8.9240	19.584
26.4639	20.577	22.1746	19.836
33.6963	20.687	35.8308	20.077
T=134.00 K		T=156.00 K	
7.2368	20.209	5.5978	19.369
20.8906	20.425	14.2846	19.545
T=136.00 K		28.6589	19.820
1.3689	20.030	T=160.00 K	
9.2490	20.167	.4675	19.091
24.5518	20.416	8.9636	19.288
34.0682	20.561	20.2324	19.524
		35.1468	19.806

Table 1 (cont'd)

P (MPa)	ρ (mol/l)	P (MPa)	ρ (mol/l)
T=164.00 K		11.9718	18.323
4.2580	19.043	17.2059	18.463
14.0474	19.250	23.3273	18.620
26.2885	19.508	32.8340	18.850
T=168.00 K		T=192.00 K	
1.7297	18.817	.9865	17.815
7.6437	18.969	5.5964	17.977
19.6507	19.230	10.6669	18.128
32.3436	19.495	16.5186	18.302
T=172.00 K		22.0330	18.447
1.2449	18.650	28.3464	18.607
5.7607	18.768	T=196.00 K	
11.8776	18.916	.4943	17.619
25.3400	19.214	4.4533	17.775
38.3722	19.482	8.4330	17.903
T=176.00 K		14.9662	18.104
1.1073	18.488	21.1586	18.286
5.2091	18.602	26.8669	18.434
8.8759	18.691	33.3677	18.595
16.9907	18.892	T=200.00 K	
31.0365	19.201	.6801	17.445
T=180.00 K		3.5738	17.581
.5247	18.295	7.3933	17.709
4.9583	18.442	12.2367	17.866
8.2782	18.525	19.4175	18.087
13.3001	18.655	25.8517	18.273
22.2633	18.876	31.6945	18.423
36.7092	19.189	T=204.00 K	
T=184.00 K		3.7760	17.411
3.9725	18.253	6.7420	17.524
7.9795	18.368	10.6983	17.658
12.4806	18.483	16.4076	17.846
18.2646	18.635	23.9051	18.074
27.5482	18.862	30.2305	18.262
T=188.00 K		36.4896	18.412
1.9817	18.021	T=208.00 K	
7.2058	18.186	.5897	17.079
		6.8033	17.354
		9.6616	17.461
		14.6253	17.634

Table 1 (cont'd)

P (MPa)	ρ (mol/l)	P (MPa)	ρ (mol/l)
20.6552	17.831	T=232.00 K	
28.3791	18.062	1.2667	15.950
35.0871	18.251	4.5825	16.167
T=212.00 K		9.4583	16.428
3.4269	17.048	13.6904	16.633
9.6570	17.293	19.2025	16.874
13.3583	17.434	28.2402	17.215
18.6673	17.619	32.7523	17.372
24.9088	17.819	T=236.00 K	
32.8419	18.051	3.8508	15.920
T=216.00 K		7.0049	16.114
2.1043	16.798	12.4747	16.403
6.4050	16.998	16.9765	16.618
13.2349	17.267	22.6904	16.862
17.2225	17.417	31.9811	17.205
22.7370	17.606	T=240.00 K	
29.1542	17.808	1.2548	15.515
T=220.00 K		2.2021	15.586
1.4301	16.567	6.3368	15.877
5.1249	16.761	9.4209	16.062
8.9985	16.934	15.5972	16.387
16.9669	17.250	20.2787	16.606
21.1113	17.404	26.1772	16.852
26.8053	17.594	35.7046	17.196
33.3471	17.798	T=244.00 K	
T=224.00 K		3.6366	15.487
4.3322	16.536	4.6703	15.556
7.6124	16.699	8.5355	15.817
12.2714	16.904	12.2246	16.039
20.7255	17.237	18.7424	16.375
25.0127	17.392	23.5869	16.595
30.8565	17.584	29.6476	16.842
T=228.00 K		T=248.00 K	
1.8552	16.198	1.7380	15.078
6.9228	16.483	5.9925	15.449
10.4762	16.654	6.8908	15.508
15.7164	16.887	11.1353	15.788
24.4895	17.225	15.1129	16.023
28.8946	17.382	21.8905	16.364
34.8859	17.574	26.8798	16.586
		33.1044	16.833

Table 1 (cont'd)

P (MPa)	ρ (mol/l)	P (MPa)	ρ (mol/l)
T=252.00 K		9.6680	14.669
1.5930	14.811	12.5033	14.914
3.9746	15.056	17.8943	15.316
8.0325	15.392	19.2306	15.395
9.0553	15.457	24.9268	15.728
13.8649	15.771	29.6684	15.973
18.0296	16.011	T=272.00 K	
25.0394	16.354	2.0844	1.243
30.1617	16.577	3.6257	13.670
T=256.00 K		4.8506	13.859
3.7062	14.790	6.0679	14.032
6.1397	15.018	8.2942	14.302
10.3740	15.358	11.8077	14.650
11.5324	15.433	14.8065	14.901
16.6249	15.758	20.4232	15.306
20.9491	16.000	21.8042	15.385
28.1716	16.345	27.6780	15.719
33.4255	16.568	32.5542	15.964
T=260.00 K		T=276.00 K	
2.6858	14.414	2.1376	1.242
5.7990	14.757	3.2684	13.256
8.0637	14.963	5.3267	13.644
12.8526	15.340	6.5457	13.824
14.0783	15.417	7.7197	13.983
19.3947	15.747	10.2212	14.275
23.8662	15.990	13.9836	14.636
31.2936	16.336	17.1196	14.890
T=264.00 K		22.9462	15.297
2.4038	14.085	24.3837	15.377
4.6766	14.389	30.4166	15.711
7.6561	14.705	35.4306	15.957
10.2294	14.931	T=280.00 K	
15.3689	15.327	2.1904	1.241
16.6466	15.405	2.9758	12.787
22.1619	15.737	4.8428	13.234
26.7721	15.981	6.9195	13.604
34.3986	16.328	8.1526	13.778
T=268.00 K		9.4890	13.951
3.0548	13.884	12.2137	14.259
4.2654	14.062	16.1653	14.625
6.5471	14.352	19.4376	14.880
		25.4635	15.288
		26.9473	15.368
		33.1520	15.703

Table 1 (cont'd)

P (MPa)	ρ (mol/l)	P (MPa)	ρ (mol/l)
T=284.00 K		3.8806	2.880
2.2428	1.240	4.3963	11.212
4.3982	12.768	4.8686	11.505
6.3596	13.203	6.4389	12.146
8.4885	13.563	8.4817	12.672
9.8840	13.751	10.8697	13.115
11.3395	13.933	13.6040	13.514
14.2261	14.247	15.2773	13.713
18.3557	14.615	16.9735	13.900
21.7505	14.872	20.2846	14.219
27.9731	15.280	24.8761	14.591
29.4971	15.360	28.6475	14.848
35.8724	15.696	35.4484	15.258
T=288.00 K		T=300.00 K	
2.2951	1.239	2.4492	1.237
3.0547	1.955	4.0309	2.875
3.9706	12.194	4.6932	10.611
5.8026	12.745	5.3970	11.196
7.7971	13.160	5.9485	11.485
10.1657	13.540	7.6275	12.109
11.6682	13.735	9.8845	12.652
13.2063	13.920	12.4490	13.102
16.2439	14.237	12.4489	13.102
20.5477	14.607	15.3377	13.504
24.0580	14.863	17.0906	13.704
30.4719	15.273	18.8621	13.892
32.0446	15.353	22.3018	14.211
T=292.00 K		27.0931	14.583
2.3466	1.239	30.9501	14.841
3.8113	11.522	T=304.00 K	
5.2158	12.173	2.4997	1.237
7.1396	12.707	3.4158	1.950
9.3105	13.131	4.1784	2.873
11.8771	13.525	4.6828	4.325
13.4688	13.723	4.7721	9.097
15.0863	13.910	4.9674	9.788
18.2640	14.228	5.3930	10.298
22.7394	14.598	5.5668	10.596
26.3645	14.855	6.3948	11.173
32.9673	15.265	6.9986	11.455
T=296.00 K		8.8474	12.082
2.3987	1.238	11.3086	12.638
3.2373	1.952	14.0362	13.092
		17.0942	13.495
		18.9013	13.696
		20.7454	13.884

Table 1 (cont'd)

P (MPa)	ρ (mol/l)	P (MPa)	ρ (mol/l)
24.3137	14.204	22.5240	13.681
29.2629	14.576	24.5119	13.869
33.2309	14.833	28.3286	14.189
		33.5824	14.562
T=306.00 K		T=316.00 K	
4.8094	4.323	2.6491	1.235
4.9441	6.533	4.6083	2.866
5.0757	9.092	5.4200	4.312
5.8014	10.290	5.9358	6.513
		6.6610	9.054
		7.1729	9.732
		7.8532	10.229
		8.1986	10.522
		9.3878	11.099
		10.1982	11.390
		12.6240	12.044
		18.8045	13.068
		22.3004	13.472
		24.3313	13.673
		26.3890	13.862
		30.3236	14.183
		T=320.00 K	
		2.6983	1.234
		3.7629	1.945
		4.7483	2.864
		5.6574	4.307
		6.3309	6.503
		7.3064	9.032
		7.9172	9.710
		8.6869	10.211
		9.0937	10.506
		10.4137	11.087
		11.2486	11.380
		13.9007	12.036
		17.0663	12.602
		20.4014	13.060
		24.0318	13.466
		26.1304	13.667
		28.2588	13.855
		32.3174	14.176
T=312.00 K			
2.5996	1.235		
3.5908	1.947		
4.4668	2.869		
5.1793	4.316		
5.5401	6.522		
6.0206	9.072		
6.4330	9.756		
7.0307	10.254		
7.3179	10.546		
8.3744	11.116		
9.1114	11.404		
11.3574	12.054		
14.1819	12.618		
17.2177	13.075		
20.5666	13.480		

Table 2

T (K)	P kPa	T (K)	P kPa
160.00	21.502	230.00	700.48
165.00	30.670	235.00	825.96
170.00	42.870	240.00	966.60
175.00	58.636	245.00	1124.4
180.00	78.734	245.00	1124.8
180.00	78.706	250.00	1300.0
185.00	103.84	250.00	1301.9
190.00	134.63	250.00	1302.1
190.00	134.72	250.00	1301.8
195.00	172.21	255.00	1495.0
195.00	172.26	260.00	1710.3
200.00	217.26	265.00	1947.9
200.00	217.32	270.00	2208.0
205.00	270.93	275.00	2493.1
205.00	271.00	275.00	2493.2
210.00	334.13	280.00	2804.6
210.00	334.17	280.00	2806.2
210.00	333.98	285.00	3144.3
210.00	333.99	290.00	3513.5
215.00	407.34	298.15	4190.9
220.00	492.16	298.15	4188.9
225.00	589.73	300.00	4353.5

APPENDIX C

Brillouin scattering techniques have been used to measure the velocity of hypersonic waves in gaseous and liquid methane. Measurements were made on the saturated liquid and vapour and along selected isotherms to a maximum pressure of about 17.5 MPa. The data, which agree well with previously measured ultrasonic velocities, have been combined with PVT data to obtain the isentropic compressibility and the ratio of specific heats.

Hypersonic velocities in saturated and compressed fluid methane

G. C. Straty

Sound velocity measurements, when combined with *PVT* data, offer a convenient way of determining certain thermodynamic quantities as well as providing a sensitive check on the equation of state and its derivatives. In a recent paper¹ we reported new measurements of the ultrasonic sound velocities in dense fluid methane. These ultrasonic measurements were limited to densities greater than about 10–14 mol l⁻¹ due to a large sound attenuation at lower densities.

In this paper we report the results of hypersonic sound velocity measurements using Brillouin scattering techniques. Measurements were made along three supercritical isotherms and on the saturated liquid and vapour to densities as low as 1 mole l⁻¹. The data have been combined with the previously measured *PVT* data² to obtain the isentropic compressibility K_s , and the ratio of the specific heats $\gamma = C_p/C_v$, using the well-known thermodynamic relation

$$W^2 = (\rho K_s)^{-1} = \gamma \left(\frac{\partial P}{\partial \rho} \right)_T$$

where W , ρ , P , and T are the sound velocity, density, pressure, and temperature, respectively.

Experimental details

The sample of high purity (99.99%) methane was placed in a high pressure cell and was illuminated with an argon-ion laser operating in a single mode at 488.0 nm with an output power of typically 20–50 mW. The frequency shifts $\Delta\nu$ of the Brillouin components at a scattering angle of 90° were determined using a pressure scanned Fabry-Perot interferometer with a finesse of about 20, as determined from the apparent width of the naturally very narrow central Rayleigh line. Interferometer spacers were chosen which avoided corrections for shrinkage effects due to neighbouring components. The light was detected with an S-20 photomultiplier and recorded on a chart recorder.

Uncertainty in the measured frequency shifts and derived sound velocities is about 0.5% as estimated from the standard deviation of replicate measurements. This uncertainty is due largely to frequency drifts of the laser and to small

thermal effects on the interferometer. The scattering angle was determined by triangulation over distances of a few metres and is not considered a significant source of error.

Temperatures were measured with a platinum resistance thermometer calibrated by the National Bureau of Standards on the IPTS 1968. Pressures were determined to within 0.02 MPa using a temperature compensated bourdon tube gauge. This gauge had been previously calibrated against a high precision commercial dead weight gauge whose uncertainty is estimated to be whichever is greater, 200 Pa or 0.015%. The experimental arrangement is similar to that used by Fleury and Boon³ for argon and neon; however, chopping the beam and phase sensitive detection of the photomultiplier output was found to be unnecessary.

Results and discussion

The Brillouin scattering data and the derived sound velocities, along with the density and derived values of isentropic compressibility and the specific heat ratio, are tabulated for the saturated fluid in Table 1 and for the compressed fluid along isotherms in Table 2. Some previously measured ultrasonic velocities¹ for the saturated liquid and for the compressed gas in the regions of overlap are also included for comparison. The velocity data are plotted as a function of density in Fig. 1 together with the ultrasonic data, which are included for completeness.

Densities and the derivatives necessary for the calculations were obtained from pressure and temperature observations and the *PVT* data and equation of state of Goodwin.² The hypersonic velocities V were determined from the observed Brillouin frequency shift $\Delta\nu$ in the usual way, using the equation

$$\Delta\nu = \frac{2nV}{\lambda} \sin \frac{\theta}{2}$$

where n is the index of refraction for the wavelength, λ of the incident radiation, and θ is the scattering angle. The index of refraction was calculated at a given density using data for the Lorentz-Lorenz function

$$R = \frac{n^2 - 1}{n^2 + 2} \frac{1}{\rho}$$

The author is with the Cryogenics Division, Institute for Basic Standards, National Bureau of Standards, Boulder, Colorado 80302, USA. Received 13 June 1975.

Table 1. Brillouin scattering data, velocity of sound W , and derived values of isentropic compressibility K_s and specific heat ratio γ of saturated vapour and liquid methane at temperature T and density ρ

T , K	$\Delta\nu$, MHz	Angle, degrees	Ref index	Density, mol l^{-1}	This work	W , m s^{-1} Ultrasonic (Ref 1)	K_s , $(\text{GPa})^{-1}$	γ
184.0	786.3	90.22	1.04800	4.751	258.4		197.1	5.052
170.0	821.2	90.22	1.02449	2.437	276.1		335.5	2.280
150.0	834.8	90.22	1.01020	1.019	284.7		756.0	1.630
170.0	2283.8	90.22	1.20153	19.356	654.7	657.7	7.528	2.675
160.0	2812.6	90.22	1.21895	20.971	794.7	795.5	4.717	2.290
112.0	4939.5	90.22	1.27698	26.310	1332.4	1334.1	1.338	1.655

Table 2. Brillouin scattering data, velocity of sound W , and derived values of isentropic compressibility K_s and specific heat ratio γ in compressed fluid methane at temperature T , pressure P , and density ρ

MPa	$\Delta\nu$, MHz	Angle, degrees	Ref index	Density, mol l^{-1}	This work	W , m s^{-1} Ultrasonic (Ref 1)	K_s , $(\text{GPa})^{-1}$	γ
$T = 300.0 \text{ K}$								
17.59	1602.0	90.22	1.08756	8.596	507.4		28.24	1.961
12.57	1428.2	90.22	1.06132	6.047	463.5		48.11	1.823
7.80	1339.9	90.22	1.03585	3.551	445.6		80.65	1.610
2.46	1312.3	90.22	1.01031	1.029	447.7		302.9	1.401
$T = 240.0 \text{ K}$								
14.47	1569.5	90.10	1.12541	12.20	480.8	480.5	22.15	2.683
12.54	1394.7	90.22	1.10907	10.63	433.1		31.34	2.729
12.50	1387.6	90.10	1.10868	10.60	431.5		31.68	2.720
10.18	1219.4	90.22	1.08361	8.226	387.6		50.58	2.688
9.778	1194.0	90.10	1.07890	7.772	381.6		55.24	2.621
8.106	1140.5	90.22	1.06001	5.940	370.6		76.62	2.311
7.640	1126.8	90.10	1.05511	5.459	368.2		84.44	2.199
6.232	1115.9	90.22	1.04156	4.126	369.0		111.2	1.926
5.451	1116.2	90.10	1.03487	3.465	371.9		130.4	1.804
3.530	1126.6	90.22	1.02051	2.045	380.3		211.3	1.561
3.415	1124.6	90.10	1.01973	1.968	380.3		219.6	1.545
2.118	1144.0	90.22	1.01154	1.153	389.7		357.0	1.445
1.824	1151.8	90.10	1.00981	0.981	393.5		411.6	1.436
$T = 210.0 \text{ K}$								
9.869	1540.8	90.22	1.14654	14.22	462.9	462.7	20.50	3.376
8.724	1315.3	90.22	1.13156	12.80	400.4		30.47	4.127
7.954	1158.5	90.22	1.11626	11.29	357.5		43.33	4.771
6.809	985.0	90.22	1.08342	8.177	313.1		77.95	4.573
5.806	957.0	90.22	1.05778	5.725	311.6		112.4	3.088
4.417	980.3	90.22	1.03589	3.574	326.0		164.6	2.087
2.300	1038.0	90.22	1.01529	1.528	352.2		329.7	1.554

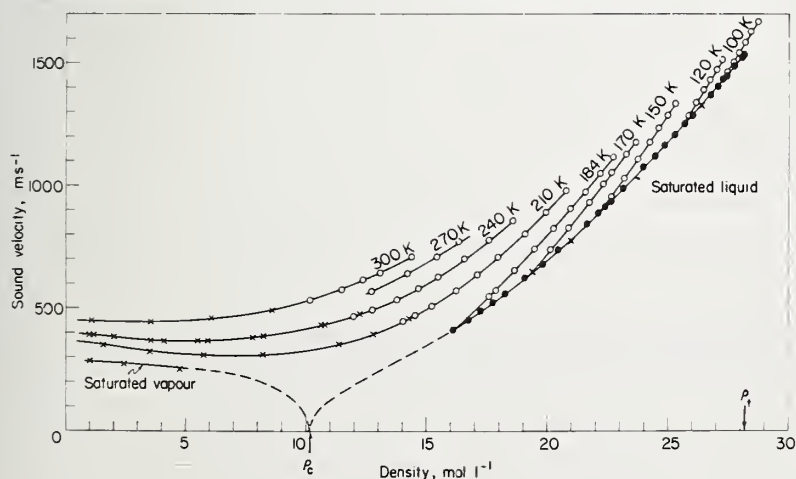


Fig.1 Velocity of sound as a function of density for saturated and compressed fluid methane
X — this work; O — ultrasonic velocities from reference 1; dashed line — qualitative estimate for the critical region

obtained by Olson⁴ for a wavelength of 546.2 nm. Adjustment to the laser wavelength was made by means of a truncated dispersion relation⁵ of the form

$$R_{\lambda} = R_{\infty} + \frac{A}{\lambda^2}$$

where R_{λ} is the value of the Lorentz-Lorenz function for wavelength λ , and the constant $A = 5.15 \times 10^{-6} \text{ cm}^5 \text{ mol}^{-1}$ was evaluated from the low pressure gas data of Cuthbertson and Cuthbertson.⁶ The index of refraction calculated in this way is rather insensitive to the exact value of R used and does not contribute significantly to the experimental error.

For comparison with ultrasonic velocity data, the experimental velocities in Table I have been adjusted for a predicted slight negative dispersion in accordance with the calculations of Mountain.⁷ At most, this correction amounts to 0.08% at the highest temperature and lowest density, decreasing rapidly by more than an order of magnitude at higher densities. The adjusted velocities are found to be in good agreement with the previously measured ultrasonic data in the regions of overlap. The data also appear to agree quite well with the data of Longequeve and Lallemand⁸ after taking into account temperature differences; however, these authors report their data in graphical form only. The measurements of Cardamone et al.⁹ are in substantial disagreement with the present measurements, being about 5% too low. More recent determinations¹⁰ at

low densities from the same laboratory, however, appear to be in better agreement with this work.

The accuracy of the density data used in the analysis is estimated by Goodwin² at $\pm 0.1\%$, resulting in a combined uncertainty in the derived isentropic compressibility, due largely to the uncertainty in the velocities, of about $\pm 1.0\%$. The uncertainty in γ is more difficult to assess depending to a large extent on the accuracy of $(\partial P / \partial \rho)_T$ used to obtain it from the velocity data. Our experience with similar analysis of more accurate ultrasonic data suggests that this derivative is probably accurate to about $\pm 1.0\%$ ^{1,11} in the region of interest here, resulting in a combined uncertainty for γ of about $\pm 2.0\%$.

References

- 1 Straty, G. C. *Cryogenics* 14 (1974) 367
- 2 Goodwin, R. D. NBS Tech Note 653 (1974), available from the Cryogenics Division, Institute for Basic Standards, National Bureau of Standards, Boulder, Colorado 80302
- 3 Fleury, P. A., Boon, J. P. *Phys Rev* 186 (1969) 186
- 4 Olsen, J. D. *J Chem Phys* 63 (1975) 474
- 5 Corruccini, R. J. NBS Tech Note 323 (1965)
- 6 Cuthbertson, C., Cuthbertson, M. *Proc Roy Soc (London)* A97 (1920) 152
- 7 Mountain, R. D. *Rev Mod Phys* 38 (1966) 205
- 8 Longequeve, A. M., Lallemand, M. P. *Comptes Rendus* 269B (1969) 1173
- 9 Cardamone, M. J., Saito, T. T., Eastman, D. P. R., Rank, D. H. *J Opt Soc of Am* 60 (1970) 1264
- 10 Wiggins, T. A. Private communication
- 11 Straty, G. C., Younglove, B. A. *J Chem Thermo* 5 (1973) 305

ICEC6

Sixth International Cryogenic Engineering Conference
11 - 14 May 1976
Alpes Congres, Grenoble, France

ICEC6 will cover all areas of current interest in cryogenic engineering. The main topics to be covered will be refrigeration; technology; superconductivity and its applications, including power generation and transmission, magnetic levitation, motors, MHD, storage; insulation; handling; properties of materials; instrumentation; and cryobiology.

Hotel accommodation in Grenoble is limited, so early registration is advisable. The deadline for registration is 1 April 1976 but early notification would enable the organizers to secure hotel bookings.

The registration fee is estimated as 500 francs. This will include pre-print of papers, refreshments, and conference dinner. Special day and student rates will be available.

A series of visits to various European laboratories will be organized, the week before or after the conference.

An exhibition is to be held in conjunction with the conference. 500 m² of exhibition area are available. Further details can be obtained from the Conference Secretary.

The deadline for the submission of abstracts of prospective papers is 15 November. All abstracts should be sent to the Conference Secretary J. Mazeur, ICEC6 Secretary, Centre de Recherches sur les Tres Basses Temperatures, BP 166 Centre de Tri, 38042 Grenoble, France.

APPENDIX D

DIELECTRIC CONSTANT DATA AND THE DERIVED CLAUSIUS-MOSSOTTI
FUNCTION FOR COMPRESSED GASEOUS AND LIQUID ETHANE

by

L. A. Weber

National Bureau of Standards
Institute for Basic Standards
Cryogenics Division
Boulder, Colorado 80302
USA

January 1976

DIELECTRIC CONSTANT DATA AND THE DERIVED CLAUSIUS-MOSSOTTI
FUNCTION FOR COMPRESSED GASEOUS AND LIQUID ETHANE

Abstract

Comprehensive, accurate measurements are presented for the dielectric constant of ethane in the saturated liquid and compressed fluid states at temperatures between 95 and 323 K. Pressures ranged up to 390 bar. The data are combined with accurate density data from several sources to produce the Clausius-Mossotti function over a wide range of temperature and density. An analytical expression of the Clausius-Mossotti function is given, and the consistency of the available density data is discussed.

DIELECTRIC CONSTANT DATA AND THE DERIVED CLAUSIUS-MOSSOTTI
FUNCTION FOR COMPRESSED GASEOUS AND LIQUID ETHANE*

L. A. Weber

National Bureau of Standards
Institute for Basic Standards
Cryogenics Division
Boulder, Colorado 80302

1. Introduction

Measurements of the dielectric constant, combined with accurate density data for compressed gases and liquids, can provide useful information about molecular polarizabilities and molecular interactions¹. Such measurements are generally combined to form the Clausius-Mossotti (CM) function, $1/\rho(\epsilon-1)/(\epsilon+2)$, where ϵ is the dielectric constant and ρ is the density. The CM function has the property of being nearly a constant, generally varying only about one percent over a wide range of density and temperature for nonpolar molecules.

A knowledge of the CM function provides a convenient and sensitive way of determining density from accurate dielectric constant measurements. Applications of this technique vary from the determination of the average density in a large tank to the use of very small density probes for study of the behavior of fluids in the vicinity of the critical point². In addition, dielectric constant data may be combined with different sets of PVT data to provide a convenient and sensitive test of agreement between the densities

*This work was carried out at the National Bureau of Standards under the sponsorship of the American Gas Association.

of different laboratories. This technique is useful even in situations where two sets of density data do not overlap.

Such measurements have been made in this laboratory on hydrogen³, oxygen⁴, fluorine⁵, nitrogen⁶, and methane⁷. This paper presents new dielectric constant measurements and the derived Clausius-Mossotti function for ethane for the saturated liquid and seven compressed fluid isotherms in the range 95 - 323.15 K. The data range in pressure up to 390 bar and in density from 0.036 to 3.16 times the critical density.

2. Experimental

Measurements were made with the highly stable cylindrical capacitor developed by Younglove and Straty⁸, which has a vacuum capacitance of about 33 pF. The curve of its vacuum capacitance versus temperature has proven to be stable to within one part in 10^5 . The dielectric constant ϵ is given by the ratio C/C_0 , where C is the capacitance with fluid between the plates and C_0 is the vacuum capacitance at the same temperature. The capacitance was measured with a three-terminal a-c bridge. Uncertainty in the determination of the dielectric constant is estimated to be less than 0.01%. Temperatures were measured with a platinum resistance thermometer calibrated on the IPTS 1968 scale and were reproducible to 0.001 K. The overall accuracy varied from 0.005 K at the lowest temperatures to 0.03 K for the room temperature measurements. Pressures were measured with an oil dead weight gage having an accuracy of about 0.01 percent. The sample holder and cryostat are similar to those described elsewhere^{5,9}. The sample used was 99.99% pure ethane which was passed through a molecular sieve trap to remove any water.

3. Results

The dielectric constant of the saturated liquid was measured at 34 temperatures between 95 and 295 K. The results are given in Table 1. Measurements were also made along seven isotherms between 120 K and 323.15 K at pressures up to 390 bar. The results are shown in Table 2. Because the cylindrical capacitor was mounted vertically, measurements at temperatures closer to the critical point (approximately 305.3 K) were not attempted. Due to the configuration of the sample holder it was also not possible to make measurements in the saturated vapor.

The results for the saturated liquid were combined with available densities to produce the Clausius-Mossotti function, and are shown in Figure 1. For temperatures up to 270 K the densities of Haynes and Hiza¹⁰ were used. At temperatures above 270 K the density data of Douslin and Harrison¹¹, represented by their smooth curve, were used. Also shown in the figure are the independent density-dielectric constant data of Sliwinski¹² for the saturated liquid and vapor near the critical point and the liquid CM data of Pan, Mady and Miller¹³ near the triple point. Three points derived from the saturated liquid density curve of Burton and Balzarini¹⁴ are shown. The error bars indicate the uncertainty involved in estimating densities from the figure given in their publication.

In Figure 2 are plotted the single phase isothermal CM function data. The isotherms at temperatures from 120 to 320 K made use of the PVT data of Straty and Tsumura¹⁵, and the CM data at 323.15 K made use of the densities of Douslin and Harrison¹¹ at that temperature. Also shown is the single CM datum of Watson, Rao and Ramaswamy¹⁶ at a pressure of one atmosphere at 298 K.

The isothermal density data were fitted with polynomials of the form,

$$P = RT\rho + \sum_i A_i \rho^i, \quad (1)$$

for the purpose of smoothing and interpolation. At temperatures below the critical, the polynomials were constrained at the saturation boundary to the densities from references 10 and 12. The density was then calculated by an iterative procedure for a given pressure.

4. Accuracy and Comparisons

The calculated CM function is extremely useful for intercomparing sets of PVT data. In Figure 1 the saturated liquid densities of Sliwinski are seen to be highly consistent with those of Haynes and Hiza. Sliwinski's estimated uncertainty in CM of 0.1% increasing to 0.4% nearest the critical point is shown in the figure. In the range 270 - 295 K Douslin's densities are seen to be 0.2 - 0.3% higher than the others. The results of Burton and Balzarini agree with those of Sliwinski within the uncertainty with which we could estimate the former. The densities of Miller et al. are in agreement with Haynes and Hiza near the triple point to within about 0.1%. The data of Canfield et al.¹⁷ lie between those of Miller et al. and Haynes and Hiza at 108 and 115 K and agree very well with Haynes and Hiza at 161 K.

In Figure 2 the isothermal CM data are compared with the best estimate of the saturation curve from Figure 1. The isotherms between 120 K and 280 K using the densities of Straty and Tsumura are seen to be in good agreement with the saturation curve. The small variation with temperature at a given density has been observed for other fluids and is believed to be real.

Their density data at 320 K may be compared directly with the density data of Douslin and Harrison at 323.15 K (assuming negligible dependence of CM on temperature over this small range), and it is seen that the latter's densities are again systematically higher by about 0.2%. The error bars indicate the deviations which would be introduced by a 0.01% uncertainty to the dielectric constant. The newer data are in good agreement with the point of Watson, Rao and Ramaswamy¹⁶.

Our dielectric constants are consistently smaller than those of Sliwinski by about 0.014%, which is about equivalent to the precision of his data. Our measurements are also smaller than those of Miller et al. by about 0.018%.

The dielectric constant measurements presented here, in combination with the saturated liquid densities of Haynes and Hiza and the PVT data of Straty and Tsumura, along with the independent measurements of Sliwinski, have been fitted with the equation,

$$CM = \frac{\epsilon-1}{\epsilon+2} \frac{1}{\rho} = A + B\rho + C\rho^2 + D T\rho \quad (2)$$

to provide an analytical expression for the results. The very precise PVT data of Douslin and Harrison were not included because of their large systematic deviation from the others. The coefficients given in Table 3 are estimated to reproduce the Clausius-Mossotti function of ethane to within 0.1%.

In Table 3 the parameter A, which is generally equated with the molar polarizability, is much larger than the corresponding parameter for methane and for the diatomic gases previously measured in this laboratory. This is to be expected based on considerations of molecular size. The dielectric second

virial coefficient, B , is also considerably larger than the coefficient found for the smaller molecules. Had the data of Douslin and Harrison been included in the fit, B would be somewhat smaller. Sliwinski found 11.22, 20, and -1460 for the values of A , B , and C from an analysis of his data alone. His value for B should be compared with the quantity $(B + DT)$ from Table 3. At room temperature this quantity has a value of about 24. However, little reliance should be placed on the significance of the value of B given here as it is based upon only one supercritical isotherm.

6. References

1. See for example, Kielich, S. Acta Phys. Polonica 27 (1975) 305; Acta Phys. Polonica 28 (1965) 95 and McQuarrie, D. A., Levine, H. B., Physica 31 (1965) 749 and references cited.
2. Weber, L. A., Phys. Rev. 2 (1970) 2379.
3. Stewart, J. W., J. Chem. Phys. 40 (1964) 3297.
4. Younglove, B. A., J. Res. NBS 76A (1972) 37.
5. Straty, G. C., Younglove, B. A., J. Chem. Phys. 57 (1972) 2255.
6. Ely, J. F., Straty, G. C., J. Chem. Phys. 61 (1974) 1480.
7. Straty, G. C., Goodwin, R. D., Cryogenics 13 (1973) 712.
8. Younglove, B. A., Straty, G. C., Rev. Sci. Instr. 41 (1970) 1087.
9. Diller, D. E., J. Chem. Phys. 47 (1968) 3096.
10. Haynes, W. M., Hiza, M. J., unpublished data.
11. Douslin, D. R., Harrison, R. H., J. Chem. Therm. 5 (1973) 491.
12. Sliwinski, P., Zeit fur Phys. Chem. 68 (1969) 91.
13. Pan, W. P., Mady, M. H., Miller, R. C., AIChE J. 21 (1975) 283.
14. Burton, M., Balzarini, D., Can. J. Phys. 52 (1974) 2011.
15. Straty, G. C., Tsumura, R., to be published.
16. Watson, H. E., Rao, G. G., Ramaswamy, K. L., Proc. Roy. Soc. Lond. A143 (1934) 558.
17. Chui, C., Canfield, F. B., Trans. Far. Soc. 67 (1971) 2933, and Shanaa, M. J., Canfield, F. B., Trans. Far. Soc. 64 (1968) 2281.

Table 1. Dielectric constant of saturated liquid ethane.

T (K)	$\rho \times 10^3$ (mol/cm ³)	ϵ	CM (cm ³ /mol)
95.00	21.520*	1.93563	11.047
100.00	21.341	1.92576	11.050
105.00	21.159	1.91590	11.054
110.00	20.975	1.90606	11.059
115.00	20.793	1.89612	11.062
120.00	20.602	1.88952	11.101
125.00	20.419	1.87661	11.074
130.00	20.232	1.86687	11.080
135.00	20.046	1.85700	11.084
140.00	19.857	1.84713	11.089
145.00	19.667	1.83721	11.094
150.00	19.475	1.82729	11.099
155.00	19.281	1.81729	11.104
160.00	19.086	1.80725	11.109
165.00	18.887	1.79714	11.115
170.00	18.687	1.78696	11.121
175.00	18.484	1.77669	11.126
180.00	18.279	1.76628	11.131
185.00	18.070	1.75576	11.136
190.00	17.861	1.74516	11.140
200.00	17.429	1.72349	11.148
210.00	16.971	1.70104	11.161
220.00	16.499	1.67786	11.171
230.00	15.997	1.65352	11.181
240.00	15.464	1.62780	11.191
250.00	14.890	1.60036	11.199
260.00	14.261	1.57076	11.208
270.00	13.549	1.53773	11.220
275.00	13.186**	1.51962	11.196
280.00	12.747	1.49994	11.206
285.00	12.258	1.47809	11.214
290.00	11.699	1.45318	11.218
295.00	11.024	1.42343	11.220

* Densities from ref. 10

** Densities from ref. 11

Table 2. Dielectric constant of compressed liquid and gaseous ethane.

T (K)	P (bar)	ϵ	$\rho \times 10^3$ (mol/cm ³)	\bar{C}_M (cm ³ /mol)
120.00	304.927	1.90928	21.026*	11.062
120.00	171.351	1.89966	20.848	11.066
120.00	66.985	1.89165	20.705	11.066
160.00	360.454	1.84490	19.827	11.083
160.00	358.376	1.84471	19.824	11.083
160.00	36.520	1.81160	19.171	11.107
160.00	36.628	1.81161	19.171	11.107
200.00	377.816	1.78020	18.564	11.118
200.00	256.633	1.76482	18.266	11.122
200.00	151.137	1.74954	17.965	11.127
200.00	69.172	1.73601	17.689	11.137
200.00	13.071	1.72560	17.472	11.147
240.00	392.029	1.71687	17.305	11.145
240.00	294.735	1.70044	16.975	11.151
240.00	211.148	1.63411	16.645	11.156
240.00	115.755	1.66165	16.186	11.164
240.00	62.930	1.64649	15.869	11.172
240.00	30.356	1.63563	15.637	11.181
280.00	376.142	1.64857	15.919	11.166
280.00	253.274	1.61794	15.274	11.182
280.00	165.058	1.58855	14.653	11.193
280.00	100.002	1.55858	14.016	11.199
280.00	54.692	1.52795	13.355	11.205
320.00	380.835	1.58441	14.579	11.183
320.00	196.092	1.51088	12.962	11.226
320.00	113.562	1.44096	11.402	11.239
320.00	79.146	1.36772	9.711	11.244
320.00	67.649	1.29621	7.894	11.256
320.00	62.595	1.22571	6.220	11.249
320.00	56.260	1.15041	4.235	11.274
320.00	40.599	1.07576	2.194	11.227

*Densities from ref. 15

Table 2. Continued

T (K)	P (bar)	ϵ	$\rho \times 10^3$ (mol/cm ³)	CM (cm ³ /mol)
323.15	318.351	1.55939	14.051**	11.185
323.15	243.358	1.52894	13.389	11.195
323.15	205.702	1.50940	12.959	11.201
323.15	184.435	1.49630	12.663	11.205
323.15	163.787	1.48155	12.339	11.210
323.15	132.020	1.45243	11.684	11.216
323.15	109.032	1.42223	10.993	11.223
323.15	94.055	1.39319	10.321	11.227
323.15	84.177	1.36464	9.650	11.230
323.15	77.255	1.33429	8.924	11.235
323.15	72.719	1.30433	8.195	11.238
323.15	69.510	1.27426	7.455	11.236
323.15	66.909	1.24358	6.686	11.231
323.15	64.448	1.21258	5.893	11.229
323.15	61.725	1.18186	5.089	11.231
323.15	58.073	1.15018	4.246	11.227
323.15	52.652	1.11762	3.362	11.221
323.15	44.559	1.08526	2.466	11.207
323.15	34.222	1.05686	1.662	11.191
323.15	62.010	1.18469	5.166	11.225
323.15	54.090	1.12503	3.566	11.220
323.15	38.024	1.06621	1.929	11.196
323.15	24.604	1.03699	1.089	11.185
323.15	16.106	1.02249	0.6660	11.174
323.15	10.202	1.01362	0.4046	11.170
323.15	6.027	1.00782	0.2326	11.171

**
Densities from ref. 11

Table 3. Parameters for equation (2); density in mol/cm³,
temperature in K.

A	11.180 ± 0.005
B	30.7 ± 2.1
C	-1627 ± 77
D	-0.021 ± 0.003

Figure Captions

Figure 1. Clausius-Mossotti function for the saturated liquid and vapor.

Figure 2. Clausius-Mossotti function for the single phase fluid.
The curve is for saturation conditions, from Figure 1.

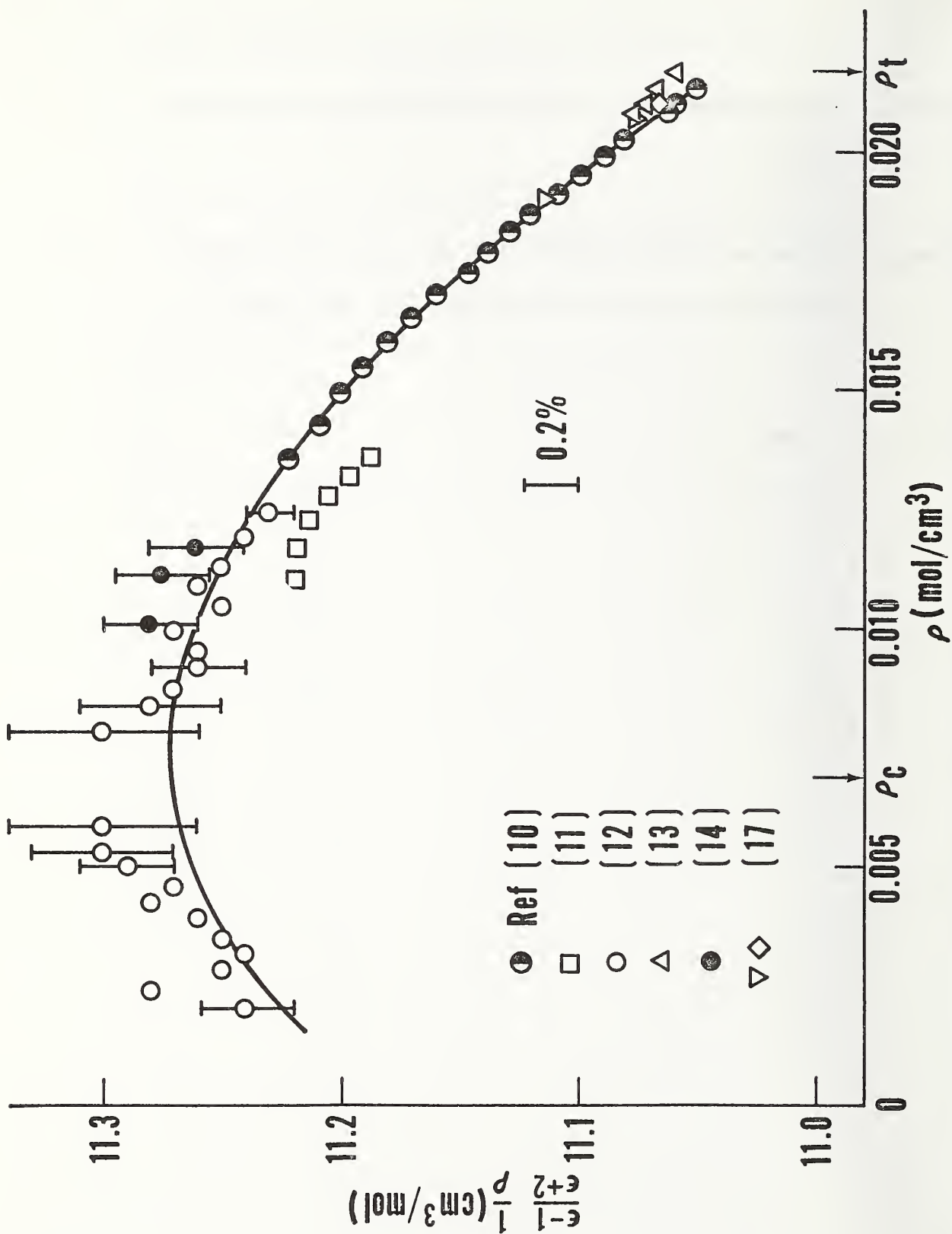


Figure 1.

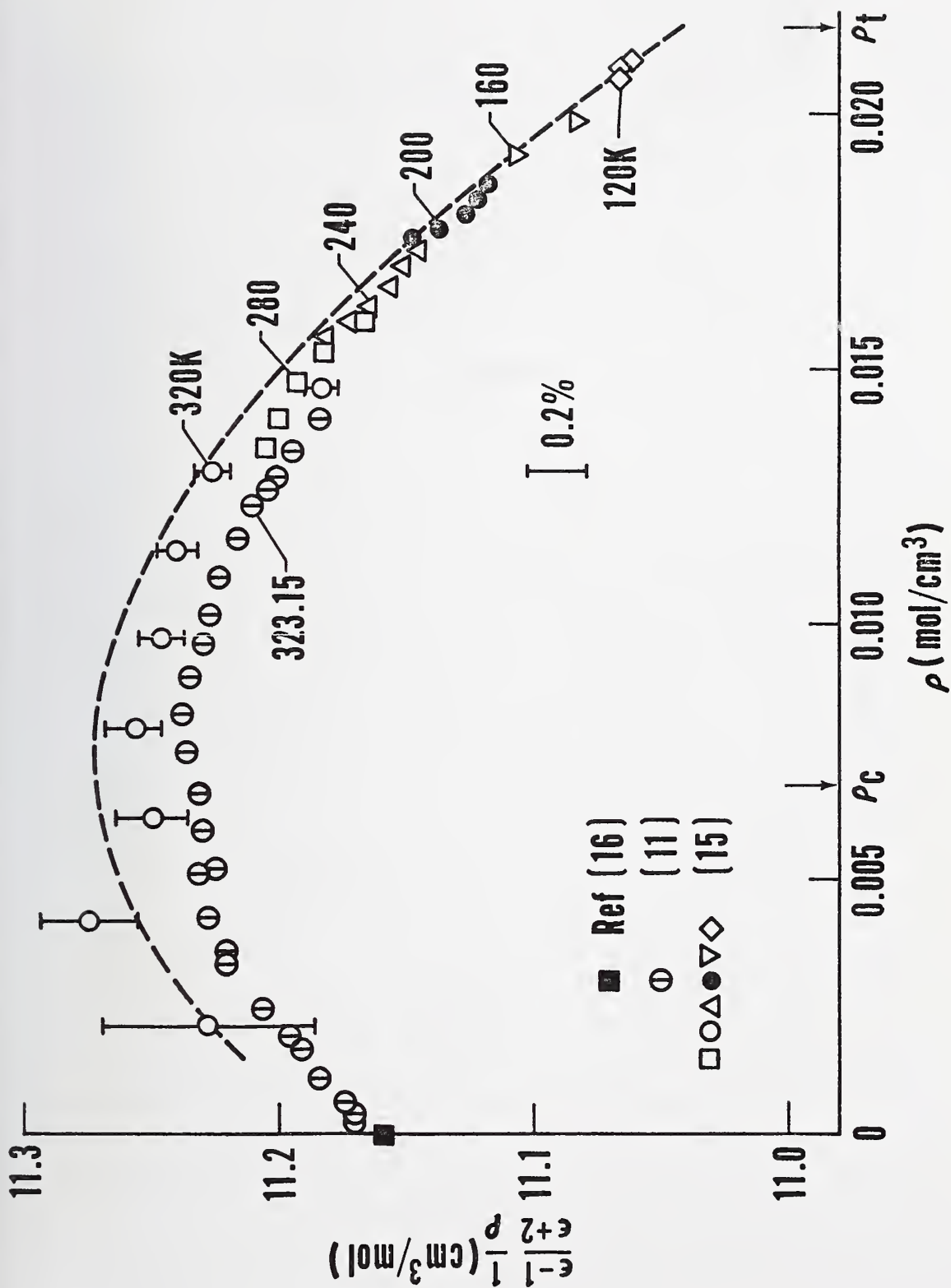


Figure 2.



APPENDIX E

Equation of State for Thermodynamic Properties of Fluids*

Robert D. Goodwin**

Institute for Basic Standards, National Bureau of Standards, Boulder, Colo. 80302

September 6, 1974

This equation of state was developed from *PVT* compressibility data on methane and ethane. The highly-constrained form originates on a given liquid-vapor coexistence boundary (described by equations for the vapor pressures and the orthobaric densities). It then requires only five least-squares coefficients, and ensures a qualitatively correct behavior of the $P(\rho, T)$ surface and of its derivatives, especially about the critical point. This nonanalytic equation yields a maximum in the specific heats $C_r(\rho, T)$ at the critical point.

Key words: Coexistence boundary; critical point; ethane; equation of state; fluids; methane; orthobaric densities; specific heats; vapor pressures.

Symbols and Units

Subscripts \underline{c} and \underline{l}	refer to critical and liquid triple points
Subscript σ	refers to liquid-vapor coexistence
α, b, δ	nonlinear constants in the equation of state
$B(\rho)$	density-dependent coefficients in the equation of state
$C(\rho)$	molal heat capacity for saturated liquid
$C_\sigma(T)$	molal heat capacity for ideal gas states
$C_r(T)$	molal heat capacity at constant density
$C_r(\rho, T)$	molal heat capacity at constant pressure
$C_p(\rho, T)$	density, mol/l
d	the Joule, 1 N·m
J	the liter, 10^{-3}m^3
l	mol, 16.043 g of CH_4 ; 30.070 g of C_2H_6 , (C^{12} scale)
P	pressure in bars, 1 bar = 10^5 N/m^2 , (1 atm = 1.01325 bar)
$P\sigma(\rho)$	the vapor pressure, bar
R	the gas constant, 8.31434 (J/mol)/K
ρ	d/d_c , density reduced at the liquid triple point
σ	d/d_c , density reduced at the critical point
T	temperature, K, (ITS-1968)
$T\sigma(\rho)$	temperature at liquid-vapor coexistence
$\theta(\rho)$	defined locus of temperatures, figure 3
$u(\rho, T)$	$T/T_\sigma(\rho)$, temperature reduced at coexistence
v	$1/d$, molal volume, l/mol
$W(\rho, T)$	the speed of sound
$x(T)$	T/T_c , temperature reduced at the critical point
$x_\sigma(\rho)$	$T_\sigma(\rho)/T_c$, reduced temperature at coexistence
$Z(P, \rho, T)$	Pv/RT , the "compressibility factor"

1. Introduction

A problem of importance for the natural gas industry is the prediction of thermodynamic properties of liquefied, multicomponent mixtures. For the wide range of compositions encountered, it may be necessary to utilize accurate properties of the pure components. We therefore believe that it will be helpful to have a relatively simple and rational equation of state of identical form for each component, such as the equation of state described below.

This equation originates on a given, liquid-vapor coexistence boundary, thus eliminating the long-standing problem of consistency between equations of state and this independently-derived envelope [26]. It ensures a maximum in the specific heats $C_r(\rho, T)$ approaching the critical point, qualitatively consistent with experimental behavior near, but not necessarily exactly at this pole [16], and it has only five arbitrary, least-squares coefficients. Experimental compressibility data for methane and ethane have been used at densities to the triple-point liquid density, temperatures to twice the critical, and pressures to 350 bar or greater.

Our objective in the present report is to give a concise description of this new type of equation of state which, with full documentation, has been presented in previous publications [14, 15].

For methane we have shown in [14] that an equation similar to that described below yields calculated specific heats, $C_\sigma(T)$, $C_r(\rho, T)$, $C_p(\rho, T)$, and speeds of sound in acceptable agreement with experimental data, without any weighting of the equation of state to those data. In a current report on ethane [15] we compute provisional thermodynamic and related properties by means of the simpler equation of state (1) described herein.

Symbols and units used here are given in a List. Fixed-point values from [14, 15] are given in table 1.

*This work at the National Bureau of Standards was supported by The American Gas Association, 1515 Wilson Boulevard, Arlington, Va. 22209.
**Cryogenics Division, National Bureau of Standards, Boulder, Colo. 80302.

For equation of state (1) the gas constant is $R \equiv (0.0831434) \cdot (d_t)$ bar/K, consistent with use of the dimensionless density, $\rho \equiv d/d_t$.

TABLE 1. Fixed-point values from [14, 15]

Triple point	Methane	Ethane
Density.....mol/l...		
Vapor.....	1.567 865·10 ⁻²	1.35114·10 ⁻⁶
Liquid.....	28.147	21.68
Temperature.....K...	90.680	89.899
Pressure.....bar ^a ...	0.1174 35675	1.009 906·10 ⁻⁵
Critical point		
Density.....mol/l...	10.0	6.74
Temperature.....K...	190.555	305.37
Pressure.....bar...	45.988	48.755

^a Precision required for vapor-pressure equation.

Various methods for utilizing the equations of state of pure components to derive properties of mixtures are described in a number of recent publications, e.g., [1, 4a, 17, 18, 19, 20, 21, 21a, 22, 23, 24, 27].

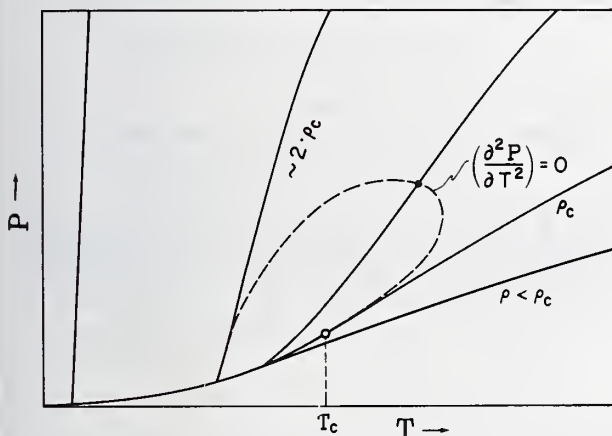


FIGURE 1. The locus of isochore inflection points.

2. The Equation of State

The $P(\rho, T)$ surface and equations of state are described in several reports, e.g., [6, 7, 10, 12, 14, 15, 20, 24, 28]. Figure 1 shows the qualitative behavior of isochores as indicated by Rowlinson [20], needed to give a calculated maximum in $C_r(\rho, T)$ at the critical point via the isothermal computation —

$$\Delta C_r = -T \cdot \int_0^{\rho} (\partial^2 P / \partial T^2) \cdot d\rho / \rho^2. \quad (a)$$

Figure 2 shows the well-known zero slope and curvature of the critical isotherm at the critical point.

This monotonic behavior (nonnegative slopes) is difficult to achieve from equations of state, yet is very important for such computations as —

$$C_p(\rho, T) = C_r(\rho, T) + T \cdot (\partial P / \partial T)^2 / (\partial P / \partial \rho) / \rho^2, \quad (b)$$

$$W(\rho, T) = [C_p \cdot (\partial P / \partial \rho) / C_r]^{1/2}. \quad (c)$$

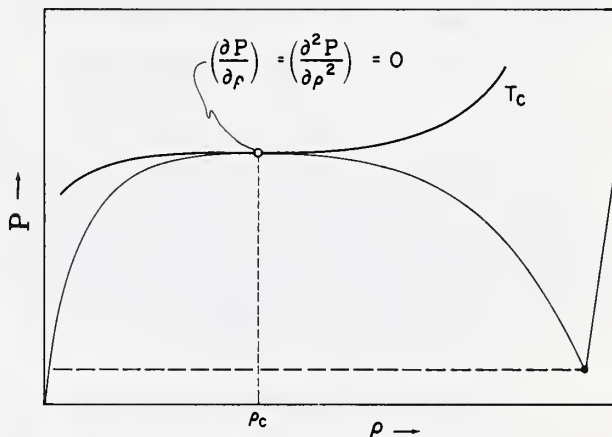


FIGURE 2. Behavior of the critical isotherm.

The liquid-vapor envelope, $T_\sigma(\rho)$, figure 3, is an important boundary of the $P(\rho, T)$ surface for the equation of state. We constrain the equation to this bound-

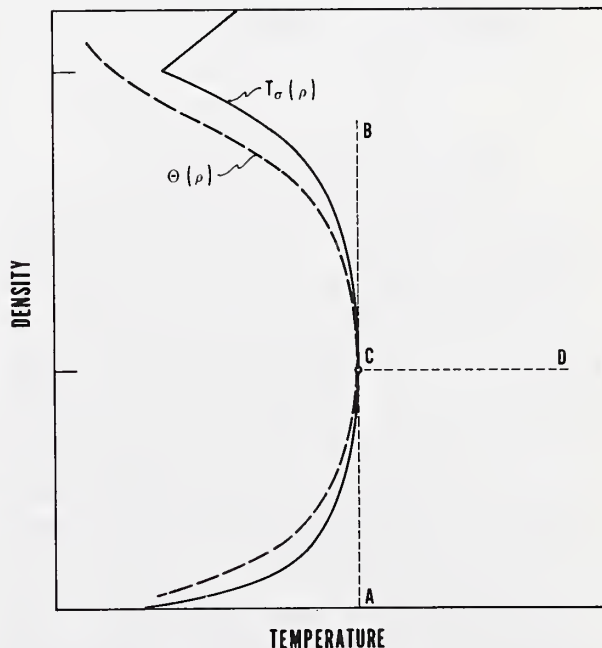


FIGURE 3. Behavior of the locus $\theta(\rho)$.

Point C is the critical point, and $T_\sigma(\rho)$ is the liquid-vapor coexistence envelope.

ary as follows, by use of the vapor pressures and the coexistence temperatures $T_\sigma(\rho)$ formulated in the appendix.

For any density (isochore), obtain the coexistence temperature from the function $T_\sigma(\rho)$. Use this to obtain the vapor pressure $P_\sigma[T_\sigma(\rho)]$ as a function of density, thus defining the equation of state at coexistence. By subtraction one then obtains an equation of the type of eq (1). The melting line is not a part of this equation of state

$$P - P_\sigma(\rho) = \rho R \cdot [T - T_\sigma(\rho)] + \rho^2 R T_c \cdot F(\rho, T),$$

where,

$$F(\rho, T) \equiv B(\rho) \cdot \Phi(\rho, T) + C(\rho) \cdot \Psi(\rho, T). \quad (1)$$

The functions $B(\rho)$ and $C(\rho)$ are polynomial coefficients to be found by least squares. The temperature-dependent functions $\Phi(\rho, T)$ and $\Psi(\rho, T)$ must be defined to be zero on the coexistence boundary at $T = T_\sigma(\rho)$, as shown by figures 4 and 5.

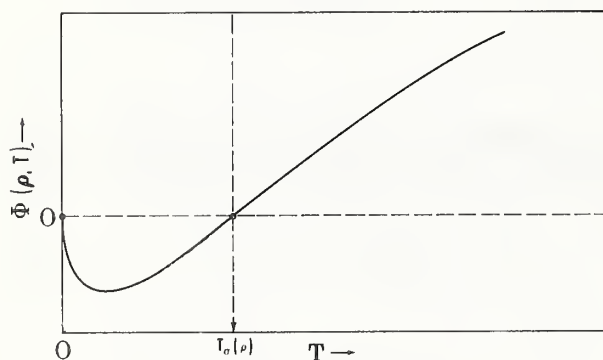


FIGURE 4. Behavior of the function $\Phi(\rho, T)$.

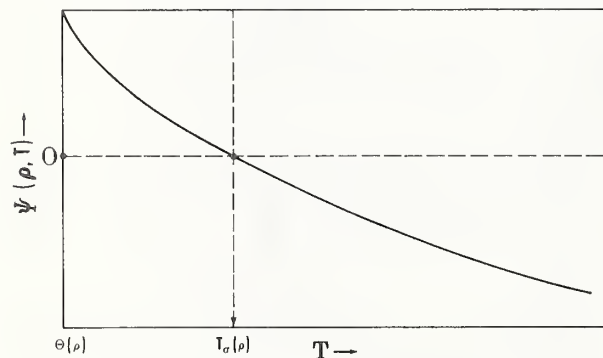


FIGURE 5. Behavior of the function $\Psi(\rho, T)$.

Equation (1) has, in addition to ρRT , only two temperature-dependent functions, which is the minimum number of functions (monotonic in T) needed to

describe the sigmoid shape of isochores in the density range $\rho_c < \rho < 2 \cdot \rho_c$, figure 1.

The first of these functions is —

$$\Phi(\rho, T) \equiv x^{1/2} \cdot \ln[u(\rho, T)], \quad (2)$$

where $u(\rho, T) \equiv T/T_\sigma(\rho)$. It is linear ($\partial^2 \Phi / \partial T^2 = 0$) everywhere on the coexistence boundary at $u = 1$, figure 4. It therefore gives a critical isochore which is linear at the critical point because $C(\rho) = 0$ by definition along this isochore, eq (6).

The second of these functions, $\Psi(\rho, T)$, is defined such that eq (1) will yield a maximum in the specific heats $C_v(\rho, T)$ at the critical point via eq (a). We first define the arguments —

$$\omega(\rho, T) \equiv \delta \cdot [T/\theta(\rho) - 1],$$

$$\omega_\sigma(\rho) \equiv \delta \cdot [T_\sigma(\rho)/\theta(\rho) - 1],$$

where δ is an arbitrary constant, and $\theta(\rho)$ is our locus of temperatures inside the coexistence envelope, figure 3,

$$\theta(\rho) \equiv T_\sigma(\rho) \cdot \exp[-\alpha \cdot f(\sigma)]. \quad (3)$$

The function $f(\sigma)$ here is normalized to unity at the liquid triple-point density —

$$f(\sigma) \equiv |\sigma - 1|^3 / (\sigma_t - 1)^3,$$

where $\sigma_t = d_l/d_c$ is a constant.

Function $\Psi(\rho, T)$ now is defined as the difference,

$$\Psi(\rho, T) \equiv \psi(\rho, T) - \psi_\sigma(\rho), \quad (4)$$

such that $\Psi = 0$ at coexistence, $T = T_\sigma(\rho)$. Component functions, $\psi(\rho, T)$, are designed to give infinite curvature ($\partial^2 \psi / \partial T^2$) at the origin, $\omega = 0$,

$$\psi_1(\rho, T) \equiv [1 - \omega \cdot \ln(1 + 1/\omega)]/x, \quad (4-a)$$

$$\psi_\sigma(\rho) \equiv [1 - \omega_\sigma \cdot \ln(1 + 1/\omega_\sigma)]/x_\sigma. \quad (4-b)$$

Figure 5 shows behavior of $\Psi(\rho, T)$. Sufficiently far away from the critical point it behaves roughly like $1/T^2$, found in the well-known, Beattie-Bridgeman equation of state.

Behavior of the coefficients $B(\rho)$ and $C(\rho)$ in eq (1) is shown by figure 6 for methane. The following polynomial representations have been developed tediously by trial,

$$B(\rho) \equiv B_0 + B_1 \cdot \rho + B_2 \cdot \rho^2 / (1 + b \cdot \rho^2), \quad (5)$$

$$C(\rho) \equiv (\sigma - 1) \cdot (\sigma - C_0) \cdot (C_1 + C_2 \cdot \rho). \quad (6)$$

The sign of the curvature of isochores ($\partial^2 P / \partial T^2$) at the coexistence boundary is determined *uniquely* by the sign of $C(\rho)$, figure 6, because $\Phi(\rho, T)$ is linear

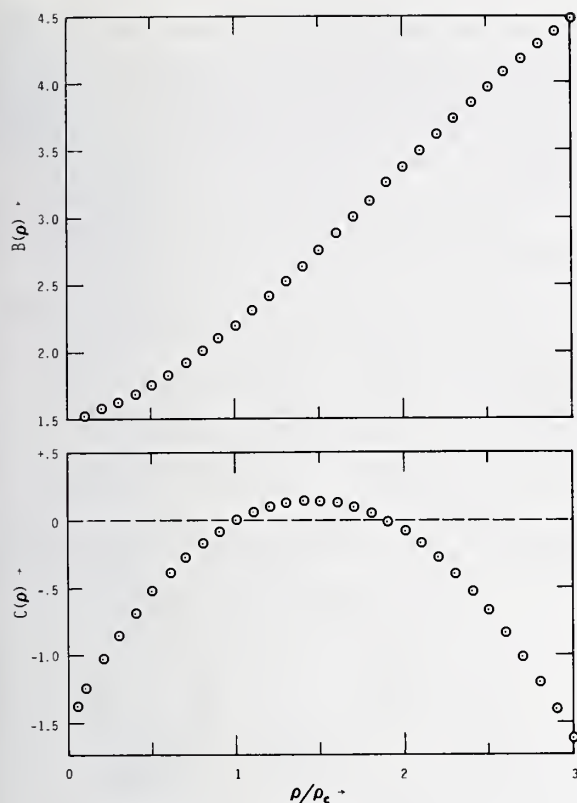


FIGURE 6. Behavior of the coefficients $B(\rho)$, $C(\rho)$ for methane.

on this boundary. The root in $C(\rho)$ at $\sigma = 1.9$ was found by least squares for methane and for ethane. It then was introduced as the constant C_0 in eq (6). This constraint is valuable because, under various conditions, we often have failed to obtain any such root from PVT data by least squares.

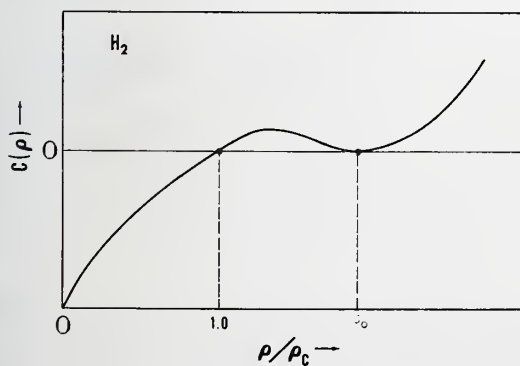


FIGURE 7. Presumed behavior of $C(\rho)$ for hydrogen, reflecting observed positive isochore curvatures in compressed liquid states at the lowest temperatures [7].

Figure 7 shows the presumed behavior of $C(\rho)$ for hydrogen, needed to give the observed positive curvature of isochores in compressed liquid states at the lowest temperatures [3, 7]. The behavior of figure 7 is described by a double root at C_0 , e.g.,

$$C(\rho) = C_1 \cdot (\sigma - 1) \cdot (\sigma - C_0)^2,$$

or without a root by—

$$C(\rho) = (\sigma - 1) \cdot (C_1 + C_2 \cdot \rho + C_3 \cdot \rho^2).$$

Table 2 presents constants of eq (1) for methane and ethane. Individual deviations of experimental PVT data from eq (1) are given for ethane in [15]. For methane with eq (1) they are comparable with those obtained in [14] using nine least-squares coefficients. Complete computer programs are reported in [15] for adjusting the vapor-pressure equation, the orthobaric-densities equations, the coexistence-temperatures equations, and the equation of state (1).

TABLE 2. Constants for equation of state (1)

	Methane	Ethane
α	2	2
b	1	1
δ	1/2	1/2
C_0	1.9	1.9
B_0	1.5082 12989	1.8481 67996
B_1	0.6544 90304	1.5697 04511
B_2	4.1320 82291	5.5601 86452
C_1	-0.7654 09076	-1.0428 42462
C_2	-0.0590 88717	+0.2249 78299
N	756	562
$\Delta P/P$, %	0.42	0.57

3. Comments on the Equation

Behavior of the critical isotherm from eq (1) at the critical point is deduced as follows. The functions $P_\sigma[T\sigma(\rho)]$ and $\Phi(\rho, T)$ depend directly upon $T_\sigma(\rho)$, which gives the overpowering factor $\exp[-\gamma/|\sigma-1|]$ for derivatives with respect to density at the critical point, $\sigma=1$. The function $\Psi(\rho, T)$ has a finite third derivative because it depends also on $\theta(\rho)$, eq (3). Its coefficient, $C(\rho)$, however, is zero at the critical density, eq (6). The first, second, and third derivatives of eq (1) therefore are zero at the critical point.

Detailed examinations of this isotherm from eq (1) show, however, that small variations in the assigned (ρ_c, T_c) critical point give small irregularities (negative slopes) nearby at $\sigma \leq 1$. We find that, given an accurate value of T_c , eq (1) serves to find the critical density which yields a well-behaved critical isotherm [15]. For methane and ethane the value of the critical density obtained by this method is roughly 1 percent lower than estimated by the conventional procedure of extrapolating the rectilinear diameter to the critical

temperature [14, 15, 20], but in each case falls within bounds of uncertainty in published works.

Ioschore inflection points figure 1, calculated from eq (1), are obtained as the difference of second derivatives (versus T) from the functions composing $F(\rho, T)$. We therefore expect high sensitivity to the analytical forms of $\Phi(\rho, T)$ and $\Psi(\rho, T)$. Variations of these forms might improve accuracy in representing PVT data. In the following we describe two alternative functions for $\Psi(\rho, T)$ from among many different functions investigated both for $\Phi(\rho, T)$ and for $\Psi(\rho, T)$. We then compare computed specific heats obtained via these two forms in the modified equation of state described below. Each of the following component functions must be differenced, as indicated by eq (4), to obtain $\Psi(\rho, T)$ for the equation of state. The argument for each of the following functions is changed to—

$$\omega(\rho, T) \equiv [1 - \theta(\rho)/T].$$

In (7) the adjustable exponent is $1 < \epsilon < 2$, and the adjustable coefficient was selected by trial to be $\delta = 1/\epsilon$,

$$\psi_2(\rho, T) \equiv 1 - (\omega - \delta \cdot \omega^\epsilon)/(1 - \delta). \quad (7)$$

This function approaches zero at high temperatures in proportion to $1/T^2$, as seen by expanding ω^ϵ . By trial with methane and ethane PVT data, we found $\epsilon = 3/2$, and hence $\partial^2 \psi_2 / \partial T^2$ behaves like $(1/\omega)^{1/2}$ on approach to the origin, $\omega = 0$.

In (8) we use the arbitrary constant $0 \leq \delta \leq 1$ to give relative weighting to two terms behaving, respectively, like $1/T$ and $1/T^2$ at high temperatures,

$$\psi_3(\rho, T) \equiv \delta \cdot (\theta/T) + (1 - \delta) \cdot [1 - \omega + \omega \cdot \ln(\omega)]. \quad (8)$$

The last term in (8) was explored for hydrogen [10]. Equation (8) can be simplified for computations. This function gives $\partial^2 \psi_3 / \partial T^2 \sim (1/\omega)$ on approach to the origin, $\omega = 0$, similar to definition (4-a) above.

With above functions, we find that coefficients B_1 and C_2 of eq (1) become nonsignificant for methane, leaving an equation of state with only three arbitrary, least-squares coefficients.

For computations on mixtures, the simplest possible equation of state is desirable. We have modified (1) such that it is suitable for corresponding-states adaptations, by specifying that densities shall be reduced at the critical point (hence $R = 0.0831434 \cdot d_c$, bar/K), and by introducing the critical pressure. The functions $\Phi(\rho, T)$ and $\Psi(\rho, T)$ remain unchanged—

$$P - P_\sigma(\rho) = \sigma R \cdot [T - T_\sigma(\rho)] + P_c \cdot \sigma^2 \cdot F(\rho, T), \quad (1-A)$$

$$B(\sigma) \equiv B_0 + B_2 \cdot \sigma^2 / (1 + b \cdot \sigma^2), \quad (5-A)$$

$$C(\sigma) \equiv C_1 \cdot (\sigma - 1) \cdot (\sigma - C_0). \quad (6-A)$$

Table 3 for methane gives the rms of relative density deviations for authors in [14], corresponding to each function $\psi(\rho, T)$ described above and, on the bottom line, the mean of combined pressure deviations. Tables 4 and 5 give the constants for eq (1-A), so that it will be possible to compute specific heats.

TABLE 3. Methane density deviations, rms percent

Equation of state.....		eq (1)	eq (1-A)	
Function $\psi(\rho, T)$		ψ_1 , eq (4-a)	ψ_2 , eq (7)	ψ_3 , eq (8)
Authors	N			
Virial eq. [14].....	46	0.06	0.12	0.16
Douslin et al. [4].....	171	.06	.13	.10
NBS [14].....	539	.51	.60	.50
Mean $\Delta P/P$, %...	756	.42	.46	.45

TABLE 4. Constants for equation of state (1-A), using $\psi_2(\rho, T)$, eq (7)

	Methane	Ethane
b	1/8	1/8
α	1/2	1/2
δ	2/3	2/3
ϵ	3/2	3/2
B_0	1.9894 21671	2.2373 56347
B_2	0.7924 35706	0.9304 97491
C_0	1.9	1.9
C_1	-0.8309 40825	-1.0494 11810
N	756	562
$\Delta P/P$, %	0.46	0.79

TABLE 5. Constants for equation of state (1-A), using $\psi_3(\rho, T)$, eq (8)

	Methane	Ethane
b	1/8	1/8
α	1/2	2/3
δ	1/3	1/2
B_0	1.9794 55787	2.1805 54662
B_2	0.8017 24817	0.9814 53571
C_0	1.9	1.9
C_1	-0.9465 70360	-1.3543 33999
N	756	562
$\Delta P/P$, %	0.45	0.75

The interaction specific heats ($C_v - C_v^0$) for methane have been compared along the critical isochore, as computed by equations (a) and (1-A), using the functions $\psi_2(\rho, T)$ and $\psi_3(\rho, T)$. Experimental behavior of specific heats suggests that these data should be described very near the critical temperature by—

$$(C_v - C_v^0) \sim (T/T_c - 1)^{-n}, \quad (9)$$

where exponent $0 < n < 1$, and usually, $0.05 \leq n \leq 0.15$, [16].

Figure 8 shows the computed results via $\psi_2(\rho, T)$, eq (7). Their qualitative behavior is correct, but they cannot be represented by (9). Instead, they are described accurately to 210 K by—

$(C_v - C_v^0) = 15.1 - 18.0 \cdot (T/T_c - 1)^{1/3}$, J/mol/K, suggesting that they might become finite at the critical temperature.

Using $\psi_3(\rho, T)$, eq (8), on the other hand, yields results on the logarithmic plot of figure 9. The slope, $n \approx 1/3$, is close to that observed for our experimental oxygen specific heats [8].

We conclude that $\psi_2(\rho, T)$ gives too weak a curvature to isochores from (1-A) approaching coexistence, and that the forms $\psi_1(\rho, T)$ and $\psi_3(\rho, T)$ may be preferable, despite the logarithmic infinity in their first derivatives versus T at the origin, $\omega = 0$.

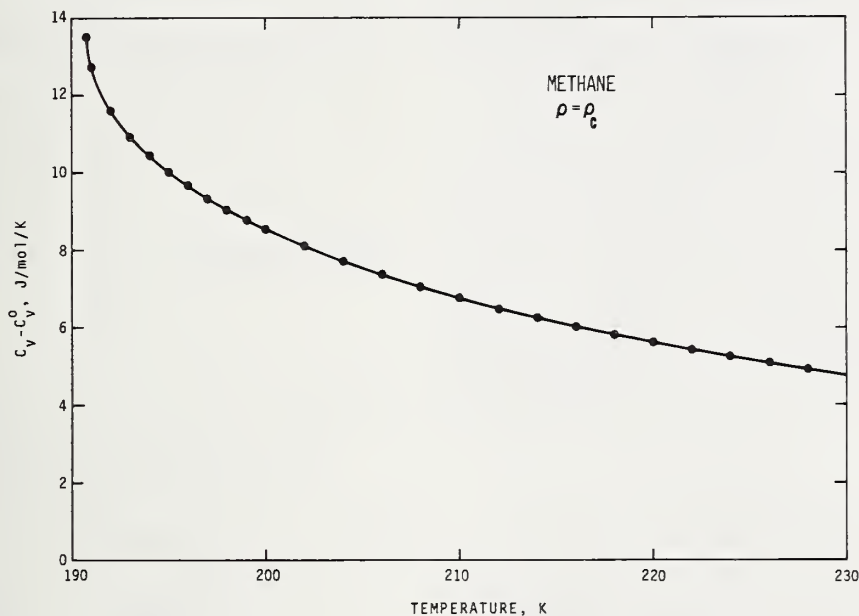


FIGURE 8. Computed interaction specific heats $(C_v - C_v^0)$ of methane along the critical isochore, via eq (1-A) and $\psi_2(\rho, T)$.

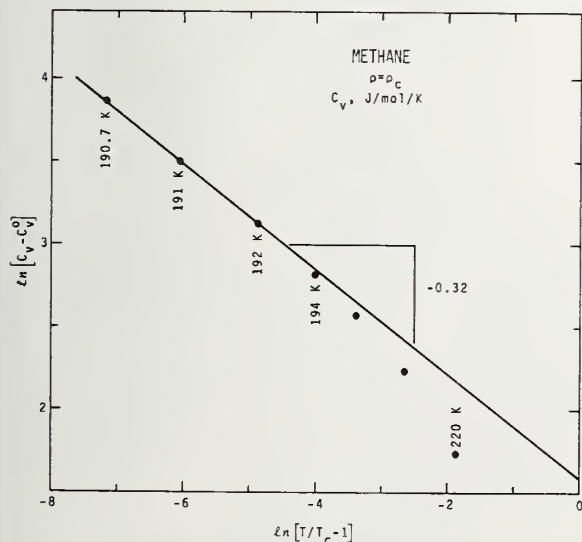


FIGURE 9. Computed interaction specific heats $(C_v - C_v^0)$ of methane along the critical isochore, via eq (1-A) and $\psi_3(\rho, T)$.

4. Conclusions

As argued above, the present equation of state (1) is rational because we understand the purpose of most of its component parts. Inclusion of the vapor pressures and orthobaric densities in this equation merely incorporates these physical properties which almost invariably must be used for a consistent network of thermodynamic functions, and eliminates the long-standing problem of continuity at the coexistence boundary [26].

We believe eq (1) to be valuable for thermal computations because it ensures an inherently correct behavior of the $P(\rho, T)$ surface, giving a maximum in the specific heats $C_v(\rho, T)$ at the critical point. The very small number of arbitrary least-squares coefficients (five, and possibly only three) facilitates comparisons of the equation of state for different substances, and may be attractive for work on mixtures.

We cannot expect eq (1) to represent some high-precision PVT data as well as equations with a much greater number of arbitrary constants. As the precision of "good" PVT data probably is often much bet-

ter than absolute accuracy, especially in the critical region, it would appear to be a self-defeating exercise to strive for the ultimate "representation" while ignoring essential features of the $P(\rho, T)$ surface. Any inaccuracies in the given, liquid-vapor, P - ρ - T boundary for eq (1), however, will be propagated along calculated isochores because eq (1) originates on this boundary.

Equation (1) almost certainly cannot be integrated analytically to express derived properties in closed form. It therefore would not be convenient for multiproperty analysis [2]. Equations amenable to integration, however, probably are not accurate in the critical region, which influences a large fraction of the $P(\rho, T)$ surface. To some extent, this must create a need for multiproperty analysis.

For methane with an equation of state similar to eq (1), on the other hand, we have used a minimum of specific heat data only to compute around the critical point for high densities near the critical temperature (fig. 3). In all other regions we computed specific heats and speeds of sound "a priori" via ideal gas specific heats and the equation of state, finding acceptable agreement with experimental data. We concluded that if such data do not exist experimentally, they could be estimated via the present type of equation of state for many but probably not all regions of the $P(\rho, T)$ surface [14].

5. Appendices

5.1. The Vapor Pressure Equation

The original form of our vapor pressure function [9] is satisfactory for methane [14], but for ethane it has been necessary to add the term $d \cdot x^4$ [15]. Define the argument—

$$x(T) \equiv (1 - T_t/T)/(1 - T_t/T_c),$$

when the function is—

$$\ln(P/P_t) = a \cdot x + b \cdot x^2 + c \cdot x^3 + d \cdot x^4 + e \cdot x \cdot (1 - x)^{3/2}. \quad (5.1)$$

Table 6 presents the coefficients.

TABLE 6. Constants for vapor-pressure equation (5.1)

	Methane	Ethane
<i>a</i>	4.7774 8580	10.7954 9166
<i>b</i>	1.7606 5363	8.3589 9001
<i>c</i>	-0.5678 8894	-3.1149 0770
<i>d</i>	0.0	-0.6496 9799
<i>e</i>	1.3278 6231	6.0734 9549

5.2. The Orthobaric Densities

The following expressions are constrained to the boundaries, the triple- and critical points [15]. In each case the basic behavior is described by—

$$Y(\rho, T) = \text{const.},$$

and polynomials are selected to represent small deviations. For the saturated liquid, define the variables,

$$x(T) \equiv (T_c - T)/(T_c - T_t),$$

$$y(\rho) \equiv (\rho - \rho_c)/(\rho_t - \rho_c),$$

$$Y(\rho, T) \equiv (y - x)/(x^e - x),$$

when the function is—

$$Y = a + b \cdot x^{2/3} + c \cdot x. \quad (5.2)$$

For the saturated vapor, define the variables,

$$x(T) \equiv (T_c/T - 1)/(T_c/T_t - 1),$$

$$y(\rho) \equiv \ln(\rho_c/\rho)/\ln(\rho_c/\rho_t)$$

$$Y(\rho, T) \equiv (y - x)/(x^e - x),$$

when the function is—

$$Y = A_1 + \sum_{i=2}^5 A_i \cdot x^{i/3}. \quad (5.3)$$

Table 7 presents constants for (5.2) and (5.3).

TABLE 7. Constants for orthobaric densities equations

	Methane	Ethane
Saturated liquid densities, eq (5.2)		
ϵ	0.36	0.33
<i>a</i>	.8595 3758	.7219 0944
<i>b</i>	.0243 6448	.2965 7790
<i>c</i>	-.0268 5285	-.3003 6548
Saturated vapor densities, eq (5.3)		
ϵ	0.41	0.39
<i>A</i> ₁	.4171 4211	.2158 7515
<i>A</i> ₂	-.5194 9762	-.0852 2342
<i>A</i> ₃	1.2077 7553	-.6152 3457
<i>A</i> ₄	-1.4613 0509	.2545 2490
<i>A</i> ₅	0.5765 8540	.1517 7230

5.3. The Coexistence Envelope, $T_\sigma(\rho)$

This envelope is shown by figure 3. For the equation of state (1) we obtain the coexistence temperature for any density from the following analytical descriptions. If the coexistence density must be found at a given temperature, it is obtained (for consistency in the equation of state) from the following expressions by iteration, using eqs (5.2) and (5.3) only to estimate an initial density.

An important feature of the present formulations [15] is that derivatives—

$$d^n T_\sigma / d\rho^n$$

of all orders, n , are zero at $\sigma = 1$, the critical point. We describe $T_\sigma(\rho)$ in two parts, according as $\sigma \leq 1$.

This simplifies constraint to the boundaries (liquid and vapor triple points). For each range the dependent variable is—

$$Y[T_{\sigma}(\rho)] \equiv (T_c/T_{\sigma} - 1)/(T_c/T_t - 1),$$

and we use the following function, infinite at the critical density

$$U(\sigma) \equiv -\gamma \cdot [1/|\sigma - 1| - 1/|\sigma_t - 1|]$$

where $\sigma_t = d_t/d_c$ is a constant, and d_t refers to vapor or liquid at the triple point according as $\sigma \leq 1$.

For the liquid range at $\sigma \geq 1$ the equation is—

$$\ln(Y) = U(\sigma) + \sum_{i=1}^5 A_i \cdot (\sigma^i - \sigma_t^i). \quad (5.4)$$

For extremely low densities in the vapor range at $\sigma \leq 1$ we modify the above expression as follows. Define the variable

$$W(\sigma) \equiv \ln(1 + s/\sigma)/\ln(1 + s/\sigma_t),$$

where s is an arbitrary constant. Our equation for the vapor range now is—

$$\begin{aligned} \ln(Y) = & U(\sigma) + B_0 \cdot \ln(W) + B_1 \cdot (\sigma^{1/3} - \sigma_t^{1/3}) \\ & + B_2 \cdot (\sigma^{2/3} - \sigma_t^{2/3}) + \sum_{i=3}^7 B_i \cdot (\sigma^{i-2} - \sigma_t^{i-2}). \end{aligned} \quad (5.5)$$

Table 8 presents constants for (5.4) and (5.5)

TABLE 8. Constants for the $T_{\sigma}(\rho)$ equations

	Methane	Ethane
Saturated liquid, eq (5.4)		
γ	1/2	1/2
A_1	11.4317 7230	23.7245 1840
A_2	-3.8765 9480	-14.8860 5161
A_3	0.5378 8326	5.4317 7443
A_4	.0	-1.0715 0566
A_5	.0	0.0913 5183
Saturated vapor, eq (5.5)		
s	1/4	1/4
B_0	0.9034 9557	0.8681 0517
B_1	.0	.0151 6978
B_2	.0	-.7296 0432
B_3	-.3834 4338	1.0096 5493
B_4	-3.9210 8638	-8.7340 2710
B_5	6.2600 3837	21.1071 2823
B_6	-9.3296 0083	-31.4499 4087
B_7	5.6060 2816	17.8637 0397

Anneke L. Sengers emphasized to us some time ago the importance of the critical region for the entire equation of state, thus motivating present developments. In this laboratory, R. D. McCarty provided the essential least-squares program, and we are indebted to D. E. Diller and L. A. Weber for discussions and valuable suggestions. The American Gas Association very kindly has supported this work.

6. References

- [1] Bazúa, E. R., and Prausnitz, J. M., Vapor-liquid equilibria for cryogenic mixtures, *Cryogenics* **11**, No. 2, 114 (April, 1971).
- [2] Cox, K. W., Bono, J. L., Kwok, Y. C., and Starling, K. E., Multiproperty analysis. Modified BWR equation for methane from PVT and enthalpy data, *Ind. Eng. Chem. Fundam.* **10**, No. 5, 245 (1971).
- [3] Diller, D. E., The specific heats (C_p) of dense simple fluids, *Cryogenics* **11**, No. 3, 186 (June, 1971).
- [4] Douslin, D. R., Harrison, R. H., Moore, R. T., and McCullough, J. P., P - V - T relations for methane, *J. Chem. Eng. Data* **9**, No. 3, 358 (1964).
- [4a] Fisher, G. D. and Leland, T. W., Jr., Corresponding states principle using shape factors, *Ind. Eng. Chem. Fundam.* **9**, No. 4, 537 (1970).
- [5] Furtado, André W., The measurement and prediction of thermal properties of selected mixtures of methane, ethane, and propane, (Ph. D. Thesis, Dept. of Chemical Engineering, Univ. of Michigan, Ann Arbor, Mich., Dec. 1973.)
- [6] Goodwin, R. D., Approximate Wide-Range Equation of State for Parahydrogen, *Advances in Cryogenic Engineering* **6**, 450 (Plenum Press, New York, 1961).
- [7] Goodwin, R. D., An equation of state for fluid parahydrogen from the triple point to 100°K at pressures to 350 atmospheres, *J. Res. Nat. Bur. Stand. (U.S.)* **71A** (Phys. and Chem.), No. 3, 203-212 (May-June 1967).
- [8] Goodwin, R. D. and Weber, L. A., Specific heats C_p of fluid oxygen from the triple point to 300 K at pressures to 350 atmospheres, *J. Res. Nat. Bur. Stand. (U.S.)* **73A** (Phys. and Chem.), No. 1, 15-24 (Jan.-Feb. 1969).
- [9] Goodwin, R. D., Nonanalytic vapor pressure equation with data for nitrogen and oxygen, *J. Res. Nat. Bur. Stand. (U.S.)* **73A** (Phys. and Chem.), No. 5, 487-491 (Sept.-Oct. 1969).
- [10] Goodwin, R. D., Formulation of a nonanalytic equation of state for parahydrogen, *J. Res. Nat. Bur. Stand. (U.S.)* **73A** (Phys. and Chem.), No. 6, 585-591 (Sept.-Oct. 1969).
- [11] Goodwin, R. D., Estimation of critical constants T_c , ρ_c , from the $\rho(T)$ and $T(\rho)$ relations at coexistence, *J. Res. Nat. Bur. Stand. (U.S.)* **74A** (Phys. and Chem.), No. 2, 221-227 (Mar.-Apr. 1970).
- [12] Goodwin, R. D. and Prydz, R., Densities of compressed liquid methane, and the equation of state, *J. Res. Nat. Bur. Stand. (U.S.)* (Phys. and Chem.), No. 2, 81-101 (Mar.-Apr. 1972).
- [13] Goodwin, R. D., Nonanalytic equation of state for methane, constrained to the vapor-liquid P - ρ - T boundary, unpublished NBS IR.
- [14] Goodwin, R. D., The thermophysical properties of methane from 90 to 500 K at pressures to 700 bar, *Nat. Bur. Stand. (U.S.)*, Tech. Note 653, 280 pages (Apr. 1974).
- [15] Goodwin, R. D., Provisional values for the thermodynamic functions of ethane, unpublished manuscript, June, 1974.
- [16] Green, M. S., and Sengers, J. V., Editors, Critical phenomena, *Nat. Bur. Stand. (U.S.)*, Misc. Publ. 273, 256 pages (Dec. 1966).
- [17] Kirk, B. S., Ziegler, W. T., and Mullins, J. C., A comparison of methods of predicting equilibrium gas phase compositions in pressurized binary systems containing an essentially pure condensed phase, *Advances in Cryogenic Engineering* **6**, 413 (1961).
- [18] Møllerup, J., and Rowlinson, J. S., The prediction of the densities of liquefied natural gas and of lower molecular weight hydrocarbons, *Chem. Eng. Sci.* **29**, 1373 (1974).

- [19] Rowlinson, J. S., Molecular theories of liquids and mixtures, Ind. Eng. Chem. **59**, No. 12, 28 (1967).
- [20] Rowlinson, J. S., Liquids and Liquid Mixtures, p. 98, (Butterworths Scientific Publications, London, 1959). See also second edition (1969).
- [21] Smith, G. E., Sonntag, R. E., and Van Wylen, G. J., Analysis of the solid-vapor equilibrium system carbon dioxide-nitrogen, Advances in Cryogenic Engineering **8**, 162 (1963).
- [21a] Smith, W. R., Perturbation theory and one-fluid corresponding states theories for fluid mixtures, The Can. J. Chem. Eng. **50**, 271 (1972).
- [22] Sood, S. K. and Haselden, G. G., Prediction methods for vapor-liquid equilibria in multicomponent cryogenic mixtures, Cryogenics **10**, No. 3, 199 (June, 1970).
- [23] Starling, K. E., Fluid Thermodynamic Properties for Light Hydrocarbon Systems (Gulf Publishing Co., Houston, Texas, 1973).
- [24] Tsonopoulos, C. and Prausnitz, J. M., Equations of state: a review for engineering applications, Cryogenics **9**, No. 5, 315 (Oct., 1969).
- [25] Verbeke, O.B., Representation of P - V - T data by means of a "universal" state equation for simple fluids, Paper F-6, Advances in Cryogenic Engineering **18**, 256 (1972).
- [26] Wagner, W., A method to establish equations of state exactly representing all saturated state variables applied to nitrogen, Cryogenics **12**, No. 3, 214 (June, 1972).
- [27] Zellner, M. G., Claitor, L. C., and Prausnitz, J. M., Prediction of vapor-liquid equilibria and enthalpies of mixtures at low temperatures, Ind. Eng. Chem. Fundam. **9**, No. 4, 549 (1970).
- [28] Zemansky, M. W., Heat and Thermodynamics (McGraw-Hill Book Co., Inc., New York, 1957).

(Paper 79A1-844)

APPENDIX F

ORTHOBARIC LIQUID DENSITIES OF NORMAL BUTANE
FROM 135 to 300 K AS DETERMINED WITH A
MAGNETIC SUSPENSION DENSIMETER

W. M. Haynes and M. J. Hiza

Cryogenics Division
Institute for Basic Standards
National Bureau of Standards
Boulder, Colorado 80302

Paper E-6

Preprinted for the
Cryogenic Engineering Conference
Kingston, Ontario, Canada
July 22-25, 1975

ORTHOBARIC LIQUID DENSITIES OF NORMAL BUTANE
FROM 135 to 300 K AS DETERMINED WITH A
MAGNETIC SUSPENSION DENSIMETER*

W. M. Haynes and M. J. Hiza

Cryogenics Division
Institute for Basic Standards
National Bureau of Standards
Boulder, Colorado 80302

Abstract

A magnetic suspension densimeter, developed for absolute density measurements of the principal components of liquefied natural gas and their mixtures, has been used to determine the orthobaric (saturated) liquid densities of normal butane from 135 to 300 K. These measurements provide the first set of density data for liquid n-butane that spans the range of temperatures from near ambient to just above the triple point, 134.8 K. These new data have been fitted to a simple analytical expression to provide a convenient and precise interpolation method. This equation has also been used to calculate densities for the subcooled liquid region at temperatures normally associated with liquefied natural gas. The precision and repeatability of measurement is within two parts in 10,000 or better. The absolute error in the densities is estimated to be less than ± 0.1 percent.

* This work was carried out at the National Bureau of Standards under the sponsorship of the LNG Density Project Steering Committee, through a grant administered by the American Gas Association, Inc.

Introduction

Of the principal constituents of natural gas, normal butane is the first in the series of paraffin hydrocarbons that has a triple-point temperature significantly higher than the normal boiling point (112 - 115 K) of methane-rich LNG (liquefied natural gas). Unlike isobutane, with a triple-point temperature (113.6 K) near the normal boiling point of methane-rich LNG, normal butane freezes at the relatively high temperature of 134.8 K. Thus any estimate of the contribution of n-butane content to the molar volume (or molar density) of LNG requires a relatively long extrapolation into the subcooled liquid region of n-butane. It is also known that n-butane is the first in the series of paraffin hydrocarbons exhibiting geometrical isomerism, with nearly instantaneous equilibrium, which contributes to the temperature dependence of the molar density [1-5]. It follows that an analytical expression that provides the most reliable means of extrapolating n-butane densities into the subcooled liquid region cannot be based on correspondence alone, but must be based on extensive and accurate data above the triple-point temperature.

Other than a few references [6, 7] that report results of saturated liquid density measurements near room temperature, no references were found that report experimental orthobaric liquid densities of n-butane below 283 K. (The results given by Klosek and McKinley [8] at temperatures below the triple-point temperature are probably based on their own data at somewhat higher temperatures.) The purposes of the present study were to obtain orthobaric liquid densities for n-butane that cover a relatively large temperature range at low temperatures, as well as some measurements up to ambient temperature, and to provide an analytical representation of these data that is used for extrapolation into the subcooled liquid region to compare with the results of reference [8].

A relatively new technique for determining absolute densities of cryogenic fluids [9] was used in the present work. It is simple in principle and is based on a straightforward application of Archimedes' principle. Using a magnetic suspension technique, a cylinder of magnetic material of known mass and volume is freely suspended by air-core solenoids in a stable configuration in the fluid whose density is to be determined. At such a stable equilibrium position, the upward magnetic force is added to the buoyancy force to balance the gravitational force. Densities of the fluid can be determined directly from the measured currents in the coils necessary to support the magnetic "float" at the same position in vacuum and in the fluid at constant temperature. The vertical position of the float is controlled by the automatic regulation of a servo-circuit, which includes a linear differential transformer for sensing inductively the position of the float. The horizontal position of the float is determined and maintained by the divergence of the magnetic field intensity.

Experimental

A complete description of the apparatus and a detailed discussion of the performance characteristics are beyond the scope of this paper and will be published elsewhere [10]. Only those essentials of the experiment necessary for clarity are included here.

The feasibility of using a magnetic suspension densimeter for measurements on cryogenic fluids had been demonstrated earlier with an absolute density measurement on liquid nitrogen at the normal boiling point [9]. The development of the present apparatus, shown in Fig. 1, was based on experience with that apparatus and incorporates a cryostat with continuous wide-range temperature control, a windowed equilibrium cell suitable for studies of the liquids and liquid mixtures of interest here, a new servo-circuit for vertical position control of the magnetic buoy, and a high-powered (125 X) microscope for monitoring the position of the magnetic buoy.

The magnetic buoy is a barium ferrite ($\text{Ba Fe}_{12} \text{O}_{19}$) ceramic magnet in the shape of a right circular cylinder, approximately 5 mm in diameter and 6 mm in length. It has been plated with approximately 0.07 mm of copper over its entire surface to prevent fluid from penetrating into the porous ceramic. Gold was flashed over the copper surface. The mass of the buoy was determined to better than 0.002% with an analytical balance. The volume of the buoy was determined within 0.02% at room temperature by using distilled water as a reference fluid of known density. At temperatures below ambient, the change in volume was calculated using the recent thermal expansion data obtained for barium ferrite [11].

Evaluation of the experimental parameters involved in this method and extensive performance tests indicate that the uncertainty in the density measurements depends primarily on the uncertainty in the determination of the position of the buoy, relative to the main coil, from vacuum to liquid measurements. The position of the float was determined to less than 10^{-3} mm with a 125 X microscope. The position of the main coil was maintained from vacuum to liquid measurements by supporting the coil at its midplane with quartz rods and by controlling the temperature of the coil with water.

The total uncertainty in the density measurements was estimated to be less than 0.1% at the lower temperatures; near room temperature the absolute error should be less than 0.05%. The imprecision of the density measurements was less than 0.02% over the complete temperature range.

A platinum resistance thermometer calibrated on the IPTS (1968) was used for the temperature measurements. The uncertainty of the calibration was approximately 0.002 K. Due to the specifications of the potentiometric measuring system, uncertainties in the temperature amounted to a maximum of 0.0135 K at 135 K, increasing to 0.030 K at 300 K. The temperature of the sample holder was controlled to better than 0.005 K, approximately the same as the reproducibility of the temperature measurements.

The purity of the n-butane used in these experiments was determined by chromatographic analysis with thermal conductivity detection. A 7.5-meter liquid partition column was used, capable of separating air (or N₂) from methane in small concentrations and the paraffinic from olefinic hydrocarbons. The only detectable impurity in this sample was air (or N₂) at approximately 25 ppm. The limits of detectability of the analyzer were approximately 20 ppm of air (or N₂) and methane and approximately 10 ppm of ethane and the higher hydrocarbons.

Results

The experimental densities for n-butane are given in Table 1 with the corresponding experimental temperatures. These data were fitted by the method of least squares to an equation of the following form:

$$\rho - \rho_c = a \left(1 - \frac{T}{T_c}\right)^{0.35} + \sum_{i=1}^3 b_i \left(1 - \frac{T}{T_c}\right)^n \quad (1)$$

where ρ = density in mol/l;

ρ_c = a characteristic density in mol/l,
approximately the critical density;

T_c = a characteristic temperature in kelvin, approximately
the critical temperature;

$n = 1 + \frac{i-1}{3}$; and

a, b_i are coefficients determined by least squares.

The parameters of equation (1) also are given in Table 1, as well as the standard deviation and the molecular weight.

In Fig. 2 the deviations of other experimental results [6, 7] and frequently used literature values [12-14] from the values calculated from equation (1) are plotted as a function of temperature. The accuracy with which equation (1), with parameters as given in Table 1, can be extrapolated above 300 K has not been investigated, but from the comparisons with Sliwinski [6] and Kahre [7] it appears that the equation gives reasonably accurate values up to 370 K.

In Fig. 3 two different methods of extrapolation to temperatures below 135 K are presented. First the present data from 135 to 170 K were fitted to equation (1) using two coefficients ($a = 7.3182177712$ and $b_1 = 3.4895578558$), and then densities were calculated for temperatures below the triple point and compared with the values of Klosek and McKinley [8]. Next the present data from 135 to 300 K were fitted using equation (1) with four coefficients, and again comparisons were made with Klosek and McKinley. The graph demonstrates the significant differences obtained for the two extrapolation methods and also provides comparisons with the only other published density values for normal butane at temperatures below 283 K. It should be noted that no effort has been expended in the present work to produce a "best" method for extrapolation into the subcooled liquid region.

Conclusions

The results of this study provide the first set of experimental density data for the orthobaric liquid phase of n-butane at temperatures between 135 and 300 K. The absolute error is estimated to be less than $\pm 0.1\%$. The analytical expression selected represents these data with a standard deviation less than the estimated imprecision of measurement, i.e. $\pm 0.02\%$. It is felt that the analytical expression given here provides a reasonable means of extrapolation of n-butane densities into the subcooled region for liquefied natural gas applications.

Acknowledgments

The authors wish to acknowledge the contributions of the LNG Density Project Steering Committee and the financial support of the companies they represent.

References

1. R. A. Bonham and L. S. Bartell, J. Am. Chem. Soc. 81, 3491 (1959).
2. R. A. Bonham, L. S. Bartell, and D. A. Kohl, J. Am. Chem. Soc. 81, 4765 (1959).
3. A. L. Verma, W. F. Murphy, and H. J. Bernatein, J. Chem. Phys. 60, 1540 (1974).
4. M. R. Cines, Phillips Petroleum Co., private communication (Jan 1974).
5. T. W. Schmidt, Phillips Petroleum Co., private communication (May 1974).
6. P. Sliwinski, Z. Phys. Chem. (Frankfurt) 63, 263 (1969).
7. L. C. Kahre, J. Chem. Eng. Data 18, 267 (1973).
8. J. Klosek and C. McKinley, Paper 22, Session 5, Proceedings of the First International Conference on LNG, Chicago, Ill. (1968).
9. W. M. Haynes and J. W. Stewart, Rev. Sci. Instr. 42, 1142 (1971).
10. W. M. Haynes, N. V. Frederick, and M. J. Hiza, manuscript in preparation.
11. A. F. Clark, W. M. Haynes, V. A. Deason, and R. J. Trapani, submitted to J. Amer. Ceramic Soc.
12. A. W. Francis, Ind. Eng. Chem. 49, 1779 (1957).
13. Natural Gas Processors Supplies Association, Engineering Data Book, Ninth Edition, NGPA, Tulsa, Oklahoma (1972).
14. American Petroleum Institute, Project 44, "Selected Values of Physical and Thermodynamic Properties of Hydrocarbons and Related Compounds," Carnegie Press, Pittsburgh, Pa. (1953).

Table 1. Densities of Saturated Liquid Normal
Butane and Parameters of Equation (1)

ρ_{exp} (mol/l)	T (K)	ρ_{calc} (mol/l)	$\frac{100 (\rho_{\text{exp}} - \rho_{\text{calc}})}{\rho_{\text{calc}}}$
12.6584	135.075	12.6590	-0.005
12.5772	140.075	12.5779	-0.006
12.4984	145.075	12.4968	0.013
12.4153	150.075	12.4157	-0.003
12.3362	155.075	12.3345	0.014
12.2544	160.075	12.2532	0.010
12.1694	165.075	12.1719	-0.020
12.0898	170.075	12.0904	-0.005
11.0955	230.000	11.0950	0.005
10.0099	290.000	10.0106	-0.006
9.8135	300.000	9.8130	0.005

Standard Deviation = 0.013%

a = 7.4784309557

b₁ = 11.182486252

b₂ = -18.803855715

b₃ = 11.170674620

T_c = 425.0 K

ρ_c = 3.876 mol/l

Molecular Weight = 58.12430

Figure Captions

- Figure 1. A magnetic suspension densimeter for cryogenic fluids.
- Figure 2. Deviation plot of densities of saturated liquid normal butane compared with values calculated from equation (1); data from this work and references 6, 7, 12-14. (Note that results from references 12-14 are not experimental data.)
- Figure 3. Deviations plot of densities of liquid normal butane of Klosek and McKinley [8] below the triple-point temperature compared with the extrapolated values calculated from equation (1) for two cases; (a) a least squares fit of the data from the present work from 135 - 170 K using two coefficients and (b) a least squares fit of the data from the present work from 135 - 300 K using four coefficients. (Note that the baseline represents two sets of extrapolated results obtained from the present data and that both curves with designated points represent a single set of values from reference [8].)

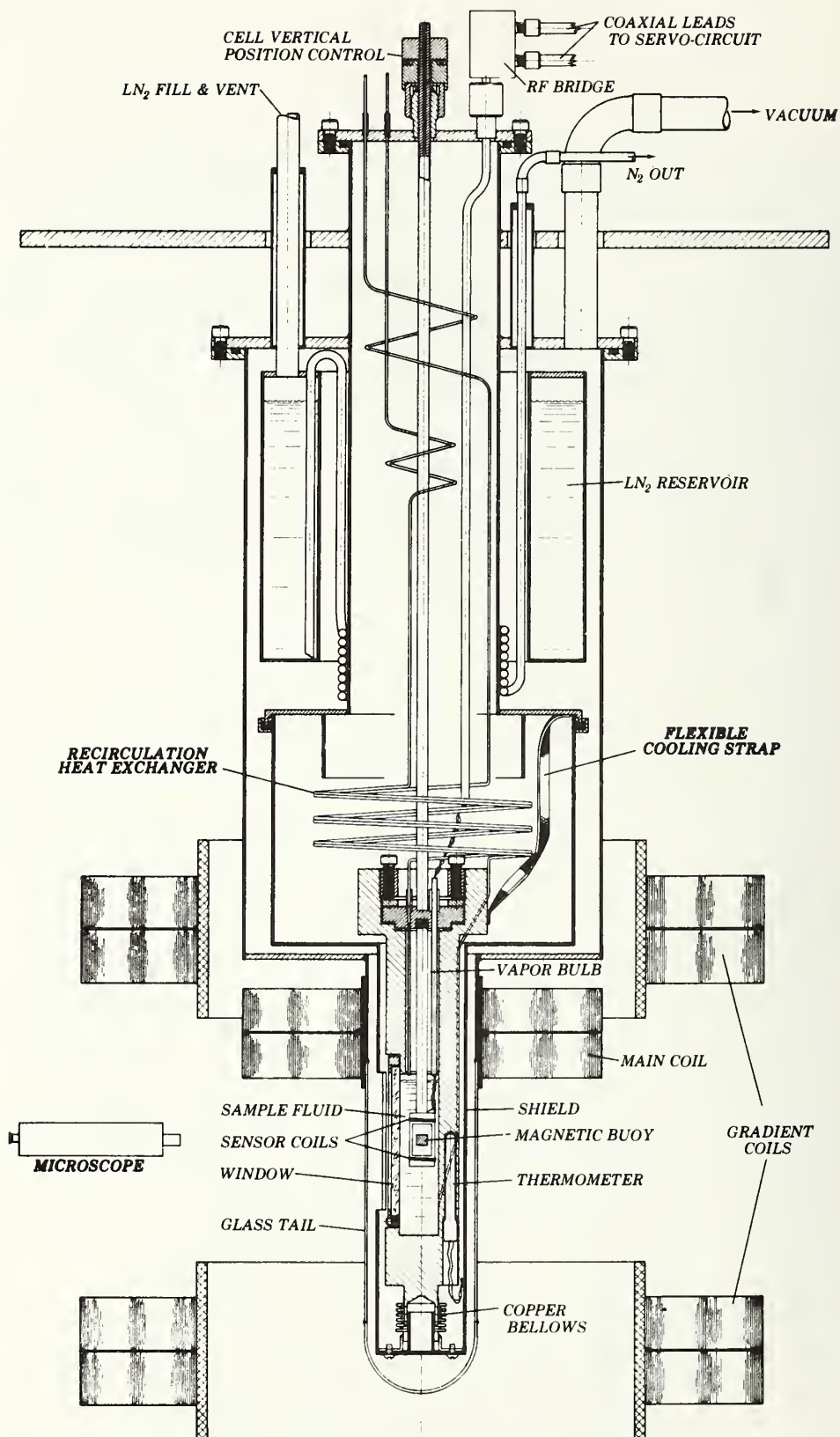


Figure 1

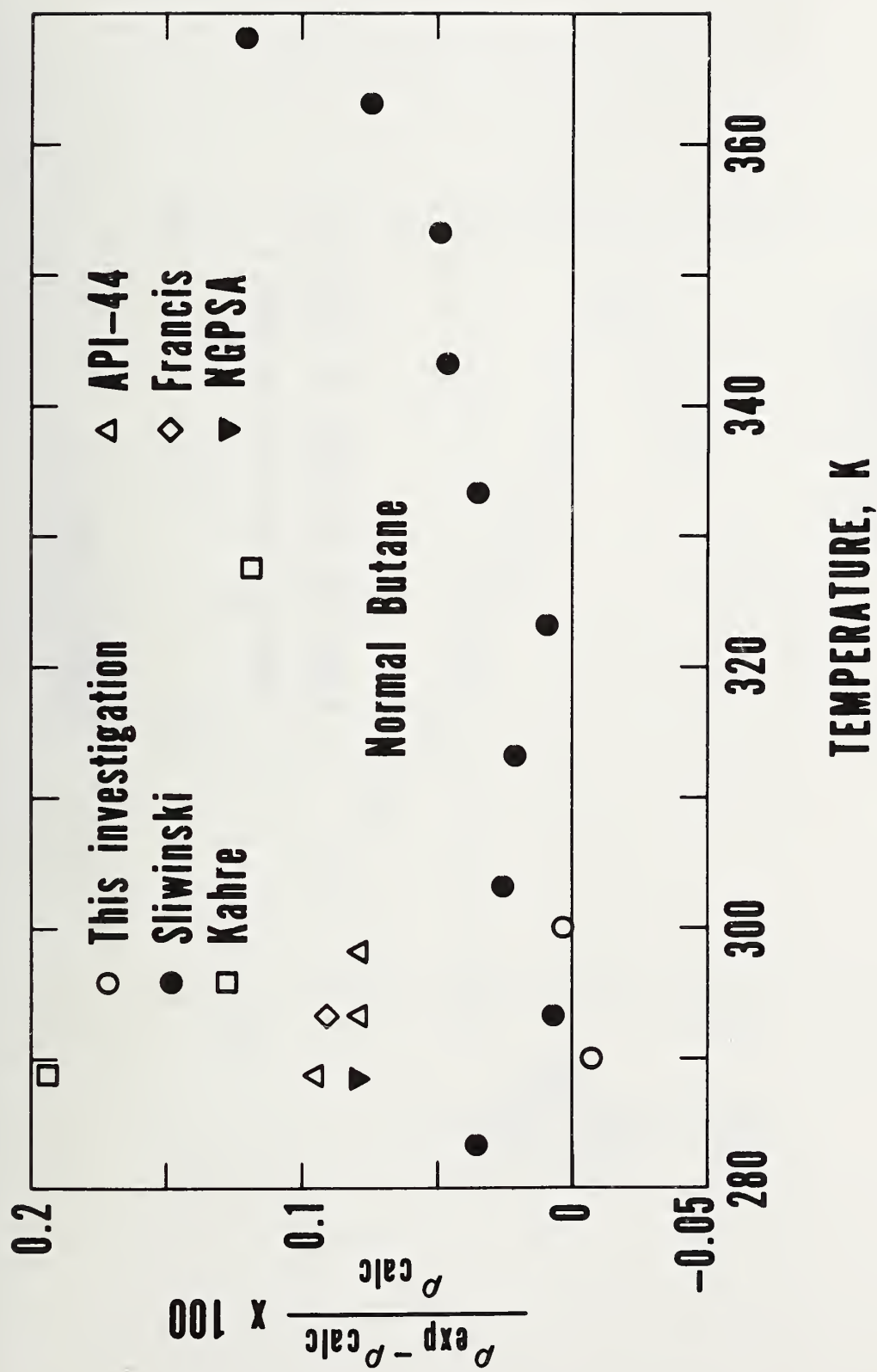


Figure 2

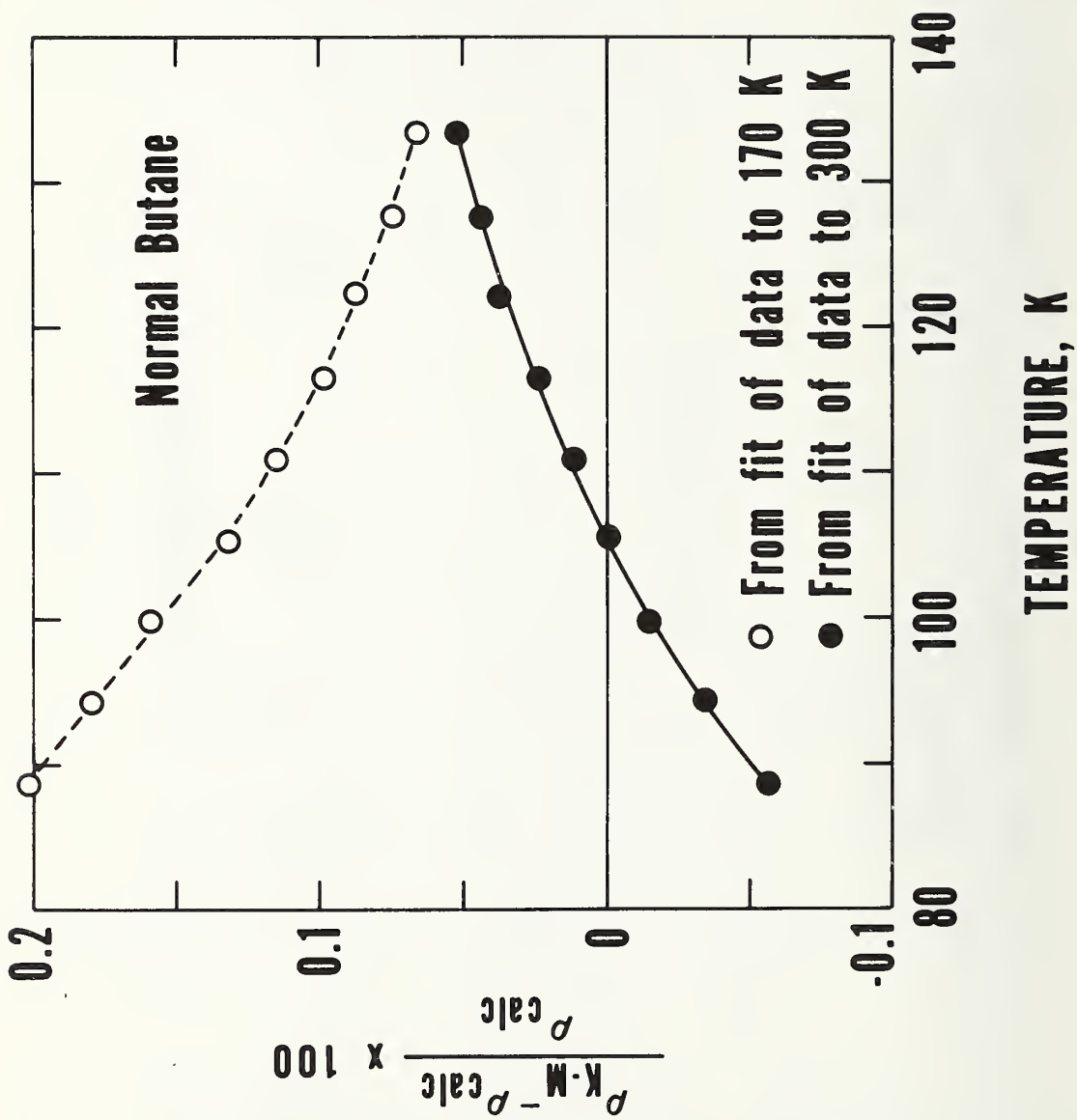


Figure 3

APPENDIX G

ON THE CONSISTENCY OF LIQUID-VAPOR EQUILIBRIA DATA
FOR BINARY MIXTURES OF METHANE WITH THE
LIGHT PARAFFIN HYDROCARBONS

W. R. Parrish and M. J. Hiza

Cryogenics Division
National Bureau of Standards
Institute for Basic Standards
Boulder, Colorado 80302

Paper E-2

Preprinted for the
Cryogenic Engineering Conference
Kingston, Ontario, Canada
July 22-25, 1975

ON THE CONSISTENCY OF LIQUID-VAPOR EQUILIBRIA DATA
FOR BINARY MIXTURES OF METHANE WITH THE
LIGHT PARAFFIN HYDROCARBONS*

W. R. Parrish and M. J. Hiza

Cryogenics Division
National Bureau of Standards
Institute for Basic Standards
Boulder, Colorado 80302

Abstract

Published experimental liquid-vapor equilibria data for the binary systems of methane with ethane, propane, isobutane, and normal butane have been compiled and evaluated for internal and mutual consistency. Equimolar excess Gibbs energies and infinite dilution Henry's constants are obtained by a method which uses only $P - x$ data. The derived equimolar excess Gibbs energies are compared with those calculated from a modified hard-sphere model for the equimolar mixtures. Critical loci (P_c , T_c , x_c) are also examined where available. Discrepancies in the data are enumerated which suggest the desirability of more precise and accurate measurements.

*

Contribution of the National Bureau of Standards, not subject to copyright.

ON THE CONSISTENCY OF LIQUID-VAPOR EQUILIBRIA DATA
FOR BINARY MIXTURES OF METHANE WITH THE
LIGHT PARAFFIN HYDROCARBONS

W. R. Parrish and M. J. Hiza

Introduction

The process design engineer usually relies upon correlations for predicting the liquid-vapor equilibria of multicomponent systems. These correlations require accurate binary data--both as a test and as a source of binary interaction parameters. With this problem in mind, we have compiled and evaluated liquid-vapor equilibria data for four binary systems of interest in LNG technology. The systems considered are methane with ethane, propane, n-butane and isobutane.

This paper gives qualitative results of the evaluation and points out the current status of each of the systems. A more detailed quantitative evaluation of these data along with volumetric and calorimetric data will be published later.

The primary source of reference for these systems (as well as other systems of cryogenic interest) is the bibliography by Kidnay et al. [1], updated through December, 1974.

Method of Evaluation

In this paper we consider only the mutual consistency between the isotherms of different investigators; the three best indicators of mutual consistency are equimolar excess Gibbs energies, G^E ($x = 0.5$), infinite dilution Henry's constants and critical loci. To calculate the first two quantities we use the

numerical technique proposed by Christiansen and Fredenslund [2]. Their method uses only total vapor pressure and liquid composition data and calculates thermodynamically consistent vapor phase values along with G^E and Henry's constants. It does not require an analytical expression to represent the liquid phase activity coefficients; vapor phase non-ideality corrections are made using the Redlich-Kwong equation of state. To find the equimolar G^E we least squares fitted the G^E values from their program to the Redlich-Kister expansion, i.e.,

$$G^E/RT = x_1 x_2 [A + B(x_1 - x_2) + C(x_1 - x_2)^2]$$

where R is the gas constant, T is the absolute temperature, x_1 and x_2 are the liquid phase mole fractions and A , B , and C are fitted coefficients. It was found that the value of the equimolar G^E can depend upon the number of interpolated points used in the numerical technique.

The equimolar G^E gives an indication of the overall shape of the $P - x$ curve for each isotherm below the critical temperature of methane (190.56 K). (It does not, in this case, give any indication of the quality of the vapor phase data. The vapor phase data are evaluated by comparing them with the calculated vapor phase values; this part of the evaluation is omitted here.) Graphical representation of equimolar G^E versus temperature provides an indication of consistency between the various isotherms. These values of G^E are compared with the values calculated using a modified hard-sphere equation of state with the parameters given by Rodosevich and Miller [3]. This equation of state seems to reliably predict the correct temperature dependence of equimolar G^E [4,5] for systems of simple molecules. Therefore, it is used as a guide for qualitatively determining which values of equimolar G^E seem to be the most reasonable. To estimate how sensitive the equimolar G^E is to systematic errors in pressure and composition, the equimolar G^E 's for the liquid phase methane-propane data of Calado et al. [16] were recalculated twice; with a systematic increase of one

percent in pressure, the equimolar G^E increased about 5 J/mol; with a systematic increase in composition of one percent, the equimolar G^E decreased about 5 J/mol (\sim 3 percent change).

Henry's constants indicate the behavior of the $P - x$ curve in the methane-lean region; they are especially useful in analyzing the data above the critical temperature of the more volatile component (methane in this case). The methane-propane data of Calado et al. [16] were used to determine the dependence of the Henry's constant on pressure and liquid phase composition errors. For a systematic one percent increase in pressure or composition the Henry's constant increased one percent.

The critical loci (P_c , T_c , x_c) are fairly difficult to determine. However, when they are reported they provide an excellent check on the consistency of the high pressure portion of the data.

Data Evaluation

Figures 1, 2 and 3 show the equimolar G^E , Henry's constants and critical loci, respectively, for the methane-ethane system. In the critical loci figures the curves were drawn to show trends in the data; no analytical model was used. Despite the many investigators, this system is clearly not well defined, especially below the critical temperature of methane. In fact, if the predicted equimolar G^E curve is qualitatively correct, one-half of the low temperature data are in error. Based on Henry's constants, the higher temperature data are in better agreement as are the critical loci. Clearly this system needs to be studied further, especially in the 90 to 190 K temperature range.

As can be seen by Figures 4, 5 and 6, the methane-propane system appears to be better defined. Based on the Henry's constants, the region above 200 K

is still not completely understood. There is good agreement in the critical loci, especially in the critical compositions. Based on these results, the methane-propane system is probably the best understood of the four systems considered here. Even so, more work is needed on this system.

Figures 7, 8 and 9 consider the methane-n-butane system. Relatively little work has been done on this system and there are no data reported below 144 K. Whereas the critical loci show good agreement, the Henry's constants show discrepancies of up to 15 percent in the 190 to 260 K range. This indicates that the data are more scattered in the low pressure and low methane concentration region. In summary, this system needs to be studied further, especially in the 100 to 150 and 190 to 260 K range.

Figures 10 and 11 show the available data for the methane-isobutane system. There are only two reported investigations of this system. The lowest temperature investigated is 190 K; there are no data in the open literature in temperature ranges of LNG applications.

Conclusions

For the four binary systems considered here, there are over 130 isotherms reported in the open literature. Even so, these systems are not as well defined as one would expect or desire. The discordant nature clearly indicates the necessity of assessing the reliability of liquid-vapor equilibria data. The preliminary evaluation given here indicates the need for more accurate liquid-vapor equilibria data, especially the methane-ethane system. Of these four systems, the methane-propane system appears to be the best defined.

Acknowledgment

The authors are grateful to L. J. Christiansen and A. Fredenslund for their computer program used in this work and to the Office of Standard Reference Data of the National Bureau of Standards for financial support.

References

1. A. J. Kidnay, M. J. Hiza, and R. C. Miller, *Cryogenics* 13, 575 (1973).
2. L. S. Christiansen and A. Fredenslund, *A.I.Ch.E. J.* 21, 49 (1975).
3. J. B. Rodosevich and R. C. Miller, *Advances in Cryogenic Engineering*, Vol. 19, Plenum Press, N. Y. (1974) p. 339.
4. W. R. Parrish and M. J. Hiza, *ibid*, p. 300.
5. A. Blinowska, T. M. Herrington, and L. A. K. Staveley, *Cryogenics* 13, 85 (1973).

Methane-Ethane System

6. O. T. Bloomer, D. C. Gami and J. D. Parent, *Inst. of Gas Technol. Res. Bull.*, No. 22 (1953).
7. Shinn-der Chang and B. C.-Y. Lu, *Chem. Eng. Progr. Symp. Ser.* 63 (81), 18 (1967).
8. M. Guter, D. M. Newitt and M. Ruhemann, *Proc. Roy. Soc. (London)* 176A, 140 (1940).
9. C. Hsi and B. C.-Y. Lu, *Can. J. Chem. Eng.* 49, 140 (1971).
10. D. W. Moran, Ph.D. Dissertation, Imperial College, University of London, London (1959).
11. A. R. Price and R. Kobayashi, *J. Chem. Eng. Data* 4, 40 (1959).
12. M. Ruhemann, *Proc. Roy. Soc. (London)* 171A, 121 (1939).

13. V. G. Skripka, I. E. Nikitina, L. A. Zhdanovich, A. G. Sirotin and O. A. Benyaminovich, *Gazov. Prom.* 15 (12), 35 (1970).
14. I. Wichterle and R. Kobayashi, *J. Chem. Eng. Data* 17, 9 (1972).

Methane-Propane System

15. W. W. Akers, J. F. Burns and W. R. Fairchild, *Ind. Eng. Chem.* 46, 2531 (1954).
16. J. C. G. Calado, G. A. Garcia, and L. A. K. Staveley, *J. Chem. Soc., Faraday Trans. 1* Vol. 70, Part 8, 1445 (1974).
17. A. J. B. Cutler and J. A. Morrison, *Trans. Faraday Soc.* 61, 429 (1965).
18. D. P. L. Poon and B. C.-Y. Lu, *Advances in Cryogenic Engineering*, Vol. 19, Plenum Press, New York (1964), p. 292.
19. A. R. Price and R. Kobayashi, *J. Chem. Eng. Data* 4, 40 (1959).
20. J. G. Roof and J. D. Baron, *ibid* 12, 292 (1967).
21. H. H. Reamer, B. H. Sage and W. N. Lacey, *Ind. Eng. Chem.* 42, 534 (1950).
22. B. H. Sage, W. N. Lacey, and J. G. Schaafsma, *ibid* 26, 214 (1934).
23. V. G. Skripka, I. E. Kikitina, L. A. Zhdanovich, A. G. Sirotin and O. A. Benyaminovich, *Gazov. Prom.* 15 (12), 35 (1970).
24. H. F. Stoeckli and L. A. K. Staveley, *Helv. Chim. Acta.* 53 (8), 1961 (1970).
25. I. Wichterle and R. Kobayashi, *J. Chem. Eng. Data* 17, 4 (1972).

Methane-n-Butane System

26. D. G. Elliot, R. J. J. Chen, P. S. Chapplear and R. Kobayashi, *J. Chem. Eng. Data* 19, 71 (1974).
27. L. C. Kahre, *ibid* 67, (1974).

28. K. L. Mulholland, Ph.D. Dissertation, University of Kansas, Manhattan (1970).
29. T. J. Rigas, D. F. Mason and G. Thodos, Ind. Eng. Chem. 50, 1297 (1958).
30. L. R. Roberts, R. H. Wang, A. Azarnoosh, and J. J. McKetta, J. Chem. Eng. Data 7, 484 (1962).
31. B. H. Sage, B. L. Hicks and W. N. Lacey, Ind. Eng. Chem. 32, 1085 (1940).
32. R. H. Wang and J. J. McKetta, J. Chem. Eng. Data 9, 30 (1964).

Methane-isobutane System

33. S. D. Barsuk, V. G. Skripka and O. A. Benyaminovich, Gazov. Prom. 15 (9), 38 (1970).
34. R. H. Olds, B. H. Sage and W. N. Lacey, Ind. Eng. Chem. 34, 1008 (1942).

List of Figures

- Figure 1. Equimolar G^E as a function of temperature for the methane-ethane system. The solid line was calculated using a modified hard-sphere equation of state [3].
- Figure 2. Infinite dilution Henry's constants as a function of temperature for the methane-ethane system.
- Figure 3. Critical pressure and composition as a function of temperature for the methane-ethane system.
- Figure 4. Equimolar G^E as a function of temperature for the methane-propane system. The solid line was calculated using a modified hard-sphere equation of state [3].
- Figure 5. Infinite dilution Henry's constants as a function of temperature for the methane-propane system.
- Figure 6. Critical pressure and composition as a function of temperature for the methane-propane system.
- Figure 7. Equimolar G^E as a function of temperature for the methane-n-butane system. The solid line was calculated using a modified hard-sphere equation of state [3].
- Figure 8. Infinite dilution Henry's constants as a function of temperature for the methane-n-butane system.
- Figure 9. Critical pressure and composition as a function of temperature for the methane-n-butane system.
- Figure 10. Infinite dilution Henry's constants as a function of temperature for the methane-isobutane system.
- Figure 11. Critical pressure and composition as a function of temperature for the methane-isobutane system.

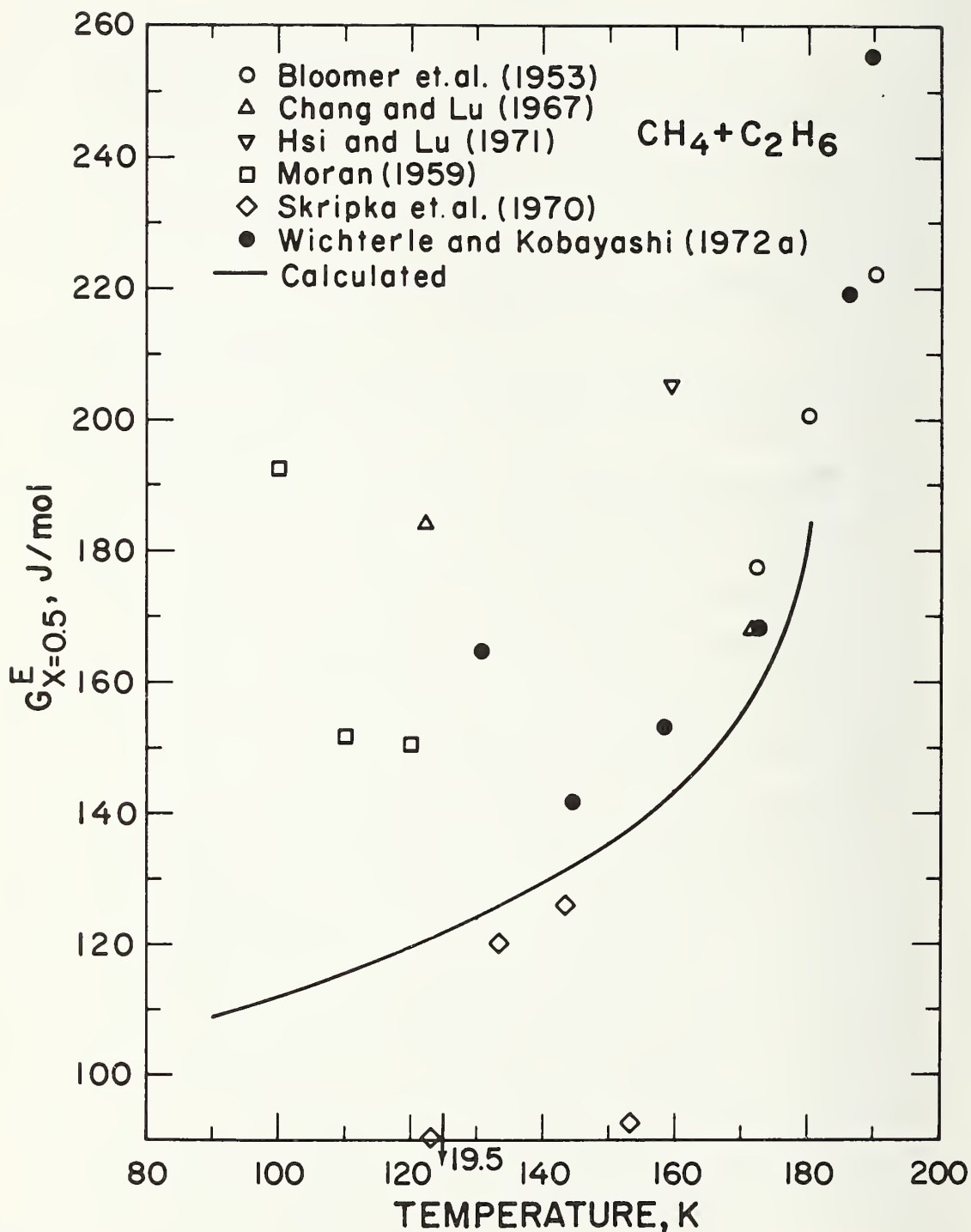


Figure 1. Equimolar G^E as a function of temperature for the methane-ethane system. The solid line was calculated using a modified hard-sphere equation of state [3].

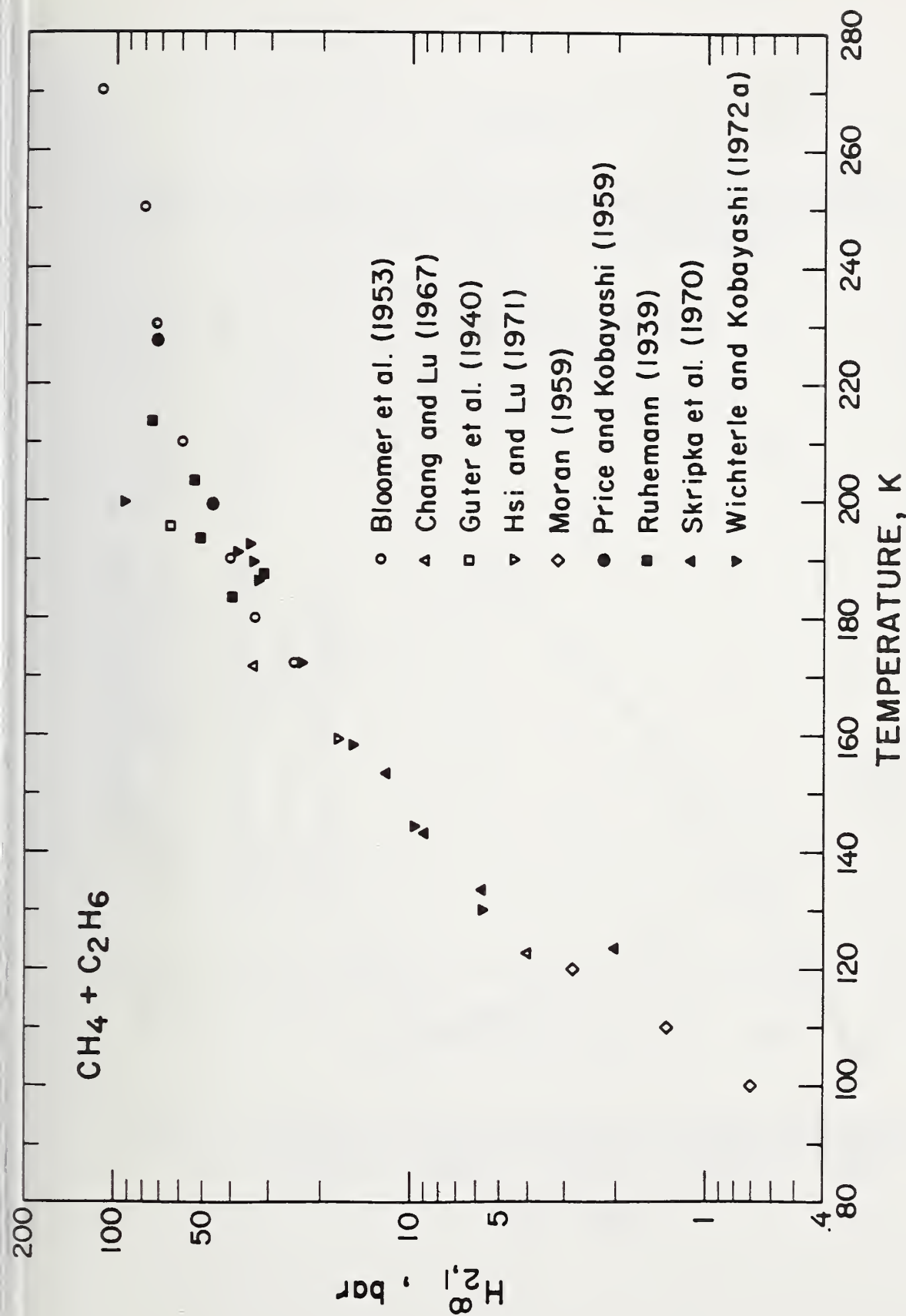


Figure 2. Infinite dilution Henry's constants as a function of temperature for the methane-ethane system.

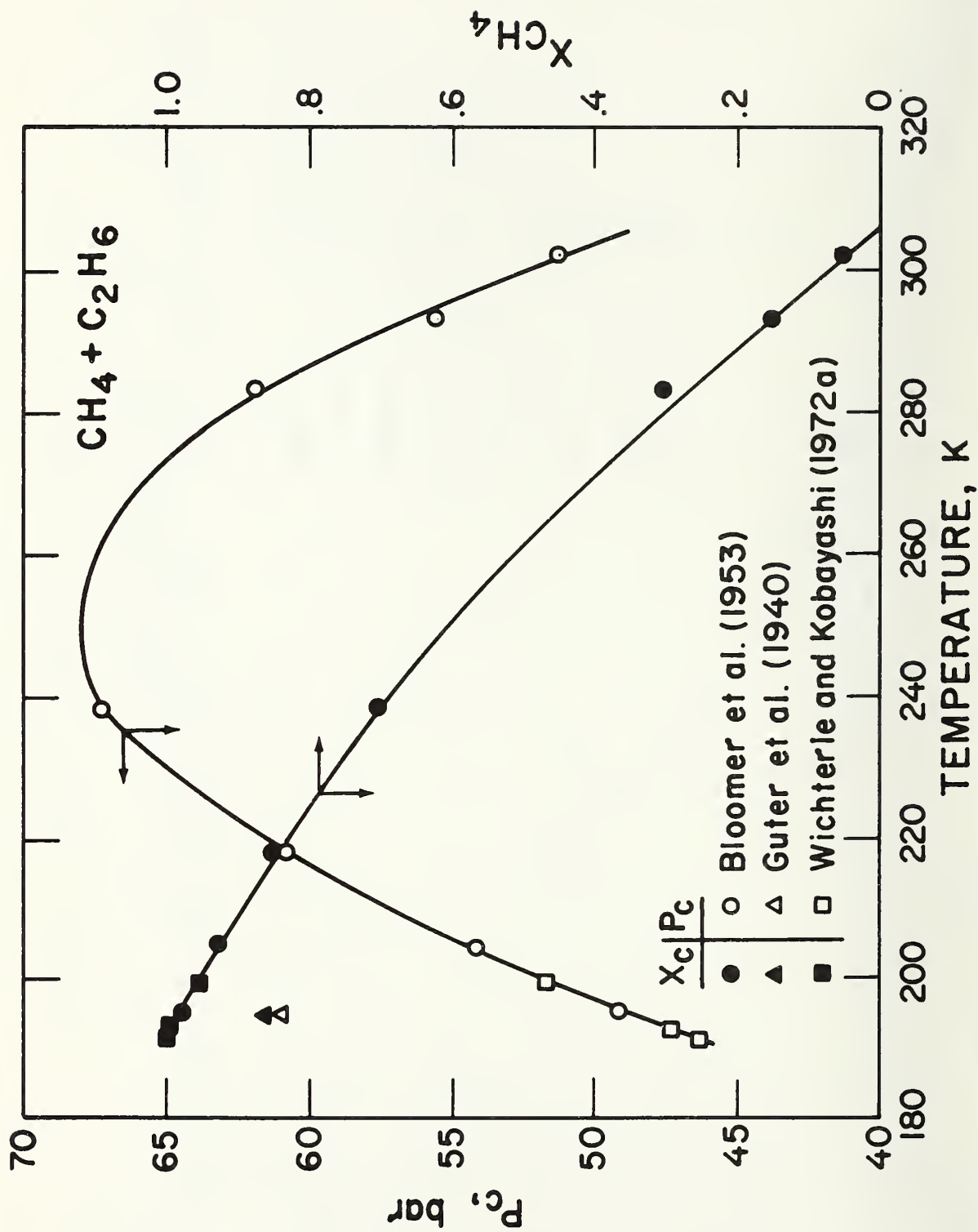


Figure 3. Critical pressure and composition as a function of temperature for the methane-ethane system.

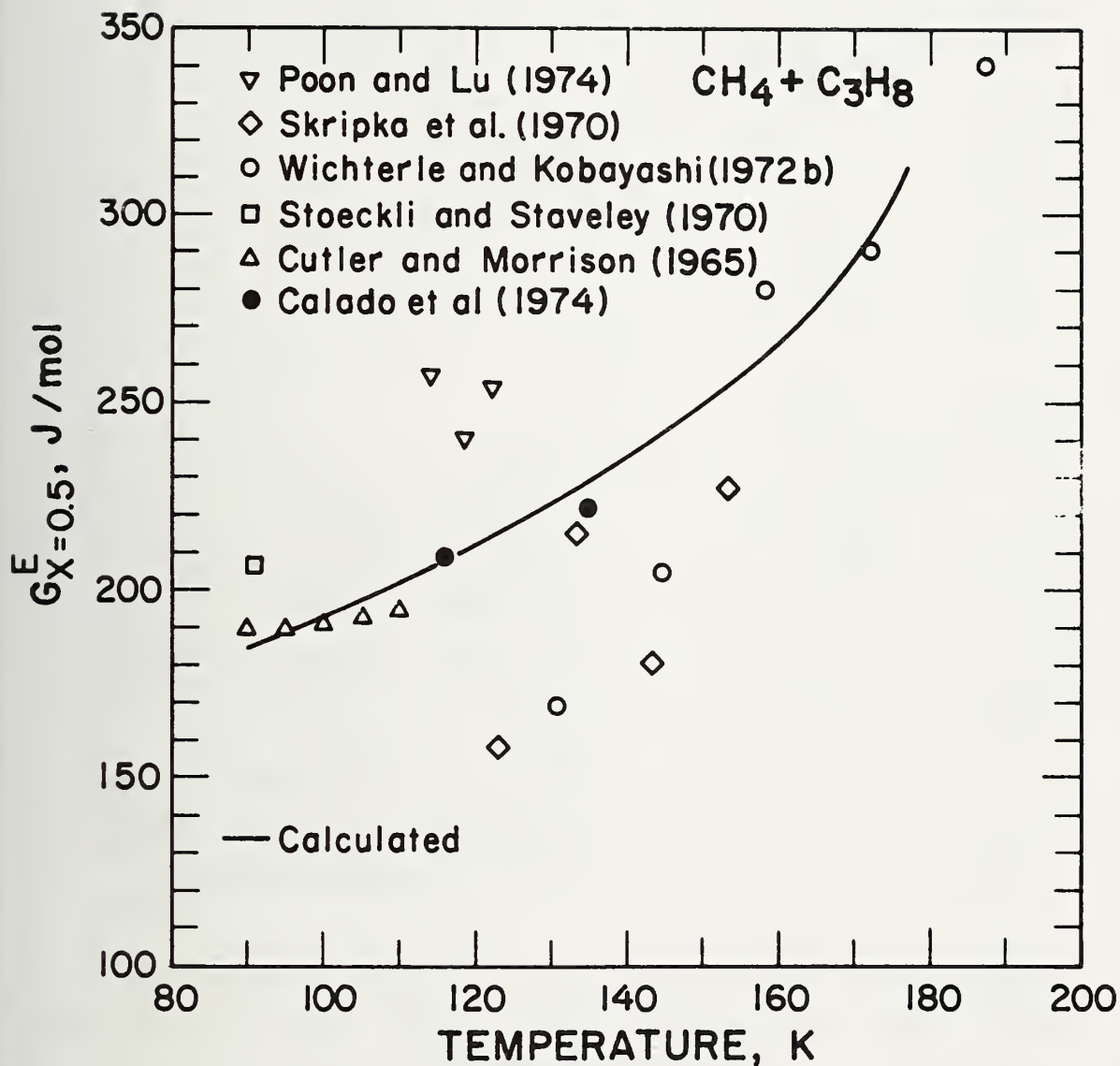


Figure 4. Equimolar G^E as a function of temperature for the methane-propane system. The solid line was calculated using a modified hard-sphere equation of state [3].

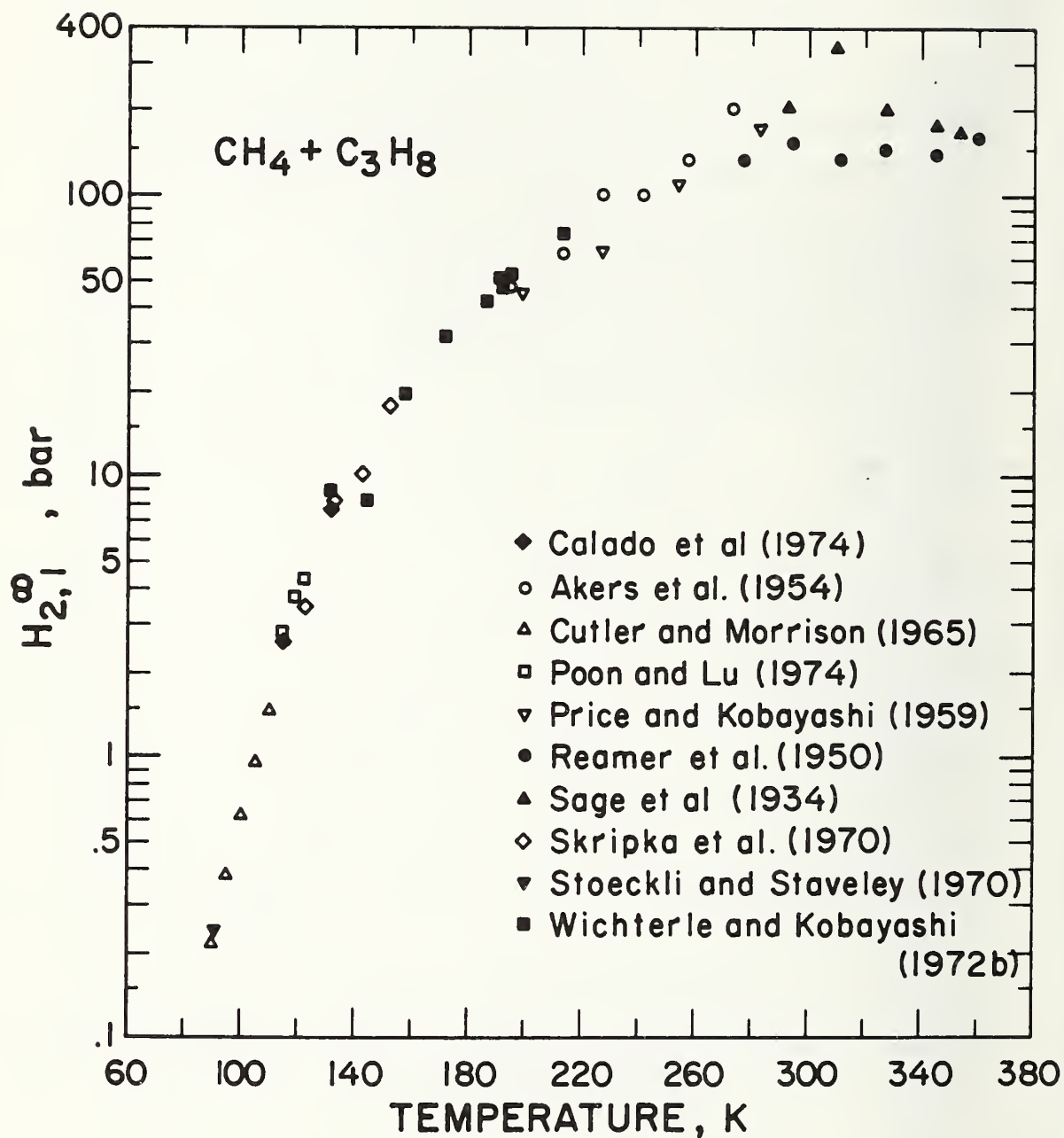


Figure 5. Infinite dilution Henry's constants as a function of temperature for the methane-propane system.

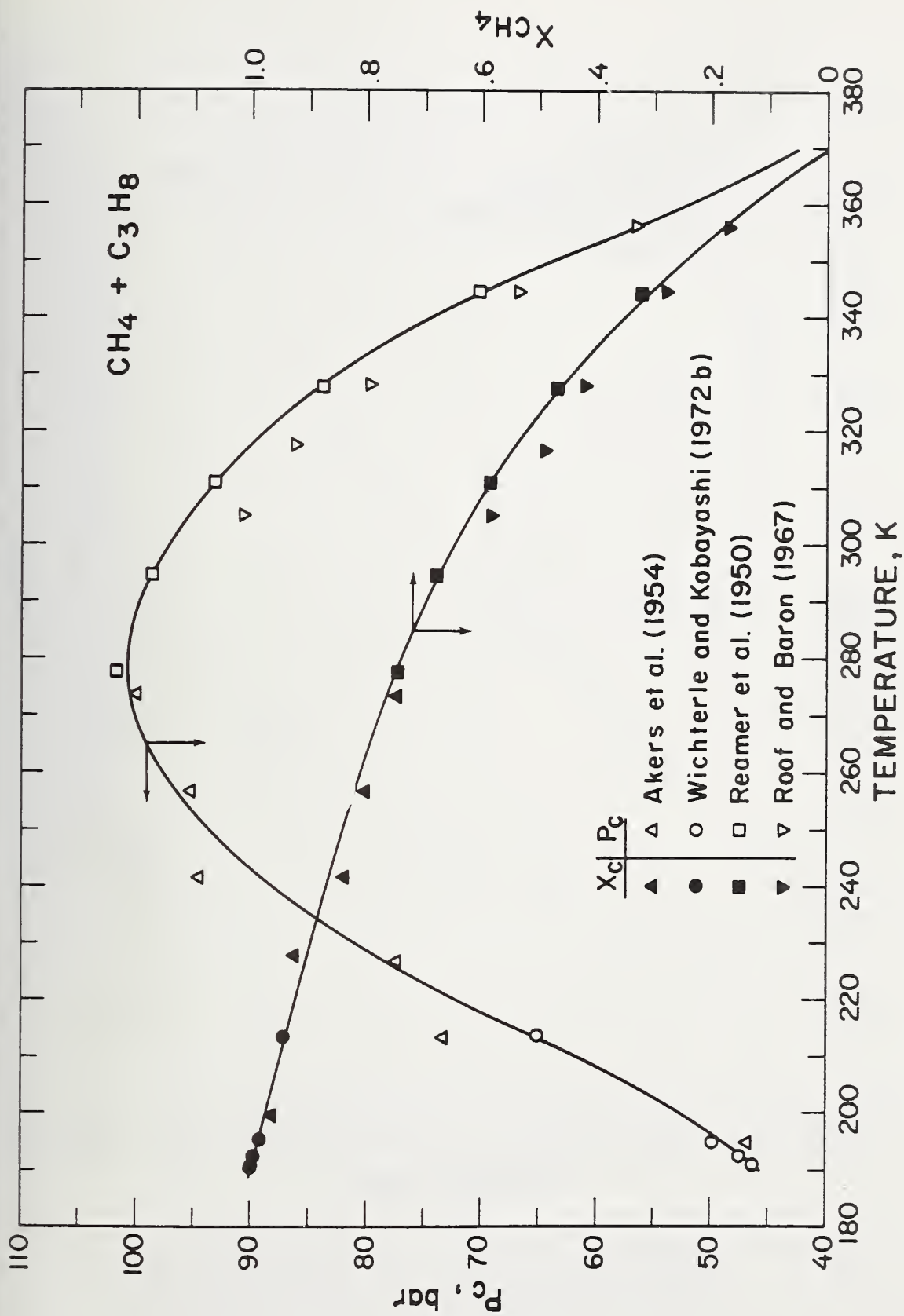


Figure 6. Critical pressure and composition as a function of temperature for the methane-propane system.

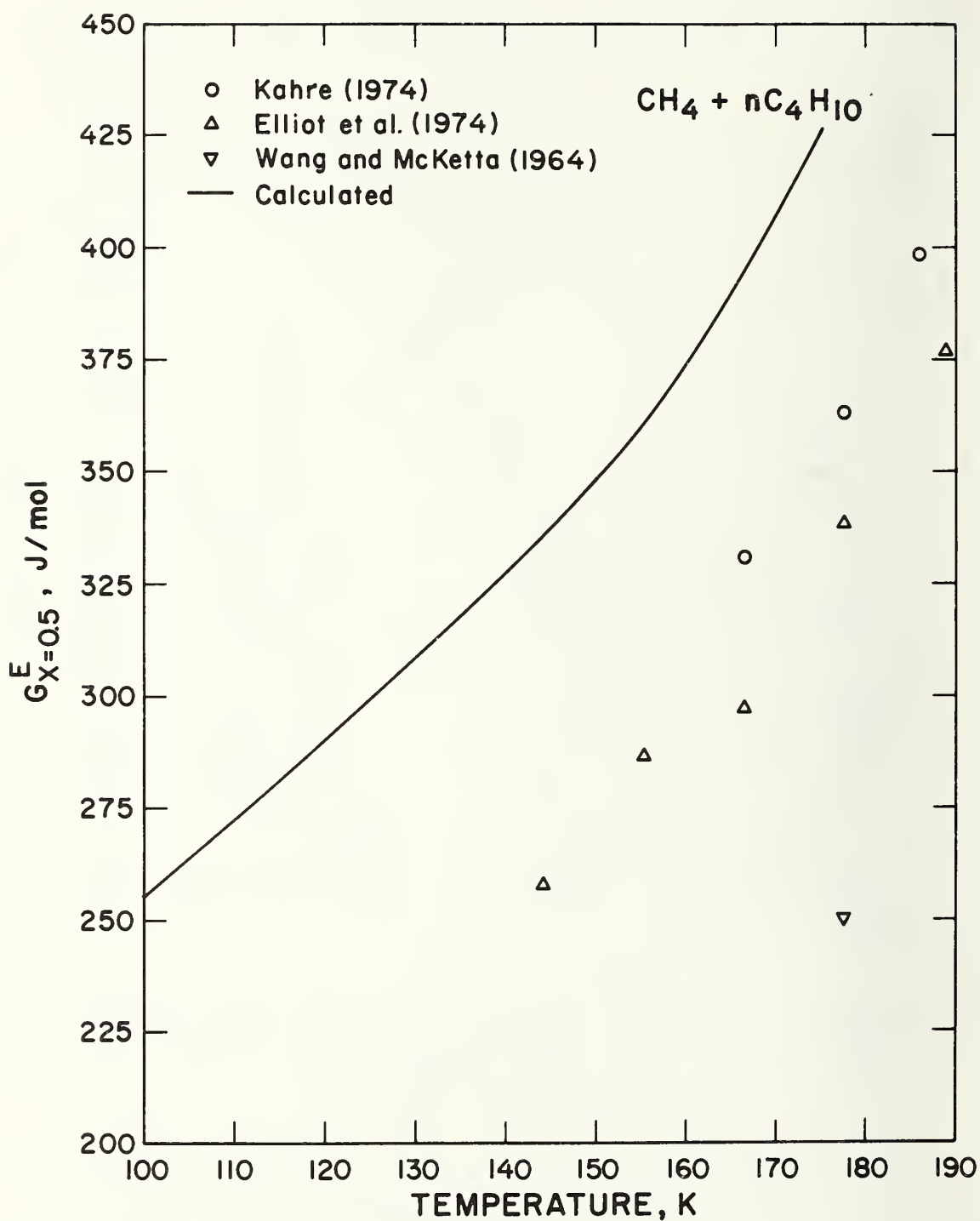


Figure 7. Equimolar G^E as a function of temperature for the methane-n-butane system. The solid line was calculated using a modified hard-sphere equation of state [3].

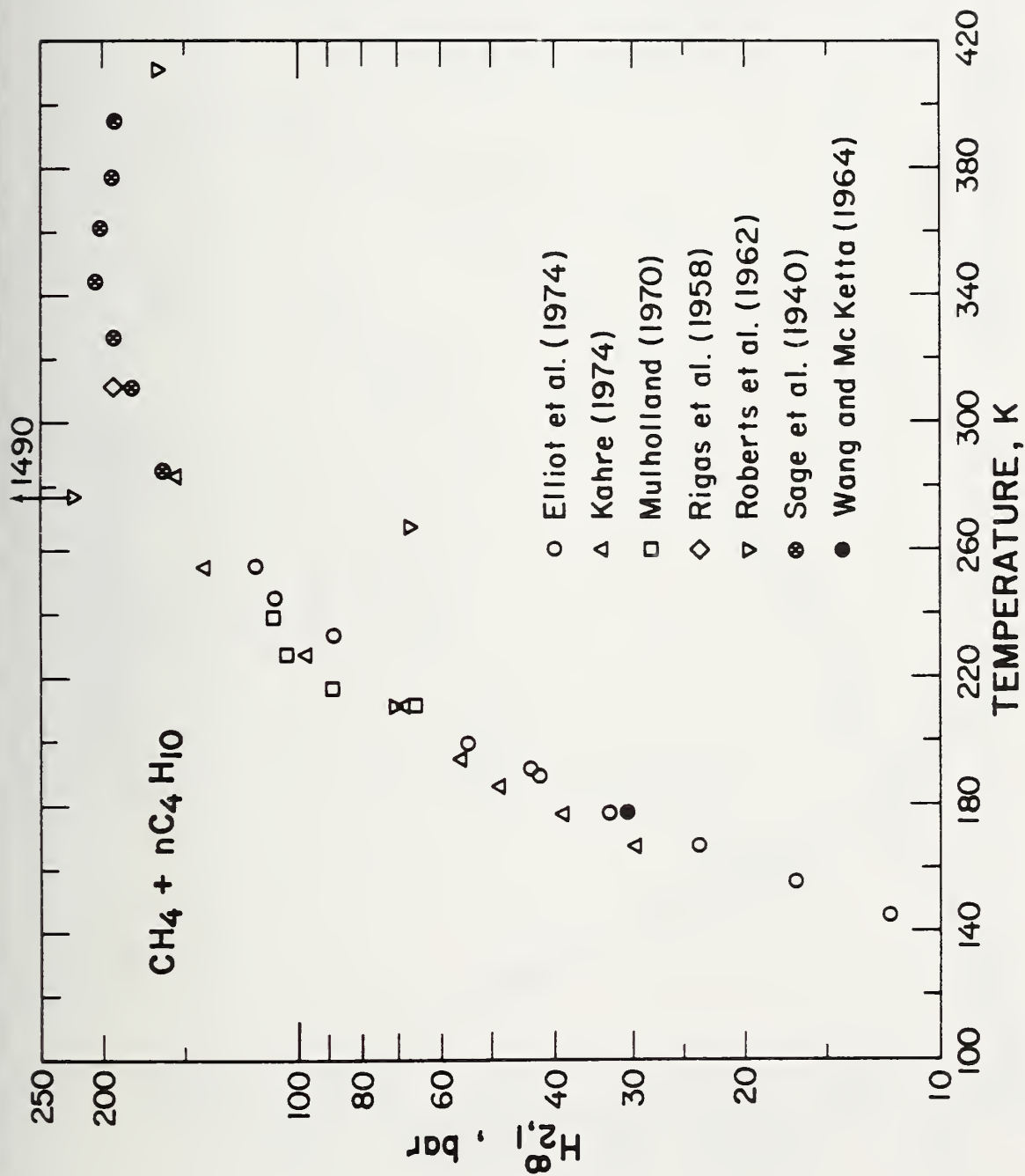


Figure 8. Infinite dilution Henry's constants as a function of temperature for the methane-n-butane system.

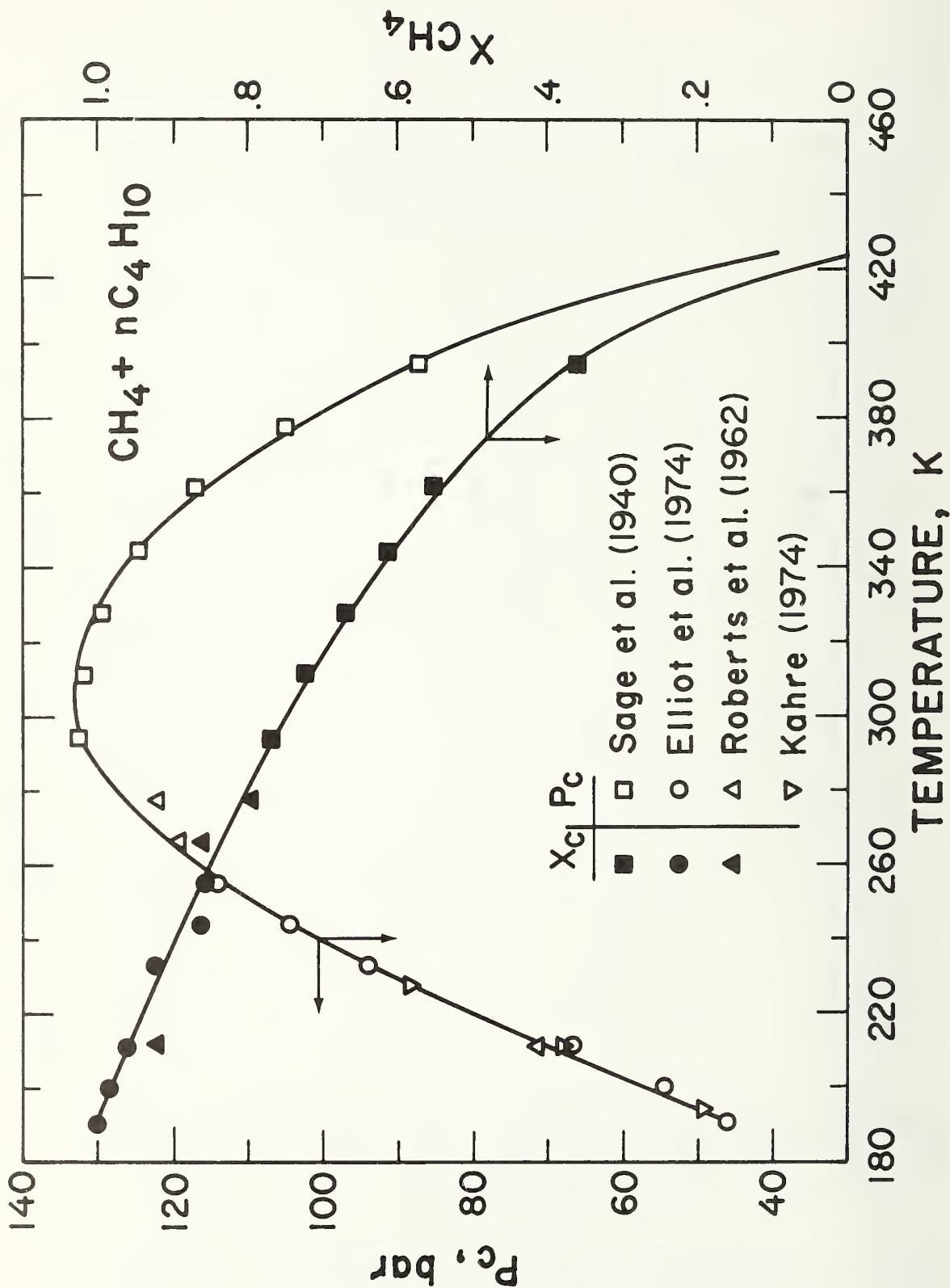


Figure 9. Critical pressure and composition as a function of temperature for the methane-n-butane system.

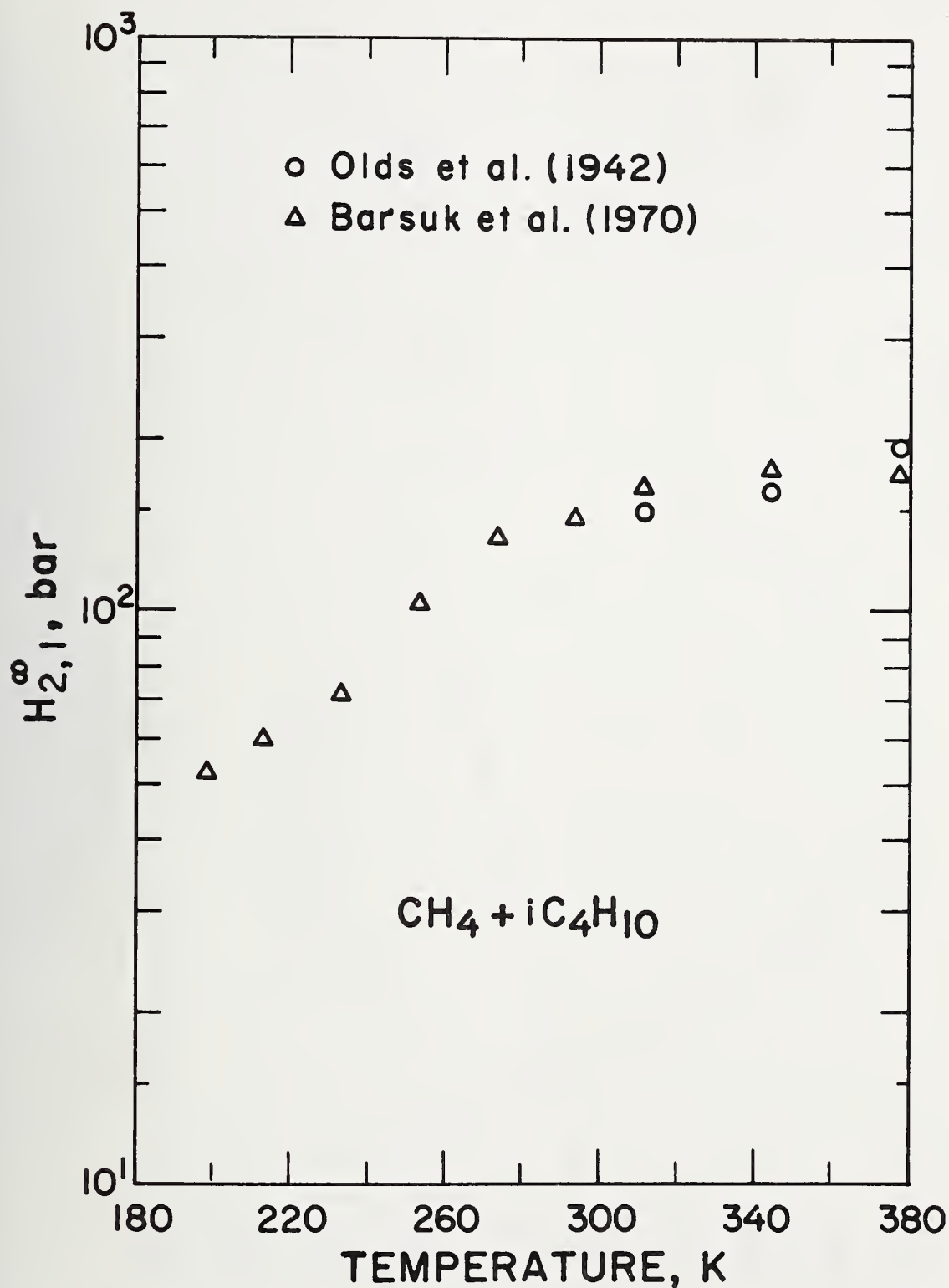


Figure 10. Infinite dilution Henry's constants as a function of temperature for the methane-isobutane system.

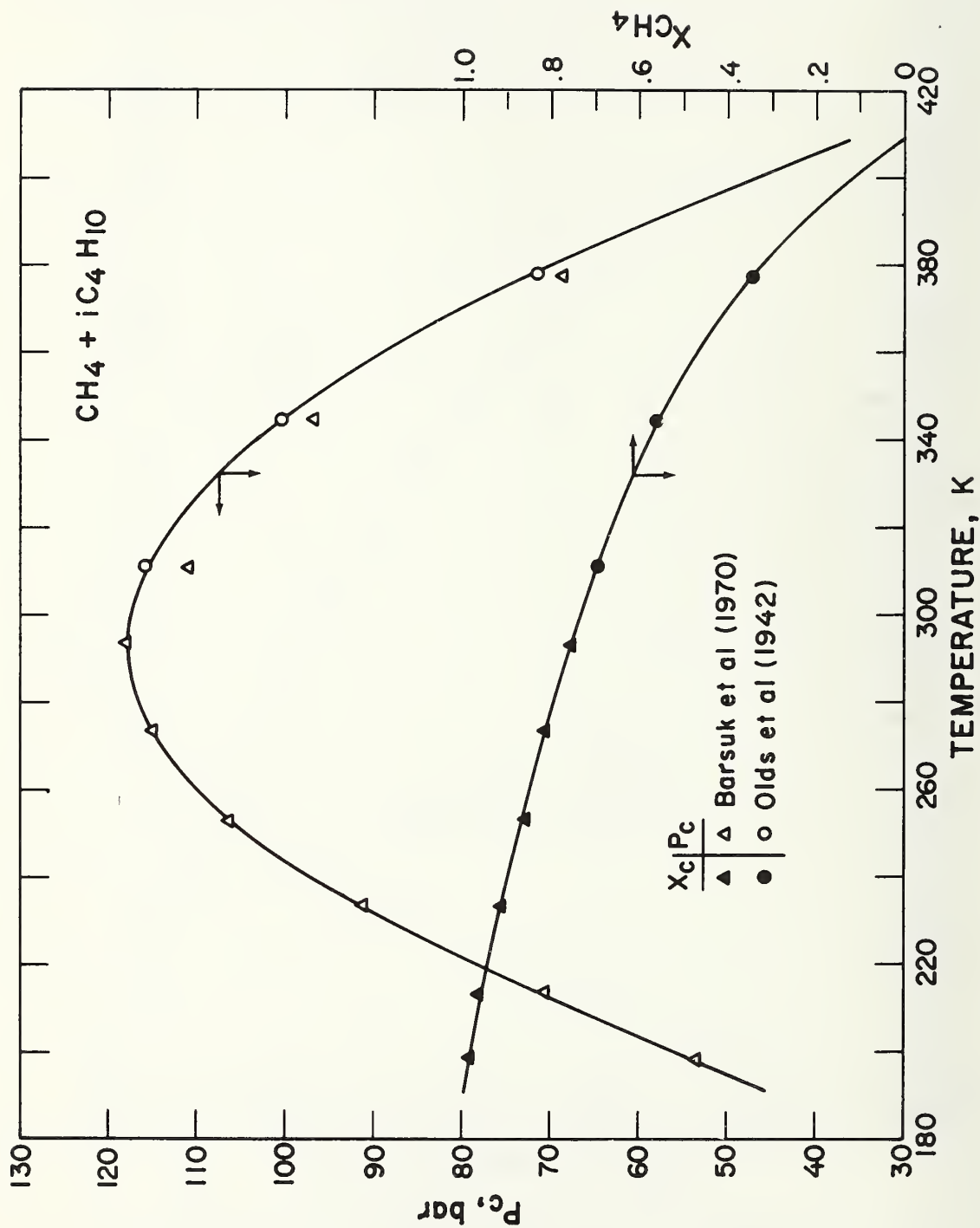


Figure 11. Critical pressure and composition as a function of temperature for the methane-isobutane system.

APPENDIX H

Isothermal composition measurements for both the equilibrium liquid and vapour phases have been determined for the nitrogen + methane system at eight temperatures between 112.00 and 180.00 K, and at pressures from 1 to 49 atm (1 to 50 bar). The internal consistency of these data is checked by comparing experimental and calculated thermodynamically consistent vapour phase compositions. Derived Henry's constants are used to provide a comparison between these data and those of other investigators.

R-917

Liquid–vapour phase equilibria in the N_2 – CH_4 system from 130 to 180 K

A. J. Kidnay, R. C. Miller, W. R. Parrish, and M. J. Hiza

Nomenclature

f	fugacity
G^l	excess Gibbs energy
H_{N_2, CH_4}	Henry's constant for N_2 in CH_4
K	equilibrium constant, y/x
P	total system pressure
p^0	vapour pressure
T	absolute temperature
x	liquid phase mole fraction
y	vapour phase mole fraction
P_c	critical pressure

Substantial quantities of nitrogen are present in most natural gases as they come from the well, and thus the design and operation of low temperature processes involving natural gas requires a knowledge of the nitrogen–methane phase equilibria over extensive ranges of pressure and temperature.

There have been two previous sets of measurements of liquid–vapour equilibria on the nitrogen–methane system at this laboratory: the work of Miller, Kidnay, and Hiza¹ at 112 K, and the work of Parrish and Hiza² at 95, 100, 105, 110, 115, and 120 K. The objective of the present research is to extend these measurements from temperatures above the critical point of nitrogen to near the critical point of methane, and thus provide an internally consistent data set over the methane liquid region. Six isotherms (130, 140, 150, 160, 170, and 180 K) have been measured over the entire liquid–vapour pressure region, and additional measurements made at 112 K and 120 K to tie in the present work with the earlier data from this laboratory.

Because of the growing interest in this system, the results of this work have been compared with existing data of other investigators, and a discussion of all liquid–vapour data for nitrogen–methane in the region above the critical point of nitrogen is given.

The authors are with the Cryogenics Division, Institute for Basic Standards, National Bureau of Standards, Boulder, Colorado 80302, USA. AJK is an Associate Professor at the Colorado School of Mines and RCM is an Associate Professor at the University of Wyoming. Received 2 May 1975.

Experimental procedure

The measurements were made in a closed-loop vapour–recirculation system. The general flow scheme is shown in Fig. 1 and the cryostat is shown in Fig. 2. The recirculation pump and the cryostat have been discussed in detail elsewhere^{3,4} and thus only a general description of the equipment and procedure will be given here.

The procedure followed was to cool (with liquid nitrogen) and evacuate the system, fill with pure methane, warm to the preselected operating temperature, and then measure the vapour pressure of the condensed methane. Measuring the vapour pressure ensures that the temperature and pressure measuring systems are functioning properly, and establishes the purity of the methane. Nitrogen gas was then introduced into the system, and recirculation of the vapour was initiated. The cold vapour from the top of the cell was heated to room temperature by exchange with the warm vapour stream returning to the cryostat. The vapour then passed through a large room temperature sample loop and was pumped back to the cell through the heat exchanger. The return vapour entered the cell near the bottom and bubbled through the liquid. When equilibrium was estab-

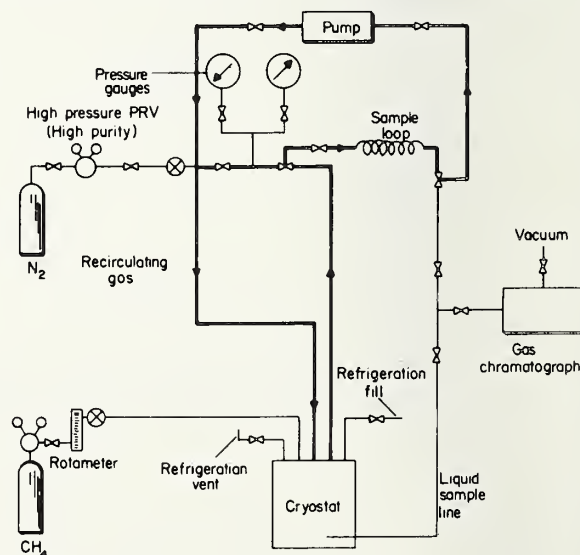


Fig. 1 Experimental apparatus

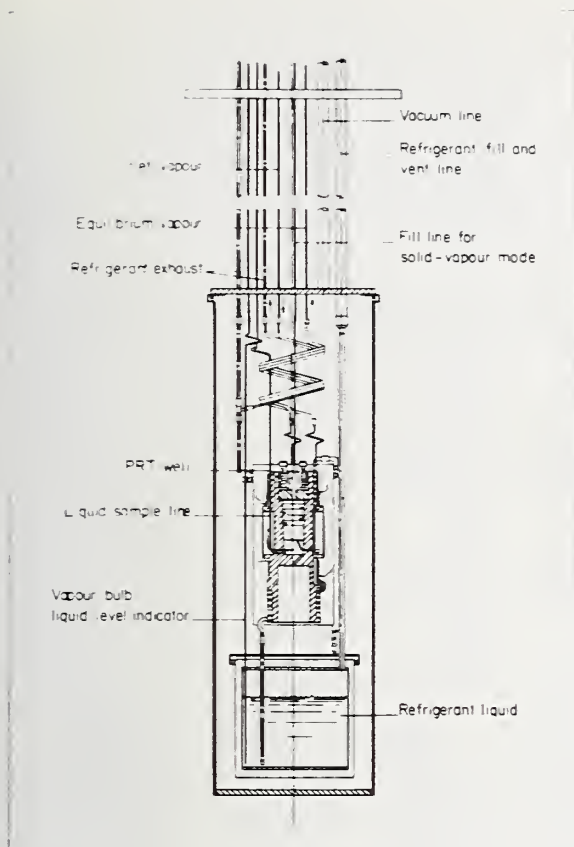


Fig. 2 Plan of cryostat

lished in the system, as determined by the constancy of the temperature and pressure measurements, the gas sample was isolated in the sample loop, and liquid samples were withdrawn through a capillary sample line, vaporized, and analysed in the gas chromatograph. Upon completion of the liquid analysis, the gas samples were withdrawn from the sample loop and analysed. The system was then repressurized with nitrogen to a new pressure, and the sequence repeated to establish another point on the isotherm.

All samples were analysed with a gas chromatograph using a thermal conductivity analyser, a 1 cm³ sample loop, helium carrier gas, and a 5 m column packed with 60/80 mesh molecular sieve 5A. The chromatograph was calibrated using samples of pure nitrogen and pure methane introduced into the chromatograph at varying pressures. When analysing samples from the equilibrium cell, the compositions of both components were determined chromatographically, and the sum of the compositions thus determined was normalized to 100%.

The temperature in the system was controlled and measured with an accuracy of ± 0.02 K using a calibrated (1PTS-68) platinum resistance thermometer. The pressures were measured with two bourdon tube gauges previously calibrated with an air piston gauge. The gauges had ranges of 0–20 bar and 0–50 atm (0–51 bar). In the range of 0 to 20 bars, the accuracy of the pressure measurements is ± 0.02 bar, while in the region above 20 bar, the accuracy is ± 0.05 bar.

The composition measurements are, in general, reproducible to 0.0005 in the mole fraction. The accuracy of the compositions is believed to be $\pm 1\%$ of the reported value or 0.001 in the mole fraction, whichever is the greater.

Results

The experimental results are presented in Table 1 and in Figs 3 and 4. The isotherms at 140.00 K and 160.00 K have been omitted to avoid cluttering the graphs. The methane vapour pressures of Table 1 were obtained from Goodwin⁵

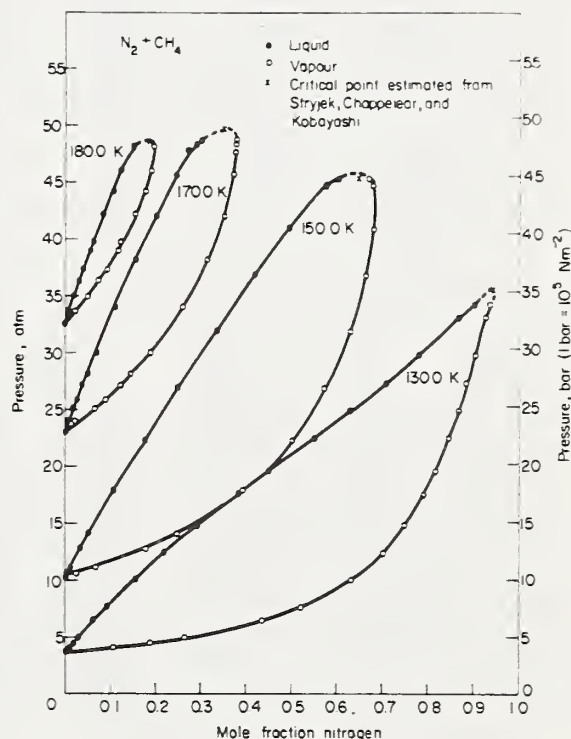


Fig. 3 Liquid and vapour compositions

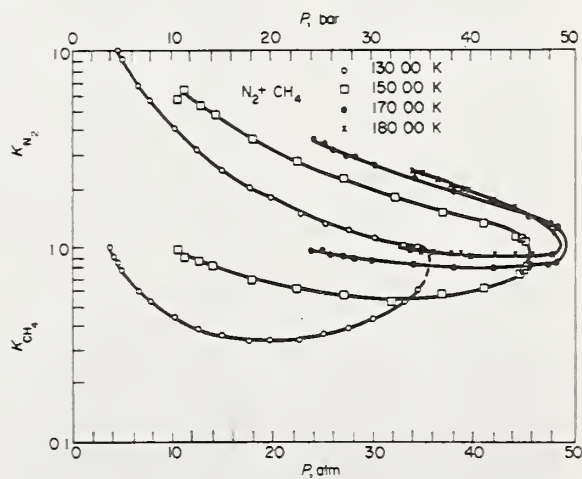


Fig. 4 K factors for nitrogen-methane

An excellent indication of the internal consistency of low pressure experimental data can be obtained by examination of pressure-composition and enhancement factor graphs for the liquid and vapour phases, respectively. For the liquid phase, a plot of $(P - p^0)$ against x_{N_2} must extrapolate smoothly to the origin as the N_2 mole fraction approaches zero. Additionally, in the region of very low N_2 concentration the relation between pressure and N_2 mole fraction

must be linear. Fig.5 is a typical graph for this investigation and it clearly shows the excellent consistency of the low pressure liquid phase data. The points at 130.00 K and 150.00 K lie on a straight line, while points at 170.00 K exhibit slight curvature. Another method for examining the liquid phase is to examine $(P - p^0)/x_{N_2}$ as a function of $(P - p^0)$ as shown in Fig.6. A plot of this type provides a severe test of the internal consistency of the experimental

Table 1. Experimental liquid-vapour equilibrium data for the nitrogen-methane system

P , bar	P , atm	x_{N_2}	x_{CH_4}	y_{N_2}	y_{CH_4}	K_{N_2}	K_{CH_4}
$T = 112.00 \text{ K}, p_{CH_4}^0 = 1.0443 \text{ bar} = 1.0306 \text{ atm}$							
1.965	1.939	0.0376	0.9624	0.4720	0.5280		
4.332	4.275	0.1504	0.8496	0.7654	0.2346		
10.538	10.400	0.5876	0.4124	0.9249	0.0751		
$T = 120.00 \text{ K}, p_{CH_4}^0 = 1.9190 \text{ bar} = 1.8939 \text{ atm}$							
5.234	5.166	0.1048	0.8952	0.6327	0.3673		
10.058	9.926	0.3012	0.6988	0.8182	0.1818		
$T = 130.00 \text{ K}, p_{CH_4}^0 = 3.681 \text{ bar} = 3.633 \text{ atm}$							
4.155	4.101	0.0097	0.9903	0.1098	0.8902	11.3196	0.8989
4.552	4.492	0.0186	0.9814	0.1862	0.8138	10.0108	0.8292
5.025	4.959	0.0292	0.9708	0.2640	0.7360	9.0411	0.7581
6.594	6.508	0.0641	0.9359	0.4339	0.5661	6.7691	0.6049
7.797	7.695	0.0926	0.9074	0.5201	0.4799	5.6166	0.5289
10.203	10.070	0.1547	0.8453	0.6316	0.3684	4.0827	0.4358
12.579	12.415	0.2188	0.7812	0.7018	0.2982	3.2075	0.3817
15.038	14.841	0.2941	0.7059	0.7508	0.2492	2.5529	0.3530
17.847	17.614	0.3822	0.6178	0.7932	0.2068	2.0754	0.3347
19.923	19.662	0.4512	0.5488	0.8166	0.1834	1.8098	0.3342
22.85	22.55	0.5516	0.4484	0.8463	0.1537	1.5343	0.3428
27.73	27.37	0.7077	0.2923	0.8860	0.1140	1.2519	0.3900
30.31	29.91	0.7828	0.2172	0.9054	0.0946	1.1566	0.4355
33.58	33.14	0.8676	0.1324	0.9285	0.0715	1.0702	0.5400
34.82	34.36	0.9017	0.0983	0.9393	0.0607	1.0417	0.6175
$T = 140.00 \text{ K}, p_{CH_4}^0 = 6.422 \text{ bar} = 6.338 \text{ atm}$							
7.221	7.127	0.0132	0.9868	0.1051	0.8949	7.9621	0.9069
8.298	8.189	0.0316	0.9684	0.2166	0.7834	6.8544	0.8090
9.258	9.137	0.0485	0.9515	0.2952	0.7048	6.0866	0.7407
10.108	9.976	0.0637	0.9363	0.3498	0.6502	5.4914	0.6944
14.056	13.872	0.1372	0.8628	0.5228	0.4772	3.8105	0.5531
18.047	17.811	0.2165	0.7835	0.6214	0.3786	2.8702	0.4832
21.94	21.65	0.3008	0.6992	0.6850	0.3150	2.2773	0.4505
26.59	26.24	0.4063	0.5937	0.7383	0.2617	1.8171	0.4408
30.76	30.36	0.5026	0.4974	0.7726	0.2274	1.5372	0.4572
32.69	32.26	0.5512	0.4488	0.7849	0.2151	1.4240	0.4793
36.33	35.85	0.6304	0.3696	0.8038	0.1962	1.2751	0.5308
37.86	37.36	0.6662	0.3338	0.8107	0.1893	1.2169	0.5671
40.39	39.86	0.7267	0.2733	0.8128	0.1872	1.1185	0.6850
42.00	41.45	0.7788	0.2212	0.8032	0.1968	1.0313	0.8897
$T = 150.00 \text{ K}, p_{CH_4}^0 = 10.414 \text{ bar} = 10.273 \text{ atm}$							
10.673	10.533	0.0038	0.9962	0.0224	0.9776	5.8947	0.9813
11.213	11.066	0.0106	0.9894	0.0675	0.9325	6.3679	0.9425
12.908	12.739	0.0333	0.9667	0.1776	0.8224	5.3333	0.8507
14.228	14.042	0.0518	0.9482	0.2479	0.7521	4.7857	0.7932
18.088	17.851	0.1082	0.8918	0.3938	0.6062	3.6396	0.6797
22.55	22.26	0.1788	0.8212	0.5026	0.4974	2.8110	0.6057

Table 1. Experimental liquid-vapor equilibrium data for the nitrogen-methane system (Cont'd)

P , bar	P , atm	x_{N_2}	x_{CH_4}	y_{N_2}	y_{CH_4}	K_{N_2}	K_{CH_4}
27.21	26.85	0.2510	0.7490	0.5742	0.4258	2.2876	0.5685
32.36	31.94	0.3377	0.6623	0.6288	0.3712	1.8620	0.5605
37.30	36.81	0.4231	0.5769	0.6630	0.3370	1.5670	0.5842
41.39	40.85	0.4951	0.5049	0.6812	0.3188	1.3759	0.6314
45.20	44.61	0.5763	0.4237	0.6813	0.3187	1.1822	0.7522
45.86	45.26	0.6042	0.3958	0.6712	0.3288	1.1109	0.8307
$T = 160.00 \text{ K}, p_{CH_4}^0 = 15.939 \text{ bar} = 15.731 \text{ atm}$							
16.813	16.593	0.0095	0.9905	0.0438	0.9562	4.611	0.9654
17.968	17.733	0.0223	0.9777	0.0979	0.9021	4.3901	0.9227
18.988	18.740	0.0334	0.9666	0.1394	0.8606	4.1737	0.8903
19.913	19.653	0.0448	0.9552	0.1742	0.8258	3.8884	0.8645
21.94	21.65	0.0684	0.9316	0.2406	0.7594	3.5175	0.8152
22.10	21.81	0.0714	0.9286	0.2458	0.7542	3.4426	0.8122
26.19	25.85	0.1205	0.8795	0.3442	0.6558	2.8564	0.7457
30.38	29.98	0.1756	0.8244	0.4184	0.5816	2.3827	0.7055
33.95	33.51	0.2243	0.7757	0.4657	0.5343	2.0762	0.6888
38.46	37.96	0.2820	0.7180	0.5051	0.4949	1.7911	0.6893
42.29	41.74	0.3333	0.6667	0.5289	0.4711	1.5869	0.7066
46.15	45.55	0.3937	0.6063	0.5422	0.4578	1.3772	0.7551
47.86	47.23	0.4246	0.5754	0.5360	0.4640	1.262	0.8064
48.38	47.75	0.4310	0.5690	0.5315	0.4685	1.233	0.8234
$T = 170.00 \text{ K}, p_{CH_4}^0 = 23.308 \text{ bar} = 23.003 \text{ atm}$							
24.27	23.95	0.0082	0.9918	0.0291	0.9709	3.5488	0.9789
25.39	25.06	0.0189	0.9811	0.0652	0.9348	3.4497	0.9538
26.20	25.86	0.0276	0.9724	0.0889	0.9111	3.2210	0.9370
27.47	27.11	0.0399	0.9601	0.1219	0.8781	3.0551	0.9146
28.43	28.06	0.0495	0.9505	0.1458	0.8542	2.9455	0.8987
30.36	29.96	0.0688	0.9312	0.1875	0.8125	2.7253	0.8725
34.43	33.98	0.1115	0.8885	0.2593	0.7407	2.3256	0.8337
38.58	38.08	0.1562	0.8438	0.3135	0.6865	2.0070	0.8136
42.52	41.96	0.2001	0.7999	0.3519	0.6481	1.7586	0.8102
46.31	45.70	0.2466	0.7534	0.3743	0.6257	1.5178	0.8305
48.33	47.70	0.2729	0.7271	0.3784	0.6216	1.3866	0.8549
48.95	48.31	0.2915	0.7085	0.3798	0.6202	1.3029	0.8754
49.39	48.74	0.3066	0.6934	0.3801	0.6199	1.240	0.894
$T = 180.00 \text{ K}, p_{CH_4}^0 = 32.883 \text{ bar} = 32.453 \text{ atm}$							
34.11	33.56	0.0089	0.9911	0.0230	0.9770	2.58	0.986
35.40	34.94	0.0202	0.9798	0.0494	0.9506	2.45	0.970
36.72	36.24	0.0327	0.9673	0.0738	0.9262	2.26	0.958
37.87	37.37	0.0434	0.9567	0.0936	0.9064	2.16	0.947
39.45	38.93	0.0588	0.9412	0.1192	0.8808	2.03	0.936
40.24	39.71	0.0632	0.9368	0.1260	0.8740	1.99	0.933
42.72	42.16	0.0863	0.9137	0.1572	0.8428	1.82	0.922
44.75	44.16	0.1083	0.8917	0.1786	0.8214	1.65	0.921
46.56	45.95	0.1254	0.8746	0.1919	0.8081	1.53	0.924
48.70	48.06	0.1567	0.8433	0.1992	0.8008	1.27	0.950

data, since very small deviations in the low concentration region are greatly magnified. Graphs of the type shown in Fig. 5, on the other hand, provide some information on the thermodynamic consistency of the data, since it is necessary that the data points be linear through the origin. For comparison, the nitrogen-methane data of Stryjek, Chapple, and Kobayashi⁶ are shown in Fig. 7. The amount of scatter exhibited by both data sets is not excessive for high quality data, and the deviation from linearity of

the isotherms as the critical temperature of the solvent is approached is also typical.

The enhancement factor, defined as $y_{CH_4}P/p_{CH_4}^0$, provides valuable insight into the vapour phase behaviour, since a plot of enhancement factor versus total pressure must form a smooth curve extrapolating to a value of unity at the vapour pressure of methane. Typical enhancement curves, shown in Fig. 8, demonstrate the high degree of consistency generally realized. Two of the isotherms measured by Stryjek,

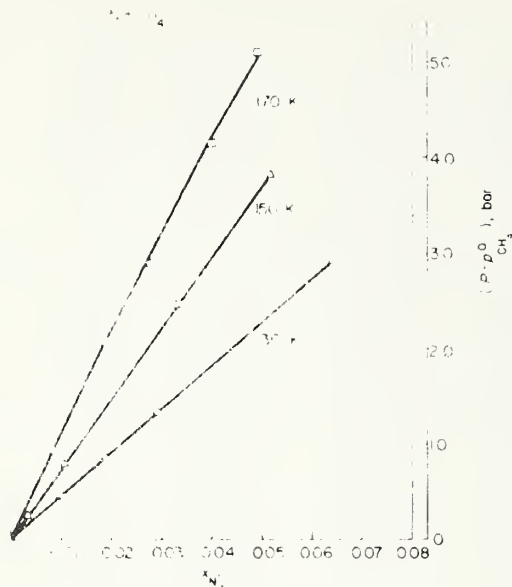


Fig. 5 Liquid phase compositions for N_2-CH_4

Chappelear, and Kobayashi are within 1 K of isotherms reported here, and in Figs 9 and 10 enhancement factors for these isotherms are compared. The agreement between the two sets of data is satisfactory.

The data of Table 1 at 112.00 K and 120.00 K are in excellent agreement with the earlier data from this laboratory.^{1,2}

Discussion

There have been nineteen previous experimental sets of measurements of liquid-vapour equilibrium in the nitrogen-methane system. Table 2 summarizes all of the previous work.

However, of the studies listed in Table 2, only those of Bloomer and Parent; Chang and Lu; Cines et al; Torochesnikov and Levius; Stryjek, Chappelear, and Kobayashi; and Yu and Lu are in the temperature region 130 to 180 K and present sufficient tabular data to attempt a meaningful comparison with the results of the present study. The data reported by Bloomer, Eakin, Ellington, and Gami as well as that reported by Ellington, Eakin, Parent et al for nitrogen-methane is the same data reported earlier by Bloomer and Parent. Brandt and Stroud, and Fastovskii and Petrovskii have very little data above 130 K and the results of Forg and Wirtz are presented only as graphs, so that comparison with our work is not worthwhile. It is also not clear whether data reported by Forg and Wirtz are original or a composite of the work of others.

Two methods are used to compare the available experimental data sets in the temperature region between the critical points of nitrogen and methane (126.20 to 190.56 K). First, a numerical method is used with the P - x data for each isotherm to calculate y values which are then compared to the experimental y values, and second, Henry's law constants are calculated from the data and plotted as a function of temperature.

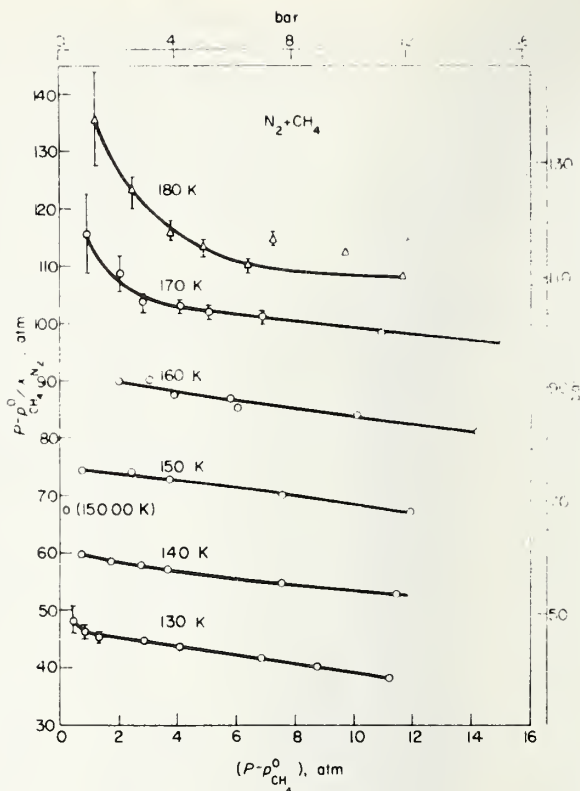


Fig. 6 Liquid phase compositions for N_2-CH_4

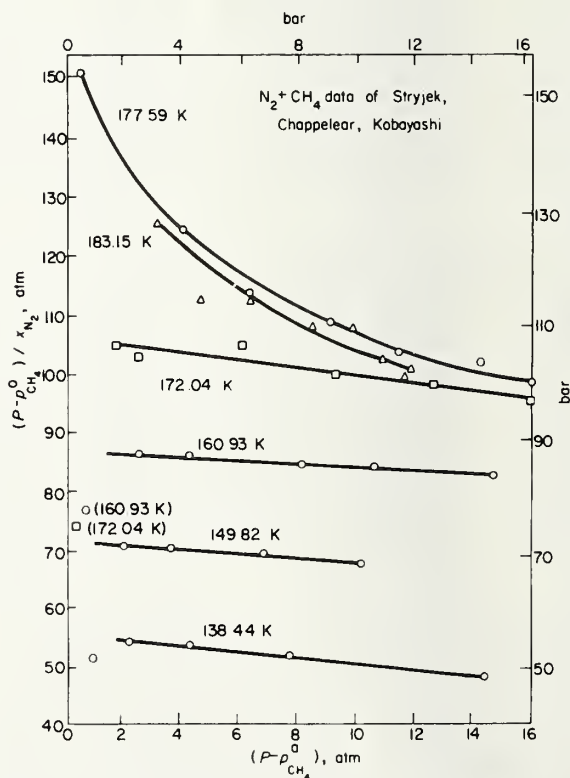


Fig. 7 Liquid phase compositions of Stryjek, Chappelear, and Kobayashi

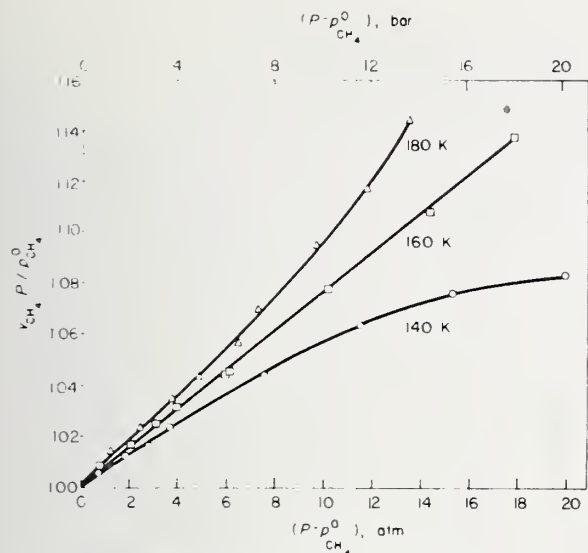


Fig.8 Enhancement factor for nitrogen-methane

Numerical method

It has been appreciated for quite some time that, in principle, the measurement of P - x - y data at a constant temperature is redundant (see for example, Redlich and Kister ²⁶ and Barker ²⁷), since it is possible in principle to calculate the third variable if two are known. Van Ness, Byer, and Gibbs ²⁸ have recently discussed this type of calculation in some detail, and Won and Prausnitz ²⁹ as well as Christiansen and Fredenslund ³⁰ have presented computational methods for determining y from constant temperature P - x data in high pressure binary systems containing one supercritical component. The work of Christiansen and Fredenslund is the basis for the comparisons presented here, and a brief description of their method follows.

Christiansen and Fredenslund use the orthogonal collocation technique to solve the non-linear differential equations relating the excess Gibbs energy to the activity coefficients that are used to calculate the mixture total pressure. The liquid phase compositions used in the calculation are roots of Legendre polynomials rather than experimentally determined x values. To determine the total pressures at the collocation points (that is, the interpolated x value at which the computations are made) the experimental P - x curve is interpolated with a cubic spline fitting procedure. The technique uses the interpolated P - x values to calculate the excess Gibbs energy, the activity coefficients, and finally the vapour phase composition at each collocation point. The calculated x versus y curve can then be interpolated to determine the y values for the experimental values of x . A modified Redlich-Kwong equation of state is used to calculate the necessary vapour phase thermodynamic properties. Since one component is supercritical the unsymmetric convention for activity coefficients is applied and the Henry's constant is required. This is obtained by extrapolating the curve of (f/x) versus x to infinite dilution using Lagrangian extrapolation. The P - x - y calculations involve a doubly iterative procedure; however, the outer iterative loop (which calculates y values)

usually takes less than ten iterations and the inner loop (which calculates the excess Gibbs energy) normally takes less than five iterations. For each isotherm, the programme is repeated seven times, using eight to fourteen collocation points. Generally, the variation in $|\Delta y|$ and the Henry's constant depend somewhat on the number of collocation points used, so at all isotherms studied the Δy and Henry's constants selected correspond to the number of collocation points yielding the minimum $|\Delta y|$.

The advantages of this technique are that it applies both above and below the solute critical temperature, provides a good estimate of the Henry's constant, and does not require an analytical expression for G^E as a function of x .

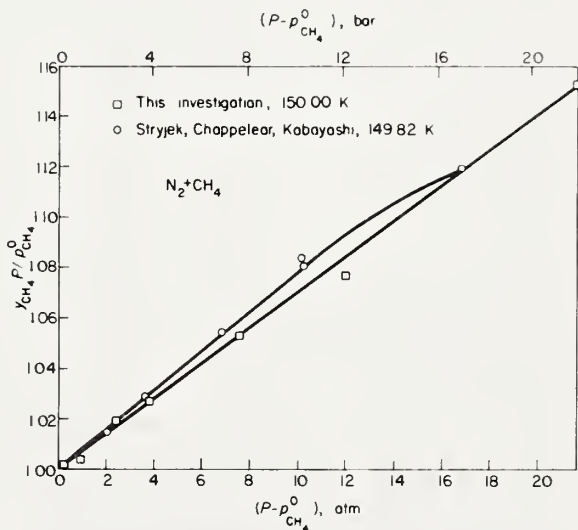


Fig.9 Comparison of enhancement factors at approximately 150 K

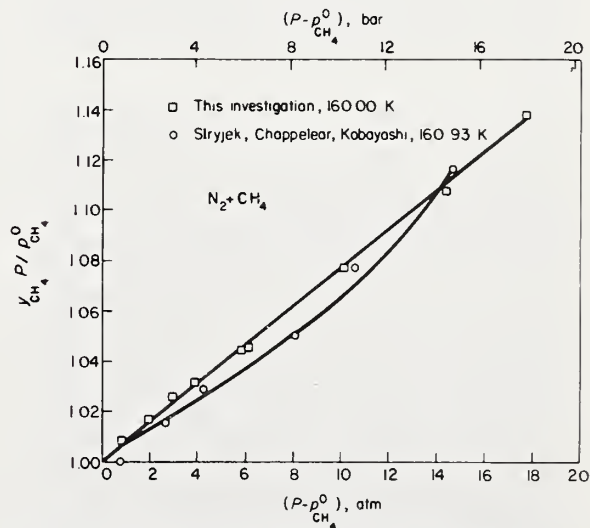


Fig.10 Comparison of enhancement factors at approximately 160 K

Table 2

Investigators	Reference No	Year	Approximate temp region covered, K	Approximate pressure region covered, ° atm	Remarks
Bloomer, Eakin, Ellington, Gami*	7	1955	100–187	7–48	Graphs only, data at constant composition
Bloomer, Parent*	8, 9	1952, 1953	91–191	1–48	Data at constant composition
Brandt, Stroud	10	1958	129–179	34	
Chang, Lu	11	1967	122, 171	3–49	
Cheung, Wang	12	1964	92–124	0–4	
Cines, Roach, Hogan, Roland	13	1953	100–172	1–44	
Ellington, Eakin,* Parent et al	14	1959	79–187	1–48	Data at constant composition
Fastovskii, Petrovskii	15	1957	90–150	1–16	
Forg, Wirtz	16	1970	80–180	1–103	Graphs only
Fuks, Bellemans	17	1967	84–89	1–2	Liquid phase only
McTaggart, Edwards	18	1919	77–109	1	
Miller, Kidnay, Hiza	1	1973	112	2–13	
Parrish, Hiza	2	Forthcoming	95–120	0–25	
Skripa, et al	19	1970	113	1–18	
Sprow, Prausnitz	20	1966	91	0–4	
Stryjek, Chappelle, Kobayashi	6	1972	114–183	1–50	
Torochesnikov, Levius	21	1939	89–133	0–24	Graphs only
Vellinger, Pons	22	1943	90	0–1	Graphs only
Yu, Lu	23	Forthcoming	130	4–34	

*Essentially the same data

The collocation technique also has several drawbacks, the major one being that it must interpolate values from the P - x curve instead of using the experimental points. This is not a serious problem if the P - x data are smooth and there are enough data points to allow a reliable interpolation, but if the data are not smooth then the method may not yield meaningful results. However, in this case the experimental data must be considered to be of questionable value.

A second disadvantage is the lack of an analytical or graphical method for eliminating the scatter in the liquid phase compositions. This failure to smooth the data means that a single bad data point on an isotherm can significantly affect the calculated results, and it also prevents the weighting of data points or the use of duplicate measurements.

Table 3 contains the Henry's constants and the average absolute deviation between experimental and calculated y values ($|\Delta y|$) calculated with the procedure of Christiansen and Fredenslund. Fig. 11 is a graphical comparison of the calculated y values, represented by the solid line, and the experimental measurements of this work at 170.00 K. The table also lists the number of experimental points where Δy is less than or greater than 1%. Predicting the critical region of a mixture is very difficult; therefore, the number of points where $|\Delta y|$ exceeds 1% is divided into two categories: those where the total pressure is less than 90% of the critical pressure and those where the total pressure

is within 10% of the critical pressure. If most of the points where $|\Delta y|$ exceed 1% are near the mixture critical point it is more than likely that the fault lies with the calculational procedure rather than the experimental data.

The failure of the 183.15 K isotherm of Stryjek et al to give consistent results is probably due to a failure in the equation of state, since the temperature is very near the critical temperature of methane (190.56 K). The 171.43 K isotherm of Chang and Lu and the 130.1 K isotherm of Yu and Lu could not be evaluated with the computer programme; this is probably due to excessive scatter in the experimental data.

Bloomer and Parent report only dew point and bubble point data. To convert their measurements into isotherms it was necessary to fit their bubble point pressures to the equation

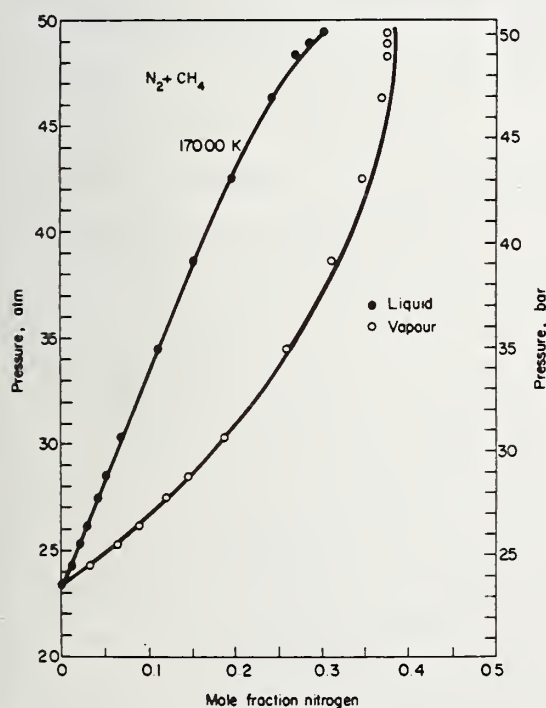
$$\log_e P = A + \frac{B}{T} + \frac{C}{T^2} \quad (1)$$

where A , B , and C are the least squares constants for each mixture. Bubble point pressures were then calculated at various temperatures. No attempt was made to interpolate y values from their dew point data.

The comparison of calculated and experimental y values shown in Table 3 indicates a high degree of internal consistency in the data of this investigation, the data of

Table 3

Investigator	T, K	H_{N_2, CH_4} , bars	Average deviation in Δy , %	Number of data points $ \Delta y > 1\%$			Remarks
				$ \Delta y < 1\%$	$P < 0.9P_c$	$P > 0.9P_c$	
This work	130.00	46.00	0.58	13	3	0	
	140.00	57.70	0.47	12	1	0	
	150.00	68.77	0.66	9	0	3	
	160.00	79.30	0.80	10	0	4	
	170.00	98.98	0.42	12	1	0	
	180.00	102.70	0.88	9	0	1	
Bloomer, Parent	127.59	42.84	—	—	—	—	Interpolated from 100 point data—see text for details of interpolation
	138.71	55.28	—	—	—	—	
	150.00	66.27	—	—	—	—	
	160.93	88.43	—	—	—	—	
Cines et al	133.15	48.97	1.00	8	5	1	
	144.26	72.00	0.63	11	1	0	
	155.37	91.48	0.74	9	1	0	
	172.04	112.83	2.23	0	6	0	
Stryjek et al	127.59	35.85	0.66	13	3	0	
	138.44	44.91	0.73	5	4	0	
	149.82	65.74	1.64	5	1	3	
	160.93	65.02	1.70	7	1	4	
	172.04	60.75	1.32	7	0	3	
	177.59	112.11	0.72	8	0	3	
	183.15	—	—	—	—	—	
Torochednikov and Levius	129.87	78.60	4.80	2	3	0	Computation method failed
	132.92	175.23	11.37	0	6	0	

Fig. 11 Comparison of calculated and experimental y values

Stryjek, Chappellear, and Kobayashi, and the data of Cines et al, with the exception of their isotherm at 172.04 K. The data of Torochednikov and Levius exhibit unacceptably high scatter, and, as noted previously, the isotherms of Chang and Lu, and Yu and Lu could not be processed with the computer programme.

Henry's constants

Henry's constant, defined by the equation

$$H_{N_2, CH_4} \equiv \lim_{x_{N_2} \rightarrow 0} \frac{f_{N_2}}{x_{N_2}} \quad (2)$$

is a valuable thermodynamic constant for two reasons. First, some of the procedures for calculating liquid–vapour equilibria of systems containing a supercritical component require the Henry's constant,²⁴ the second, it proves useful in testing the internal consistency of a set of experimental data and in comparing data sets from different investigations.

There are two basic approaches to the evaluation of Henry's constant from experimental data. In the first method, the vapour phase fugacity of the supercritical component is evaluated with a suitable equation of state, and (2) is directly applied to the data by preparing graphs of f_{N_2} versus x_{N_2} or (f_{N_2}/x_{N_2}) versus x_{N_2} and evaluating the slope of the curve at infinite dilution or the intercept, respectively. The disadvantage of this method is that it uses only the data in the region of very low nitrogen concen-

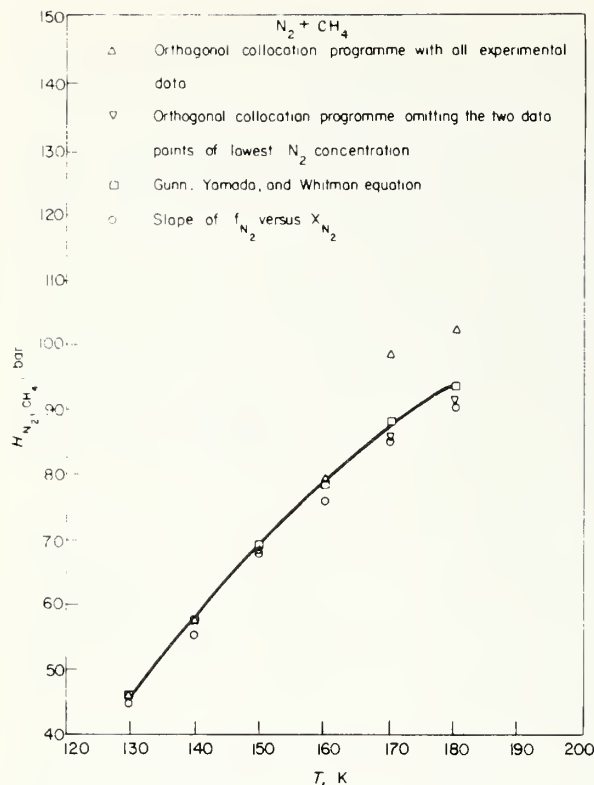


Fig.12 Henry's constants

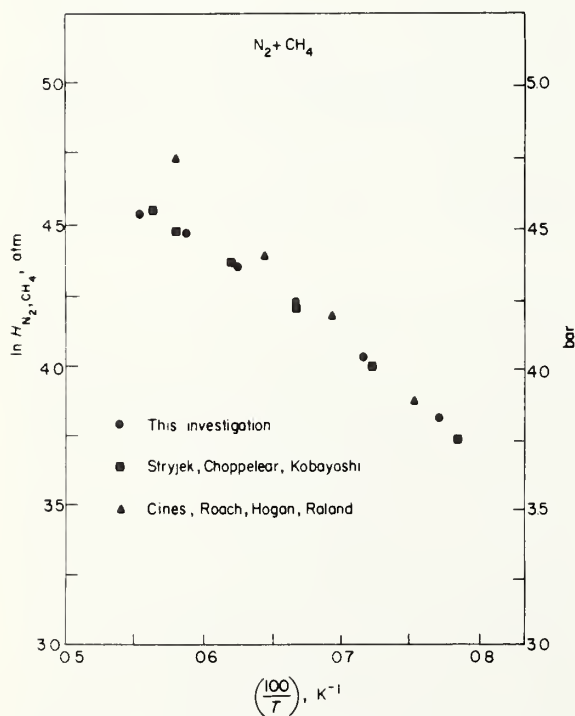


Fig.13 Comparison of Henry's constants

tration, which is a difficult region to measure experimentally. The second approach makes use of an integrated form of (2), such as the Krichevsky-Kasarnovsky equation,²⁴ the Krichevsky-Ilinskaya equation,²⁴ or the equation proposed recently by Gunn, Yamada, and Whitman.²⁵ These equations have the advantage of utilizing data in the mid-range of nitrogen concentrations, but have the drawback of requiring assumptions regarding the liquid-phase behaviour of the system. All of the methods for evaluating Henry's constant require the use of an equation-of-state for the vapour phase.

In Fig.12, Henry's constants determined by several different methods from the data of this investigation are shown. The isotherms at 170 and 180 K (Fig.12) were treated with the orthogonal collocation programme in two ways; first, using all of the experimental data, and second, omitting for each isotherm the two data points of lowest nitrogen concentration. Using all the data, the Henry's constants are in serious disagreement with values obtained from the other methods, while elimination of the two data points on each isotherm results in reasonably satisfactory agreement (5%) among the Henry's constants.

The difficulty encountered with the orthogonal collocation programme is due primarily to the particular extrapolation method used in obtaining the Henry's constants. With the method employed, very small errors in x_{N_2} at the lowest concentration level of N_2 can significantly alter the value of the Henry's constant. The effect of analytical imprecision in the liquid phase concentration measurements is shown by the vertical lines in Fig.6 for 130, 170, and 180 K.

To compare the Henry's constants from this work with those of previous investigations, the method of Gunn, Yamada, and Whitman was selected, and the comparison is made in Fig.13. The Henry's constants of this work and that of Stryjek, Chapple, and Kobayashi are in excellent agreement over the entire temperature region studied. The data of Cines et al are in good agreement at the lower temperatures, but show marked deviations at the higher temperatures. The smooth behaviour of the data in Fig.13 indicates good internal consistency for all the data.

Conclusions

The 'enhancement factor' graphs (Figs 8, 9, and 10), the pressure-composition graphs (Fig.5), and the Henry's constant graphs (Figs 12 and 13), as well as the results of the orthogonal collocation programme (Table 3, Fig.11) all demonstrate the high degree of internal consistency and the probable thermodynamic consistency of the data reported here. Unfortunately, there exists no technique for establishing beyond doubt the thermodynamic consistency of any high pressure liquid-vapour equilibria data.

The data of Stryjek, Chapple, and Kobayashi are in good agreement with this study, as are the lower temperature data of Cines et al. The isotherm of Cines et al at 172.04 K disagrees markedly with this study (Fig.13), and shows considerable internal scatter (Table 3). The reliability of the data reported by Chang and Lu, Yu and Lu, and Torochesnikov and Levius is questionable. Since Bloomer and Parent did not measure isothermal data, as was the case in all of the other studies, it is difficult to make a meaningful comparison with their results. However, the Henry's constants obtained from their data with the numerical orthogonal collocation programme appear to be in sub-

stantial agreement with those of Stryjek, Chapple, and Kobayashi, and with this study.

Summarizing, it appears that highly reliable data for the N_2 - CH_4 system are now available over the temperature region near the nitrogen critical point to approximately the methane critical point.

The authors are grateful to L. J. Christiansen and A. Fredenslund for the orthogonal collocation computer programme used in this work, to R. D. Gunn for calculating the Henry's constants of Fig. 13, and to the Office of Standard Reference Data of the National Bureau of Standards for partial financial support.

References

1. Miller, R. C., Kidnay, A. J., Iliza, M. J. *AIChE J* 19 (1973) 145
2. Parrish, W. R., and Iliza, M. J. *Advances in Cryogenic Engineering* 19 (Plenum Press, New York, 1974) 300
3. Iliza, M. J., Duncan, A. G. *Rev Sci Instr* 40 (1969) 513
4. Duncan, A. G., Iliza, M. J. *Advances in Cryogenic Engineering* 15 (Plenum Press, New York, 1970) 42
5. Goodwin, R. D. 'The thermophysical properties of methane, from 90 to 500 K at pressures to 700 bar,' US Dept of Commerce, NBS Tech Note 653
6. Stryjek, R., Chapple, P., Kobayashi, R. *J Chem Eng Data* 19 (1974) 334
7. Bloomer, O. T., Eakin, B. E., Ellington, R. T., Gami, D. C. 'Thermodynamic properties of methane-nitrogen mixtures', *Inst Gas Techn Res Bull* No 21 (1955).
8. Bloomer, O. T., Parent, J. D., 'Physical-chemical properties of methane-nitrogen mixtures', *Inst of Gas Techn Res Bull* No 17 (1952)
9. Bloomer, O. T., Parent, J. D. *Chem Eng Progr Symp Ser* 49, No 6 (1953) 11
10. Brandt, L. W., Stroud, L. *Ind Eng Chem* 50 (1958) 849
11. Chang, Shinn-der, Lu, B. C.-Y. *Chem Eng Progr Symp Ser* 63, No 81 (1967) 18
12. Cheung, H., Wang, D. I.-J. *Ind Eng Chem Fundam* 3 No 4 (1964) 355
13. Cines, M. R., Roach, J. T., Hogan, R. J., Roland, C. H. *Chem Eng Progr Symp Ser* 49 No 6 (1953) 1
14. Ellington, R. T., Eakin, B. E., Parent, J. D., Gami, D. C., and Bloomer, O. T. *Thermodynamic and Transport Properties of Gases, Liquids, and Solids*, Am Soc Mech Engrs, Heat Transfer Div (McGraw-Hill, New York, 1959) 180
15. Fastovskii, V. G., Petrovskii, Yu. *Zh Fiz Khim* 31 (1957) 231
16. Forg, W., Wirtz, P. *Linde Rep Sci Technol* 15 (1970) 46
17. Fuks, S., Bellemans, A. *Bull Soc Chim Belges* 76 (1963) No 5, 6, 290
18. McTaggart, H. A., Edwards, E. *Trans Roy Soc Can* 13 (1919) 47
19. Skripka, V. G., Nikitina, I. E., Zhdanovich, L. A., Sirotin, A. G., Benyaminovich, O. A. *Gasov Prom* 15, No 12 (1970) 35
20. Sprow, F. B., Prausnitz, J. M. *Cryogenics* 6 (1966) 338
21. Torochesnikov, N. S., Levius, L. A. *Zh Khim Prom* 16 (1971) 19. This data appears in graphical form in Ruhemann, M. *The Separation of Gases* (Oxford Univ Press, 1949) 54
22. Vellinger, E., Pons, E. *Compt Rend* 217 (1943) 689
23. Yu, P., Lu, B. C.-Y. *Advances in Cryogenic Engineering* 20 (1975)
24. Prausnitz, J. M. *Molecular Thermodynamics of Fluid-Phase Equilibria*, (Prentice-Hall, Englewood-Cliffs, NJ, 1969)
25. Gunn, R. D., Yamada, T., Whitman, D. *AIChE J* 20 (1974) 906
26. Redlich, O., Kister, A. T. *J Am Chem Soc* 71 (1949) 505
27. Barker, J. A. *Australian Jour of Chem* 6 (1953) 207
28. Van Ness, H. C., Byer, S. M., Gibbs, R. E. *AIChE J* 19 (1973) 238
29. Won, K. W., Prausnitz, J. M. *Ind Eng Chem Fund* 12 (1973) 459
30. Christiansen, L. J., Fredenslund, Aa. *AIChE J* 21 (1975) 49

SCIENCE & PUBLIC POLICY

the international journal of the Science Policy Foundation

current awareness for busy people in

**government · industry · business ·
education · research**

SCIENCE & PUBLIC POLICY

- provides information on national policies for science and technology and their effects
- examines the roles of science and technology in the operations of government (local, national and international), industry and business
- analyses the social and political environments within which science and technology operate
- assesses appropriate methodologies, information systems and organisational forms
- explores various types of public participation and their influence on national and international policies

The journal contains short, pithy news items, concise reports, comment, commissioned reviews, facts in figures, book reviews and extensive bibliographies.

The information is gathered through a worldwide network of national correspondents who are intimately involved in researching and applying science and public policy in their country.

Subscription £25.00 (\$65.00) per year (12 issues) including postage by fastest route. A special annual rate of £10.00 (\$26.00) is available for the individual who certifies that the copies are for his/her personal use and who is the full-time employee of a current full-price establishment subscriber at the same address.

IPC Business Press Ltd, Oakfield House, Perrymount Road, Haywards Heath, Sussex, England

Published monthly by IPC Science and Technology Press Ltd: publishers of *FUTURES*, *ENERGY POLICY* and *RESOURCES POLICY*.



APPENDIX I

FRACTURE MECHANICS AND ITS APPLICATION TO CRYOGENIC STRUCTURES*

H. I. McHenry

Cryogenics Division
Institute for Basic Standards
National Bureau of Standards
Boulder, Colorado 80302

ABSTRACT

A tutorial review of fracture mechanics is presented with emphasis on the application of this technology to cryogenic structures. The concepts of linear-elastic and elastic-plastic fracture mechanics are briefly reviewed. Test methods and representative data for fatigue crack growth and fracture toughness of structural alloys at cryogenic temperatures are summarized. The elements of a fracture control plan are presented and applications of fracture mechanics to cryogenic structures are described.

Key Words: Crack propagation; cryogenics; fracture mechanics; fracture toughness; material properties; structures.

* Contribution of NBS--not subject to copyright.

FRACTURE MECHANICS AND ITS APPLICATION TO CRYOGENIC STRUCTURES*

H. I. McHenry

Cryogenics Division
Institute for Basic Standards
National Bureau of Standards
Boulder, Colorado 80302

INTRODUCTION

The hazardous nature of many cryogenic fluids requires the use of conservative design procedures to assure adequate structural safety. The prevention of brittle fracture is an important consideration because of the sudden and uncontrolled nature of such failures. Experience gained from service failures of many engineering structures indicates that most brittle fractures are initiated by small flaws that grow, as cracks, to a critical size during operation. Accordingly, there are three elements to the fracture problem: 1) the initial flaw, 2) crack growth and 3) crack tolerance. To account for these factors, a new design approach, based on fracture mechanics, is being developed and applied in varying degrees to the design of nuclear pressure vessels,¹ bridges,² aircraft³ and missiles.⁴

Fracture mechanics is the study of the influence of loading, crack size and structural geometry on the fracture resistance of materials containing cracks. When applied to design the objective of the fracture mechanics analysis is to limit operating stresses such that a pre-existing flaw of assumed initial size will not grow to critical size during the desired service life of the structure. Service life is calculated on the basis of probable initial flaw sizes limited by inspection, a stress analysis of the structure and experimental data relating crack growth and fracture to fracture mechanics parameters.

In this paper, the concepts of fracture mechanics and their application to the design of cryogenic structures are reviewed. Emphasis is placed on imparting an understanding of the technology, a review of the information available and an appreciation of the many factors contributing to the fracture problem.

* Contribution of NBS--not subject to copyright.

LINEAR ELASTIC FRACTURE MECHANICS

The physical basis of fracture mechanics stems from the work of Griffith⁵ who demonstrated that the strain energy released upon crack extension is the driving force for fracture. The strain energy, V , is the work done by load, P , causing a displacement, Δ :

$$V = \frac{P\Delta}{2} = \frac{CP^2}{2} \quad (1)$$

where, $C = \frac{\Delta}{P}$ = elastic compliance.

The loss of elastic energy upon crack extension of unit area, A , is defined as the strain energy release rate, G :

$$G = - \left. \frac{dV}{dA} \right|_{\Delta} = \frac{P^2}{2} \frac{dC}{dA} = \left. \frac{dV}{dA} \right|_P \quad (2)$$

Irwin and Kies⁶ used this relationship to determine the fracture resistance of structural materials, G_c , by measuring the critical load, P_c , in a specimen with a known compliance function, dC/dA .

The Stress Intensity Factor

Irwin,⁷ who determined the stress distribution near the tip of a crack located in a linear elastic body, developed a stress analysis basis for fracture mechanics. The magnitude of the crack tip stress field, σ_{ij} , was found to be proportional to a single parameter, K , the stress intensity factor:

$$\sigma_{ij} = \frac{K}{\sqrt{2\pi r}} f_{ij}(\theta) = K \cdot f(\text{position}) \quad (3)$$

where, r and θ are cylindrical position coordinates; $r = 0$ at the crack tip and $\theta = 0$ in the crack plane. K is a function of the applied stress, σ , crack length, a , and a factor dependent on structural geometry, $Y(a)$:

$$K = Y(a)\sigma\sqrt{\pi a} \quad (4)$$

Tada, Paris and Irwin⁸ and Sih⁹ have published handbooks of K formulae for various geometries and boundary conditions.

Irwin⁷ demonstrated that the strain energy-release rate and stress intensity approaches are related:

$$K^2 = E'G \quad (5)$$

where, for plane stress, $E' = E$, the elastic modulus; and for plane strain, $E' = E/(1-\nu^2)$, where ν is Poisson's ratio. Thus, it is equivalent to attribute the driving force for fracture to the crack tip stress field, which is proportional to K , or to the elastic strain energy release rate, G . The stress intensity, K , is used more commonly than G because K can be computed for different structural geometries using stress analysis techniques.

Fracture Toughness

Fracture occurs when the crack tip stress field reaches a critical magnitude, i.e., when K reaches K_C , the fracture toughness of the material. K_C is a mechanical property that is a function of temperature, loading rate and microstructure, much the same as yield strength is; however, K_C is also a function of the extent of crack tip plasticity relative to the other specimen (or structural) dimensions. If the plasticity is small compared to the specimen dimensions and the crack size, then K_C approaches a constant minimum value defined as K_{IC} , the plane strain fracture toughness.

Measurements of fracture toughness based on linear elastic theory are limited to the case of plane strain testing in accordance with ASTM E 399.¹⁰ The dimensional criteria in this specification are:

$$B, a, W-a \geq 2.5 \left(\frac{K_{IC}}{\sigma_{ys}} \right)^2 \quad (6)$$

where, B , a and W are defined in Figure 1. The specimens are precracked by fatigue cycling to an initial crack length of $a/W = 0.5$ and subsequently loaded to failure. K_{IC} is calculated from the critical load, P_Q , the measured crack length, the specimen dimensions and the specimen calibration function, $Y(\frac{a}{W})$, as follows:

$$K_Q = \frac{P_Q}{B\sqrt{W}} Y\left(\frac{a}{W}\right) \quad (7)$$

$K_{IC} = K_Q$ if all the conditions of ASTM E 399 are met, i.e., precracking procedures, load-displacement record, specimen dimensions, etc. At cryogenic temperatures, the test procedures are similar to those employed at room temperature.¹¹ A cryostat, such as the one shown in Figure 2, is used to contain the cryogen for obtaining the desired test temperature.

Crack Tip Plasticity

Applicability of the linear elastic analysis has been extended to conditions approaching net section yielding by correcting for the zone of plasticity that exists at the crack tip.¹² The idea is that the plastic material at the crack tip strains without carrying the incremental load; therefore, in the elastic sense, the crack behaves as if it were slightly longer. The adjustment is made by adding the radius of the plastic zone, r_y , to the apparent crack length:

$$K = Y(a+r_y) \sigma \sqrt{a+r_y} \quad (8)$$

$$r_y = \frac{1}{2\pi} \left(\frac{K}{\sigma_Y} \right)^2 \quad (9)$$

where, σ_Y is the yield strength at the crack tip.

The r_y correction modifies the crack tip stress field to account for the elastic stress redistribution due to the localized plasticity.

The extent of crack tip plasticity is influenced by specimen dimensions. This is particularly true for thickness. As specimen thickness increases, σ_Y increases from σ_{ys} to $\sqrt{3} \sigma_{ys}$ due to through-the-thickness elastic constraint.¹³ The maximum value of σ_Y is reached when the plastic zone size is limited to about 5 percent of the thickness. Thus, in a given material, the plastic zone size as computed by Equation 9 can vary with thickness by a factor of three--leading to a strong dependence of K_{IC} on thickness as shown in Figure 3. The inflection point of the curve in Figure 3 occurs at approximately $(K_{IC}/\sigma_{ys})^2$; thus, for maximum toughness:

$$B < \left(\frac{K_{IC}}{\sigma_{ys}} \right)^2 \text{ or } K_{IC} > \sigma_{ys} \sqrt{B}. \quad (10)$$

Equation 8 is often useful in material selection.¹⁴

Summary Comments

The crack tip stress field is the driving force for fracture and the magnitude of this stress field is proportional to the stress intensity factor, K . K is a function of crack size, applied stress and structural geometry and can be computed using stress analysis methods. The resistance to fracture is a material property defined as the fracture toughness, K_c ; fracture occurs when $K = K_c$. Thus, for a given structural geometry and material, critical crack sizes can be determined as a function of applied stress and vice-versa:

$$a_c = \left[\frac{K_c}{\sigma Y(a)} \right]^2. \quad (11)$$

The approach is applicable to conditions of localized crack tip plasticity, i.e., where $\sigma \leq .8\sigma_{ys}$ or $r_y \leq 0.3a$, when the r_y correction is used to account for crack tip plasticity.¹⁵

ELASTIC PLASTIC FRACTURE MECHANICS

Many of the high toughness structural materials used for cryogenic structures undergo extensive plastic deformation prior to fracture. Thus, the concepts of linear elastic fracture mechanics are being extended to account for elastic-plastic behavior. Three approaches currently under development include: the crack opening displacement (COD), the J integral and the R-curve.

The Crack Opening Displacement

The crack opening displacement concept is a crack tip strain criterion for fracture stemming primarily from the work of Wells.¹⁶ For a crack in an elastic body, the crack opening displacement, v , at a distance r from the crack tip is given by Westergaard's¹⁷ displacement equation:

$$v = \frac{2K}{\pi E'} \sqrt{2\pi r}. \quad (12)$$

Under conditions of small scale yielding, the displacement at the crack tip, δ , can be calculated by assuming the effective crack tip ($a_{\text{effective}} = a + r_y$) is at a distance r_y from the actual crack tip:

$$\delta = 2v = \frac{4}{\pi} \frac{K}{E'} \sqrt{2\pi r_y} = \frac{4}{\pi} \frac{K^2}{E' \sigma_Y}. \quad (13)$$

Theoretically, fracture occurs when $\delta = \delta_c$, the critical COD. In practice, a characteristic value for δ exists only for the crack initiation event; significantly more scatter exists for δ measured at maximum load or final fracture.

The COD approach is limited by the analytical and experimental uncertainties of the crack tip region. Analytically, δ is defined as the COD at the interface of the elastic plastic boundary and the crack surface. Experimentally, δ is calculated from displacement measurements taken remotely from the crack tip; direct physical measurements of δ have been abandoned due to lack of precision. Further uncertainty is introduced by the term σ_Y in Equation 13, which may vary by 75 percent depending upon the degree of elastic constraint--a crack tip characteristic that cannot be measured directly.

Despite these shortcomings, the COD approach is being widely used, particularly in Great Britain, because it offers a significant improvement over linear elastic methods in the plastic range. Several useful empirical correlations have been developed relating COD, crack size and applied strain for specific structure/material combinations.¹⁸ Test methods for measuring δ have been standardized¹⁹ and found to be useful as a comparative measure of material toughness.

J-Integral

The J-integral is a characterization developed by Rice²⁰ of the elastic-plastic field in the vicinity of the crack tip. The use of the J-integral as a fracture criterion was suggested and experimentally demonstrated by Begley and Landes.²¹ J is defined as the line integral:

$$J = \int_{\Gamma} [w dy - \vec{T} \left(\frac{\partial \vec{u}}{\partial x} \right) ds] \quad (14)$$

where, Γ is any contour surrounding the crack tip,
 w is the strain-energy density,
 \vec{T} is the stress vector normal to Γ ,
 \vec{u} is the displacement vector and
 s is the arc length along Γ .

The J-integral is path independent for linear and non-linear elastic materials²⁰ and nearly so for most structural materials under monotonic loading conditions.²² Thus, J can be computed using numerical methods by analyzing along a contour away from the crack tip, i.e., in a region where the analysis methods are quite accurate. This relieves the uncertainties of the crack tip region--a problem that seriously limits the usefulness of the COD method.

An equivalent interpretation is that J is equal to the change of potential energy, U, upon an increment of crack extension of unit area, A:

$$J = - \frac{dU}{dA} . \quad (15)$$

For the linear elastic case the potential energy equals the strain energy ($U = V$) and, therefore, Equation 15 is the same as Equation 2 and $J = G$. Thus, J appears to be a logical extension of linear elastic fracture mechanics into the elastic-plastic range. Due to the irreversibility of plastic deformation, the energy interpretation of the J-integral does not apply to the process of crack extension, and J is not equal to the energy available for crack extension in elastic-plastic materials--as G is for elastic materials. J is simply an analytically convenient, measurable parameter that is a characteristic of the elastic-plastic field at the crack tip. The contribution of Begley and Landes²¹ was to demonstrate that crack initiation under elastic-plastic conditions occurs at a characteristic value of J, called J_{IC} , that is related to K_{IC} in the same way G is related to K in Equation 5. Thus, J integral methods can be used to determine K_{IC} in specimens significantly smaller than the size requirements of Equation 6.

Methods of measuring J_{IC} are not yet standardized; however, the method proposed by Landes and Begley²³ is receiving widespread use. A deeply notched compact specimen of ASTM E 399 design is precracked to $a/W \approx 0.6$ and loaded to a predetermined J-level in the region where crack extension is anticipated. The load-displacement curve is recorded on an X-Y plotter. Displacement is measured along the load line. Subsequently, the specimen is unloaded and heat tinted to mark the region of crack extension. The specimen is fractured and the crack extension, Δa , is measured from the exposed fracture surface. J is calculated from the load displacement record and specimen dimensions using the approximation of Rice, Paris and Merkle.²⁴

$$J = \frac{2A}{bB}, \quad (16)$$

where, A is the area under the load displacement record and B is the ligament ($W-a$).

The results of a test series are plotted as J vs. Δa , and the J_{IC} is defined as the extrapolation of the best-fit curve to $\Delta a = 0$. Data for ASTM A453 stainless steel at 4 K are shown in Figure 4.²⁵ K_{IC} is related to J_{IC} as follows:

$$K_{IC}(J) = \sqrt{E'} J_{IC}. \quad (17)$$

The principal limitation of the J-integral concept is that it is only applicable to crack initiation. In most of the materials that fail in the elastic-plastic range, significant fracture resistance exists after crack initiation. Thus, in some cases the J-integral may be unduly conservative as a fracture criterion. Another factor currently limiting the routine application of J is the analytical complexity in determining J. The stress-strain characteristics of the material must be properly accounted for in the analysis. Thus, for a given structural configuration, J solutions are required for each distinct material instead of the single solution needed for K analyses.

R-Curves

The R-curve concept, introduced by Krafft, Sullivan and Boyle²⁶, is a characterization of the increase in fracture resistance accompanying the slow crack extension that precedes unstable fracture. The R-curve is determined by measuring crack extension, Δa , as a function of the driving force for fracture expressed in terms of G, K, J or δ . The level of driving force required to extend the crack is defined as the resistance, R, of the material. An R-curve is a plot of R vs Δa as shown in Figure 5, where R is expressed in terms of K and is denoted by K_R . The R-curve may be used as a fracture criterion when crack driving force curves, expressed in terms of K vs a at constant load in Figure 5, are shown on the same plot. Fracture is predicted when the following conditions are met:²⁷

$$K = K_R \text{ and } \frac{\partial K}{\partial a} = \frac{\partial K_R}{\partial a} \quad (18)$$

K_R and K are computed for the test specimen and structure respectively using the appropriate value of $Y(a)$ in Equation 8.

In applying the R-curve concept as a fracture criterion, it is assumed that: 1) the R-curve is a property of the material for a given thickness and temperature and 2) the influence of planar geometry on the predicted instability point is accounted for in the calculation of K for the driving force curves. The first assumption implies that the R-curve is independent of specimen size and configuration and the initial crack size. This assumption has not been clearly established because results which both agree²⁸ and disagree²⁹ with this hypothesis have been reported. The validity of the second assumption is limited to the case of small scale yielding where the K-analysis is appropriate. These uncertainties, coupled with the complexity of the proposed test method,³⁰ have limited the applicability of the R-curve approach.

The R-curve approach is used as a measure of fracture toughness for plate thicknesses where valid K_{IC} data cannot be obtained because of the size requirement of Equation 9. For example, the nickel steels have been evaluated at temperatures down to 76 K using the R-curve approach.³¹ The results can be misleading if one compares materials on the basis of fracture toughness, i.e., an initiation criterion such as K_{IC} indicates a substantially lower toughness than an instability criterion such as the R-curve.

Summary Comments

The COD and J-integral concepts are efforts to define single parameter characterizations of the fracture process that are applicable to linear elastic and general yielding fracture. In the COD concept, attention is focused at the crack tip; fracture theoretically occurs when a critical displacement develops at the crack tip. The J-integral concept examines the stress-strain conditions along an arbitrary contour away from the crack tip; fracture theoretically occurs when the potential energy available for crack extension reaches a critical value defined by J . For the linear elastic case, δ_c and J_{IC} are consistent with the linear elastic fracture criteria:

$$G_c = \frac{K_{IC}^2}{E'} = \sigma_Y \delta_c. \quad (19)$$

The principal limitation in extending these criteria to general yielding fracture is that both δ_c and J_{IC} are only applicable to the onset of crack extension. Only the R-curve approach accounts for the significant increase in fracture resistance that accompanies the slow crack growth preceding unstable fracture. The application of the COD, J-integral and R-curve approaches to the design of cryogenic structures has been limited to characterizing the fracture toughness of the materials.

SUBCRITICAL CRACK GROWTH

In linear elastic fracture mechanics, the crack tip stress field represented by K is the driving force for fracture. It is logical then that K would also describe the conditions for incremental extension of the crack due to fatigue cycling, stress corrosion and hydrogen embrittlement. Extensive experimental evidence indicates that this is indeed the case.

Fatigue Crack Growth

Fracture mechanics concepts have been applied to the study of fatigue crack propagation. In reviews of extensive crack propagation data, Paris³² observed that a log-log plot of the crack growth rate, da/dN , versus the stress intensity range, ΔK , is a straight line of the form:

$$\frac{da}{dN} = c(\Delta K)^n \quad (20)$$

where, c and n are empirical constants; and $\Delta K = K_{MAX} - K_{MIN}$, where K_{MAX} and K_{MIN} are the maximum and minimum stress intensity factors of the fatigue cycle, respectively. This relation implies that the cyclic crack tip stress field described by ΔK is the driving force for fatigue crack extension. Cyclic profile and frequency, mean load and stress state are of secondary importance. The principal limitation of the Paris equation is the failure to account for environmental-enhanced fatigue crack growth.³³ Environmental factors, including temperature, increase the importance of the secondary variables; however, Equation (20) still provides a useful basis for the empirical analysis of crack growth data. Accordingly, most data are presented as log-log plots of da/dN vs. ΔK .

Equation (20) is frequently used to estimate the life of a cracked structure subject to fatigue. A crack is assumed to exist at a selected location in the structure. For this location, the relationship between K and crack length is determined by stress analysis or by handbook values. Experimental data for the material of construction relate the fatigue crack growth rate and the critical crack size to ΔK and K_c , respectively. Life is calculated by integrating Equation (20) between the limits set by the initial flaw size and the final size based on fracture toughness data:

$$N = \int_{a_i}^{a_c} \frac{da}{c(\Delta K)^n} = \frac{1}{c(\Delta \sigma)^n} \int_{a_i}^{a_c} \frac{da}{[f(a)]^n} . \quad (21)$$

For complex load histories, $\Delta \sigma$ takes on many values as a function of time, and Equation (21) must be integrated sequentially using numerical methods. Several computerized techniques have been developed to evaluate Equation (21), including some to account for load interaction effects.^{34,35} These latter methods attempt to account for the beneficial effect of peak loads on subsequent low load growth rates, i.e., da/dN is frequently reduced below expected values during low stress amplitude cycles that follow high stress amplitude cycles.

Stress Corrosion Cracking

Stress corrosion cracking is a type of crack extension that occurs in susceptible materials under the combined action of corrosion and static tensile stress.³⁶ Experimental studies indicate that for a given material and environment, a threshold stress intensity (K_{ISCC}) exists below which crack extension does not occur. K_{ISCC} has been shown to be independent of specimen configuration and thus may be regarded as a material property for a given environment.³⁷ Kinetic studies also indicate that the crack tip stress field is the driving force for stress corrosion cracking, i.e., the crack growth rate, da/dt , is a repeatable function of K .³⁸

Stress corrosion cracking is an important consideration for many engineering structures because of the wide range of susceptible materials and aggressive environments. To date, however, stress corrosion cracking has not been reported to occur at cryogenic temperatures. It is likely that stress corrosion cracking is less a problem in cryogenic structures because the low temperatures preclude the existence of an aggressive environment.

Hydrogen Embrittlement

Sustained load cracking may occur in a high pressure hydrogen environment in a manner analogous to stress corrosion cracking;³⁹ i.e., the time to initiate cracking is a function of K and a threshold K exists below which cracking will not occur. Cracking may also occur due to hydrogen reaction embrittlement, e.g., cracking of copper alloys due to the formation of high pressure water vapor in voids; or due to internal hydrogen embrittlement, where the hydrogen is introduced by electrolytic charging. At cryogenic temperatures, cracking due to hydrogen embrittlement has not been observed. However, in liquid hydrogen vessels, materials in the ullage space that are near ambient temperature may be susceptible to hydrogen environment cracking.

FRACTURE PROPERTIES OF MATERIALS AT CRYOGENIC TEMPERATURES

In applying fracture mechanics to design, the material properties of interest are the fracture toughness, which is used to compute critical crack sizes, and the fatigue crack growth rate, which is used to estimate the cycle life expectancy of a cracked structure. At cryogenic temperatures, sustained load flaw growth is presumed negligible; however, caution should be taken for components of the cryogenic system subjected to ambient temperature conditions.

When comparing alloys of different base-metal systems, it is important to recall how critical flaw sizes are influenced by fracture toughness and by stress level as shown in Equation (11). In most design codes, the design allowable stress levels are related to the strength of the material. Since critical flaw sizes are proportional to the ratio $(K_{IC}/\sigma)^2$, high strength materials need greater fracture toughness than low strength materials. For comparable fracture resistance, a steel alloy with an allowable stress of 30 ksi must have a fracture toughness 9 times greater than an aluminum alloy with an allowable stress of 10 ksi. Similarly, the fatigue crack growth rates are strongly related to operating stress levels as shown in Equation (20). Thus, in comparing growth rates of different alloys, the ΔK ordinate of the da/dN - ΔK curve should be normalized for operating stress, i.e., $\Delta K/\Delta\sigma$.

Mechanical property tests have been conducted at cryogenic temperatures on most of the metals and alloys of practical interest. Extensive reviews and compilations of these data are given in References 40, 41, 42. The fracture test methods most generally employed were the Charpy and Izod impact tests, notched tensile tests and tear tests. Although these data are not suitable for a fracture mechanics analysis, they are indicative of relative toughness. These data indicate that the fracture properties of metals at cryogenic temperatures are primarily controlled by yield strength within a given base metal system and by crystalline structure when comparing different systems. As yield strength increases, fracture toughness generally decreases due to diminishing plastic strain energy dissipation upon fracture—a trend that is apparent in the data in aluminum alloys at 76 K shown in Figure 6.⁴³⁻⁴⁸ Fracture toughness tends to be high for face-centered cubic (FCC) metals, e.g., Al, Cu, Ni and austenitic stainless steels, and low for body-centered cubic (BCC) metals, e.g., most steels and refractory metals. Metals with a hexagonal close packed (HCP) structure exhibit mixed behavior at cryogenic temperatures; HCP titanium alloys are reasonably tough, but magnesium and beryllium alloys are brittle.

Fracture mechanics test methods have been used to determine fracture toughness and fatigue crack growth on materials for aerospace pressure vessels, LNG tankers and superconducting machinery. Several reviews of fracture toughness data at cryogenic temperatures have been prepared recently; Matthews⁴⁹ compiled K_{IC} data for aerospace materials at temperatures ranging from 20 to 300 K, Campbell⁵⁰ reviewed the fracture toughness of high strength alloys at low temperatures, and Pense and Stout⁵¹ included extensive fracture data in their review of cryogenic nickel steels. The available fatigue crack growth data at 4 K have been reviewed by Tobler and Reed.⁵² The fatigue crack growth rates tend to decrease at low temperature except for steels at temperatures below their ductile-to-brittle transition temperature. The data for materials being used for LNG applications are summarized in Figure 7.^{53,54}

FRACTURE CONTROL PLANS

Many factors contribute to brittle fracture and its prevention. Consider, for example, Equations 11 and 21 for determining critical crack size and

cycle life, respectively. These relations require an understanding of the material properties, the service load history, probable initial flaw sizes and the functionality of K vs. a for the locations of interest. A complete understanding of all these aspects is obviously not possible for a complex structure. Thus, to assure safety, it is necessary to devise a plan to limit the uncertainties. Such a plan, referred to as a fracture control plan, consists of the following elements:

1. Establish design criteria and analysis assumptions
2. Design for damage tolerance
3. Implement the controls necessary to assure the validity of the design assumptions.

Design Criteria and Analysis Assumptions

The design criteria and analysis assumptions need to be clearly defined in the procurement specification or agreed upon early in the design phase. Criteria relevant to fracture control include the design service life, the anticipated service load history and the thermal and chemical environment. The principal analysis assumptions are the initial flaw size and location, the fracture criterion (plane strain or plane stress) and the load for use in critical flaw size calculations.

The U.S. Air Force has recently developed a rigorous set of damage tolerance requirements to augment the standard strength and fatigue requirements for military aircraft.⁵⁵ Primary structure must be designed such that assumed initial flaws of prescribed size and location do not grow to critical size within either a specified inspection interval or the entire service life depending upon the inspectability of the structure. Damage tolerance requirements are also specified for nuclear reactor⁵⁶ and spacecraft pressure vessels.⁵⁷ These requirements, although currently of limited applicability, may be the precursors of requirements for cryogenic structures where public safety is a prominent consideration.

Design for Damage Tolerance

The role of the design function is to integrate materials and structures technology into the design of a safe, functional and economical structure. The design should incorporate the results of the structural analyses for

strength, rigidity, fatigue life and fracture resistance. Careful attention to design detail is essential because fatigue cracks initiating at stress concentrations are perhaps the most likely source of failures.

The two principal design options for providing damage tolerance are the fail safe and the safe life approaches. In the fail safe approach, fracture safety is provided by structural redundancy. Inspectability is essential to fail safe design to assure detection of the initial failure before the damage spreads beyond control. In the safe life approach, the stress levels are limited such that a flaw will not grow to critical size during the life of the structure. When sufficient inspectability exists, this latter approach can be modified to provide for a safe inspection interval--at which time the structure is inspected and certified for another interval of safe operation.

Fracture mechanics analyses are complex and costly and thus must be conducted judiciously on the parts and locations deemed most susceptible to fracture. These parts, identified as fracture critical parts, are also subjected to more stringent controls during material procurement and fabrication as outlined in the next section.

Specifications and Controls

A variety of controls are necessary to assure that the fabricated structure is adequately represented by the design and analyses. Material procurement and processing are controlled by specifications that are sufficient to preclude use of materials in the structure that have fracture properties inferior to those assumed in design. Inspection of the raw material and the final assembly should be sufficient to assure that the flaws in the fabricated structure are smaller than those assumed in the crack growth analysis. For fracture critical parts, records are needed to provide traceability of product quality from the raw material heat identification, through all manufacturing operations, to final assembly. These records are needed to limit the scope of a retrofit program in case of service failure due to inferior material quality.

The engineering drawing is a convenient vehicle for transmitting the requirements of a fracture control plan. Drawing notes can be used to identify the part as fracture critical, to invoke material and process specifications and to specify inspection and corrosion protection requirements.

The control measures discussed above are sufficient to provide the customer with a safe structure. It is the responsibility of the user to exercise control over usage of the structure such that service operations do not exceed the design limits.

APPLICATIONS

Structural safety has always been a primary consideration in the design of cryogenic structures. Thus, it is not surprising to find the essential fracture control implemented in their design and fabrication. However, as cryogenic technology advances, there is an increased tendency to use higher strength materials, higher operating stresses and/or thick sections to build larger and more complex structures. These trends increase the hazard of brittle fracture and sometimes justify the use of fracture mechanics methods. In this section the potential uses of fracture mechanics in conventional structures are proposed and sophisticated applications of fracture mechanics to the design of LNG ships and aerospace pressure vessels are reviewed.

Storage Tanks and Piping System

For cryogenic structures such as storage tanks and piping systems, there exists a considerable body of favorable service experience. Thus, the design practices, the fabrication methods and the type and extent of inspection have proven satisfactory, and there is little need for a fracture mechanics analysis. The existing design codes published by ASME,⁵⁸ API⁵⁹ and ANSI⁶⁰ fulfill the need for a fracture control plan. There is, however, a trend in engineering design toward increased structural efficiency through the rational determination of structural loads, working stresses and material properties. This trend has created pressure for changing certain aspects of the design codes in the interest of cost reduction. Fracture mechanics is a useful tool for assessing the impact of these changes on structural safety.

In most cases, the design allowable stress level for a material used at cryogenic structures is based on the strength of that material at room temperature. Generally, the strength increases at cryogenic temperatures and thus a higher allowable might be appropriate. Fracture mechanics can provide a quantitative assessment of the effect of increased stress levels on the flaw tolerance of the material at low temperatures and, therefore, can provide a rational basis for modifying stress allowables.

The qualification of materials and welding procedures for fabricating cryogenic structures in accordance with the ASME Pressure Vessel Code⁵⁸ of the ANSI Piping Code⁶⁰ is difficult. Charpy impact tests are not appropriate at temperatures below 76 K because of testing difficulties and adiabatic heating of the test specimen. Standards have not been established for alternative tests such as the notched tension test. Fracture mechanics tests are a bit cumbersome for qualification testing, but may provide a useful basis for comparison with other tests. The correlations of unit propagation energy in the tear test for aluminum alloys⁶¹ and impact energy in Charpy tests for steel alloys⁶² as functions of fracture toughness are good examples of this approach.

Shipboard LNG Tanks

Several types of containment systems have been devised for the marine transport of liquefied natural gas (LNG).⁶³ In general, the containment system consists of a primary barrier to contain the cargo for the life of the ship, and a secondary barrier to contain the cargo for 15 days in case the primary barrier fails. Spherical free standing tank designs do not require a secondary barrier if fracture mechanics analysis indicates satisfactory leak-before-break behavior.⁶⁴

The leak-before-break criterion requires demonstration by test and analysis that a subcritical crack will grow through the thickness of the tank wall and cause a detectable amount of cargo leakage for a safe period of operation prior to failure. The minimum period of safe operation is defined as 15 days at sea under storm conditions. Fracture mechanics analysis is used to compute the minimum flaw size that will allow leakage of sufficient gas to be sensed by the gas detectors.⁵³ The period of safe operation is determined by integrating Equation 21 between the limits set by this minimum flaw size and the critical flaw size determined from fracture toughness measurements; crack growth data for the tank material and the appropriate cyclic stress history for storm conditions are used.

Aerospace Pressure Vessels

Cryogenic vessels used by NASA for launch vehicles and spacecraft gas containers are designed, fabricated and tested in accordance with an overall

fracture control plan.⁵⁷ One of the principal elements of this plan is the proof pressure test. The proof test concept is shown schematically in Figure 8. The proof test is conducted at a pressure (and stress level, σ_{pr}) which exceeds the maximum service pressure (and stress level, σ_s); thus, the critical crack size during proof test, a_{pt} , is smaller than the critical crack size during service, a_s . The flaw size that could exist in the pressure vessel following proof test is conservatively estimated to be equal to a_{pt} , i.e., any flaw larger than a_{pt} would have caused failure during proof test. During service, this initial flaw is stable until it grows to critical size, a_s , and thus a period of safe operation exists. This period of safe operation is determined using empirical data (or Equation 21) relating crack length to service time, t , where all the appropriate loads and environments are simulated in the test and/or analysis.

Future Applications

In the coming years, many applications of fracture mechanics will be directed toward the establishment of a more rational basis for design codes and improved standards for material acceptance, welding procedure qualification and nondestructive inspection. In addition, many new design ideas will be developed for constructing superconducting devices and hydrogen fuel equipment. Superconducting systems for energy storage and for fusion magnets will involve enormous structures and capital investment considerations may justify the use of fracture mechanics methods. Public safety considerations will probably lead to the application of fracture mechanics to the design of equipment for storing, handling and transporting cryogenic hydrogen fuel.

SOURCES OF INFORMATION

An abundance of information is available for those interested in further study of fracture mechanics. Textbooks have been written by Knott,⁶⁵ Brock⁶⁶ and Lawn and Wilshaw.⁶⁷ Extensive surveys on specific applications have been prepared for aircraft structures⁶⁸ and for space vehicles.⁶⁹ Analysis handbooks which include compilations of stress intensity factor solutions have been written by Tada et al.⁸ and by Sih.⁹ Material property handbooks are generally beginning to include fracture mechanics test data and one handbook⁷⁰ is specifically for the compilation of fracture mechanics data on aerospace

materials. Experimental methods in fracture mechanics are reviewed in a training manual written by Hickerson⁷¹ and in a monograph edited by Kobayashi.⁷² Fracture mechanics concepts are applied to failure analysis in a book by Colangelo and Heiser.⁷³

Current research in fracture mechanics is published quarterly by two journals: Engineering Fracture Mechanics and International Journal of Fracture. The American Society for Testing Materials (ASTM) regularly publishes the proceedings of symposia on topics in fracture mechanics including the papers presented at the annual National Symposium on Fracture Mechanics. Work in progress is presented at the semi-annual meetings of ASTM committee E-24 on Fracture Testing of Metals.

SUMMARY

Fracture mechanics has made significant contributions to our understanding of the fracture process. Yet, much remains to be learned--particularly in the area of elastic-plastic fracture. The design methodology limits stress levels throughout the structure such that initial flaws will not grow to critical size during the desired service life. Further progress in fracture mechanics should lead to acceptance of this approach to structural safety by those responsible for the design, operation and regulation of cryogenic structures.

NOMENCLATURE

a	crack length
A	crack surface area
a_c	critical crack size
a_i	initial crack size
a_s	critical crack size at maximum stress in service
a_{pt}	critical crack size at maximum stress in proof test
B	thickness
b	ligament, $b = W-a$
c	empirical coefficient in crack growth rate equation
C	elastic compliance
COD	crack opening displacement
da/dN	crack growth per load cycle in fatigue
da/dt	crack growth per unit time
E	elastic modulus
E'	reduced modulus, $E/(1-\nu^2)$
f(a)	function of crack length
$f_{ij}(\theta)$	generalized distribution function
G	strain energy release rate
G_c	strain energy release rate at fracture
J	the line integral of Equation 14 or the potential energy difference of Equation 15
J_{IC}	the critical value of J for crack initiation
K	degrees kelvin
K	stress intensity factor
K_c	fracture toughness
K_{MAX}	maximum K in fatigue cycle
K_{MIN}	minimum K in fatigue cycle
K_{IC}	plane strain fracture toughness
$K_{IC}(J)$	K_{IC} computed from J_{IC}
K_R	crack growth resistance
K_{ISCC}	stress corrosion cracking threshold
n	empirical exponent in crack growth rate equation
N	number of load cycles in fatigue
P	applied load
P_c	critical load

P_Q	candidate critical load per ASTM 399
r	radial coordinate from a crack tip
r_y	radius of the plastic zone at the crack tip
s	arc length along the contour Γ
t	time
\vec{T}	stress vector normal to Γ
T	temperature
\vec{u}	displacement vector
U	potential energy per unit thickness
v	displacement in the Y direction
V	elastic strain energy
w	strain energy density
W	width
x	coordinate in the plane of the crack
$Y(a)$	geometry correction factor
$Y(\frac{a}{W})$	specimen calibration function
Δ	displacement
δ	crack opening displacement at the crack tip
δ_c	δ at the onset of fracture
Δa	increment of crack extension
ΔK	stress intensity factor range during fatigue cycling
$\Delta \sigma$	stress range during fatigue cycling
Γ	any contour surrounding the crack tip
θ	angular coordinate measure from the crack plane
ν	Poisson's ratio
σ	applied stress
σ_{ij}	tensor notation for the crack tip stress field
σ_s	maximum stress in service
σ_{pt}	maximum stress in proof test
σ_c	critical stress
σ_Y	yield stress of the material local to the crack tip
σ_{ys}	0.2% offset yield strength

REFERENCES

1. E. T. Wessel and T. R. Mager, "Fracture Mechanics Technology as Applied to Thick-Walled Nuclear Pressure Vessels," Conference on Practical Applications of Fracture Mechanics to Pressure Vessel Technology, Institution of Mechanical Engineers, London, England, May 1971.
2. J. M. Barsom, "The Development of AASHTO Fracture-Toughness Requirements for Bridge Steels," U.S.-Japan Cooperative Science Seminar, Tohoko University, Sendai, Japan, August 1974.
3. H. A. Wood, "Fracture Control Procedures for Aircraft Structural Integrity," Advanced Approaches to Fatigue Evaluation, NASA SP-309, 1972.
4. C. F. Tiffany, G. T. Smith and S. Glorioso, "Fracture Control of Aerospace Pressure Vessels," American Society for Metals, Conference on Fracture Control, Philadelphia, PA, 1970.
5. A. A. Griffith, "The Phenomena of Rupture and Flow in Solids," Philosophical Transactions of the Royal Society, 221A: 163, 1920.
6. G. R. Irwin and J. A. Kies, "Critical Energy Data Analysis of Fracture Strength," Welding Journal, 33: 193s, 1954.
7. G. R. Irwin, "Analysis of Stresses and Strains Near the End of a Crack Traversing a Plate," Transactions of the ASME, Journal of Applied Mechanics, 24: 361, 1957.
8. H. Tada, P. C. Paris and G. R. Irwin, The Stress Analysis of Cracks Handbook, Del Research Corporation, Hellertown, PA, 1973.
9. G. C. Sih, Handbook of Stress Intensity Factors for Researchers and Engineers, Institute of Fracture and Solid Mechanics, Lehigh University, Bethlehem, PA, 1973.
10. Standard Method of Test for Plane Strain Fracture Toughness of Metallic Materials (Designation E 399-74), 1974 Annual Book of ASTM Standards, Part 10, 1974, pp. 432-451.
11. C. W. Fowlkes and R. L. Tobler, "Fracture Testing and Results for a Ti 6Al-4V alloy at Liquid Helium Temperature," Engineering Fracture Mechanics, submitted for publication.
12. G. R. Irwin, "Plastic Zone Near a Crack and Fracture Toughness," Proceedings, Seventh Sagamore Ordnance Materials Research Conference, Syracuse University Press, Syracuse, N.Y., 1960, pp. IV-63 to IV-78.
13. G. R. Irwin, "Fracture Mode Transition of a Crack Traversing a Plate," Transactions of the ASME, Journal of Basic Engineering, 82: 417, 1960.
14. S. T. Rolfe, "Fracture Criteria for Structural Steels," American Society for Metals, Conference on Fracture Control, Philadelphia, PA, 1970.
15. P. C. Paris and G. C. Sih, "Stress Analysis of Cracks," Fracture Toughness Testing and Its Applications, ASTM STP 381, 1965, pp. 30-81.

16. A. A. Wells, "Notched Bar Tests, Fracture Mechanics, and the Brittle Strength of Welded Structures," *British Welding Journal*, 12:2, 1965.
17. H. M. Westergaard, "Bearing Pressures and Cracks," *Transactions of the ASME, Journal of Applied Mechanics*, 61: A49, 1939.
18. C. E. Turner, and F. M. Burdekin, "Review of Current Status of Yielding Fracture Mechanics," *Atomic Energy Reviews*, 12: 439, 1974.
19. British Standards Publication, Draft for Development on Crack Opening Displacement (COD) Testing, DD 19, 1972.
20. J. R. Rice, "A Path Independent Integral and Approximate Analysis of Strain Concentration by Notches and Cracks," *Transactions of the ASME, Journal of Applied Mechanics*, 35: 379, 1968.
21. J. A. Begley and J. D. Landes, The J-Integral as a Fracture Criterion, Fracture Toughness, ASTM STP 514, 1972, pp. 1-20.
22. D. J. Hayes, "Some Applications of Elastic Plastic Analysis to Fracture Mechanics," Ph.D. Thesis, University of London, 1970.
23. J. D. Landes and J. A. Begley, "Test Results from J-Integral Studies--An Attempt to Establish a J_{IC} Testing Procedure," *Westinghouse Research Laboratory Scientific Paper 73-1E7-FMPWR-P3*, 1973.
24. J. R. Rice, P. C. Paris and J. G. Merkle, Some Further Results of J-Integral Analysis and Estimates, Progress in Flaw Growth and Fracture Toughness Testing, ASTM STP 536, 1973, pp. 231-245.
25. R. P. Reed, R. L. Tobler and R. P. Mikesell, "The Fracture Toughness and Fatigue Crack Growth Rate of an Fe-Ni-Cr Superalloy at 298, 76 and 4 K," *International Cryogenic Materials Conference, Cryogenic Engineering Conference, Kingston, Ontario, 1975*.
26. J. M. Krafft, A. M. Sullivan and R. W. Boyle, "Effect of Dimensions on Fast Fracture Instability of Notched Sheets," *Proceedings, Crack Propagation Symposium, College of Aeronautics, Cranfield England, 1961 Vol. 1*, pp. 8-28.
27. J. E. Srawley and W. F. Brown, Jr., "Fracture Toughness Testing Methods, Fracture Toughness Testing and Its Applications", ASTM STP 381, 1965, pp. 133-196.
28. D. E. McCabe and R. H. Heyer, "R-Curve Determination Using a Crack-Line-Wedge-Loaded (CLWL) Specimen," Fracture Toughness Evaluation by R-Curve Methods, ASTM STP 527, 1973 pp. 17-35.
29. A. M. Sullivan, C. N. Freed and J. S. Stoop, "Comparison of R-Curves Determined from Different Specimen Types," Fracture Toughness Evaluation by R-Curve Methods, ASTM STP No. 527, 1973, pp. 85-104.

30. Anon., "Proposed Recommended Practice for R-Curve Determination," 1974 Annual Book of ASTM Standards, American Society for Testing Materials, 1974, pp. 669-683.
31. D. A. Sarno, J. P. Bruner and G. E. Kampschaefer, "Fracture Toughness of 5% Nickel Steel Weldments," Welding Journal, 53: 486, 1974.
32. P. C. Paris, "The Fracture Mechanics Approach to Fatigue," Proceedings, Tenth Sagamore Army Materials Research Conference, Syracuse University Press, Syracuse, N.Y., 1964, pp. 107-127.
33. R. P. Wei, "Some Aspects of Environment-Enhanced Fatigue Crack Growth," Engineering Fracture Mechanics, 1: 633, 1970.
34. R. M. Engle, "CRACKS, A Fortran IV Digital Computer Program for Crack Propagation Analysis," Air Force Flight Dynamics Laboratory, AFFDL-TR-70-107, October 1970.
35. O. E. Wheeler, "Spectrum Loading and Crack Growth," Transactions of the ASME, Journal of Basic Engineering, 94: 181, 1972.
36. Anon., "Stress Corrosion Cracking in Metals," NASA Space Vehicle Design Criteria (Structures), NASA SP-8032, August 1971.
37. C. D. Beachem and B. F. Brown, "A Comparison of Three Specimens for Evaluating the Susceptibility of High Strength Steel to Stress Corrosion Cracking," Internal Report, U.S. Naval Research Laboratory, 1967.
38. H. H. Johnson and A. M. Willner, "Moisture and Stable Crack Growth in a High Strength Steel," Applied Materials Research, 4: 34, 1965.
39. P. M. Lorenz, Effect of Pressurized Hydrogen Upon Inconel 718 and 2219 Aluminum, The Boeing Company, Document D2-114417-1, Seattle, Washington, February 1969.
40. F. R. Schwartzberg, "Cryogenic Materials Data Handbook, Air Force Materials Laboratory, AFML-TDR-64-680, 1964 and 1968.
41. Anon., "Handbook on Materials for Superconducting Machinery," Metals and Ceramics Information Center, MCIC-HB-04, Battelle, Columbus, Ohio, November 1974.
42. R. P. Reed and R. P. Mikesell, "Low Temperature Mechanical Properties of Copper and Selected Copper Alloys," NBS, Monograph 101, 1967.
43. W. L. Engstrom, "Determination of Design Allowable Properties, Fracture of 2219-T87 Aluminum Alloy," NASA CR-115388, March 1972.
44. C. Vishnevsky and E. A. Steigerwald, "Plane Strain Fracture Toughness of Some Cryogenic Materials at Room and Subzero Temperatures," Fracture Toughness Testing at Cryogenic Temperatures, ASTM STP 496, 1971, pp. 3-26.

45. J. G. Kaufman, F. G. Nelson and R. H. Wygonic, "Large Scale Fracture Toughness Tests of Thick 5083-0 Plate and 5183 Welded Panels at Room Temperature, -260 and -320°F," Fatigue and Fracture Toughness-Cryogenic Behavior, ASTM STP 556, 1974, pp. 125-158.
46. L. R. Hall and R. W. Finger, "Investigation of Flaw Geometry and Loading Effects on Plane Strain Fracture in Metallic Structures," NASA Report CR-72659, December 1971.
47. F. G. Nelson and J. G. Kaufman, "Plane Strain Fracture Toughness of Aluminum Alloys at Room and Subzero Temperatures," Fracture Toughness Testing at Cryogenic Temperatures, ASTM STP 496, 1971, pp. 27-39.
48. F. R. Schwartzberg, R. D. Keys and T. F. Kiefer, "Cryogenic Alloy Screening," NASA Report CR-72733, November 1970.
49. W. T. Matthews, "Plain Strain Fracture Toughness (K_{IC}) Data Handbook for Metals," Army Materials and Mechanics Research Center, AMMRC MS 73-6, Watertown, Massachusetts, 1973.
50. J. E. Campbell, "Fracture Toughness of High-Strength Alloys at Low Temperatures -- A Review," Fatigue and Fracture Toughness-Cryogenic Behavior, ASTM STP 556, 1974, pp. 3-25.
51. A. W. Pense and R. D. Stout, "Fracture Toughness and Related Characteristics of the Cryogenic Nickel Steels," Welding Research Council, WRC Bulletin 204, March 1975.
52. R. L. Tobler and R. P. Reed, "Fatigue Crack Growth Rates of Structural Alloys at Four Kelvin," International Cryogenic Materials Conference, Cryogenic Engineering Conference, Kingston, Ontario, 1975.
53. P. Tenge and O. Solli, "Fracture Mechanics in the Design of Large Spherical Tanks for Ship Transport of LNG," Norwegian Maritime Research, Vol. 1, No. 2, p. 1, 1973.
54. R. J. Bucci, B. N. Greene and P. C. Paris, "Fatigue Crack Propagation and Fracture Toughness of 5 Nickel and 9 Nickel Steels at Cryogenic Temperatures," Progress in Flaw Growth and Fracture Toughness Testing, ASTM STP 536, 1973, pp. 206-228.
55. Anon., "Airplane Damage Tolerance Requirements," Military Specification MIC-A-83444.
56. Anon., "The 1974 ASME Boiler and Pressure Vessel Code, Section III, Nuclear Power Plant Components," The American Society of Mechanical Engineers, New York, N.Y., 1974.
57. Anon., "Fracture Control of Metallic Pressure Vessels, NASA Space Vehicle Design Criteria (Structures), NASA SP-8040, May 1970.

58. Anon., "The 1974 ASME Boiler and Pressure Vessel Code, Section VIII, Pressure Vessels," The American Society of Mechanical Engineers, New York, N.Y., 1974.
59. Anon., "Low Pressure Storage Tanks for Liquefied Hydrocarbon Gases," Appendix Q, Supplement to API Standard 620: Recommended Rules for Design and Construction of Large, Welded, Low Pressure Storage Tanks, American Petroleum Institute, New York, 1973.
60. Anon., "Petroleum Refinery Piping," ANSI B 31.3, The American Society for Mechanical Engineers, New York, N.Y., 1973.
61. J. G. Kaufman and M. Holt, "Fracture Characteristics of Aluminum Alloys," Aluminum Company of America, ARL Technical Paper No. 18, 1965.
62. J. M. Barsom and S. T. Rolfe, "Correlations Between K_{IC} and Charpy V-Notch Test Results in the Transition-Temperature Range," Impact Testing of Metals, ASTM STP 466, 1970, pp. 281-302.
63. W. D. Thomas and A. H. Schwendtner, "LNG Carriers: The Current State of the Art," Oceanology International, 7: 1A, 1972.
64. Anon., "Rules and Regulations for Tank Vessels," CG-123, Part 38, "Liquefied Flammable Gases," Title 46 Code of Federal Regulations, Subchapter D of Chapter 1, 1973.
65. J. F. Knott, Fundamentals of Fracture Mechanics, Halsted Press, John Wiley and Sons, New York, 1973.
66. D. Brock, Elementary Engineering Fracture Mechanics, Noordhoff International, Leyden, 1974.
67. B. R. Lawn and T. R. Wilshaw, Fracture of Brittle Solids, Cambridge University Press, London, 1975.
68. H. Liebowitz, Editor, Fracture Mechanics of Aircraft Structures, NATO Advisory Group for Aerospace Research and Development, AGARDograph No. 176, 1974.
69. A. F. Liu, R. M. Ehret and E. J. Malcahy, Fracture Control Methods for Space Vehicles, NASA, CR-134596 (Vol. 1), CR-134597 (Vol. 2) and CR-134598 (Vol. 3), 1974.
70. Anon., Damage Tolerant Design Handbook, Metals and Ceramics Information Center, MCIC HB-01, 1972, and MCIC HB-01S, 1973, Columbus.
71. J. P. Hickerson, Elements of Experimental Fracture Mechanics, Sandia Laboratories, SLA-73-0424, Albuquerque, 1973.
72. A. S. Kobayashi, Editor, Experimental Techniques in Fracture Mechanics, Society for Experimental Stress Analysis, SESA Monograph No. 1, 1973.
73. V. J. Colangelo and F. A. Heiser, Analysis of Metallurgical Failures, John Wiley and Sons, New York, 1974.

LIST OF FIGURES

- Fig. 1. ASTM E399 Compact Specimen for Fracture Toughness Testing [10].
- Fig. 2. Cryostat for Fracture Testing in Liquid Helium [11].
- Fig. 3. Fracture Toughness Transition in Structural Alloys.
- Fig. 4. J-Integral Crack Growth Resistance Curves for an Fe-Ni-Cr Superalloy [25].
- Fig. 5. Crack Growth Resistance Curve and Crack Driving Force Curves in R-Curve Format [28].
- Fig. 6. Fracture Toughness of Aluminum Alloys at 76 K.
- Fig. 7. Fatigue Crack Growth Behavior of 5083-0 Aluminum and 9% Ni Steel at LNG Temperature (111 K).
- Fig. 8. The Proof Test Concept [57].

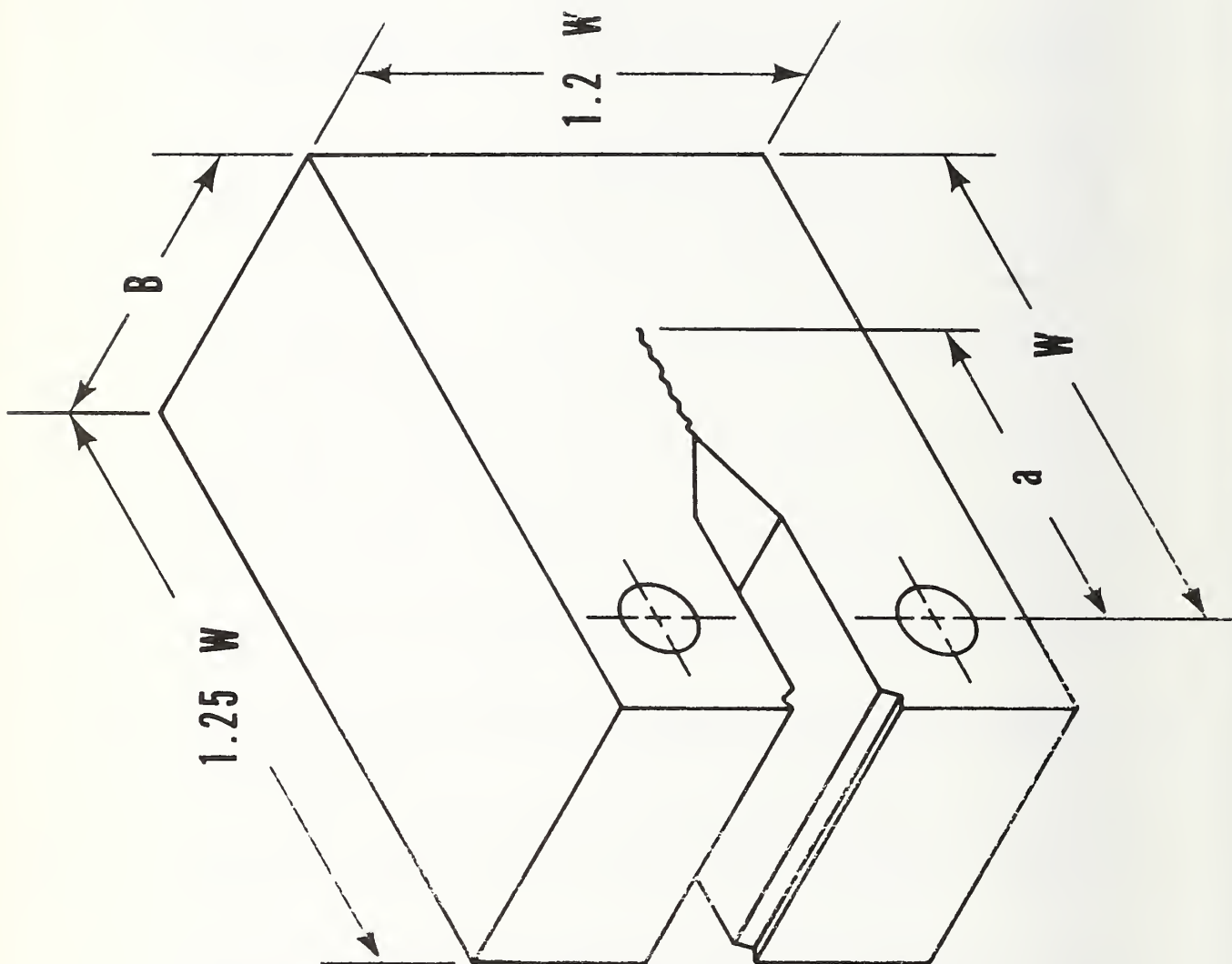


FIG. 1. ASTM E399 Compact Specimen for Fracture Toughness Testing [10].

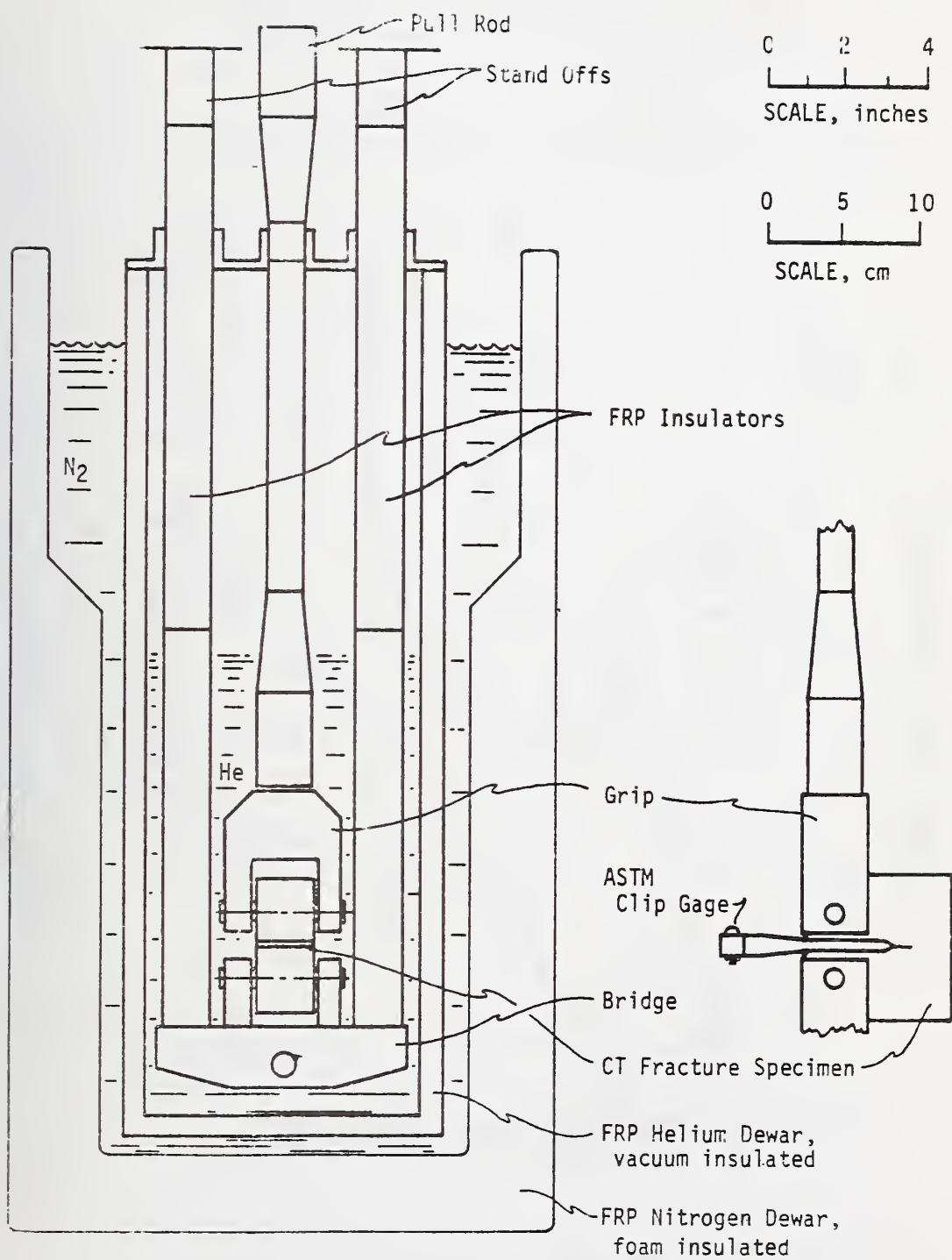


Fig. 2. Cryostat for Fracture Testing in Liquid Helium [11].

FRACTURE TOUGHNESS

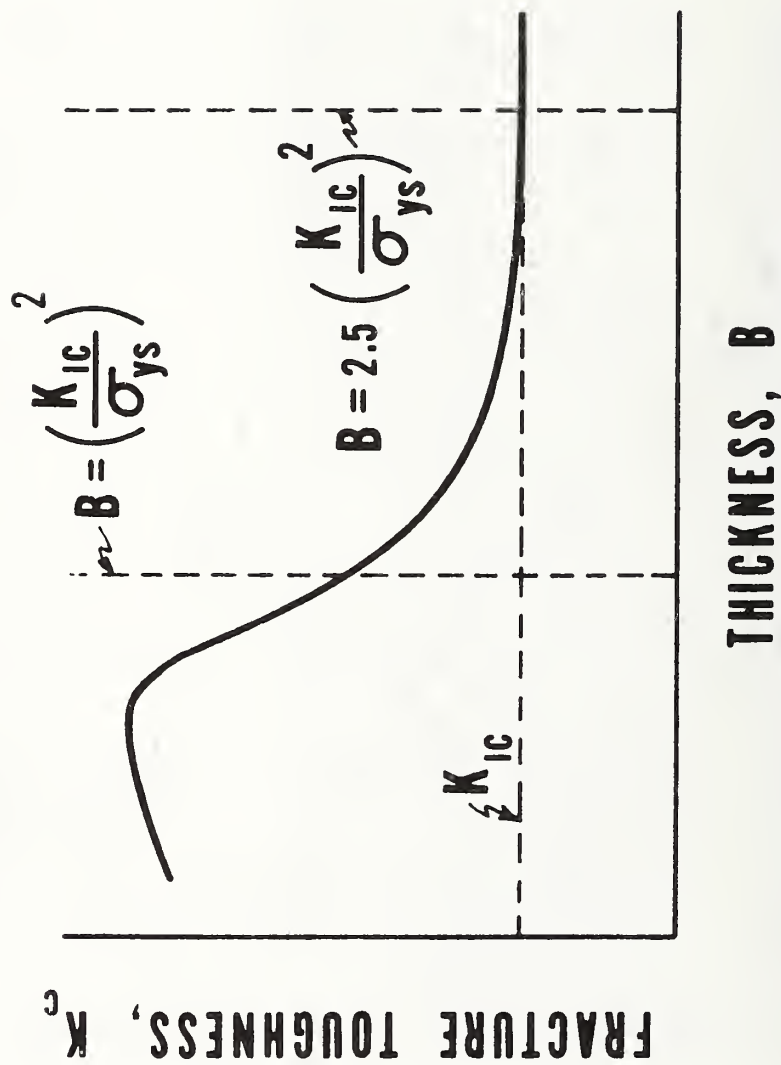


Fig. 3. Fracture Toughness Transition in Structural Alloys.

CRACK EXTENSION, Δa , cm

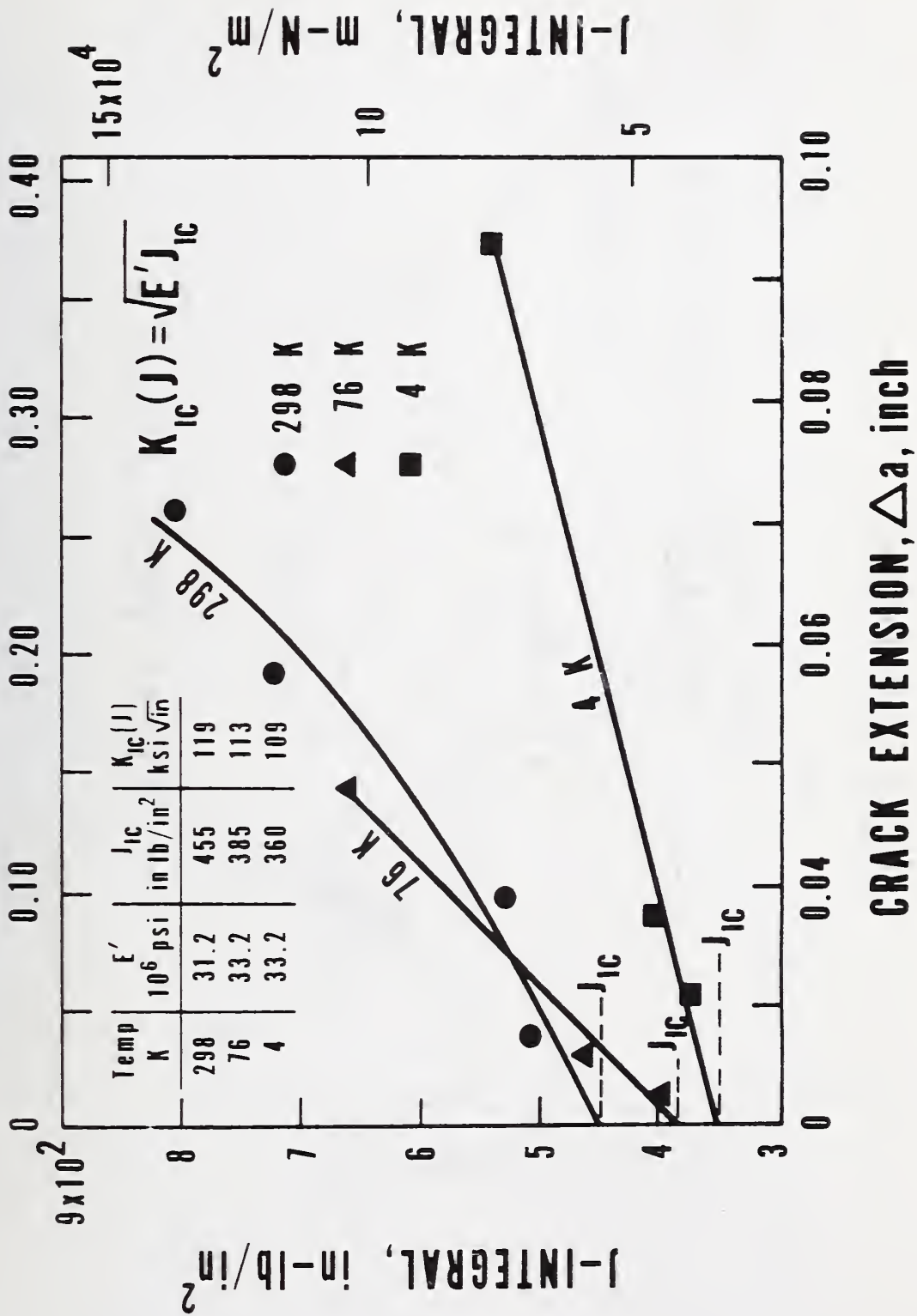


Fig. 4. J-Integral Crack Growth Resistance Curves for an Fe-Ni-Cr Superalloy [25].

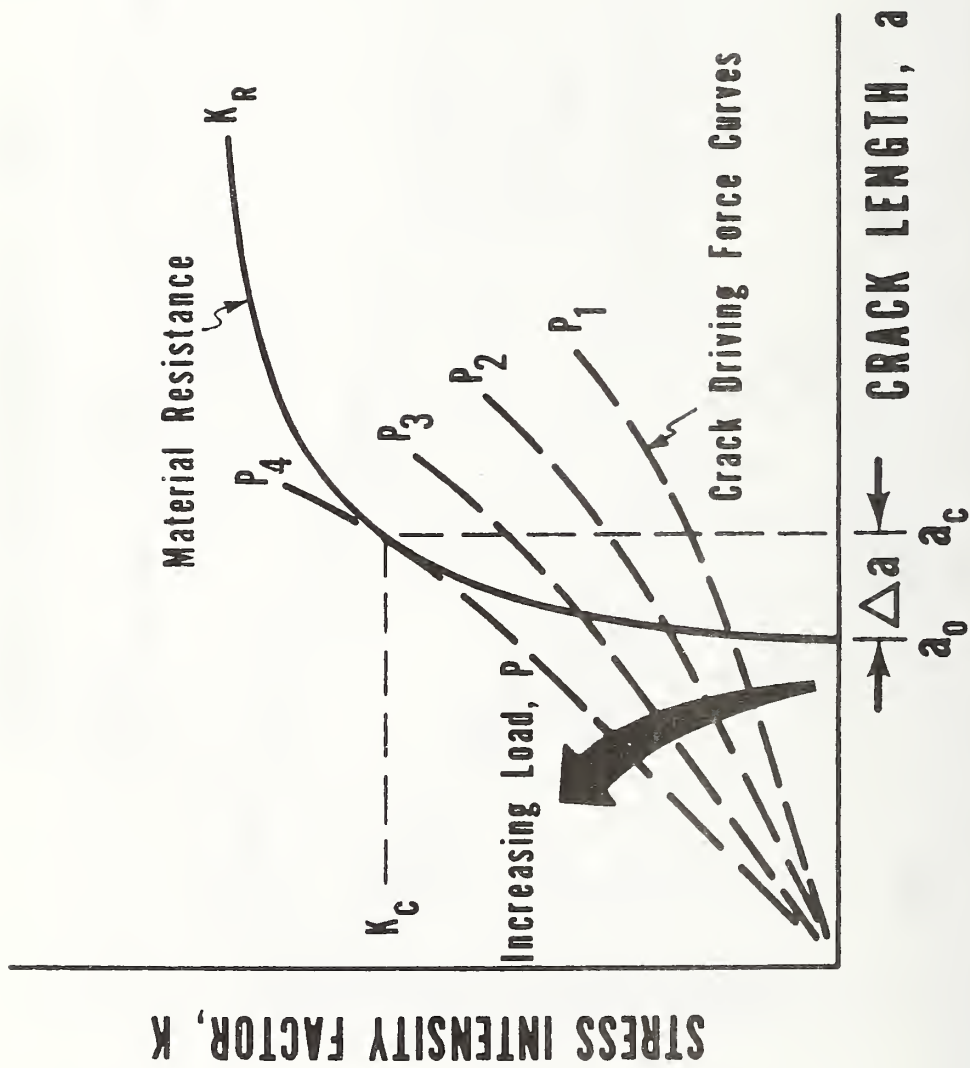


Fig. 5. Crack Growth Resistance Curve and Crack Driving Force Curves in R-Curve Format [28].

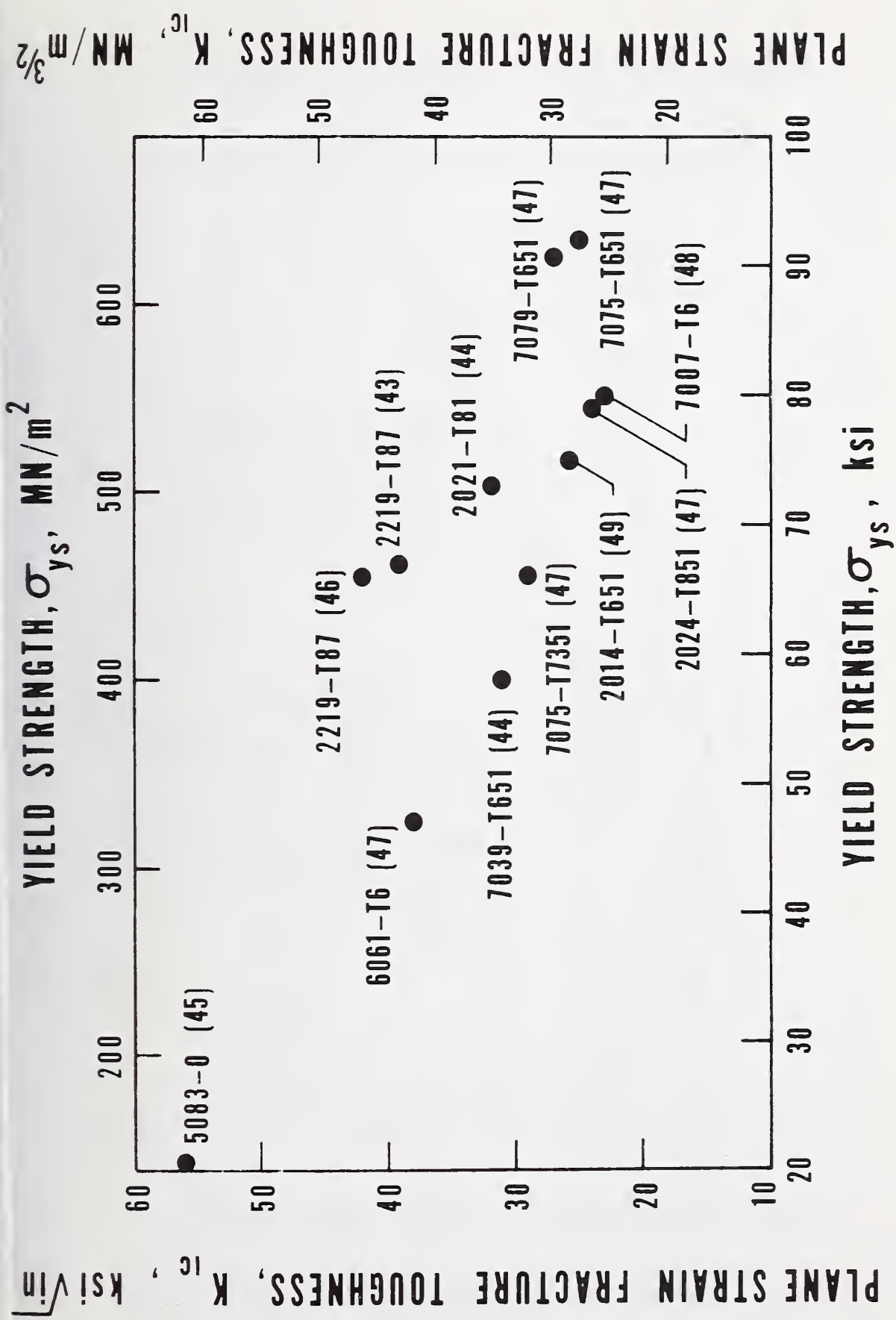


Fig. 6. Fracture Toughness of Aluminum Alloys at 76 K.

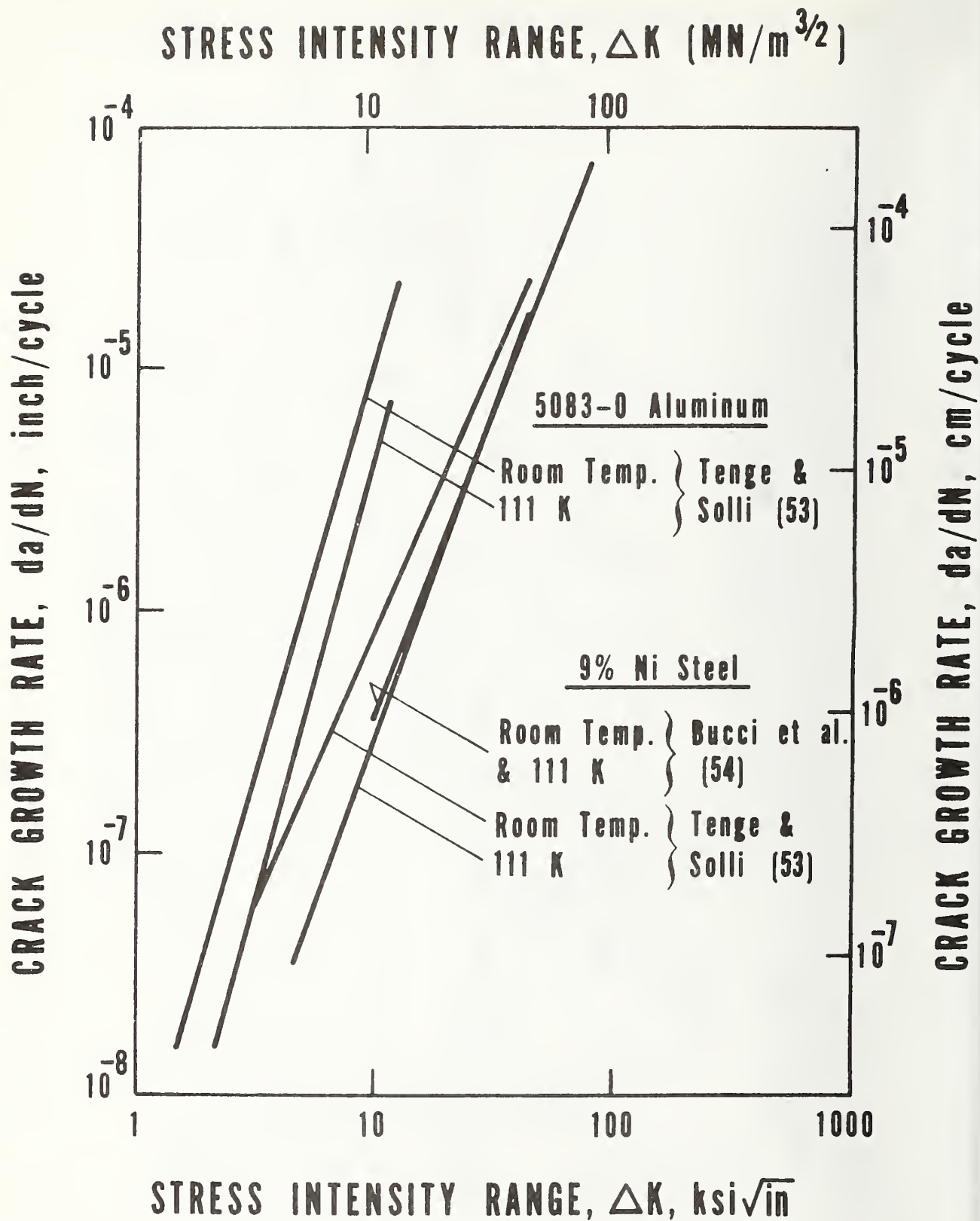


Fig. 7. Fatigue Crack Growth Behavior of 5083-0 Aluminum and 9% Ni Steel at LNG Temperature (111 K).

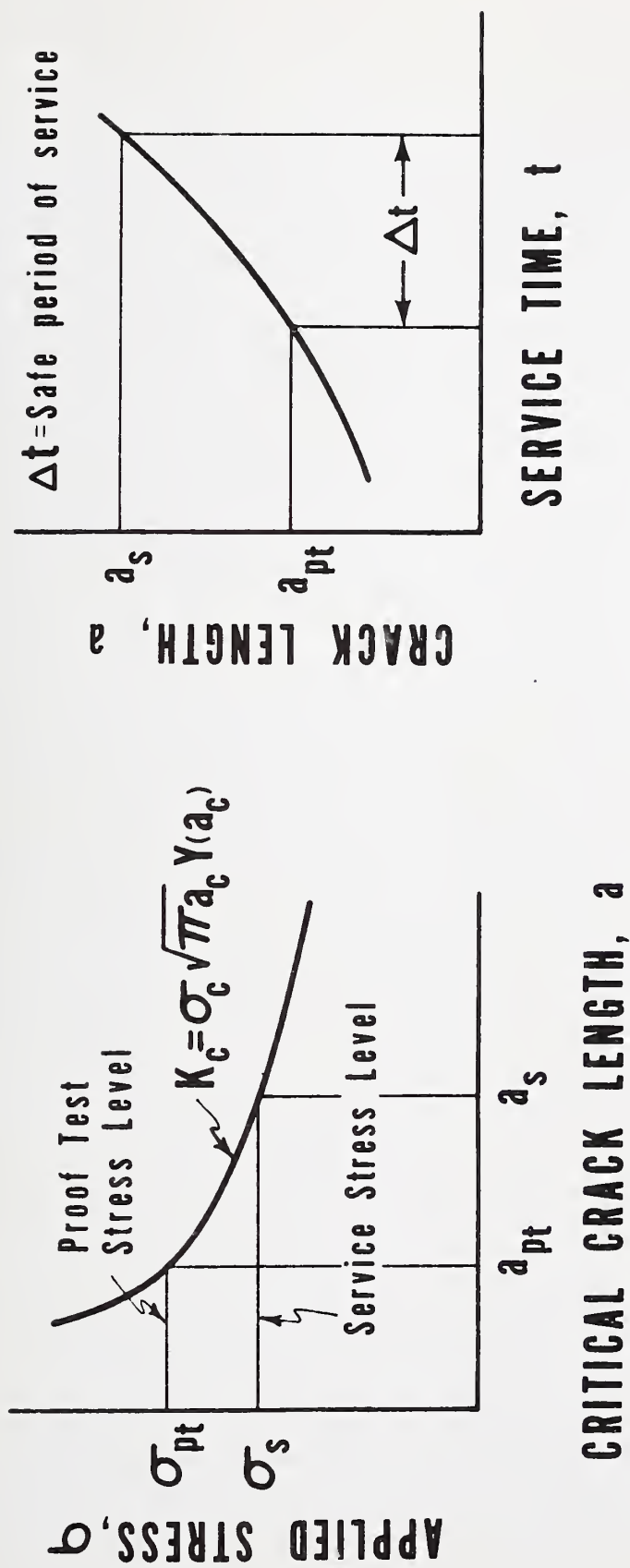


Fig. 8. The Proof Test Concept [57].

APPENDIX J

SHIP STEEL WELDMENTS FOR LOW TEMPERATURE SERVICE *

by

Harry I. McHenry

Cryogenics Division
Institute for Basic Standards
National Bureau of Standards
Boulder, Colorado 80302

Preprint of paper prepared for presentation at the Fourth Army Materials Technology Conference, Advances in Joining Technology, Boston, MA, September 16-19, 1975.

SHIP STEEL WELDMENTS FOR LOW TEMPERATURE SERVICE*

H. I. McHenry
National Bureau of Standards
Cryogenics Division
Boulder, Colorado

ABSTRACT

The ship steels, welding practices and weldment toughness requirements applicable to low temperature (to -46°C) regions of liquefied-natural-gas (LNG) tankers are reviewed. In the construction of LNG ships, the principal welding productivity problem is the low deposition rate associated with the low heat input welding practices required to provide sufficient toughness in the weld heat-affected-zone (HAZ). A potential solution to this problem is to use improved steels which can be welded using efficient procedures and still provide satisfactory HAZ toughness. The steelmaking practices that contribute to low temperature toughness are reviewed with respect to economic limitations associated with ship steels and to their potential for improving HAZ toughness.

* Contribution of NBS -- not subject to copyright.

INTRODUCTION

A large fleet of tankers is under construction for the marine transport of liquefied natural gas (LNG). In LNG ships, significant portions of the hull are cooled by the cryogenic cargo to temperatures ranging from 0 to -46°C . At these temperatures many ship steels exhibit brittle behavior. Consequently, the U.S. Coast Guard (USCG),¹ the American Bureau of Shipping (ABS)² and comparable regulatory agencies around the world have established strict requirements on the ship steels and weld procedure qualifications for weldments subjected to low temperatures. To meet these requirements, shipyards generally employ low-heat-input, multipass welding practices for welds in the low temperature regions of the hull. As a result, welding productivity is being limited to a level far below the capability of the equipment and facilities.

The Maritime Administration (MarAd) was advised of the increased costs of welding LNG ship hulls by the Welding Panel of the Ship Production Committee, a group of industry experts organized by the Society of Naval Architects and Marine Engineers to advise MarAd on how to improve shipyard productivity. In their efforts to reduce the cost of ship construction, MarAd requested the National Bureau of Standards to conduct a survey to establish the feasibility of improving the efficiency of welding ship steels for low temperature service. The survey included visits to the shipyards involved in LNG construction, to the appropriate regulatory agencies, to the steel plate producers and to other companies engaged in fabricating structures for low temperature service. These visits clarified the problem and the rules, and provided a review of the technology available for improving welding efficiency. The survey has been completed and the results are presented herein.

SHIPYARD PRACTICE

The LNG ships under construction in the United States are approximately 280 m long, 42 m wide and 30 m deep and have a cargo capacity of 125,000 cubic meters. The ships are double-hull vessels with transverse bulkheads dividing the ship into several cargo bays as shown in Figure 1.³ The cryogenic containment system fitted within each cargo bay consists of the cargo tank, the insulation and a secondary barrier to contain the

LNG in case of tank failure. Thomas and Schwendtner⁴ have described eight types of containment systems in use or under consideration worldwide. In the U.S., three designs are under construction: The Conch free-standing prismatic tank, the Gazocean membrane prismatic tank and the Kvaerner-Moss free-standing spherical tank. For each system, the insulation is sufficient to permit transport of the LNG at approximately -162°C and atmospheric pressure with boil-off rates less than .25% per day.

The temperature environment within the hull is a function of the ambient air and water conditions, the effectiveness of the insulation system and the proximity of the cargo. For North Atlantic routes, the USCG specifies that the design temperatures be based on assumed ambient conditions of -18°C air, a 5 MPH (2.33 m/s) wind and still water at 0°C. The inner hull, the transverse bulkheads and the tank support structure are the principal areas cooled by proximity to the cargo. Minimum design temperatures in these areas range from 0°C to -46°C. The coldest locations are the inner side-shell above waterline and parts of the tank support structure.

STEEL SELECTION

The chemistry, processing and testing requirements of steels used in LNG ships being made in the U.S. are summarized in Table I. These steel selections are generally in accordance with the proposed (1975) regulations of the International Maritime Consultive Organization (IMCO) as outlined in Tables II and III. For temperatures below -10°C, fully-killed, aluminum treated, fine grain, C-Mn-Si steels are used. For temperatures below -25°C, the steel must also be either normalized or quenched and tempered. The most commonly used steels are the ABS ordinary strength grades; CN is used for temperatures to -23°C, CS for temperatures to -34°C and V-051 for temperatures to -46°C. For high strength applications, ABS grade EH steel is commonly used for temperatures to -34°C and ASTM grade A537 Modified is used for temperatures to -46°C.

Approximately 28,000 metric tons of steel are required for the hull of a 125,000 cubic meters LNG ship. The tonnage requirements for all grades of hull steel and for low temperature steels are summarized in Table IV. These data are indicative of the total usage of low temperature

steels and include significant tonnage selected for improved toughness and used in parts of the ship not exposed to temperatures below 0°C.

WELD PROCEDURE QUALIFICATION

For service temperatures less than -18°C, the welding procedures must be qualified in accordance with USCG and ABS requirements. Procedures are specific for each base metal, wire and flux combination and must be established for each welding process and position. The joint preparation, preheat and interpass temperatures, root coping and other aspects of the procedure must be representative of the procedures used in production. Generally, two qualifications are required to cover the range of plate thicknesses: $9.5 < t \leq 19$ mm and $t > 19$ mm. Test plates for these qualifications are usually 19 mm thick for the lower thickness range and the maximum thickness used in production for thicknesses greater than 19 mm. The test plates are oriented such that the weld axis is parallel to the rolling direction.

The qualification requirements include the room temperature tensile and guided bend tests specified by ABS for all weld procedure qualifications plus a series of Charpy V-notch impact tests. The Charpy tests are conducted at 5.5°C below the minimum service temperature in accordance with ASTM A 370, using type A specimens. The specimens are cut transverse to the weld axis with the notches normal to the plate surface. Three specimens are tested for each of the following notch locations: centered in the weld metal; on the fusion line; and in the heat affected zone (HAZ) 1, 3 and 5 mm from the fusion line. The impact specimen location requirements are summarized in Figure 2. The average Charpy value must equal or exceed 2.8 kgm (20 ft lb); the minimum value for one specimen is 1.9 kgm (13.3 ft lb).

WELDING PROCESSES AND CONSUMMABLES

Conventional shipyard welding practices are generally being used to fabricate low temperature steels; however, the heat inputs are restricted in order to meet the Charpy impact requirements. Consequently, the deposition rates are far below the equipment capabilities. The principal welding processes are submerged arc (SA), shielded metal arc (SMA) and gas metal arc (GMA). For flat position welds and horizontal fillet welds, SA is the most efficient and reliable process, and therefore is widely used on automated panel-lines.

Both SMA and GMA are used for most of the other welding; the selection of one process over the other varies widely from yard to yard. Variations of these processes such as one-sided welding, gravity welding, tandem arc and 3 o'clock sub-arc welding are used in specific instances depending on the capabilities of the shipyard. High-heat-input processes such as the electro-slag and electro-gas processes are not approved by ABS for use on low temperature steels.

A wide range of wires, rods and fluxes are used to weld ship steels for low temperature service. For submerged arc welding, two approaches have been taken: 1) use a mild steel wire and an alloy flux, or 2) use an alloy wire and a neutral flux. The mild steel wires conform to AWS specification AS.17-69 Class EM12K, and the alloy fluxes are of a proprietary nature. The alloy wires, which contain 1 to 2% Mn, .1 to .5% Mo and .5 to 2.0% Ni, are welded with a neutral flux suitable for multipass welding. For SMA welding, the most common electrode is AWS E 8018-C3 which contains 1% Ni. In some cases, E 7018 electrodes, which contain 0.5% Mo, are used for moderately low temperatures and E 8018-C1 electrodes, which contain 2 to 2.75% Ni, are used for the lowest temperatures. Both solid and flux-core wires are used for GMA welding. The solid wires are alloyed with Mn, Mo and Ni for low temperature toughness and the cored wire generally has a mild steel sheath and a proprietary flux.

Low-heat-input welding practices are necessary to meet the USCG impact requirements in the HAZ of low temperature ship plate weldments. This poses a significant productivity problem to the LNG shipyards because deposition rate is proportional to heat input, and their welding equipment is capable of far greater deposition rates than are possible using the low-heat-input practices. Consider, for example, the welding procedures that are representative for welding 19mm plate. For X-ray quality welds in steels such as ABS grade B, the following conditions are recommended:⁵

Joint preparation: double V groove with an 8 mm land

Backing weld: 850 amps, 33 volts, 16 in/min (.68 cm/sec), 105 kJ/in.
(267 kJ/cm)

Finishing weld: 1150 amps, 35 volts, 13 in/min (.55 cm/sec),
186 kJ/in. (472 kJ/cm)

In contrast, 19 mm ship plate for low temperature service must be multipass welded with the heat input limits ranging from about 40 to 80 kJ/in. (102 to 203 kJ/cm) depending on the particular combination of steel grade and service temperature. At heat input levels within this range, anywhere from 4 to 14 passes may be required to weld 19 mm plate.

Two approaches to solving the productivity problem are apparent: either change the weldment toughness requirements or improve the tolerance of the base metal to higher heat input welding practices. Changing the rules is not a viable solution to the problem, because strict requirements are appropriate for hazardous cargo such as LNG. In addition, the requirements have recently been adapted by IMCO as standards acceptable to all major shipping countries. Thus, any change in the existing requirements would probably be contingent upon agreement by both the USCG and IMCO, certainly a long term proposition. The alternative solution would be to make available an economical steel which, when welded using efficient procedures, provides the required level of toughness. This potential solution is attractive because it is based on steelmaking technology and shipyard economics instead of international agreements. The feasibility of this solution is addressed in the next section.

STEELMAKING TECHNOLOGY

Current steelmaking technology offers several methods for providing improved toughness at low temperatures. The methods include alloying, rolling practice, sulfide shape control and heat treating. The extent to which the improvements are reflected in HAZ toughness of high heat input welds is not well documented. Nevertheless, there exists reason to believe that one or a combination of the available metallurgical treatments will permit higher heat inputs than currently being used. Whether or not the improvement will be economically justifiable depends on the cost increment added to the price of the steel and the extent of the improvement. Because of the large tonnages involved, the added cost of an improved ship steel will likely be limited to a maximum of \$20 to \$60 per ton, depending on the specific application.

ALLOYING

The use of additional alloying to improve ship steels is severely constrained by steel pricing practices. Steel prices are comprised of a base price and extras for the specification, plate dimensions and quantity. There are two base prices; the carbon steel base and the alloy steel base, the latter of which is about 40% higher. The carbon steel base price is applicable to all the steels used in LNG ship hulls. The American Iron and Steel Institute (AISI) considers a steel to be an alloy steel when either (1) the maximum of the range given for the content of alloying elements exceeds one or more of the following limits: Mn, 1.65%; Si, 0.60%; Cu, 0.60%; or (2) a definite range or a definite minimum quantity of any other element is specified to obtain a desired alloyed effect.⁶ The chemistry specification for ABS EH 36 shown in Table I is typical of the degree of alloying permissible in carbon steels. Notice that there are no minimum requirements on alloying elements such as Cr, Mo, Ni, V and Nb. Thus, the steelmaker has flexibility on how best to achieve the required tensile and impact properties. These pricing practices preclude the use of 0.4 to 0.8% Ni additions that are frequently specified for low temperature applications by Japanese and European shipbuilders. However, the transition temperature of ship steels can be reduced by alloy adjustments within the AISI limits for carbon steels. As shown in Figure 3, the transition temperature is reduced by increasing the Mn content and by lowering C, Si and N.⁷

Microalloying with Nb or V is an economical approach to providing strength and good low temperature properties in the base plate, and is currently used in EH 36 and A537 Modified steels. Strengthening is provided by a combination of reduced grain size and precipitation hardening. The low temperature toughness is improved because of the small grain size--an improvement that is only partially offset by the precipitation hardening effect shown in Figure 3. However, the HAZ toughness near the fusion line is adversely affected by grain coarsening and further reduced by the strengthening effect of carbonitride precipitation.^{8,9} This embrittlement is almost always observed in simulated HAZ specimens, but is frequently not evident in Charpy specimens taken from weldments. The absence of embrittlement in high-heat-input weldments such as shown in Figure 4 suggests that the high toughness material surrounding the

embrittled region substantially reduces the embrittlement.¹⁰ It is not clear at this time whether this can be attributed to an averaging effect, i.e., the Charpy impact specimen samples a composite of high and low toughness material, or to a reduction of constraint provided by the ductile material surrounding the embrittled region. In either case, it appears that the problem of Cb or V embrittlement in the HAZ may not be as significant in real weldments as suggested by some investigators^{8,9} on the basis of simulated HAZ studies.

INCLUSION CONTROL

Nonmetallic inclusions are an intrinsic constituent of all steels. There are two main types of inclusions: 1) the indigenous inclusions which precipitate in the molten or solidifying metal due to decreased solubility of oxygen and sulfur upon cooling, and 2) the exogenous inclusions which are introduced into the steel from materials such as the refractories which come in contact with the molten steel. The indigenous inclusions are far more numerous and predictable in their behavior than the exogenous types, which occur sporadically. The principal types of indigenous inclusions are oxides and sulfides. In Al-killed steels, the dominate oxide is Al_2O_3 , which precipitates as small refractory crystals that do not agglomerate and do not change shape appreciably during rolling operations.

The principal sulfide inclusion in C-Mn steels is MnS. In low oxygen steels (e.g., Al-killed), the MnS inclusions are quite plastic and tend to elongate during rolling. These stringer-shaped inclusions separate readily from the steel matrix, and have a higher surface-to-volume ratio and a shorter interparticle spacing than globular inclusions. Consequently, the MnS stringers serve as initiation sites for low energy fracture when the steel is loaded transverse to the direction of rolling.

Sulfide shape control is rapidly emerging as a practical tool for eliminating stringers and thereby improving the transverse toughness of structural steels.¹¹ The process generally consists of lowering the sulfur content of the heat below .015% and then adding elements to the melt which form refractory sulfides. The refractory sulfides take on a spherical shape in the liquid steel and tend to retain this shape upon solidification and during the rolling process. Several elements, including Ti, Zr, Ca, Mg and the rare

earth metals, form refractory sulfides. Although practices vary widely, sulfide shape control by the ladle addition of rare-earth metal (REM) in the form of mischmetal, a mixture of rare earths containing about 50% Ce, appears to be gaining favor. The rare earths are preferred over Ti and Zr because, in addition to shape control, an appreciable reduction in sulfur content occurs due to the solution of rare earth sulfides and oxysulfides in the slag. Calcium and magnesium are effective for both sulfide shape control and sulfur reduction; however, Mg is difficult to introduce into molten steel because of its high vapor pressure; and Ca, which is not soluble in liquid iron, does not mix readily enough to assure complete sulfide shape control. The influences of sulfur content and REM additions on toughness are shown in Figure 5.¹²

ROLLING PRACTICE

Significant toughness improvements can be obtained by altering the rolling practice. Cross rolling can improve transverse properties at a moderate increase in steel cost; however, substantial improvements require rolling ratios that approach unity. Steel specifications rarely include cross rolling requirements; however, a guaranteed transverse Charpy requirement generally implies that cross rolling will be used. Thus, the principal use for cross rolling is to make moderate improvements in transverse properties to assure conformance to a transverse toughness guarantee.

Controlled rolling can improve strength and low temperature toughness by substantially reducing the austenite grain size and the fineness and nature of the transformation products.¹³ It involves a schedule of reductions at specified temperatures, sometimes coupled with controlled cooling between passes and after the final pass. Most commonly, controlled rolling is limited to performing the final reduction at a specified temperature which is lower than normally employed. As shown in Figure 6, the reduction below 900°C causes a significant decrease in transition temperature. It is particularly useful for the production of line pipe, where the large tonnage involved permits optimization of the rolling schedules on an economical basis. For ship steels, the large variety of plate sizes, thickness and

grades, and the lack of facilities for producing controlled-rolled plates greater than 16 mm thick, limit the practicability of controlled rolling. In addition, the large variety of rolling schedules can lead to more scatter in the material properties than is associated with more easily controlled procedures such as normalizing. Due to these limitations, controlled rolling is not considered practical for improving the toughness of ship plate.

HEAT TREATMENT

Nearly all of the ship steels used for low temperature (to -46°C) applications are normalized. The typical normalizing heat treatment involves heating the as-rolled plate to $925 \pm 25^{\circ}\text{C}$ and air cooling to room temperature. As shown in Figure 7, the low temperature toughness of these steels could be improved by a quench and temper (Q and T) heat treatment.¹⁴ For C-Mn steels such as ship plate, Q and T involves heating to $925 \pm 25^{\circ}\text{C}$, quenching in water and subsequently tempering at $650 \pm 50^{\circ}\text{C}$. This heat treatment is nearly twice as expensive as normalizing. Although Q and T improves base plate toughness, it is not clear whether this benefit will be apparent in the heat affected zone of weldments. It is considered likely that the reheat-treatment caused by the weld thermal cycle will impart the same toughness to the heat affected zone regardless of prior heat treatment. Thus, the extra cost of Q and T over normalizing (\$30 to \$40/metric ton) is not considered a cost effective means of improving heat affected zone toughness.

WORK IN PROGRESS

On the basis of the shipbuilding and steel industry survey, MarAd requested NBS to conduct a follow-on program in cooperation with the LNG shipbuilders to evaluate improved ship steels for low temperature service. In this program, the major steel companies are providing the LNG shipyards with production heats of ABS steels, modified to possess improved transverse fracture properties at the appropriate test temperatures. The shipyards will evaluate these steels by qualifying optimum weld procedures in accordance with the USCG requirements. A comparison of the optimized procedures with those currently employed will be indicative

of the cost reduction possible through the use of improved steels. As a result, each participating shipyard will be in a position to make a rational decision regarding the cost effectiveness of premium quality steels. The program, currently in the formative stages, will be completed in mid-1976, and the results will be published shortly thereafter.

SUMMARY

A survey of the U.S. shipyards engaged in LNG ship construction, the major steel plate producers and the maritime regulatory agencies has been conducted to establish the feasibility of improving the efficiency of welding ship steels for low temperature service. The results of this survey suggest that application of state-of-the-art steelmaking technology can substantially improve the low temperature toughness of ship steels. A program is being conducted to determine if steels with improved toughness retain satisfactory toughness in the HAZ when higher-heat-input welding practices are used.

ACKNOWLEDGEMENTS

This work was sponsored by the U.S. Maritime Administration. The author wishes to acknowledge the many contributions of M. B. Kasen and R. P. Reed of NBS who collaborated on all aspects of the program described herein. The author also expresses appreciation to R. W. Schaffran of the U.S. Maritime Administration and W. C. Brayton of Bethlehem Steel Corporation who were responsible for initiating the program.

REFERENCES

1. Anon., U.S. Coast Guard Marine Engineering Regulations, Subchapter F, CG-115, July 1970.
2. Anon., Rules for Building and Classing Steel Vessels, American Bureau of Shipping, New York, 1974.
3. Emery II, W. B., Sterrett, E. L. and Moore, C. S., "Alaskan Liquefaction Plant to Supply Gas for Japanese Use," Oil and Gas Journal, 66(1), 55-59.
4. Thomas, W. D. and Schwendtner, A. H., "LNG Carriers: The Current State of the Art," 1971 Annual New York Meeting, The Society of Naval Architects and Marine Engineers, 1971.
5. Anon., "Submerged Arc Welding Handbook," Linde Reference Library, Union Carbide Corp., New York, 1974.
6. Anon., "Alloy Steel Plates," American Iron and Steel Institute, New York, April 1970.
7. Cordea, J. N. "Niobium-and Vanadium-Containing Steels for Pressure Vessel Service," Welding Research Council Bulletin No. 203, February 1975.
8. Hannerz, N. E., "Effect of Cb on HAZ Ductility in Constructional HT Steels," Welding Journal, 54, No. 5 (1975) 1625-1685.
9. Hannerz, N. E. and Jonsson-Holmquist, B. M., "Influence of V on the HAZ Properties of Mild Steel," Metal Science 8 (1974) 228-233.
10. Alia, B. L., Stern, I. L. and Null, C., "Toughness Evaluation of Electrodeposited and Electroslag Weldments," Project Report, The National Shipbuilding Research Program, U.S. Maritime Administration, March 1975.
11. Korchynsky, M., "The Relationships Between Sulfide Composition Morphology and Distribution on Mechanical Properties of HSLA Steels," presented at the International Symposium on Sulfide Inclusions in Steel, American Society for Metals, Port Chester N.Y., November 1974.
12. Kozasu, I. and Osuka, T., "Processing Conditions and Properties of Control-Rolled Steel Plates," in Processing and Properties of Low Carbon Steel, Gray, J. M. (editor), The Metallurgical Society of AIME, New York, 1973.
13. Gray, J. M., "Columbium (Niobium) as a Grain Refiner in Hot Rolled Steels," in Processing and Properties of Low Carbon Steel, Gray, J. M. (editor), The Metallurgical Society of AIME, New York, 1973.
14. Anon., "N-Tuf, Low Temperature Steels," Nippon Steel Corp., Tokyo, 1972.

Table 1. Specifications for Steel Plates Used in LNG Ship Hulls

	Ordinary Strength Grades			Higher Strength Grades	
	CN -23 (ABS 1972 Rules)	CS -34 (ABS 1974 Rules)	V-051 -46 (ABS 1974 Rules)	ELI-36 -34 (ABS 1974 Rules)	A537-A, Modified -46 (ASTM 1970 Standards)
	(ABS 1972 Rules)	(ABS 1974 Rules)	(ABS 1974 Rules)	(ABS 1974 Rules)	(ASTM 1970 Standards)
Minimum Design Temp, °C					
Chemical Composition, %					
C, Max	0.23	0.16	0.16	0.18	0.16
Mn	0.6-0.9	1.00-1.35	1.15-1.50	0.90-1.60	1.15-1.50
Si	0.1-0.35	0.10-0.35	0.10-0.35	0.10-0.50	0.15-0.50
P, Max	0.05	0.04	0.04	0.04	0.04
S, Max	0.05	0.04	0.04	0.04	0.04
Al	0.02-0.06	0.02-0.06	-	0.06 Max	-
Ni, Max				0.40	0.25
Cr, Max				0.25	0.25
Mo, Max				0.08	0.08
Cu, Max				0.35	0.35
Cb, Max				0.05	-
V, Max				0.10	0.08
Mechanical Properties					
Tensile, kg/mm ² (KSI)	41-50(58-71)	41-50(58-71)	41(58),Min	50-63(71-90)	46(65),Min
Yield, kg/mm ² (KSI)	-	24(34),Min	25(35),Min	36(51),Min	32(47),Min
Elongation in 50 mm	24%	24%,Min	24%,Min	22%,Min	22%,Min
Charpy Impact Requirements					
Test Temperature					
Energy, Min Avg. kg-m(ft-lb)			-51	-40	-51
No. of Specimens			2.8(20) Transverse 3/Plate	3.5(24) Longitudinal 3/Plate	4.2(30) Longitudinal 3/Plate
Heat Treatment	All grades normalized				
Deoxidation	All grades aluminum killed, fine grain practice				

Table II. IMCO Requirements for LNG Hull Steels

Minimum Design Temperature, T, °C	Plate Thickness, t mm	Approved ABS Steel Grades
$T \geq 0$	--	Normal Practice
$0 > T \geq -10$	$t \leq 12.5$	B
	$12.5 < t \leq 25.5$	D
	$t > 25.5$	
$-10 > T \geq -25$	$t \leq 12.5$	D
	$t > 12.5$	E
$-25 > T \geq -55$	--	See Table III

Table III. IMCO Requirements for LNG Hull Steels for
Design Temperatures of -25 to -55°C

Chemical Composition

C	Mn	Si	S	P	
.16% max	0.70-1.60%	0.10-0.50%	0.035% max	0.035% max	
Optional additions:					
Ni	Cr	Mo	Cu	Cb	V
0.80% max	0.25% max	0.08% max	0.35% max	0.05% max	0.10% max

Heat Treatment

Normalized or quenched and tempered.

Deoxidation

Fully killed, aluminum treated, fine grain practice.

Toughness Requirements

Temperature: 5°C below design temperature

Specimens: Charpy V-notch-transverse

Energy, min. avg.: 2.8 kg m

No. of Tests: 3 from each plate

Table IV. Usage of Low Temperature Steels in LNG Ship Hulls

Ship Design	Steel	Weldment Test Temp °C	Tonnage		Applications
			Long tons	(1000 Kg)	
Gazoclean Membrane Prismatic	All Grades	---	29,573		Total hull plus scrap and spare
	ABS CS	-34	9,666		Inner bottom, web frames, gunwale, bilge
	ABS V-051	-43	2,695		Inner side shell, transverse deck box
Conch Free Standing Prismatic	All Grades	---	17,810		Midbody (hull less bow and stern)
	ABS CN	-23	6,058		Trans. Bulkhead, inner side shell, deck
	ABS CS	-21 to -32	4,602		Inner bottom, gunwale, bilge
	CS Q&T	-45	418		Roll key
Kvaerner-Moss Free Standing Spherical	All Grades	---	17,393		Midbody
	ABS CN	-23	1,408		Inner hull
	ABS CS	-33	1,602		Transverse bulkheads
	ABS EH-36	-29	1,515		Deck girders
	ASTM A537 (Mod)	-51	1,185		Cylindrical tank support

LIST OF FIGURES

- Figure 1. Structural Arrangement of an LNG Ship Hull [3].
- Figure 2. Charpy V-notch Specimen Locations for Weld Procedure Qualification [1].
- Figure 3. Strength Toughness Vectors for Structural Steels [7].*
- Figure 4. Charpy Toughness Traverse for Cb-Treated EH-36 Weldment [10].
- Figure 5. The Effect of Rare Earth Metal Treatments on the Transverse Shelf Energy of Low Sulfur C-Mn Steel [12].**
- Figure 6. The Effect of Rolling Reduction Below 900°C on the Fracture Appearance Transition Temperature [13].**
- Figure 7. Charpy Impact Transition Curves for Normalized and for Quenched and Tempered CS Steel [14].

* Reprinted with permission of the Welding Research Council.

** Reprinted with permission of the Metallurgical Society of AIME.

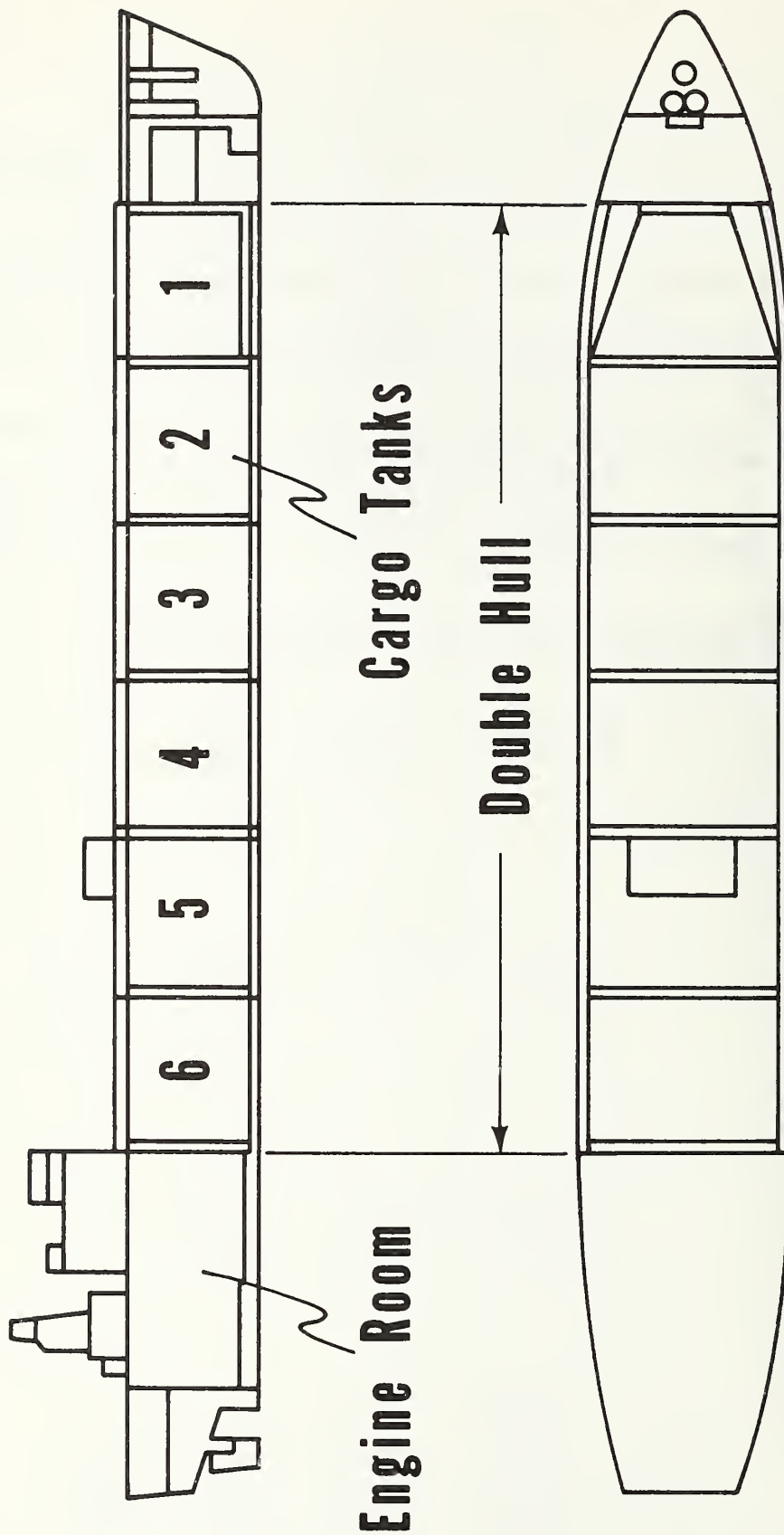
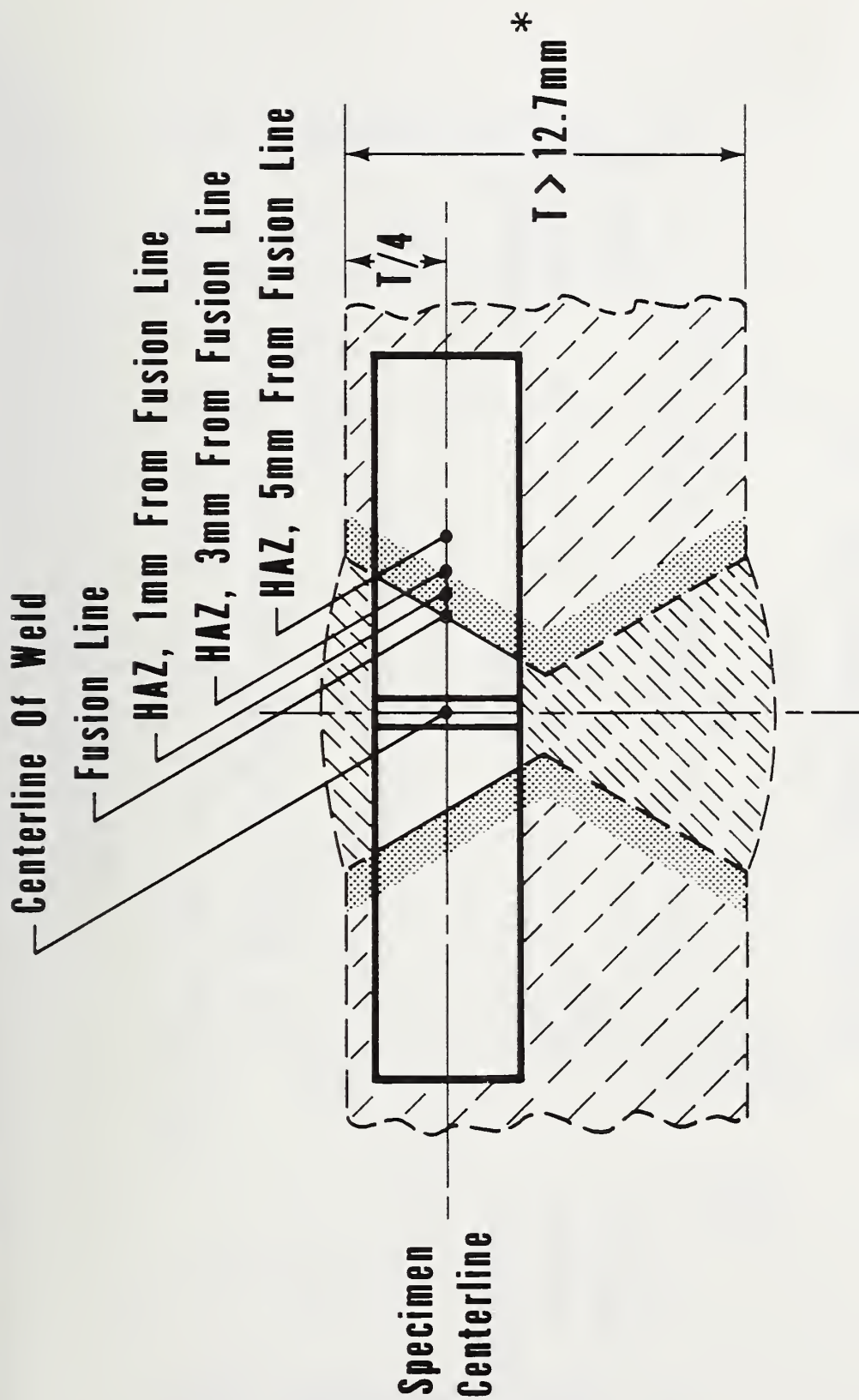


Figure 1.



* For $T \leq 12.7\text{mm}$, Specimen Centerline At $T/2$

Figure 2.

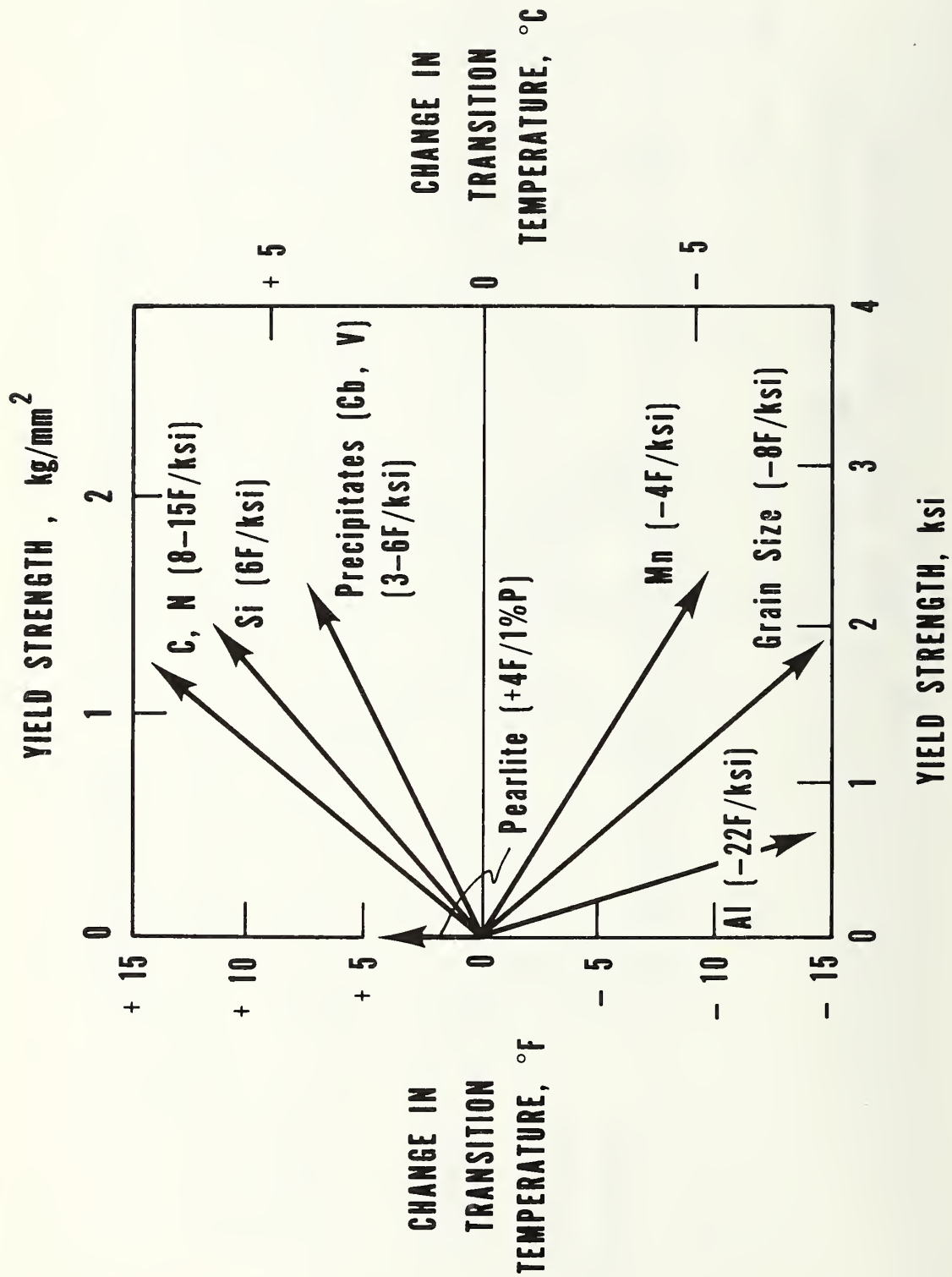


Figure 3.

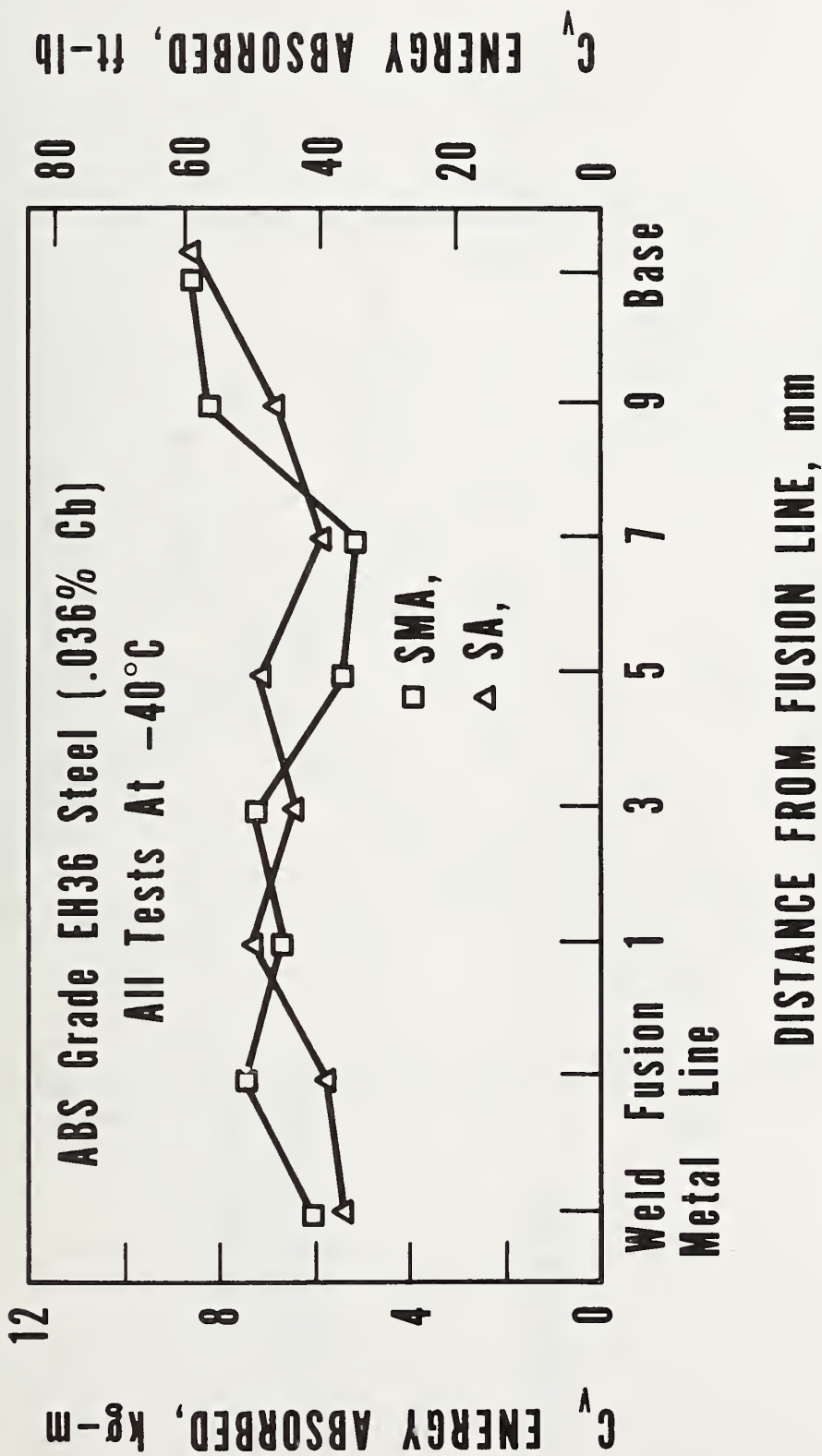


Figure 4.

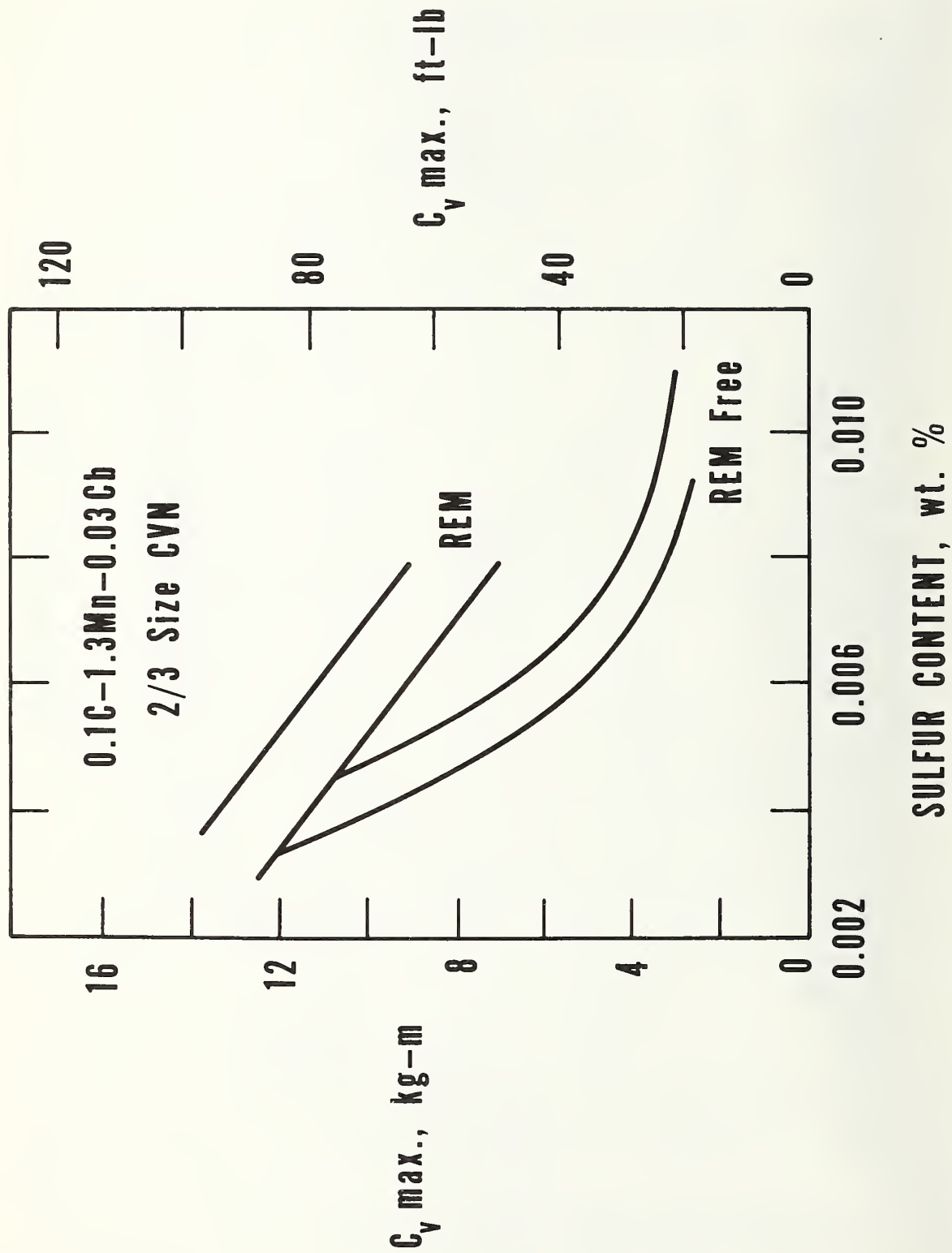


Figure 5.

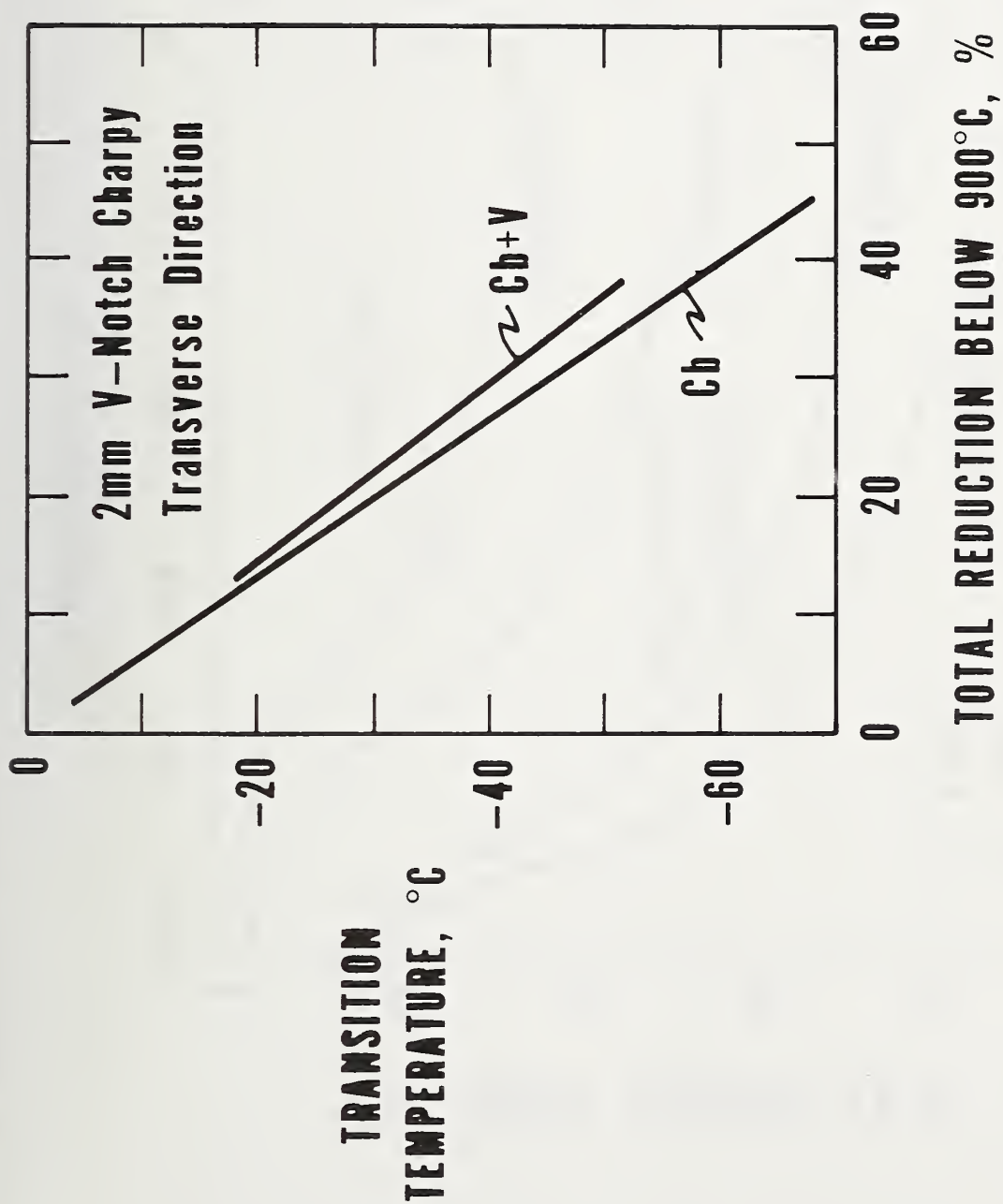


Figure 6.

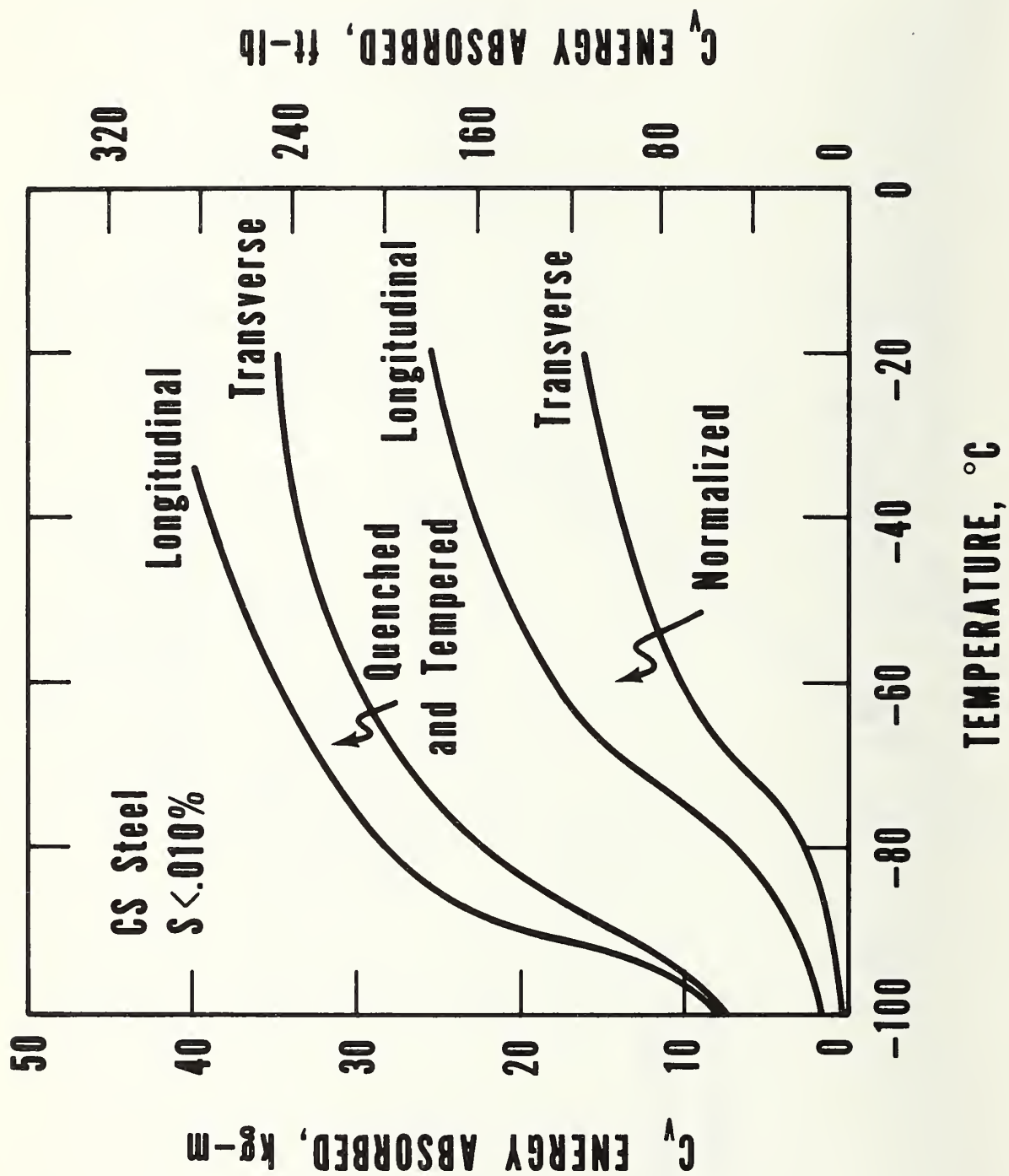


Figure 7.

APPENDIX K

The refractive index and Lorenz-Lorentz function of fluid methane*

James D. Olson†

Institute for Basic Standards, National Bureau of Standards, Boulder, Colorado 80302

(Received 13 February 1975)

The refractive index of gaseous and liquid methane was measured between 95 and 300 K and to pressures of 225 bar (1 bar = 10^5 Pa). The measurements were performed at the ^{198}Hg vapor green line, $\lambda = 546.2$ nm, with a Fabry-Perot interferometer referred to vacuum. The refractive index data were combined with the previously measured densities of methane to calculate the Lorenz-Lorentz (LL) function. Refractometric virial coefficients were obtained from analysis of the small ($\sim 0.5\%$) maximum exhibited by the (LL) function with increasing density. B_R , the second refractometric virial coefficient, is estimated to be ~ 6.0 (cm^3/mol)² and is almost independent of temperature between 220 and 300 K. The critical point refractive index, $n_c = 1.10333$, was extrapolated from a rectilinear diameter treatment of the saturated liquid and vapor results. The critical point refractive index was combined with an estimate of the critical point (LL) function to yield a critical density of methane, $\rho_c = 10.16 \pm 0.01$ mol/l.

I. INTRODUCTION

The refractive index n and the molar density ρ are related by the Lorenz-Lorentz (LL) electromagnetic equation of state:

$$(\text{LL}) = \frac{n^2 - 1}{n^2 + 2} \frac{1}{\rho} = \frac{4\pi N_A}{3} \alpha_e^0, \quad (1)$$

where N_A is Avogadro's number and α_e^0 is the isolated molecular electronic polarizability. For real nondipolar gases, the (LL) function shows small ($\approx 1\%$) deviations from the rhs of Eq. (1). These deviations may be represented by a density expansion analogous to the thermodynamic virial equation of state,

$$(\text{LL}) = A_R + B_R \rho + C_R \rho^2 + \dots, \quad (2)$$

where A_R, B_R, C_R are the refractometric virial coefficients. Similarly, the dielectric constant ϵ is related to the molar density by the Clausius-Mossotti (CM) equation and the dielectric virial coefficients,

$$(\text{CM}) = \frac{\epsilon - 1}{\epsilon + 2} \frac{1}{\rho} = A_D + B_D \rho + C_D \rho^2 + \dots. \quad (3)$$

This article reports the experimental determination of the refractive indices of methane at temperatures between 95 and 300 K and at pressures to 220 bar. The (LL) function was calculated by combining these data with the experimental densities of Goodwin and Prydz.¹ The purposes of this study are twofold: (i) To provide data with which to test the (LL) relation and estimate the magnitude of the refractometric virial coefficients. This type of study is useful in assessing the details of the intermolecular potential function and in the correlation of the macroscopic properties of nondipolar fluids.² (ii) To provide additional thermophysical properties data for methane whose other macroscopic properties have been measured in this laboratory. In particular, this study will suggest refinements in the PVT surface of methane near the critical point, similar to a recent analysis on hydrogen.³

The microscopic expressions for the refractometric and dielectric virial coefficients have been derived in

many forms.⁴⁻⁸ Careful experiments are required to provide data sufficiently precise to obtain refractometric virial coefficients and to test molecular theories of refractive index. Unlike the more abundant studies of the CM function and the dielectric virial coefficients,⁸ there have been few experimental determinations which provide data over large ranges of density and temperature. Michels and co-workers measured the refractive index of carbon dioxide,⁹ nitrogen,¹⁰ ethylene,¹¹ and argon¹² interferometrically to high pressures (2.5 kbar) at room temperature and above. As the precision of these measurements decreased rapidly at lower densities, their chief achievement was to determine the behavior of the (LL) function at densities above the critical density. Teague and Pings¹³ measured the refractive index of argon from temperatures near the triple point temperature to temperatures above the critical point and to pressures of 100 bar. Diller¹⁴ of this laboratory performed precise interferometric measurements of the refractive index of hydrogen at temperatures from 15 to 300 K and at pressures to 230 bar. This work indicated significant deviations from Eq. (1) in qualitative agreement with molecular theory. Buckingham and Graham¹⁵ recently measured the first and second refractometric virial coefficients, A_R and B_R , for several gases at room temperature using a differential interferometric expansion technique.

II. EXPERIMENTAL METHOD AND APPARATUS

The refractive index was measured with a Fabry-Perot interferometer immersed in the fluid methane. The absolute index was obtained by monitoring the change in interference order while venting the fluid to vacuum. This reference to vacuum is necessary because interferometric measurements record only changes in refractive index. In this particular experimental arrangement, a change of one order in the interference pattern (passage of one fringe) corresponded to a change in refractive index of about 5×10^{-5} . Fractional order changes of about ± 0.025 could be detected, indicating an uncertainty of about $\pm 1 \times 10^{-6}$ in refractive index. This is about 100 times more sensitive than non-

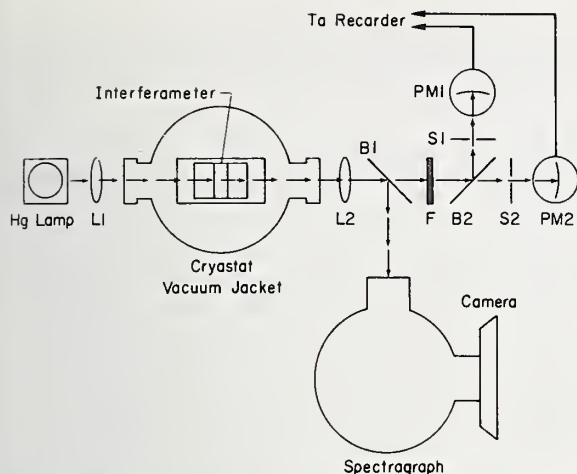


FIG. 1. Schematic diagram of optical arrangement, top view. Arrows indicate optical path.

interferometric methods of refractive index measurement. This procedure also has the advantage of not requiring a calibration experiment with a fluid of known refractive index.

The sample holder and cryostat were built from the original plans of Diller¹⁴ based on a general cryostat arrangement for hydrogen studies suggested by Goodwin.¹⁶ Complete details of this and other aspects of the experimental arrangement are discussed in the paper by Diller.¹⁴ Liquid nitrogen was used as the refrigerant except at 300 K. The high pressure sample holder is suspended from the refrigerant tanks by a reflux tube. Low temperature shields from these tanks attenuate radiation heat leaks. This assembly is contained in an evacuated cryostat equipped with windows to accommodate optical measurements.

Temperatures were measured on the IPTS-68 scale with a platinum resistance thermometer calibrated by the NBS Temperature Section. The sample holder temperature was proportionally controlled by electrical heating in a feedback loop from the output of the potentiometer used for the thermometer measurements. A guard ring and adiabatic shield were controlled to the sample temperature by differential thermocouples. This arrangement typically controlled the steady state temperature of the sample holder to ± 1.5 mK.

Fluid pressures were referenced from the sample holder system through a null pressure detector to an oil dead weight piston gauge. Equilibrium pressures derived in this manner are accurate to 0.04% or 0.007 bar whichever is greater.

The Fabry-Perot interferometer consisted of two fused-silica cylinders 1.1 cm in length which were wrung to a 0.5 cm tungsten spacer. The cylinders were vacuum coated with aluminum to about 50% transmission. The spacer is spacer #2 from the hydrogen work.¹⁴ A ¹⁹⁸Hg vapor lamp was used as the light source because the vacuum wavelength of the green line is precisely known to be 546.22705 ± 10^{-5} nm.¹⁷ The inter-

ferometer was entirely immersed in the fluid methane which allowed an unambiguous calculation of the pressure correction to the spacer length.

The sample was 99.99 mol% methane from a commercial supplier (1 mol CH₄ = 16.0430 g).¹⁸ Any residual water vapor was removed by passage of the methane through a molecular sieve trap immersed in an ice bath.

III. EXPERIMENTAL PROCEDURE

Absolute refractive indices were calculated from laboratory measurements by means of the data reduction formula,

$$n_\lambda = 1 + \frac{\lambda_{vac}(\Delta N)}{2t_{vac}} + \frac{P}{3B} + \frac{P}{3B} \left[\frac{\lambda_{vac}(\Delta N)}{2t_{vac}} \right], \quad (4)$$

where ΔN = total fringe count to vacuum, λ_{vac} = vacuum wavelength of light, t_{vac} = vacuum spacer length at the temperature of the fluid, P = pressure of the fluid, and B = bulk modulus of tungsten, taken to be $3.14 \pm 0.03 \times 10^6$ bar. The spacer length was determined by observation of the coincidence of the vacuum fringe patterns for the different wave lengths of ¹⁹⁸Hg light by means of the method of exact fractions.¹⁹ The fractional part of the total fringe count was calculated from photographs of the ring diameters of the initial and final interference patterns.²⁰ The application of those techniques and the derivation of Eq. (4) is discussed in detail by Diller.¹⁴

A major difficulty is the unambiguous determination of the total fringe count between an initial point in the fluid and vacuum. A decrease in the interference order, which is caused by a decrease in the spacer length or a decrease in the refractive index of the fluid, is indicated by the collapse of the concentric Fabry-Perot rings toward the center of the fringe pattern. The reverse direction of fringe travel indicates an increase in the spacer length or refractive index of the fluid. The integral interference order change (fringe count) may be recorded by focusing the center of the ring pattern upon a photoelectric device. A strip chart record of the periodic intensity changes of the interference pattern allows one to count the total number of fringes. However, temporary reversals in the fringe direction may occur while venting the fluid to vacuum, particularly while making pressure measurements at intermediate points between the highest pressure and vacuum. This problem was overcome by monitoring the output of two photomultipliers which were positioned to observe slightly different parts of the ring pattern. The two strip chart fringe records were, therefore, slightly out of phase and reversals in the fringe count could be unambiguously determined.

The dual fringe patterns were monitored in the optical arrangement shown in top view by Fig. 1. These optical components were aligned with a small He-Ne laser. Light from the extended ¹⁹⁸Hg lamp source is focused by lens L1 into the interferometer through the vacuum window of the cryostat and the high pressure window of the sample holder. The ring pattern produced by the interferometer is imaged by lens L2 on the slit of a spectrograph after passage through a beamsplitter B1. The other branch of the optical train passes through a green

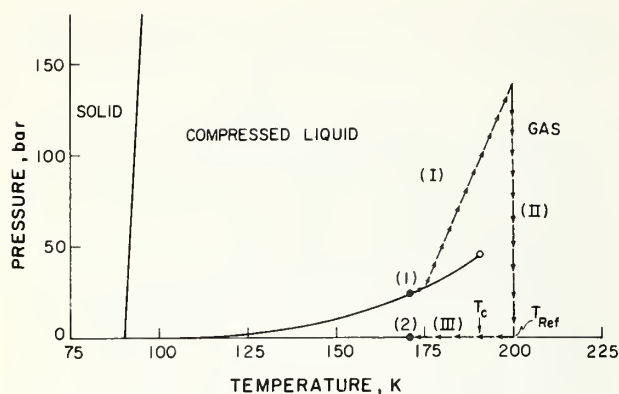


FIG. 2. Pressure-temperature phase diagram of methane. Arrows indicate fringe count path for measurement of saturated liquid refractive index.

filter F and second beamsplitter B2. These two images are focused on adjustable pinhole targets, S1 and S2. The pinhole targets admit light from slightly different parts of the ring pattern to two photomultiplier tubes, PM1 and PM2, whose output is recorded on a dual channel stripchart recorder. In addition, the output from the pinhole aligned exactly with ring pattern center is fed into a digital counter. This eliminates the tedious procedure of counting several thousand fringes from the strip chart record. However, the strip chart provided a permanent record of the fringe count that could be checked for discrepancies indicated by the (LL) function.

The experimental procedure for gas isotherms above the critical point was as follows: The sample holder was filled to the highest pressure for the particular run. After steady-state conditions were attained (about 30 min), the pressure was measured with the dead weight piston gauge and a photograph of the ring pattern was taken. The pressure gauge was then isolated from the sample system by a needle valve and an amount of gas was slowly vented from the pressure bomb. The integer fringe count was monitored during this attenuation of the fluid pressure. The sample system was again equilibrated at a lower pressure, after which another photograph and pressure measurement were taken. This process continued to vacuum. The cumulative fringe count could then be added up for each pressure measurement and the refractive index calculated from Eq. (4).

Determinations of the refractive index of saturated vapor methane were carried out along isotherms. Methane was admitted to the evacuated sample holder at a subcritical temperature and the fringe count increase was recorded. When the increasing gas pressure reached the vapor pressure, the fringe pattern ceased changing as liquid condensed in the sample holder. The intersection with the two phase boundary was also indicated by a sudden increase in sample holder temperature as the liquid condensed. The fractional fringe count was estimated directly from the strip chart record to ± 0.1 fringe. This was necessary because of the poor quality of the equilibrium fringe pattern photographed on the saturation boundary. The vapor pressure was

either measured or calculated from the experimental results of Goodwin.²¹ In either case, these data were then substituted into Eq. (4) to yield the refractive index.

Nonisothermal measurements along the coexistence boundary were complicated because t_{vac} must be known or calculated for each temperature, and the presence of the vapor-liquid meniscus prevented the direct fringe count from a point in the liquid to vacuum. To overcome these difficulties, the fringe count was measured from a point on the coexistence boundary to vacuum at a reference temperature above the critical point. Two adjustments were made on the data before using Eq. (4): (i) The vacuum spacer length was calculated from an equation derived from the experimental measurements of the temperature dependence of the length of the spacer. (ii) The total fringe count was adjusted to correspond to the fringe count from the point on the coexistence boundary to vacuum at the same temperature. This correction is illustrated for the saturated liquid data by the methane phase diagram, Fig. 2. Because the refractive index is a thermodynamic state function, a measurement of Δn depends only on the initial and final states. The absolute index of the saturated liquid point labeled (1) on the phase diagram is obtained from the fringe count between (1) and (2) which is vacuum at the same temperature. The dotted line shows the actual temperature-pressure path used to measure the different parts of the fringe count. Part (I), an isochoric fringe count, and Part (II), an isothermal fringe count, are measured directly by counting the fringe count decrease to vacuum at the reference temperature (200 K) above the critical point. Part (III), from vacuum at the reference temperature to vacuum at the initial temperature, is calculated from the change in the vacuum spacer length:

$$\lambda_{vac} N_{vac} = 2t_{vac} \quad (5)$$

$$\Delta N^{(III)} = N_{vac}^{T(1)} - N_{vac}^{T_{Ref}} = 2(t_{vac}^{T(1)} - t_{vac}^{T_{Ref}})/\lambda_{vac} \quad (6)$$

The change in t_{vac} is calculated from experimental measurements as described above. $\Delta N^{(III)}$ is added to the total fringe count from Secs. (I) and (II) and this total is substituted into Eq. (4) as usual.

The effect of the adjustment on the spacer length had a relatively small effect on (LL), typically a few parts in 100 000. However, the adjustment to the fringe count, $\Delta N^{(III)}$, was relatively large for the low temperature liquid. For methane at 95 K, $\Delta N^{(III)}$ was about 0.13% of the fringe count which increased the (LL) function by about 0.1%. A nonisothermal fringe count path from a point in the saturated vapor passed beneath the critical point; hence a reference temperature less than the critical point temperature could be used in this case. Because the fringe counts were small for low temperature saturated vapor data, the amount of the correction, $\Delta N^{(III)}$, was similar in magnitude to the total fringe count. Consequently, the saturated vapor refractive index data below 160 K decreases rapidly in accuracy. The tables of experimental results for the coexistence boundary nonisothermal runs include the calculated spacer length and fringe count adjustment for each temperature.

TABLE I. Experimental results for methane at 300 K.

ID	P (bar)	n	ρ (mol/l)	(LL) (cm ³ /mol)	Fringe (count)
615	1.278	1.000508	9.34
615	1.701	1.000679	12.49
614	2.116	1.000844	15.52
613	2.523	1.001008	18.53
612	2.937	1.001174	21.58
512	2.998	1.001199	22.03
526	3.000	1.001199	22.04
525	3.000	1.001199	22.04
524	3.003	1.001203	22.11
523	3.005	1.001203	22.11
513	3.022	1.001209	22.23
611	3.290	1.001319	24.24
511	3.328	1.001331	24.46
518	3.706	1.001484	27.28
610	3.742	1.001500	27.57
510	3.744	1.001498	27.54
609	4.126	1.001654	30.41
509	4.150	1.001662	30.56
514	4.375	1.001755	32.26
608	4.543	1.001825	33.55
508	4.553	1.001826	33.57
607	4.949	1.001890	36.57
507	4.983	1.002001	36.78
506	5.329	1.002141	39.35
606	5.360	1.002155	39.61
605	5.749	1.002311	42.47
505	5.770	1.002320	42.64
517	6.129	1.002468	45.37
604	6.162	1.002480	45.58
504	6.186	1.002488	45.72
603	6.570	1.002646	48.64
503	6.593	1.002655	48.80
602	6.927	1.002793	51.33
502	6.958	1.002815	51.74
521	7.418	1.002992	54.99
522	7.418	1.002992	54.99
520	7.422	1.002993	55.02
519	7.423	1.002993	55.02
501	7.429	1.002997	55.08
516	7.473	1.003013	55.38
515	7.473	1.003013	55.38
601	7.479	1.003020	55.51
2805	17.154	1.007043	129.45
2804	32.150	1.013562	249.23
2803	46.433	1.020091	369.30
2802	60.092	1.026622	489.36
201	65.927	1.029497	2.949	6.6340	542.20
105	65.983	1.029525	2.952	6.6341	542.71
307	68.965	1.031011	3.100	6.6334	570.03
407	69.038	1.031048	3.104	6.6334	570.70
2801	73.195	1.033136	3.312	6.6319	609.09
406	75.924	1.034524	3.449	6.6322	634.61
306	76.180	1.034653	3.463	6.6319	636.98
305	82.705	1.038005	3.785	6.6319	698.59
405	82.854	1.038098	3.804	6.6321	700.31
107	85.211	1.039300	3.924	6.6311	722.39
304	89.053	1.041309	4.122	6.6320	759.32
404	89.512	1.041705	4.162	6.6319	766.61
303	96.923	1.045455	4.532	6.6324	835.53
403	96.946	1.045469	4.534	6.6326	835.79
402	104.118	1.049236	4.910	6.6331	905.96
302	105.113	1.049820	4.963	6.6335	915.78
106	105.638	1.050101	4.990	6.6335	920.94
401	113.950	1.054566	5.430	6.6346	1003.02
301	114.430	1.054824	5.455	6.6346	1007.76
105	124.534	1.060275	5.990	6.6364	1107.95
104	144.848	1.071146	7.052	6.6389	1307.79
103	163.592	1.080853	8.000	6.6405	1486.77
102	184.859	1.091353	9.015	6.6413	1679.22
101	214.779	1.104755	10.308	6.6417	1925.57

The optical path of the light undergoing multiple reflections in the etalon was distorted whenever large density gradients were present in the fluid. This caused a degradation of the ring pattern that reduced the amplitude of the recorded interference fringes and destroyed the continuous fringe count. To prevent this, data were taken by slowly venting the fluid or slowly heating along the coexistence boundary in order to maintain near-equilibrium conditions.

The absolute fringe count to vacuum was measured for only one point in the saturated liquid, 183 K. The refractive indices at the other temperatures were determined by measuring the fringe count difference between those temperatures and 183 K. This was necessary because the entire coexistence boundary (91–190 K) could not be covered with one filling of the pressure bomb as Diller had previously done for hydrogen.¹⁴ The fluid methane passed into the saturated vapor or compressed liquid after a large enough temperature change. Also, the time required to count fringes along the path above the critical point (see Fig. 2) was prohibitive because the sample holder was heated very slowly to prevent density gradients that could destroy the fringe pattern.

IV. EXPERIMENTAL RESULTS

The results for 255 determinations of the refractive index of methane are displayed in Tables I–VII. The experimental ID numbers indicated the chronological order in which the data were taken. A change in the first two digits of the ID number indicates a new filling of the sample holder. Table VIII contains the vacuum spacer length measurements for the gas isotherm results. These data were combined with previous measurements on the same spacer¹⁴ to produce a correlation from which the spacer length could be calculated for measurements on the coexistence boundary as described in Sec. III.

The densities used to calculate the (LL) function for the gas isotherms were obtained in exactly the same manner as those used by Straty²² for Clausius–Mossotti (CM) experiments on methane. Experimental gas densities¹ were interpolated along an isotherm with a polynomial equation. However, these experimental data had a lower bound of about 3 mol/l; hence extrapolation to lower densities was not valid and the LL function was not evaluated. The low pressure data (3–7 bar) at 300 K were used to estimate the zero density limit, A_R , of the LL function as discussed in Sec. V.

The densities for saturated liquid methane were also calculated as described by Straty.²² At temperatures above 175 K, these numbers are obtained from an extrapolation²³ which is highly sensitive to the form of the fitting equation. This problem will be discussed further in Sec. V. The ID numbers for different temperature regions indicate the data were taken in several overlapping segments. The junction points between these runs were reproduced to 0.15 fringe.

Accurate densities for saturated vapor methane are especially difficult to measure. The LL function for

TABLE II. Experimental results for methane at 280 K.

ID	P (bar)	n	ρ (mol/l)	(LL) (cm ³ /mol)	Fringe (count)
2910	7.644	1.003318	60.98
2909	14.905	1.006580	120.94
2908	21.936	1.009844	180.94
2907	28.742	1.013110	240.96
704	32.373	1.014895	273.77
2906	35.341	1.016376	300.99
2905	41.728	1.019639	360.98
2904	47.970	1.022914	421.16
2903	54.007	1.026173	481.07
703	55.778	1.027143	498.89
2902	59.901	1.029439	2.944	6.6323	541.09
701	62.476	1.030893	3.089	6.6319	567.83
702	62.476	1.030893	3.089	6.6319	567.83
805	62.703	1.031021	3.102	6.6317	570.18
2901	65.699	1.032733	3.272	6.6311	601.64
705	77.783	1.039842	3.978	6.6303	732.30
804	78.314	1.040161	4.010	6.6303	738.18
803	95.770	1.050957	5.075	6.6328	936.61
706	96.399	1.051356	5.115	6.6331	943.95
708	107.895	1.058704	5.836	6.6352	1079.02
707	108.797	1.059287	5.893	6.6355	1089.73
802	111.339	1.060924	6.054	6.6356	1119.81
906	125.805	1.070278	6.968	6.6385	1291.76
801	128.082	1.071738	7.111	6.6383	1318.58
905	142.739	1.081039	8.016	6.6399	1489.56
904	159.312	1.091102	8.992	6.6401	1674.50
903	178.249	1.101772	10.023	6.6402	1870.62
902	200.126	1.112835	11.086	6.6403	2073.96
901	222.740	1.122864	12.046	6.6400	2258.29

the saturated vapor was calculated using the densities obtained by Goodwin²⁴ from intersection of his virial equation densities with the vapor pressure curve. These

TABLE III. Experimental results for methane at 250 K.

ID	P (bar)	n	ρ (mol/l)	(LL) (cm ³ /mol)	Fringe (count)
3010	6.174	1.003012	55.35
3009	12.598	1.006282	115.45
3008	18.722	1.009537	175.27
3007	24.600	1.012805	235.34
3006	30.233	1.016078	295.48
3005	35.942	1.019541	359.13
3004	41.107	1.022817	419.34
3003	46.058	1.026084	479.39
3002	50.804	1.029344	2.935	6.6306	539.30
1008	52.940	1.030858	3.085	6.6316	567.11
1001	54.677	1.032102	3.209	6.6311	589.98
3001	55.362	1.032598	3.259	6.6311	599.11
1007	66.726	1.041260	4.117	6.6329	758.31
1006	78.391	1.050972	5.076	6.6342	936.80
1005	90.025	1.061420	6.102	6.6365	1128.83
1004	100.300	1.071081	7.047	6.6377	1306.40
1003	109.979	1.080309	7.946	6.6392	1476.01
1107	122.379	1.091852	9.065	6.6400	1688.17
1002	123.304	1.092684	9.146	6.6398	1703.45
1106	134.331	1.102257	10.069	6.6405	1879.39
1105	146.728	1.112018	11.008	6.6405	2058.79
1104	162.000	1.122518	12.013	6.6399	2251.77
1103	180.747	1.133356	13.048	6.6386	2450.94
1102	201.627	1.143297	13.994	6.6361	2633.62
1101	222.795	1.151671	14.790	6.6334	2787.51

vapor (LL) results should not be considered comparable in accuracy with the more accurate values obtained for the supercritical isotherms.

Figure 3 shows a plot of refractive index vs temperature for the two phase region. The critical refractive index n_c was obtained by extrapolation from a rectilinear diameter treatment^{13,25} of the saturated liquid and vapor results. The more abundant liquid refractive index data were used to interpolate values for sparse refractive index vapor points above 160 K. These data were fit to a straight line:

$$n(T) = \frac{1}{2}[n(T)_{\text{mean}} + n(T)_{\text{liquid}}] = AT + B \quad (7)$$

An ordinary least squares fit to the nine data pairs yields these results for A , B , n_c , and their standard deviation estimates:

$$A = -4.423 \times 10^{-4}, \quad \text{S. D.}(A) = 1.5 \times 10^{-6},$$

$$B = 1.187615, \quad \text{S. D.}(B) = 3 \times 10^{-4},$$

$$n_c = 1.10333, \quad \text{S. D.}(n_c) = 2 \times 10^{-5}.$$

The refractive index at the triple point, 90.680 K, was

TABLE IV. Experimental results for methane at 220 K.

ID	P (bar)	n	ρ (mol/l)	(LL) (cm ³ /mol)	Fringe (count)
3110	6.187	1.003465	63.68
3109	11.669	1.006723	123.54
3108	16.837	1.009991	183.61
3107	21.709	1.013263	243.73
3106	26.267	1.016522	303.61
3105	30.569	1.019790	363.68
3104	34.606	1.023054	423.67
3103	38.401	1.026319	483.66
3102	41.950	1.029572	2.958	6.6307	543.45
1210	43.632	1.031188	3.119	6.6308	573.14
1201	44.447	1.031982	3.198	6.6293	587.72
3101	45.315	1.032855	3.284	6.6309	603.78
1209	52.806	1.040980	4.091	6.6308	753.09
1208	61.290	1.051908	5.168	6.6338	953.93
1207	67.935	1.062057	6.164	6.6365	1140.44
1206	74.042	1.072713	7.206	6.6378	1336.29
1205	79.797	1.083718	8.275	6.6410	1538.55
1204	84.324	1.092565	9.133	6.6405	1701.14
1203	89.922	1.103091	10.151	6.6399	1894.59
1202	95.669	1.112834	11.087	6.6399	2073.65
1308	95.730	1.112944	11.096	6.6407	2075.67
3210	98.966	1.117832	11.565	6.6403	2165.52
1307	102.714	1.122997	12.058	6.6406	2260.43
3209	106.914	1.128180	12.552	6.6406	2355.69
1306	111.034	1.132727	12.984	6.6405	2439.25
3208	116.854	1.138388	13.522	6.6400	2543.30
1305	122.856	1.143457	14.004	6.6388	2636.43
3207	130.205	1.148850	14.516	6.6373	2735.55
1304	138.604	1.154149	15.020	6.6348	2832.91
3206	144.959	1.157695	15.357	6.6332	2898.07
3205	151.826	1.161162	15.686	6.6314	2961.78
1303	159.298	1.164578	16.011	6.6293	3024.54
3204	167.767	1.168095	16.345	6.6274	3089.17
3203	176.997	1.171557	16.674	6.6251	3152.79
1302	186.786	1.174899	16.990	6.6231	3214.16
3202	198.015	1.178378	17.320	6.6208	3278.10
3201	210.288	1.181825	17.647	6.6183	3341.43
1301	222.462	1.184964	17.943	6.6167	3399.08

TABLE V. Experimental results for methane at 200 K and subcritical isotherms.

ID	T (K)	P (bar)	n	Fringe (count)
3612	140,000	2.974	1.002687	49.37
3611	140,000	3.314	1.003020	55.48
3610	140,000	3.594	1.003288	60.42
3609	140,000	3.866	1.003563	65.47
3608	140,000	4.137	1.003836	70.48
3607	140,000	4.405	1.004109	75.49
3606	140,000	4.664	1.004379	80.46
3605	140,000	4.921	1.004647	85.38
3604	140,000	5.181	1.004920	90.40
3603	140,000	5.437	1.005194	95.43
3602	140,000	5.689	1.005472	100.54
3601	140,000	5.959	1.005777	106.15
3511	160,000	3.944	1.003095	56.87
3510	160,000	5.355	1.004288	78.78
3509	160,000	6.704	1.005489	100.86
3508	160,000	8.002	1.006689	122.91
3507	160,000	9.232	1.007882	144.83
3506	160,000	10.392	1.009063	166.54
3505	160,000	11.521	1.010275	188.80
3504	160,000	12.579	1.011471	210.78
3503	160,000	13.589	1.012665	232.72
3502	160,000	14.530	1.013863	254.73
3501	160,000	15.409	1.015044	276.43
3410	180,000	5.030	1.003498	64.27
3409	180,000	9.307	1.006763	124.26
3408	180,000	13.194	1.010027	184.25
3407	180,000	16.724	1.013313	244.63
3406	180,000	19.901	1.016611	305.23
3405	180,000	22.697	1.019869	365.10
3404	180,000	25.172	1.023141	425.22
3403	180,000	27.323	1.026387	484.87
3402	180,000	29.187	1.029643	544.71
3401	180,000	30.785	1.032925	605.01
3310	200,000	5.451	1.003376	62.04
3309	200,000	10.351	1.006640	122.01
3308	200,000	14.900	1.009912	182.14
3307	200,000	19.107	1.013177	242.13
3306	200,000	22.983	1.016439	302.08
3305	200,000	26.572	1.019710	362.18
3304	200,000	29.846	1.022966	422.02
3303	200,000	32.868	1.026238	482.14
3302	200,000	35.618	1.029503	542.14
3301	200,000	38.133	1.032776	602.30

calculated from a second order Lagrange interpolating polynomial fit to the refractive index data at 95, 100, and 105 K.

The Lorenz-Lorentz function for fluid methane is plotted vs density in Fig. 4. Several replicate isothermal results are not included in the figure. Note the increase in the (LL) function as the lower limit of accurate gas densities is approached. Also, the oscillatory behavior of the 220 K results in an artifact of the polynomial interpolating function. The accuracy of the (LL) values is limited by the accuracy of the PVT surface because the refractive index is known much more precisely than the pressure-density relationship. Uncertainties as large as 0.1% could exist in the experimental densities of Ref. 1.

The precision of the experimental data is best indicated by replicates of experimental measurements. Rep-

licate determinations starting from the same initial density and pressure generally agreed within 0.05% in the derived (LL) function, as indicated by Fig. 4 and Tables I-VII. The two replicates of the 183 K saturated liquid reference point agreed within 0.003% in $(n-1)$.

The evaluation of the accuracy of experimental measurements in the absence of exactly known reference values is a difficult and ill-defined process.²⁶ An estimate of the accuracy of the quantity $(n-1)$ may be calculated from the upper bounds of the possible systematic errors in the quantities appearing in Eq. (4). Not surprisingly, this number is most directly influenced by the percentage of uncertainty in the total fringe count. This suggests that accuracy of the measurements is on the same order as the precision described above. The percentage uncertainty varies from 0.1% at small fringe counts to 0.002% at the largest fringe counts. Additional uncertainty due to the calculated fringe count adjustment has been discussed in Sec. III for the results on the coexistence boundary.

V. DISCUSSION

A. Comparisons with other work

The refractive index of methane has been previously measured at room temperature and low pressure by several workers,²⁷⁻²⁹ and by Abbiss *et al.*³⁰ for the saturated liquid at 588.3 nm. None of these results can be directly compared with the present experiments because of differences in pressure, temperature, and wavelength of light used.

The widely referenced work by Ramaswamy and Watson²⁷ was performed with a Rayleigh interferometer designed for determinations at pressure near or below 1 bar. Also, the temperature of their apparatus was not closely controlled. However, extrapolation of the low pressure 300 K results of Table I to a pressure of 1 atm and temperature of 298.15 K agrees within experimental error with the 25 °C $(n-1)_{\text{atm}}^{546.2}$ number of Ramaswamy and Watson.

Pings and co-workers³⁰ used a minimum deviation angle refractometer that required a room temperature calibration with water. The uncertainty in the refractive indices was estimated to be ± 0.0001 . Unfortunately, their results are at 588.3 nm and no dispersion data exists for liquid methane. However, these refractive index results at 588.3 nm are about 0.8% lower than our results at 546.2 nm at the common temperatures. This is in qualitative agreement with the normal wavelength dependence of refractive index observed for other cryogenic fluids.

The (LL) vs density behavior shown in Fig. 4 is similar to the (CM) and (LL) density behavior observed for other nondipolar fluids. This behavior is in qualitative agreement with the predictions of theoretical calculations,³¹ that is, a slight increase with density to the critical density, then a decreasing (LL) or (CM) function at higher densities. No temperature dependence among the gas isotherm results is distinguishable at densities below 12.0 mol/l. At higher densities, the 220 K data are higher than the 250 K data in qualitative agreement

TABLE VI. Experimental results for saturated liquid methane.

ID	T (K)	P ^a (bar)	ρ (mol/l)	n	(LL) (cm ³ /mol)	Fringe ^b (count)	t_{vac} (cm)
c	90,680		28.15	1.29581	6.5580		
2501	95,000	0.199	27.789	1.291899	6.5615	5362.83(6.23)	0.501770
2502	100,000	0.345	27.367	1.287255	6.5650	5277.58(5.97)	0.501777
2503	105,000	0.566	26.934	1.282490	6.5680	5190.12(5.72)	0.501784
2504	110,000	0.884	26.491	1.277612	6.5711	5100.56(5.46)	0.501791
2505	115,000	1.326	26.035	1.272619	6.5745	5008.89(5.19)	0.501798
2506	120,000	1.919	25.566	1.267479	6.5779	4914.52(4.92)	0.501806
2507	125,000	2.694	25.081	1.262181	6.5814	4817.25(4.65)	0.501813
2508	130,000	3.681	24.578	1.256692	6.5848	4716.47(4.37)	0.501821
2509	135,000	4.912	24.055	1.251007	6.5887	4612.08(4.08)	0.501828
2401	140,000	6.422	23.508	1.245061	6.5924	4502.89(3.79)	0.501836
2402	145,000	8.244	22.933	1.238832	6.5962	4388.50(3.50)	0.501844
2403	150,000	10.414	22.325	1.232260	6.6003	4267.81(3.21)	0.501852
2404	155,000	12.966	21.678	1.225253	6.6041	4139.11(2.91)	0.501861
2405	160,000	15.939	20.980	1.217723	6.6079	4000.80(2.60)	0.501869
2301	165,000	19.372	20.219	1.209524	6.6119	3850.19(2.29)	0.501877
2302	170,000	23.308	19.371	1.200443	6.6168	3683.38(1.98)	0.501886
2303	175,000	27.794	18.401	1.190045	6.6212	3492.36(1.66)	0.501895
2304	178,000	30.771	17.731	1.182905	6.6244	3361.17(1.46)	0.501900
2203	180,000	32.884	17.232	1.177607	6.6271	3263.83(1.33)	0.501903
2204	181,000	33.980	16.962	1.174741	6.6284	3211.17(1.27)	0.501905
2205	182,000	35.104	16.675	1.171701	6.6298	3155.31(1.20)	0.501907
2001	183,000	36.256	16.368	1.168454	6.6315	3095.64(1.14)	0.501909
2201	184,000	37.437	16.036	1.164951	6.6334	3031.27(1.07)	0.501911
2202	185,000	38.648	15.673	1.161132	6.6358	2961.11(1.01)	0.501912
2101	186,000	39.890	15.269	1.156884	6.6384	2883.04(0.94)	0.501914
2102	187,000	41.165	14.808	1.152051	6.6417	2794.23(0.88)	0.501916
2103	188,000	42.473	14.260	1.146355	6.6469	2689.56(0.81)	0.501918
2104	189,000	43.818	13.561	1.139103	6.6539	2556.29(0.74)	0.501920
2105	189,404	44.372	13.201	1.135379	6.6582	2487.87(0.72)	0.501920
d	190,555		10.16	1.10333	6.6475		

^aCalculated from vapor pressure equation (Ref. 21).^bCalculated fringe count correction in parenthesis.^cTriple point extrapolation.^dCritical point extrapolation.

with a negative temperature dependence of refractometric virial coefficients. In addition, an isochoric comparison of the saturated liquid results with the gas isotherms indicates the same trend.

An interesting comparison may be made between the present (LL) results and the earlier (CM) results determined by Straty.²² Figure 6 is a plot of the (LL) and (CM) results for methane, with the zero density limit, A_R or A_D , subtracted to illustrate the relative change in polarization as a function of density. The sharper decrease in the (LL) function at higher (liquid) densities was also noted in the case of the carbon dioxide.⁵ However, experiments on argon³² exhibited the same relative behavior for both the (CM) and (LL) functions. There is presently no theoretical explanation for this difference in behavior at high densities. However, the importance of three-body interactions on the induced dipole forces at high densities may explain the relatively higher polarization in the (CM) case.

B. Refractometric virial coefficients

Estimates of second and third refractometric virial coefficients, B_R and C_R , were obtained from a least squares fit of Eq. (2) to the gas isotherm data. Several

assumptions are implicit in this type of analysis³³: (i) The truncated form of the virial equation, Eq. (2), is truly representative of the (LL) function over the density range $0 \leq \rho \leq 18$ mol/l. If a real fourth term, $D_R \rho^4$, is in fact neglected, then the adjusted values of B_R and C_R are in error. (ii) Systematic deviations from Eq. (2) due to the form of density interpolating functions are small compared to the overall (LL) trend with density. (iii) The temperature dependence of the (LL) function is small so that the 220 K isotherm, which includes data over the largest density range, may be combined with an estimate of A_R at 300 K. (iv) An independent method of determining A_R , the zero density limit, is available. The results of the least squares fit are extremely sensitive to a choice of A_R . Moreover, a fit of only the 3–18 mol/l data cannot be attempted because the value of A_R obtained in this case was found to be heavily influenced by meaningless random variations in the data.

The low pressure refractive index data at 300 K may be used to estimate A_R , the zero density limit of the LL function, with the use of the thermodynamic virial equation of state:

$$P/RT = \rho + B_R \rho^2 + C_R \rho^3 + \dots \quad (8)$$

TABLE VII. Experimental results for saturated vapor methane.

ID	T (K)	P ^a (bar)	ρ (mol/l)	n	(LL) (cm ³ /mol)	Fringe ^b (count)	t _{vac} (cm)
1905	99.290	0.320	...	1.000403	...	7.41(3.41)	0.501797
1904	114.403	1.266	...	1.001378	...	25.32(2.62)	0.501819
1903	129.865	3.651	...	1.003738	...	68.67(1.77)	0.501842
2601	138.000	5.783	...	1.005704	...	104.80(0.00)	0.501833
1902	139.649	6.307	...	1.006216	...	114.21(1.21)	0.501857
1901	150.000	10.414	...	1.010161	...	186.71(0.61)	0.510874
1406	158.411	14.946	...	1.014804	...	272.00(2.70)	0.501866
2701	160.000	15.939	1.589	1.015772	6.6010	289.80(0.00)	0.501891
1803	160.000	15.927	1.589	1.015739	6.5875	289.20(1.39)	0.501875
1405	166.136	20.221	2.069	1.020622	6.6210	378.92(2.22)	0.501879
1404	171.307	24.426	2.588	1.025774	6.6112	473.59(1.89)	0.501888
1802	172.386	25.358	2.713	1.026973	6.5977	495.62(0.62)	0.501897
1403	175.711	28.479	3.146	1.031356	6.6076	576.16(1.61)	0.501896
1801	176.928	22.773	3.327	1.033132	6.6016	608.83(0.33)	0.501904
1402	179.077	31.896	3.680	1.036723	6.6095	674.80(1.39)	0.501902
1501	180.000	32.865	3.849	1.038404	6.6072	705.70(0.00)	0.501915
1401	181.560	34.606	4.162	1.041568	6.6095	763.83(1.23)	0.501906
1703	182.000	35.104	4.258	1.042540	6.6105	781.70(0.00)	0.501913
1702	184.000	37.415	4.747	1.047515	6.6164	873.13(0.13)	0.501915
1701	186.000	39.870	5.362	1.053738	6.6171	987.50(0.00)	0.501919
1601	190.000	45.192	7.829	1.078959	6.6262	1451.00(0.00)	0.501925
c	190.555		10.16	1.10333	6.6475		

^aCalculated from vapor pressure equation (Ref. 21).^bCalculated fringe count correction in parenthesis. Zero correction indicates isothermal determination.^cCritical point extrapolation.

Upon elimination of density between Eq. (2) and Eq. (8), a "pseudo" (LL) function expansion is obtained:

$$\frac{n^2 - 1}{n^2 + 2} \frac{RT}{P} = A_R + (B_R - A_R B_p) \frac{P}{RT} + O\left(\frac{P}{RT}\right)^2 \quad (9)$$

Figure 5 is a plot of Eq. (9) for the low pressure (3–7 bar) data of Table I. Note the dramatic increase in the scatter of replicates at low pressure. The percentage amount of the fringe fraction error compared to the total fringe count has increased from 0.06 to 0.12%. The interferometer was originally designed for use at moder-

ate and high densities. To restore its optimal sensitivity for the low pressure experiment, the spacer length would have to increase from 0.5 cm to, say 10 cm. Moreover, these low pressure results are very sensitive to the determination of the fractional order measured at vacuum because this number enters the calculation of $(n - 1)$ for each point in the run.

An ordinary least squares fit to Eq. (9) gave these values for B_p and A_R at 300 K (assuming $B_R \approx 5.0$ to 7.0

TABLE VIII. Experimental vacuum spacer lengths.

ID	T (K)	t _{vac} (cm)
100–400	300.000	0.502146
500–600	300.000	0.502145
2800	300.000	0.502150
700–900	280.000	0.502101
2900	280.000	0.502106
1000–1100	250.000	0.502036
3000	250.000	0.502041
1200–1300	220.000	0.501976
3100	220.000	0.501977
3200	220.000	0.501978
3300	200.000	0.501938
3400	180.000	0.501906
3500	160.000	0.501892
3600	140.000	0.501874
a	100.000	0.501756
a	80.000	0.501729

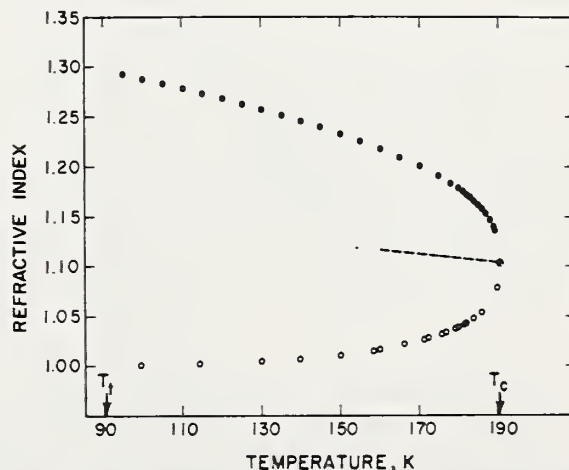
^aExperimental measurement on same spacer from Ref. 14.

FIG. 3. The refractive index of saturated liquid and saturated vapor methane as a function of temperature: ●, saturated liquid; ○, saturated vapor; --- is rectilinear diameter line; ⊗ indicates extrapolated critical point refractive index.

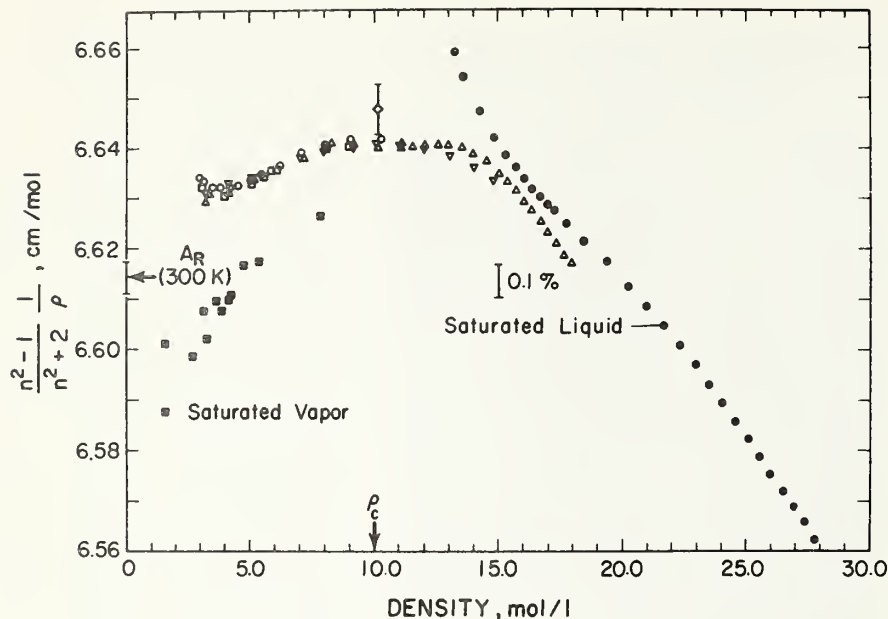


FIG. 4. The density dependence of the Lorenz-Lorentz function of fluid methane; \circ , 300 K; \square , 280 K; ∇ , 250 K; Δ , 220 K; \bullet , saturated liquid; \blacksquare , saturated vapor. A_R is the zero density limit at 300 K. \diamond is estimated value of critical point (LL) function with error bar.

(cm^3/mol)²):

$$A_R = 6.614_3 \text{ (cm}^3/\text{mol)}, \text{ S.D. } (A_R) = 0.002 \text{ (cm}^3/\text{mol)},$$

$$B_p = -44.0 \text{ (cm}^3/\text{mol)}, \text{ S.D. } (B_p) = 3.0 \text{ (cm}^3/\text{mol)}.$$

The second pressure virial coefficient agrees within the experimental error with the 300 K value from the correlation of Goodwin.²⁴ A_R should be weakly temperature dependent, decreasing slightly with decreasing temperature. Direct determination of A_R at low tem-

peratures was not attempted because B_p becomes more negative as temperature decreases. The slope of the fitted line in Fig. 5 increases as B_p becomes more negative and the large scatter in the data owing to the fractional fringe uncertainty would vitiate any attempt to estimate an intercept.

Buckingham and Graham¹⁵ reported a value of 6.600 (cm^3/mol) for A_R measured at 299 K and $\lambda = 632.8 \text{ nm}$. Their measurement required previous knowledge of the second pressure virial coefficient B_p . There are no other direct determinations of A_R for methane. However, the low pressure measurements of $(n-1)^{27-29}$ may be combined with the STP density to estimate A_R . Values of 6.584, 6.608, and 6.615 (cm^3/mol) were calculated from this analysis for A_R at $\lambda = 546.2 \text{ nm}$.

The results of an ordinary least squares fit to Eq. (2) of the gas isotherm data and A_R , the zero density limit, are shown in Table IX. Two fits were performed; first, a fit of all the gas isotherm data in the (3–18) mol/l range, and second, a fit of the 220 K gas isotherm. The uncertainty in B_R is about 1 (cm^3/mol)² in both cases. Buckingham and Graham¹⁵ obtained a value of $7.15 \pm 0.35 \text{ (cm}^3/\text{mol})^2$ for B_R from their differential interferometric expansion experiments. Our value is in substantial agreement with theirs when the limitations of the curve fitting procedure discussed above are considered.

TABLE IX. Refractometric virial coefficients of methane at $\lambda = 546.2 \text{ nm}$.

Data used for fit	A_R (cm^3/mol)	B_R (cm^3/mol) ²	C_R (cm^3/mol) ³
All isotherms	6.615	5.5	-290
220 K isotherm	6.613	6.1	-320

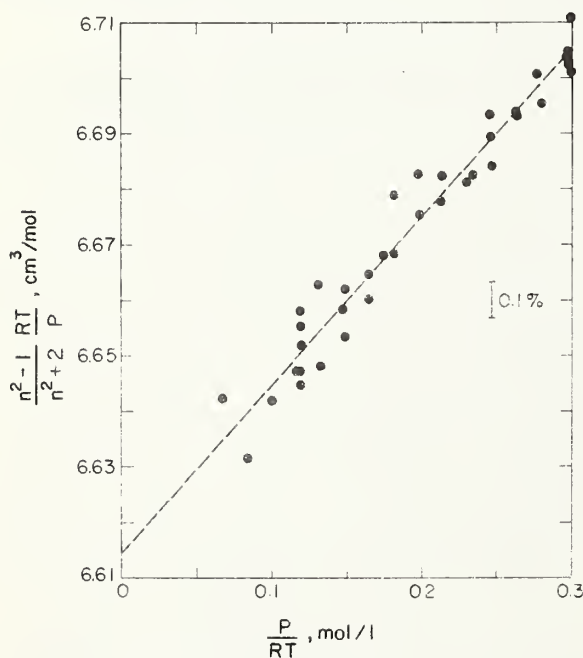


FIG. 5. Ideal gas Lorenz-Lorentz function for methane low pressure (3–7 bar) data at 300 K; --- is least-squares-fit to Eq. (9).

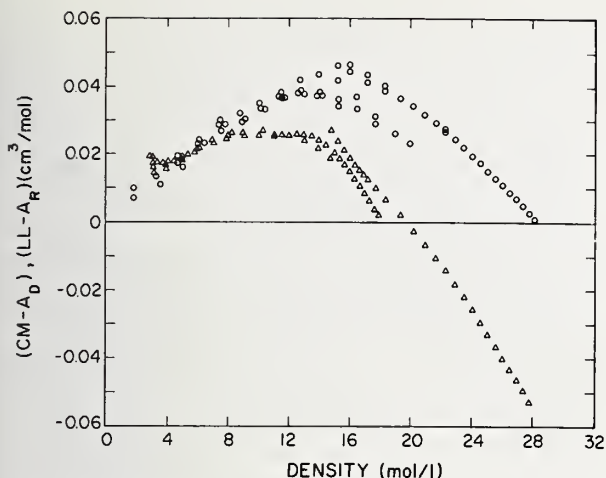


FIG. 6. The density dependence of the reduced Lorentz-Lorentz and Clausius-Mossotti functions of fluid methane: Δ , $(LL - A_R)$; O , $(CM - A_D)$.

C. Octopole moment of methane

The first nonvanishing molecular moment of methane is the octopole moment because of the T_d symmetry. Attempts to determine the magnitude of this moment include analyses of the second pressure virial coefficient data,³⁴⁻³⁶ but these analyses were hampered by the lack of a suitable reference intermolecular potential function. For example, it is common practice to fit the viscosity coefficients assuming spherical intermolecular interactions. However, proper fits of this type have only recently been possible.³⁷

Alternatively, analysis⁷ of experimental dielectric virial coefficients may also indicate the magnitude of the octopole moment. B_D is separated into two parts:

$$B_D = B_{ind} + B_{O_r}, \quad (10)$$

where B_{ind} results from the dipolar induced polarization of the external field and B_{O_r} results from octopolar interaction with induced dipoles. It is B_{O_r} that is used to estimate the octopole moment from the experimental measurements. Unfortunately, it is difficult to estimate B_{O_r} , for example, Bose, Sochanski, and Cole³⁸ measured B_D to be $6.75 \text{ (cm}^3/\text{mol)}^2$ at 373.4 K and $8.14 \text{ (cm}^3/\text{mol)}^2$ at 279.8 K. They estimate a value of $B_{ind} \approx 2.5 \text{ (cm}^3/\text{mol)}^2$ on the basis of this temperature dependence. However, both our results and those of Buckingham and Graham¹⁵ suggest that if $B_R \approx B_{ind}$ (Bose *et al.* suggest this approach at the end of their paper), then B_{ind} is on the order of $5.5\text{--}7.5 \text{ (cm}^3/\text{mol)}^2$. Further work is necessary here to show exactly how B_R and B_{ind} are related and how a more significant value of B_{O_r} may be estimated from B_D before a definitive value of the octopole moment may be determined from electromagnetic virial coefficients. Furthermore, it may be that an analysis of the temperature and higher density dependence of (CM) and (LL) taken together, as shown in Fig. 6, would indicate the octopolar contribution to the molecular polarization.

D. The critical density and PVT surface of methane

Electromagnetic equation of state data provide a sensitive test of the P - ρ - T relationship, especially near the vapor-liquid critical point. This section will be concluded with some comments on the thermodynamic implications of the methane refractive index and (LL) function data. It is expected that the saturated vapor (LL) function would be as large or larger than the gas isotherm values. Hence, our data suggests the calculated vapor densities²⁴ may be 0.3%–0.5% too large. Adsorption of a film of liquid methane on the interferometer optical surfaces during the saturated vapor measurements would increase the apparent refractive index and, therefore, raise, not lower, the calculated (LL) values.

The low pressure refractive index data at the eight temperatures between 140 and 300 K provide a basis for examination of the virial equation of state representation for methane. This type of procedure was recently applied to dielectric constant measurements on nitrogen.³⁹

The behavior of the saturated liquid (LL) function near the critical point (see Fig. 4) does not represent the real (LL) behavior, but rather indicates inaccuracy in the liquid density determinations. Experimental data¹ were not available above 175 K so that densities at higher temperatures were essentially obtained from an extrapolation that is very sensitive to the choice of critical parameters in the fitting equation. Previous workers^{13,14} also observed anomalous deviations in the (LL) function of simple fluids as the critical point was approached.

The diamond in Fig. 4 represents a "reasonable" extrapolation of the critical Lorentz-Lorentz function, $(LL)_c$, from the saturated liquid values. This value of $(LL)_c$ was combined with n_c , the critical point refractive index, to calculate a value of the critical density of methane,

$$\rho_c = 10.16 \pm 0.01 \text{ mol/l}.$$

The uncertainty in the critical density was calculated from the error bounds on the extrapolated value of $(LL)_c$. All methods of determining the critical density depend on some form of extrapolation,⁴⁰ usually with a rectilinear diameter analysis. The high precision of interferometric refractive index measurements coupled with the relative constancy of the (LL) function suggests that the method described in our work is the most accurate technique currently available for determination of the critical density.

ACKNOWLEDGMENTS

The author expresses his appreciation to B. A. Younglove, G. C. Straty, and W. M. Haynes for their advice on cryogenic instrumentation and experimental technique. D. E. Diller suggested the project and provided valuable comments on all aspects of the work. Finally, the author gratefully acknowledges the encouragement and perceptive guidance of H. J. M. Hanley.

- *Contribution of the National Bureau of Standards, not subject to copyright.
- †NRC-NBS Postdoctoral Research Associate, 1972-74.
- ¹R. D. Goodwin and R. Prydz, J. Res. Natl. Bur. Stand. (U.S.) A 76, 81 (1972).
- ²J. F. Ely, H. J. M. Hanley, and G. C. Straty, J. Chem. Phys. 59, 842 (1973).
- ³R. D. McCarty, NBSIR 74-357 (1974); Available from the National Bureau of Standards, Cryogenic Data Center, Boulder, CO 80302.
- ⁴J. G. Kirkwood, J. Chem. Phys. 4, 592 (1936).
- ⁵A. D. Buckingham, Trans. Faraday Soc. 52, 747 (1956).
- ⁶H. B. Levine and D. A. McQuarrie, J. Chem. Phys. 44, 3500 (1966).
- ⁷C. J. F. Bottcher, *Theory of Electric Polarization*, revised by O. C. Van Belle, P. Bordewijk, and A. Rip [Elsevier, New York, 1973], 2nd ed., Vol. I, Chap. VI.
- ⁸H. Sutter, "Dielectric Polarization in Gases," in *Dielectric and Related Molecular Process*, Specialist Periodical Report, edited by M. Davies (The Chemical Society, London, 1972).
- ⁹A. Michels and J. Hamers, Physica (Utr.) 4, 995 (1937).
- ¹⁰A. Michels, H. Lebesque, L. Lebesque, and S. R. De Groot, Physica (Utr.) 13, 337 (1947).
- ¹¹A. Michels, A. Brotzen, and S. R. De Groot, Physica (Utr.) 13, 343 (1947).
- ¹²A. Michels and A. Brotzen, Physica (Utr.) 15, 769 (1949).
- ¹³R. K. Teague and C. J. Pings, J. Chem. Phys. 48, 4973 (1968).
- ¹⁴D. E. Diller, J. Chem. Phys. 49, 3096 (1968).
- ¹⁵A. D. Buckingham and C. Graham, Proc. R. Soc. A 336, 275 (1974).
- ¹⁶R. D. Goodwin, J. Res. Natl. Bur. Stand. (U.S.) C 65, 231 (1961).
- ¹⁷B. Edlon, Rep. Int. Astron. Union 12, 138 (1964).
- ¹⁸H. Remy, Chem. Ber. 101, 1 (1968).
- ¹⁹C. Candler, *Modern Interferometers* (Hilger, London, 1951), p. 218.
- ²⁰F. H. Rolt and H. Barrell, Proc. R. Soc. A 122, 122 (1929).
- ²¹R. Prydz and R. D. Goodwin, J. Chem. Thermodyn. 4, 127 (1972).
- ²²G. C. Straty and R. D. Goodwin, Cryogenics 13, 712 (1973).
- ²³R. D. Goodwin, J. Res. Natl. Bur. Stand. (U.S.) A 75, 15 (1971).
- ²⁴R. D. Goodwin, Tech. Note U. S. Natl. Bur. Stand. 653, (1974); Available from Superintendent of Documents, U. S. Govt. Printing Office, Washington, D.C., Order No. C13.46:653, \$2.25.
- ²⁵J. R. Partington, *Treatise on Physical Chemistry* (Longmans, Green, London, 1949), Vol. 1, p. 639.
- ²⁶J. Mandel, *The Statistical Analysis of Experimental Data* (Interscience, New York, 1964), p. 125.
- ²⁷H. E. Watson and K. L. Ramaswamy, Proc. R. Soc. A 156, 144 (1936).
- ²⁸C. Cuthbertson and M. Cuthbertson, Proc. R. Soc. A 97, 152 (1920).
- ²⁹*Landolt-Börnstein* (Springer-Verlag, Berlin, 1962), Band II, Teil 8.
- ³⁰C. P. Abliss, C. M. Knobler, R. K. Teague, and C. J. Pings, J. Chem. Phys. 42, 4145 (1965).
- ³¹G. Stell and G. S. Rushbrooke, Chem. Phys. Lett. 24, 531 (1974).
- ³²J. de Boer, F. van der Maeson, and C. A. ten Seldam, Physica (Utr.) 19, 265 (1953).
- ³³H. J. M. Hanley, R. D. McCarty, and J. V. Sengers, J. Chem. Phys. 50, 857 (1969).
- ³⁴S. Kielich, Acta Phys. Pol. 27, 475 (1965).
- ³⁵T. H. Spurling, A. G. DeRocco, and T. S. Storvich, J. Chem. Phys. 48, 1006 (1968).
- ³⁶K. K. Datta and Y. Singh, J. Chem. Phys. 55, 3541 (1971).
- ³⁷J. F. Ely and H. J. M. Hanley, Mol. Phys. 24, 683 (1972).
- ³⁸T. K. Bose, J. S. Sochanski, and R. H. Cole, J. Chem. Phys. 57, 3592 (1972).
- ³⁹J. F. Ely and G. C. Straty, J. Chem. Phys. 61, 1480 (1974).
- ⁴⁰M. R. Moldover, J. Chem. Phys. 61, 1766 (1974).

APPENDIX L

THERMOPHYSICAL PROPERTIES DATA RESEARCH
ON COMPRESSED AND LIQUEFIED GASES
AT THE NBS CRYOGENICS DIVISION

Dwain E. Diller

Cryogenics Division
Institute for Basic Standards
National Bureau of Standards
Boulder, Colorado

Paper E-4

Preprinted for the
Cryogenic Engineering Conference
Kingston, Ontario, Canada
July 22-25, 1975

THERMOPHYSICAL PROPERTIES DATA RESEARCH
ON COMPRESSED AND LIQUEFIED GASES
AT THE NBS CRYOGENICS DIVISION*

Dwain E. Diller

Cryogenics Division
Institute for Basic Standards
National Bureau of Standards
Boulder, Colorado

Abstract

This report summarizes important NBS contributions to accurate thermophysical properties data for compressed and liquefied gases (helium, hydrogen, nitrogen, oxygen, fluorine and argon), and discusses research on liquefied hydrocarbon gases (methane, ethane, ethylene etc.) and their mixtures. Representative results of research on the thermophysical properties of methane and mixtures containing methane are presented. Additional contributions expected through 1977 are summarized.

*

Contribution of the National Bureau of Standards, not subject to copyright.

THERMOPHYSICAL PROPERTIES DATA RESEARCH
ON COMPRESSED AND LIQUEFIED GASES
AT THE NBS CRYOGENICS DIVISION

Dwain E. Diller

Introduction

The Cryogenics Division of the National Bureau of Standards, with support from the NBS Office of Standard Reference Data, the National Aeronautics and Space Administration, the American Gas Association, Inc., and the LNG Density Project Steering Committee*, is engaged in a program of thermophysical properties data research on compressed and liquefied gases and their mixtures in support of advanced cryogenic technology. New technologies are continually being developed to promote efficient, economical and safe utilization of the country's material and energy resources. Important cryogenic processes, such as the separation, liquefaction, storage, transport and custody transfer of gases, are being used in much larger projects than ever before, and will benefit greatly from comprehensive accurate thermophysical properties data. The purpose of the NBS program is to provide critically evaluated data and calculation methods, original experimental measurements, new measurement technology, and data awareness and dissemination services in support of these projects. Our technical goal is to provide a range and quality of data which will be recognized as definitive or standard for all foreseeable low temperature engineering calculations. Our

*The LNG Density Project Steering Committee is a consortium of national and international energy companies which includes representatives from British Gas Corporation, Chicago Bridge and Iron Co., Columbia Gas Service Corp., Distrigas Corp., Easco Gas LNG, Inc., El Paso Natural Gas, Gaz de France, Marathon Oil Co., Mobil Oil Corp., Natural Gas Pipeline Co., Phillips Petroleum Co., Shell International Gas Ltd., Sonatrach, Southern Calif. Gas Co., Tennessee Gas Pipeline, Texas Eastern Pipeline Co., Tokyo Gas, Ltd., and Transcontinental Gas Pipeline Corp.

scientific goal is to understand the relationships between molecular structure, dense fluid structure, and the behavior of simple molecular fluids, which are the basis for developing accurate predictive calculation methods. The purpose of this report is to summarize important NBS contributions to thermophysical properties data research on the monatomic and diatomic gases (helium, hydrogen, nitrogen, oxygen, fluorine and argon), and to discuss NBS research on the hydrocarbon gases (methane, ethane, ethylene, etc.) and their mixtures. Table 1 gives references to selected NBS publications on the equation of state, thermodynamic, electromagnetic and transport properties of the monatomic and diatomic gases. Accurate equations of state and thermodynamic property data tables for these substances are among the most important NBS contributions to cryogenic technology.

NBS Research on Compressed and Liquefied Hydrocarbon Gases

In 1970 the American Gas Association, Inc. initiated a project at the NBS Cryogenics Division on the thermophysical properties of compressed and liquefied hydrocarbon gases (methane, ethane, propane etc.) in support of liquefied natural gas (LNG) technology. There are few accurate thermophysical properties data available, even for the simplest pure hydrocarbon gases and liquids, at temperatures below 200 K. Table 2 shows the hydrocarbon gases having freezing and normal boiling temperatures in this range. We expect that the demand for accurate data for these fluids and their mixtures will continue to increase with the necessity for efficient distribution and utilization of energy and chemical feed stock supplies.

The most important NBS contribution to liquefied hydrocarbon gas technology to date is comprehensive accurate thermophysical properties data for pure compressed and liquefied methane, the most abundant constituent in natural gas.

Table 3 summarizes selected NBS publications of this data [29-40]. The most useful publication for engineering calculations is NBS Technical Note 653, "The Thermophysical Properties of Methane, from 90 to 500 K at Pressures to 700 Bar" [36]. This publication contains a critical evaluation and correlation of all of the accurate equation of state (PVT) and thermodynamic properties data available for methane through April 1974, and reports original NBS measurements and interpolation functions for the vapor pressures, melting pressures, orthobaric densities, equation of state (PVT) and specific heats. The thermodynamic property tables were calculated using an isochoric equation of state, which typically differs from the experimental PVT data by less than 0.2% in density, except in the critical region. The calculated calorimetric and sound velocity data, obtained without recourse to multiproperty analysis, typically differ less than 3% from their measured values. The data, equations, and computer programs given in this report have already found important applications in recent calculations of the phase equilibria, orthobaric densities and thermodynamic properties of LNG mixtures [50].

A similar project on the thermophysical properties of compressed and liquefied ethane is underway. An isochoric equation of state has been used to analyze all of the volumetric and calorimetric data available for ethane, and to compute provisional thermodynamic property tables covering the temperature range 90 - 600 K at pressures to 70 MPa (10,000 psia) [51]. New measurements of the vapor pressures, melting pressures, orthobaric densities, equation of state, dielectric constants and specific heats are being performed to extend the experimental data down to the triple point temperature, 89.9 K. A revision of the provisional thermodynamic tables, incorporating all available new measurements is planned. A project on the thermophysical properties of propane will be initiated in 1976.

The Cryogenics Division is also participating in a joint industry-government project on the thermophysical properties of ethylene. This project was initiated in 1974 by the NBS Office of Standard Reference Data and a consortium of seven industrial firms^{*} to provide accurate equation of state and thermodynamic properties data for ethylene for improved plant design and custody transfer operations. New measurements are being carried out at NBS-Washington, NBS-Boulder, the ERDA Energy Center at Bartlesville, Oklahoma and at the University of Michigan. Evaluation and correlation of the data are now underway at NBS Boulder with completion scheduled for 1979.

Properties of Methane: Representative Results

High priority has been given to obtaining comprehensive accurate thermophysical properties data for compressed and liquefied pure methane, the most abundant constituent in natural gas. Methane also has the simplest structure of any of the hydrocarbon gases and is therefore a useful model for theoretical calculations of dense fluid structure and properties. Representative results of thermophysical properties data research on methane are given in Figures 1 - 4.

Figure 1 shows the dependences of the Clausius-Mossotti function, $V(\epsilon-1)/(\epsilon+2)$, on density and temperature [37]. The behavior of the Clausius-Mossotti function, C-M, for methane is typical of the behavior of other non-polar fluids; the dependence on density is less than 1% at fixed temperatures, and the dependence on temperature is less than 0.5% at fixed densities. Figure 1 demonstrates the utility of the Clausius-Mossotti function for evaluating the consistency and accuracy of equation of state measurements. As the quantity $(\epsilon-1)$ can easily

^{*}The NBS-Industry Project on the Thermophysical Properties of Ethylene is jointly supported by the NBS Office of Standard Reference Data and seven industrial firms including Celanese Chemical Co., Cities Service Oil Co., Continental Oil Co., Gulf Research and Development Co., Mobil Chemical Co., Monsanto Polymers and Petrochemicals Co., and Union Carbide Corp.

be measured with an accuracy better than 0.1%, equation of state inconsistencies of this magnitude are readily visible. The figure also demonstrates the utility of accurate Clausius-Mossotti function data for density gauging. Once the Clausius-Mossotti function has been determined for a particular fluid, the density can easily be obtained from a capacitance gauge measuring the dielectric constant.

Figure 2 shows Lorentz-Lorenz function, $V(n_\lambda^2 - 1)/(n_\lambda^2 + 2)$, data for methane, recently obtained from precise refractive index n_λ measurements [38] and the equation of state. The dependences of the Lorentz-Lorenz function, L-L, for methane on density and temperature are typical of other non-polar fluids, and are similar to the behavior of the Clausius-Mossotti function. There are subtle differences between the behavior of the L-L and C-M functions at high densities which have not been satisfactorily explained, even for the simplest gases and liquids. Figure 2 shows inconsistencies in the orthobaric density data used to compute L-L near the critical temperature. Unlike many other physical properties, the C-M and L-L functions appear to be well-behaved near the critical point; this fact has been utilized to obtain very precise equation of state data near the critical point from precise dielectric constant and refractive index measurements [64].

Figure 3 shows the dependences of the sound velocities in gaseous and liquid methane on density and temperature. The circles indicate conventional ultrasonic measurements [34] and the crosses indicate light scattering spectroscopy measurements [35] obtained in this laboratory. The light scattering measurements were made in a density range inaccessible to conventional ultrasonic measurements on methane. Accurate sound velocity measurements give a valuable

check on the consistency of the equation of state derivatives and calorimetric data using the thermodynamic relationship $W_S^2 = \gamma(\partial P/\partial \rho)_T$, where W_S is the sound velocity and $\gamma \equiv C_p/C_v$ is the specific heat ratio. Both sets of measurements are consistent with each other and with the thermodynamic sound velocities within their combined uncertainties.

New equations have been developed to calculate the dependences of the transport properties of gaseous and liquid methane on density and temperature [40]. The behavior of the thermal conductivity coefficients for methane can be calculated to good approximation with

$$\lambda(\rho, T) = \lambda_0(T) + \lambda_1(T)\rho + \Delta\lambda'(\rho, T) + \Delta\lambda_c(\rho, T), \quad (1)$$

where λ_0 is the dilute gas coefficient, λ_1 is the first density correction coefficient, $\Delta\lambda'$ is a remainder term and $\Delta\lambda_c$ gives the enhancement of the thermal conductivity coefficient near the critical point. The enhancement occurs at densities within about 50% of the critical density and at temperatures within about 20% of the critical temperature. Detailed equations for each term are given in reference [40]. In the absence of systematic measurements for methane, the last term $\Delta\lambda_c$ has been estimated from scaling law relations [53], mode-mode coupling theory [54] and by corresponding states with data for CO_2 [55].

Figure 4 shows the predicted dependences of the excess thermal conductivity, $(\lambda_1\rho + \Delta\lambda' + \Delta\lambda_c)$, on the density and temperature as these parameters approach their critical values. The estimated accuracy of equation (1) is better than 5% outside the critical region, and about 20% in the region of the predicted enhancement. Preparations are underway for systematic light scattering measurements of the thermal diffusivity coefficients, $\chi \equiv \lambda/\rho C_p$, to provide additional information on the behavior in the critical region.

NBS Research on Compressed and Liquefied Gas Mixtures

The National Bureau of Standards has supported thermophysical properties data research on cryogenic fluid mixtures since 1959. The purpose of this research is to provide critically evaluated physical and thermodynamic properties data and accurate original measurements needed to evaluate and optimize predictive calculation methods. One of the most valuable NBS contributions to date is a comprehensive bibliography of experimental phase equilibrium data [56]. This report has been revised and expanded and now gives references to all experimental phase equilibrium, volumetric and calorimetric data available for fluid mixtures through 1974 [41]. Information is given on the composition, temperature and pressure ranges investigated for mixtures (mostly binary) of 26 molecular species, consisting mainly of the monatomic, diatomic and hydrocarbon gases. Because of the vast scope of this subject it is extremely important that additional research be carried out primarily on carefully selected simple representative systems, which have most of the features of technically important multicomponent mixtures. We have therefore given high priority to experimental and analytical research on binary mixtures of the simplest molecular gases. We are evaluating the available phase equilibrium and volumetric data for carefully selected binary mixtures, and performing precise liquid-vapor equilibrium and orthobaric density measurements to fill important data gaps and reconcile inconsistencies.

Properties of Mixtures Containing Methane: Representative Results

The evaluation of available phase equilibrium data for compressed and liquefied gas mixtures has been hampered by the lack of generally accepted rigorous analytical methods. Several approaches have been explored. One approach involves the comparison of excess thermodynamic properties data derived

from different kinds of measurements. For example, direct calorimetric measurements of the enthalpies of mixing H^E can be compared with the estimates of H^E derived from the temperature dependence of the excess Gibbs energies G^E (obtained from precise phase equilibrium measurements) and the thermodynamic relationship

$$H^E = G^E - T (\partial G^E / \partial T)_P. \quad (2)$$

There are, however, very few sets of sufficiently comprehensive and accurate data, obtained for the same mixtures in similar composition, temperature and pressure ranges, to make this type of comparison possible. We have analyzed the available phase equilibrium data for several carefully selected mixtures containing methane, with typical results shown for methane-nitrogen mixtures in Figure 5.

This figure indicates relatively good agreement at temperatures above 110 K and relatively poor agreement below 110 K among data from different laboratories. There is considerable uncertainty in estimating the temperature dependence of the excess Gibbs energy from these data. As a result of this analysis we have performed new high precision liquid-vapor equilibrium composition measurements for this mixture in the temperature range 95 - 120 K [43]. Figure 6 shows the excess Gibbs energies derived for equimolar methane-nitrogen mixtures in this range. The results give an improved estimate of the temperature dependence of G^E , which is in satisfactory agreement with direct calorimetric measurements [44]. Similar analyses of the data available for other mixtures containing methane are underway. Paper E-2 at this conference gives additional details of this work [57].

The evaluation of phase equilibrium data is even more difficult at temperatures above the critical temperature of one of the components, where direct comparison of the excess thermodynamic functions is not possible. In this case it is useful to compare Henry's constants, derived from the data using the definition

$$H_{2,1} \equiv \lim_{x_2 \rightarrow 0} (f_2/x_2), \quad (3)$$

where f_2 is the vapor phase fugacity of the supercritical component. Figure 7 shows the dependence of the Henry's constants, derived from phase-equilibrium data for methane-nitrogen mixtures, on temperature in the range 130 - 180 K [45]. It appears that there are now highly consistent phase equilibrium data available for methane-nitrogen mixtures throughout the entire temperature range 95 - 180 K.

The LNG Density Project Steering Committee, a consortium of 13 U.S. and 5 international energy companies initiated a project at the Cryogenics Division in 1972 on the orthobaric densities of liquefied hydrocarbon gases and their mixtures. The goal of this project is to obtain accurate (0.1%) measurements and evaluated calculation methods for the orthobaric densities of LNG mixtures having arbitrary compositions for custody transfer operations. Several promising calculation methods of varying complexity are being evaluated and optimized for this purpose [46, 47, 48]. A magnetic suspension densimeter, based on Archimedes' principle, has been constructed and thoroughly performance tested to obtain accurate absolute density measurements on liquefied gases at temperatures down to 90 K and pressures to 5 MPa. The densities measured typically range from 0.3 to 1.3 g/cm³. Accurate orthobaric density data have

been obtained for liquefied methane, ethane, propane, butanes and nitrogen, mainly at temperatures between 100 and 150 K, with a typical repeatability of 0.02% and an estimated accuracy better than 0.1%. Preliminary comparisons with measurements from other laboratories show differences smaller than 0.2% in most cases. Paper E-6 at this conference gives additional information on the apparatus and presents results for liquefied normal butane [49], which are typical of data for the other components.

Extensive measurements are now being performed on carefully selected and gravimetrically prepared mixtures of LNG components. The scope of this project is shown in Table 4. High priority has been given to equimolar binary mixtures containing methane. Data for the dependences of the densities of the binary mixtures on both composition and temperature will be obtained to test several mathematical models and optimize the adjustable coefficients. Data for multi-component mixtures will be obtained to evaluate the accuracy of the optimized calculation methods and to discriminate between the models.

Discussion

Thermophysical properties data research at the NBS Cryogenics Division is currently concentrated on obtaining comprehensive accurate data and predictive calculation methods for compressed and liquefied hydrocarbon gases and their mixtures. This report summarizes important NBS contribution on the thermophysical properties of methane and binary mixtures containing methane, and discusses typical current and planned projects. Table 5 summarizes some additional NBS contributions expected through 1977, and suggests that emphasis on liquefied hydrocarbon gases will likely continue through the rest of the

seventies. It is hoped that the systematic approach being taken to the phase equilibrium properties and the orthobaric liquid densities will soon be extended to include the equation of state, thermodynamic and transport properties of several carefully selected simple representative liquefied gas mixtures.

Acknowledgments

The contributions of all members of the Properties of Cryogenic Fluids Section, the Cryogenic Data Center, and of various university groups, especially at Rice University and the University of Michigan, are gratefully acknowledged.

References

1. R. D. McCarty, J. Phys. and Chem. Ref Data 2, 923 (1973).
2. R. D. McCarty, "Thermophysical Properties of Helium-4 from 2 to 1500 K with Pressures to 1000 Atmospheres," NBS Tech. Note 631 (1972).
3. H. J. M. Hanley and G. E. Childs, Cryogenics 9, 106 (1969).
4. W. G. Steward and G. H. Wallace, unpublished data (1971).
5. R. D. Goodwin, J. Res. NBS 73A, 585 (1969).
6. H. M. Roder, L. A. Weber, and R. D. Goodwin, "Thermodynamic and Related Properties of Parahydrogen from the Triple Point to 100 K at Pressures to 340 Atm," NBS Monograph 74 (1965).
7. H. M. Roder and R. D. McCarty, "Modified Benedict-Webb-Rubin Equation of State for Parahydrogen II," NBSIR 75- 814 (1975).
8. R. D. McCarty and L. A. Weber, "Thermophysical Properties of Hydrogen from the Freezing Liquid Line to 5000 R for Pressures to 10,000 PSIA," NBS Tech. Note 617 (1972).
9. L. A. Weber, "Thermodynamic and Related Properties of Parahydrogen from the Triple Point to 300 K at Pressures to 1000 Bar," NBSIR 74-374/ NASA SP-3088 (1974).
10. R. D. McCarty, "ASRDI Hydrogen Technology Survey, Volume I: Thermophysical Properties, NASA SP-3089 (1975).
11. J. W. Stewart, J. Chem. Phys. 40, 3297 (1964).
12. D. E. Diller, J. Chem. Phys. 49, 3096 (1968).
13. D. E. Diller, J. Chem. Phys. 42, 2089 (1965).
14. H. M. Roder and D. E. Diller, J. Chem. Phys. 52, 5028 (1970).
15. R. T. Jacobsen, R. B. Stewart, R. D. McCarty, H. J. M. Hanley, "Thermophysical Properties of Nitrogen from the Fusion Line to 3500 R for Pressures to 150,000 PSIA," NBS Tech. Note 648 (1973).
16. J. F. Ely and G. C. Straty, J. Chem. Phys. 61, 1480 (1974).
17. H. J. M. Hanley, R. D. McCarty and W. M. Haynes, J. Phys. Chem. Ref. Data 3, 979 (1974).

18. L. A. Weber, J. Res. NBS 74A, 93 (1970).
19. R. D. McCarty and L. A. Weber, "Thermophysical Properties of Oxygen from the Freezing Liquid Line to 600 R for Pressures to 5000 PSIA," NBS Tech. Note 384 (1971).
20. H. M. Roder and L. A. Weber, "ASRDI Oxygen Technology Survey, Volume I: Thermophysical Properties," NASA SP-3071 (1972).
21. B. A. Younglove, J. Res. NBS 76A, 37 (1972).
22. W. M. Haynes, unpublished data (1972).
23. A. L. Gosman, R. D. McCarty and J. G. Hust, "Thermodynamic Properties of Argon from the Triple Point to 300 K at Pressures to 1000 Atmospheres," NSRDS-NBS Monograph 27 (1969).
24. W. M. Haynes, Physica 67, 440 (1973).
25. R. Prydz and G. C. Straty, "The Thermodynamic Properties of Compressed Gaseous and Liquid Fluorine," NBS Tech. Note 392 (revised), (1973).
26. G. C. Straty and B. A. Younglove, J. Chem. Phys. 57, 2255 (1972).
27. H. J. M. Hanley and R. Prydz, J. Phys. Chem. Ref. Data 1, 1101 (1972).
28. W. M. Haynes, Physica 76, 1 (1974).
29. Prydz and R. D. Goodwin, J. Chem. Thermo. 4, 127 (1972).
30. R. D. Goodwin and R. Prydz 76A, 81 (1972).
31. R. D. McCarty, Cryogenics 14, 276 (1974).
32. R. D. Goodwin, J. Res. NBS 79A, 71 (1975).
33. B. A. Younglove, J. Res. NBS, 78A, 401 (1974).
34. G. C. Straty, Cryogenics 14, 367 (1974).
35. G. C. Straty, Cryogenics (in press, 1975).
36. R. D. Goodwin, "Thermophysical Properties of Methane, from 90 to 500 K at Pressures to 700 Bar," NBS Tech. Note 653 (1974).
37. G. C. Straty and R. D. Goodwin, Cryogenics 13, 712 (1973).
38. J. D. Olson, J. Chem. Phys. (in press, 1975).

39. W. M. Haynes, *Physica* 70, 410 (1973).
40. H. J. M. Hanley, R. D. McCarty and W. M. Haynes, *Cryogenics* (in press, 1975).
41. M. J. Hiza, A. J. Kidnay and R. C. Miller, Equilibrium Properties of Fluid Mixtures; A Bibliography of Cryogenic Data to 1975 (Plenum Press, 1975).
42. A. G. Duncan and M. J. Hiza, *Ind. and Eng. Chem. Fund.* 11, 38 (1972).
43. W. R. Parrish and M. J. Hiza, Advances in Cryogenic Engineering 19, 300 (Plenum Press, 1974).
44. R. C. Miller, private communication.
45. A. J. Kidnay, R. C. Miller, W. R. Parrish and M. J. Hiza, *Cryogenics* (in press, 1975).
46. M. A. Albright, Technical Publication No. 3, A Report to the GPA, Tulsa, OK (1973).
47. J. B. Rodosevich and R. C. Miller, Advances in Cryogenic Engineering 19, 339 (Plenum Press, 1974).
48. J. Mollerup and J. S. Rowlinson, *Chemical Engineering Science* 29, 1373 (1974).
49. W. M. Haynes and M. J. Hiza, "Orthobaric Liquid Densities of Normal Butane from 135 to 300 K as Determined with a Magnetic Suspension Densimeter," Paper E-6, Cryogenic Engineering Conference, Kingston, Ontario, Canada, July 22-25, 1975.
50. J. M. Mollerup, Advances in Cryogenic Engineering 20, (in press, 1975).
51. R. D. Goodwin, "Provisional Values for the Thermodynamic Functions of Ethane," NBSIR 74-398 (1974).
52. G. C. Straty, *Cryogenics* (in press, 1975).
53. M. Vincenti-Missoni, J. M. H. Levelt Sengers and M. S. Green, *J. Res. Nat. Bur. Std.* 73A, 563 (1969).
54. M. E. Fisher, *J. Math. Phys.* 6, 944 (1964).
55. A. Michels, J. V. Sengers and P. S. Van der Gulik, *Physica* 28, 1216 (1962).
56. T. M. Flynn, "A Bibliography of the Physical Equilibria and Related Properties of Some Cryogenic Systems," NBS Tech. Note 56 (1960).
57. W. R. Parrish and M. J. Hiza, "On the Consistency of Liquid-Vapor Equilibria Data for Binary Mixtures of Methane with the Light Paraffin Hydrocarbons," Paper E-2, Cryogenic Engineering Conference, Kingston, Ontario, Canada, July 22-25, 1975.

58. R. L. Amey and R. H. Cole, J. Chem. Phys. 40, 146 (1964).
59. L. D. Ikenberry and S. A. Rice, J. Chem. Phys. 39, 1561 (1963)
60. N. Mani, "Precise Determination of the Thermal Conductivity of Fluids using the Absolute Transient Hot Wire Technique," Ph.D. Thesis, Univ. of Calgary (1971).
61. R. C. Miller, A. J. Kidnay and M. J. Hiza, A.I.Ch.E. J. 19, 145 (1973).
62. R. Stryjek, P. Chapplelear and R. Kobayashi, J. Chem. Eng. Data 19, 334 (1974).
63. M. R. Cines, J. T. Roach, R. J. Hogan and C. H. Roland, Chem. Eng. Progr. Symp. Ser. 49, No. 6, 1 (1953).
64. L. A. Weber, Phys. Rev. A2, 2379 (1970).
65. F. B. Sprow and J. M. Prausnitz, A.I.Ch.E.J., 12, 780 (1966).
66. R. Stryjek, P. S. Chapplelear, and R. Kobayashi, J. Chem. and Eng. Data 19, 334 (1974).
67. S. D. Chang and B. C.-Y. Lu, Chem. Eng. Prog. Symp. Series, 63, 18 (1967).
68. V. G. Fastovskii and Yu. V. Petrovskii, Zh. Fiz. Khim. 31, 2317 (1957).
69. S. Fuks and A. Bellemans, Bull. Soc. Chim. Belg., 76, 290 (1967).

List of Symbols

C_v	Specific heat at fixed volume, J/mol · K
C_p	Specific heat at fixed pressure, J/mol · K
C-M	Clausius-Mossotti function, $V(\epsilon-1)/(\epsilon+2)$, cm ³ /mol
χ	Thermal diffusivity coefficient, $\lambda/\rho C_p$, cm ² /s
ϵ	Dielectric constant
f_i	Fugacity of component i, Pa
G^E	Excess Gibbs energy, J/mol
	Specific heat ratio, C_p/C_v
H^E	Excess enthalpy (heat of mixing), J/mol
$H_{2,1}$	Henry's constant, Pa
L-L	Lorentz-Lorenz function $V(n_\lambda^2-1)/(n_\lambda^2+2)$, cm ³ /mol
λ	Thermal conductivity coefficient, W/m · K
n_λ	Refractive index at wave length λ
ρ	Density, mol/l
ρ_c	Critical density, mol/l
T	Temperature, K
T_t	Triple point temperature, K
T_{bp}	Normal boiling point temperature, K
T_c	Critical temperature, K
V	Specific volume, cm ³ /mol
W_s	Sound velocity, m/s
x_i	Mole fraction of component i

Table 1. Selected NBS Publications on the Thermophysical Properties of Compressed and Liquefied Monatomic and Diatomic Gases.

	HELIUM	HYDROGEN	NITROGEN	OXYGEN	FLUORINE	ARGON
Equation of state (PVT)	1	5,7	15	18	25	23
Thermodynamic properties	2	6,8,9	15	18,19,20	25	23
Electromagnetic properties	2	8,11,12	16	19,20,21	26	
Transport properties	3,4	13,14	17	19,20,22	27,28	24

The numbers refer to the reports and publications given in References.

Table 2. Thermophysical Properties of Liquefied Hydrocarbon Gases :
Triple Point, Normal Boiling Point and Critical Temperatures;
Critical Densities.

	M	T _t ,K	T _{bp} ,K	T _c ,K	ρ _c ,mol/l
methane	CH ₄	16.043	111.7	190.5	10.1
ethylene	C ₂ H ₄	28.054	169.4	282.3	7.6
ethane	C ₂ H ₆	30.070	184.5	305.4	6.9
Propylene	C ₃ H ₆	42.081	225.5	365.	5.5
Propane	C ₃ H ₈	44.097	231.1	370.	5.1
1-butene	C ₄ H ₈	56.108	266.9	419.6	4.2
isobutane	C ₄ H ₁₀	58.124	261.4	408.1	3.8
n-butane	C ₄ H ₁₀	58.124	272.7	425.	3.9
n-pentane	C ₅ H ₁₂	72.151	309.0	469.5	3.2

Table 3. Selected NBS Publications on the Thermophysical Properties of Methane.

★ *Equation of State*

R. D. Goodwin, J. Res. NBS 79A, 71 (1975)
R. D. McCarty, Cryogenics 14, 276 (1974)

★ *Specific Heats*

B. A. Younglove, J. Res. NBS 78A, 401 (1974)

★ *Sound Velocities*

G. C. Straty, Cryogenics 14, 367 (1974)

★ *Thermodynamic Functions*

R. D. Goodwin et al., NBS Tech. Note 653 (1974)

★ *Dielectric Constants*

G. C. Straty & R. D. Goodwin, Cryogenics 13, 712 (1973)

★ *Refractive Indices*

J. D. Olson, J.Chem. Phys. (in press, 1975)

★ *Transport Properties*

H. J. M. Hanley et al., Cryogenics (in press, 1975)
W. M. Haynes, Physica 70, 410 (1973)

Table 4. LNG Density Project: Scope of Work

★ *Pure Components*

methane	isobutane
ethane	n-butane
propane	nitrogen

★ *Binary Mixtures*

methane-ethane	ethane-propane	propane-isobutane
methane-propane	ethane-isobutane	propane-n-butane
methane-isobutane	ethane-n-butane	propane-nitrogen
methane-n-butane	ethane-nitrogen	
methane-nitrogen		

★ *Multicomponent Mixtures*

methane-ethane-propane

methane-ethane-nitrogen

methane-ethane-propane-n-butane

methane-ethane-propane-nitrogen

methane-ethane-propane-n-butane-nitrogen

typical LNG mixtures

Table 5. Expected NBS Publications on the Thermophysical Properties of Compressed and Liquefied Hydrocarbon Gases and Their Mixtures

- ★ Refractive Indices of Methane (1975)
 - ★ Hypersonic Velocities in Methane (1975)
 - ★ Thermal Diffusivity Coefficients for Methane (1977)
 - ★ Equation of State (PVT) for Ethane (1976)
 - ★ Dielectric Constants of Ethane (1976)
 - ★ Specific Heats of Ethane (1977)
 - ★ Thermodynamic Properties of Ethane (1977)
 - ★ Bibliography - Equilibrium Properties Data for Fluid Mixtures (1975)
 - ★ Liquid-Vapor Equilibrium Data for Methane-Nitrogen Mixtures (1975)
 - ★ Liquid-Vapor Equilibrium Data for Methane-Ethane Mixtures (1977)
 - ★ Magnetic Densimeter for Liquefied Gases and Their Mixtures (1976)
 - ★ Densities of LNG Components (1976)
 - ★ Densities of Mixtures of LNG Components (1976)
 - ★ Accurate Calculation Methods for LNG Densities (1977)
-

Figure Captions

- Figure 1. Clausius-Mossotti function for saturated and compressed fluid methane.
○ 220 K; X 250 K; Δ 280 K; □ 300 K; ● saturated and compressed liquid as indicated; ■ and - - - from reference [58];
◇ estimated C-M at the critical density.
- Figure 2. Lorentz-Lorenz function for saturated and compressed fluid methane.
○ 300 K; □ 280 K; ▽ 250 K; Δ 220 K; ● saturated liquid;
■ saturated vapor; A_R is the estimated zero density limit at 300 K; ◇ estimated L-L at the critical density.
- Figure 3. Sound velocities in saturated and compressed fluid methane.
X - hypersonic (light scattering velocities;
● ○ ultrasonic velocities;
- - - estimated thermodynamic sound velocities.
- Figure 4. Excess thermal conductivity coefficient ($\Delta\lambda^T \equiv \lambda_1\rho + \Delta\lambda' + \Delta\lambda_c$) for compressed gaseous methane.
● 235 K [59]; ○ 200 K [59]; □ 200 K [60]; - - - calculated [40].
- Figure 5. Excess Gibbs energies for equimolar methane-nitrogen mixtures obtained in different laboratories. The key to the symbols is given on the figure.
- Figure 6. Excess Gibbs energies for equimolar methane-nitrogen mixtures.
● ○ [43]; ▲ Δ [61]; — — — calculated from modified hard-sphere equation of state with $k_{12} = 0.035$.
- Figure 7. Henry's constants for methane-nitrogen mixtures in the temperature range 130 - 180 K.
○ [45]; □ [62]; Δ [63].

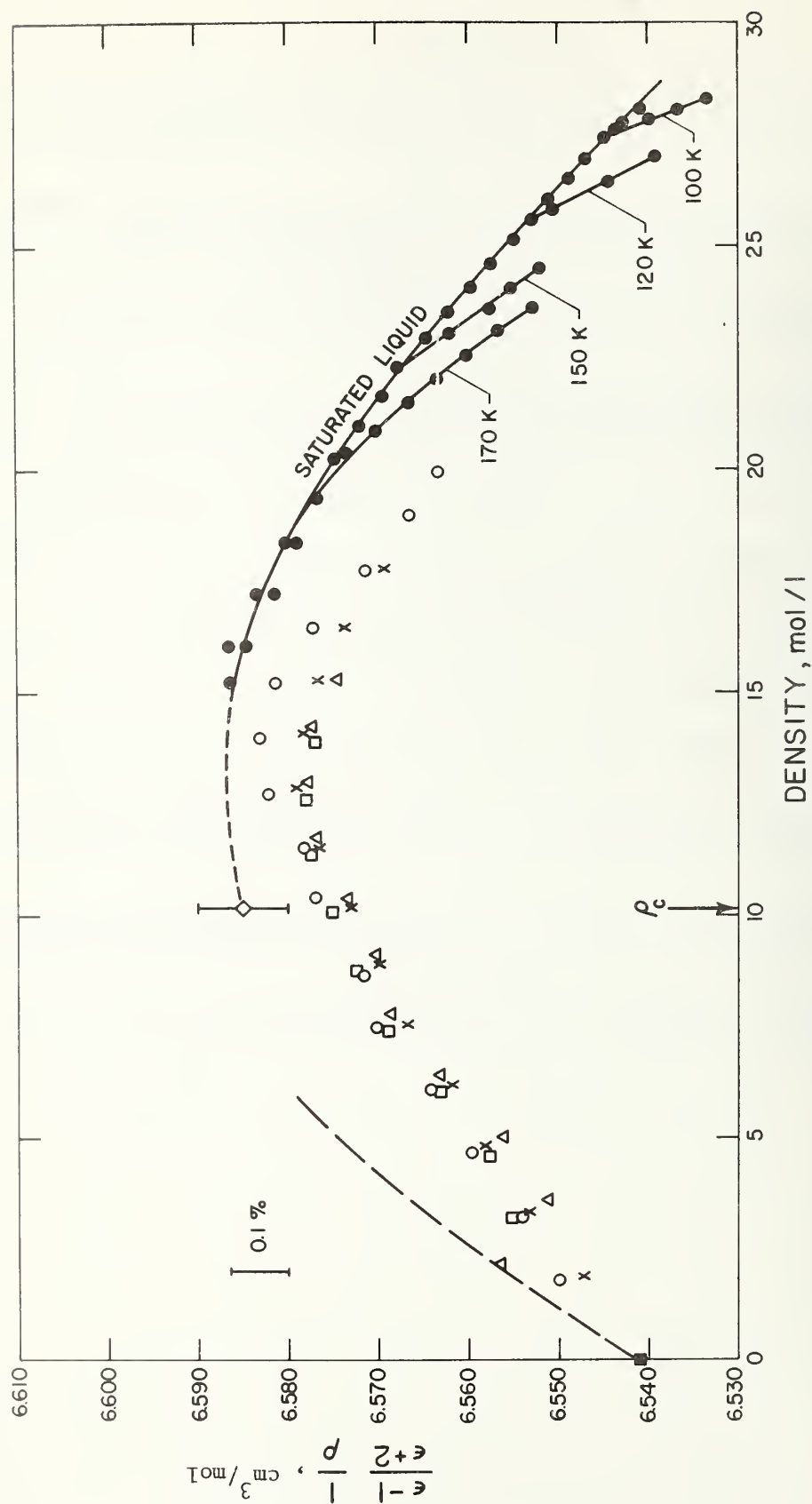


Figure 1

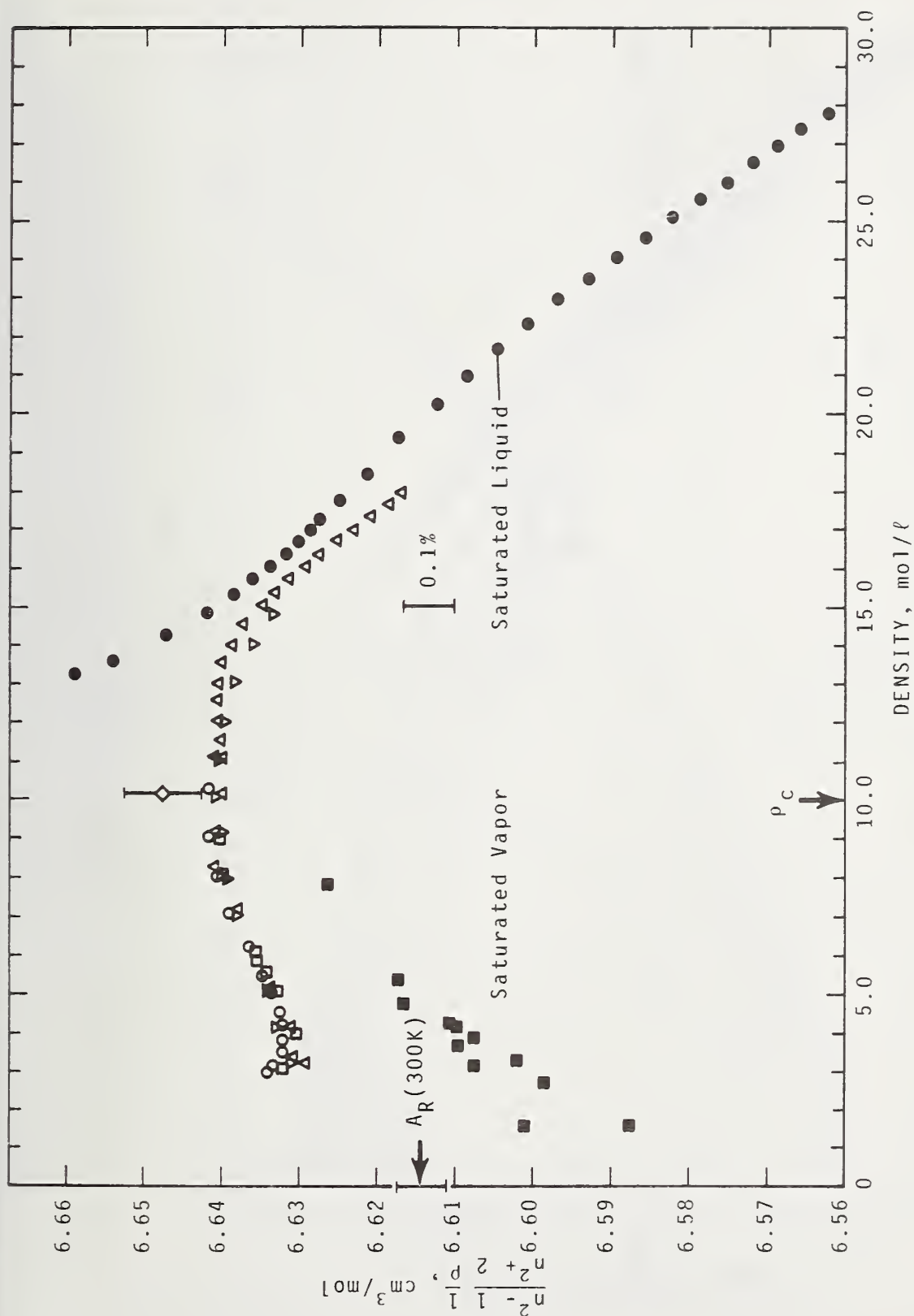


Figure 2

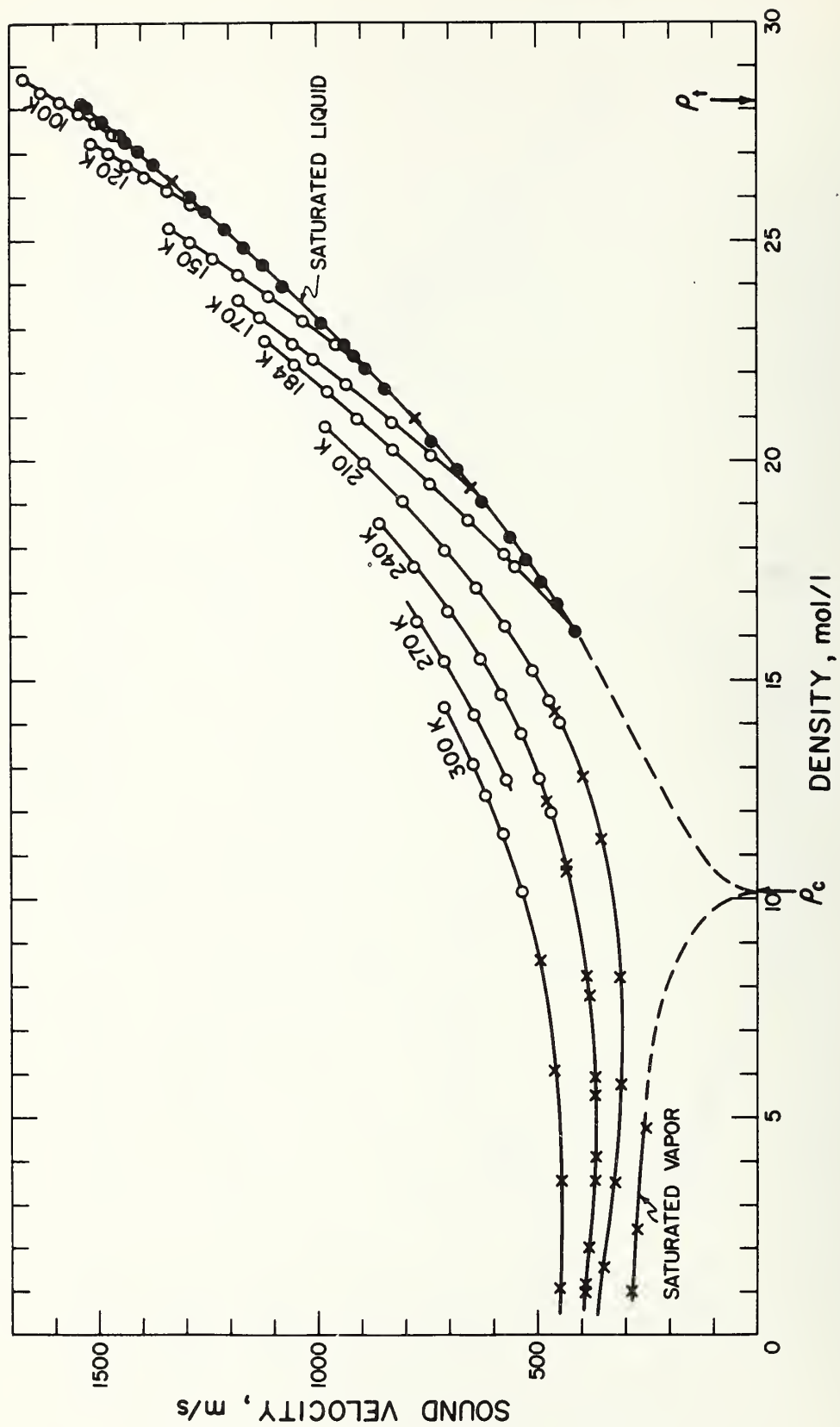


Figure 3

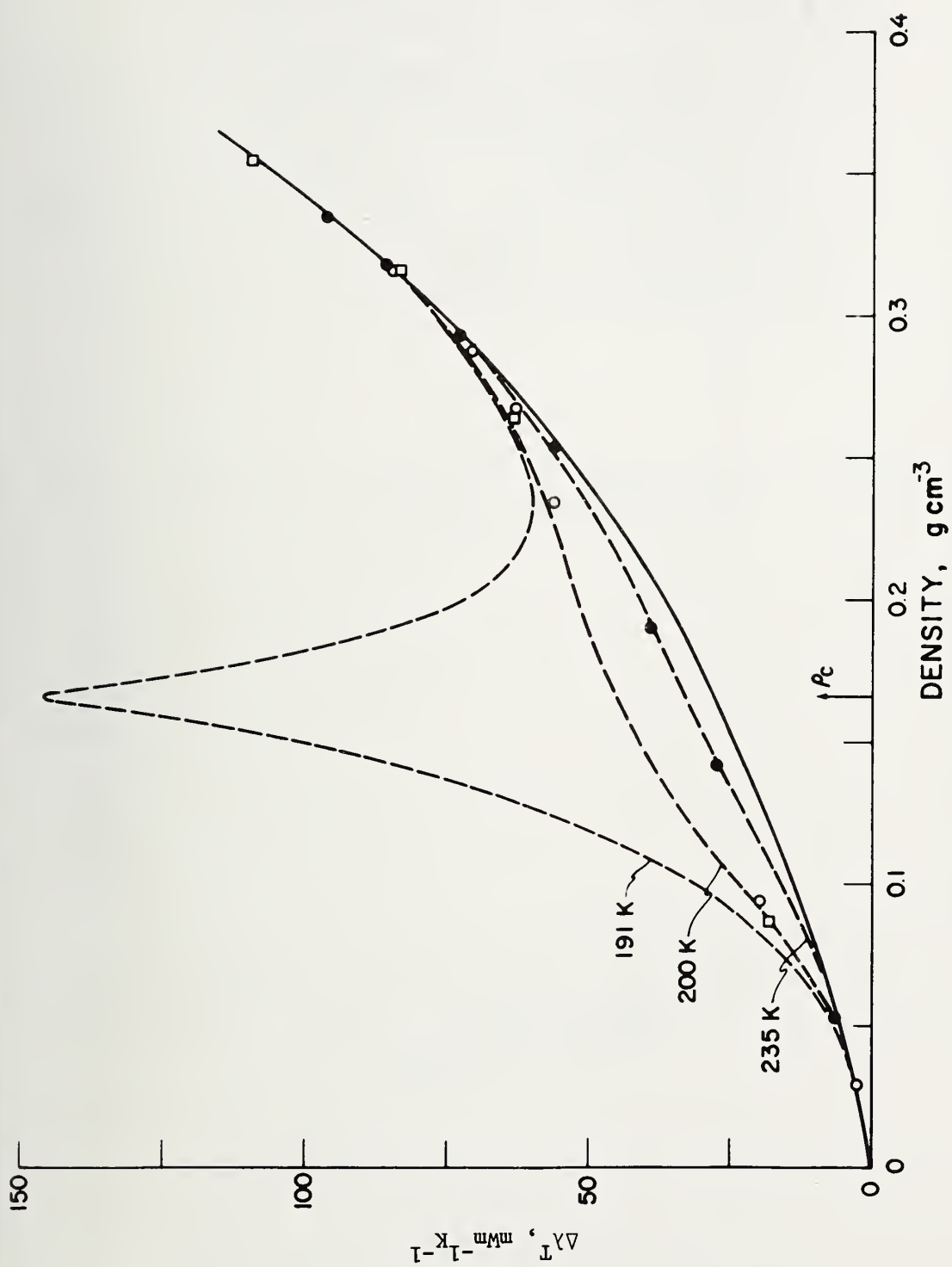


Figure 4

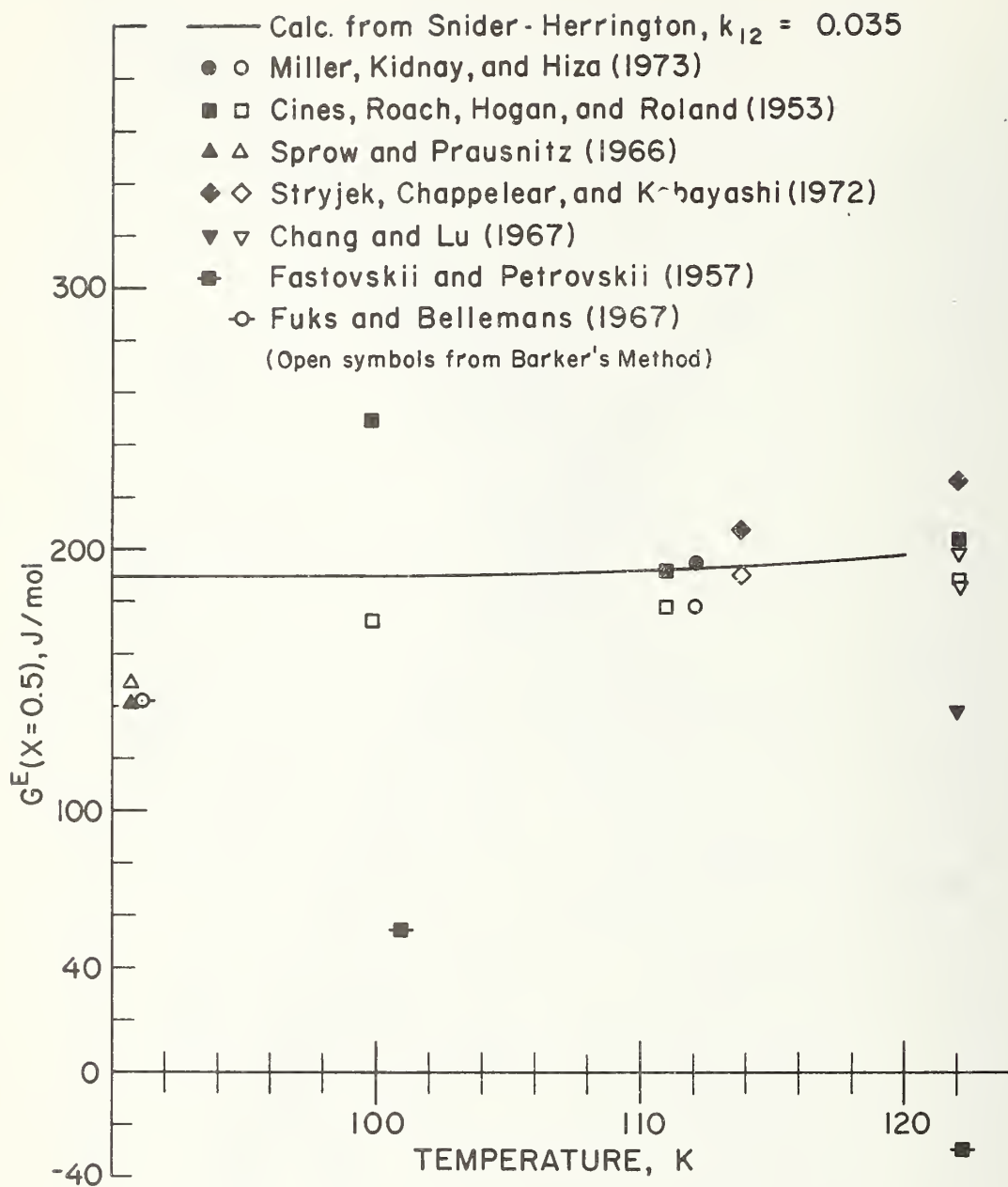


Figure 5

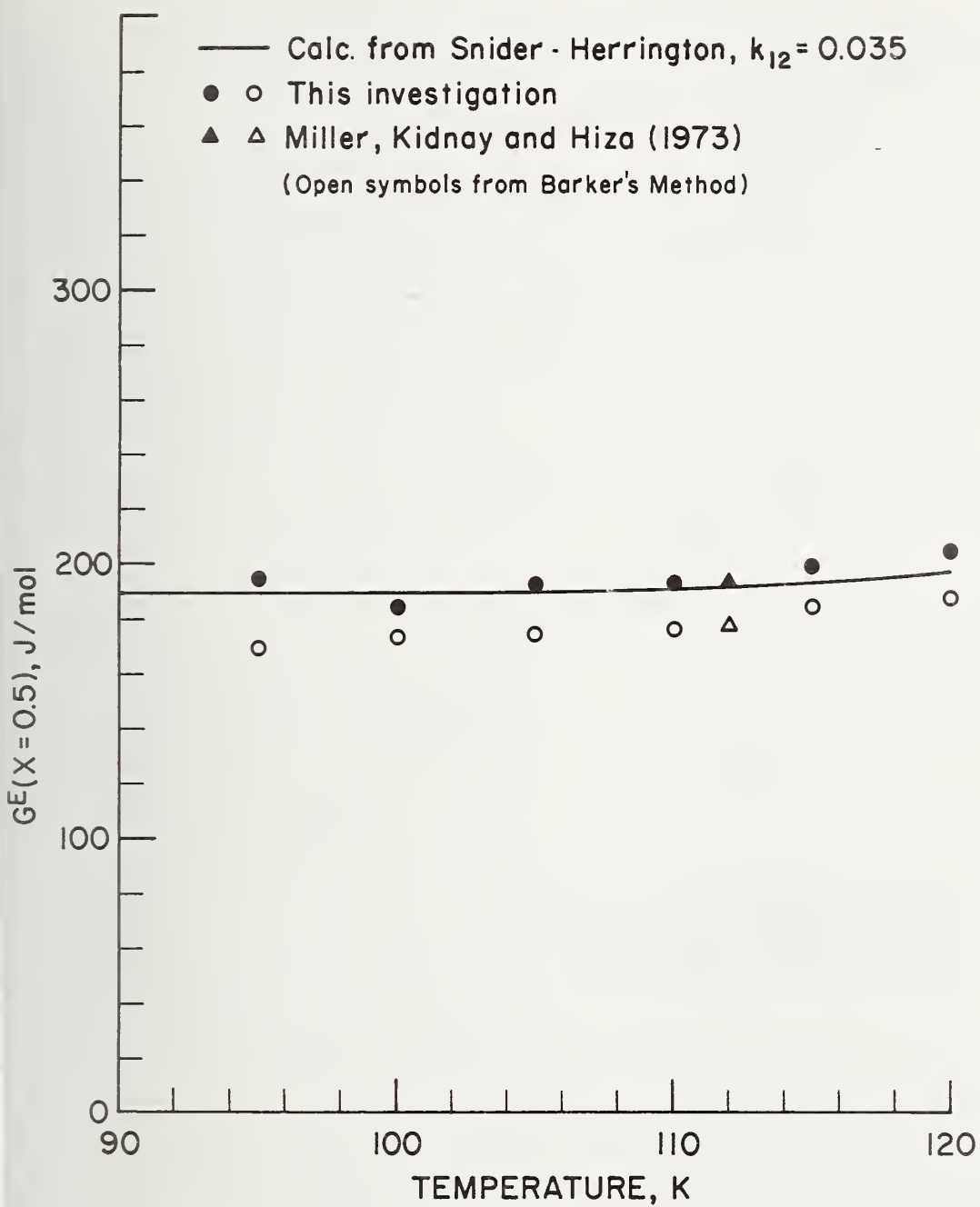


Figure 6

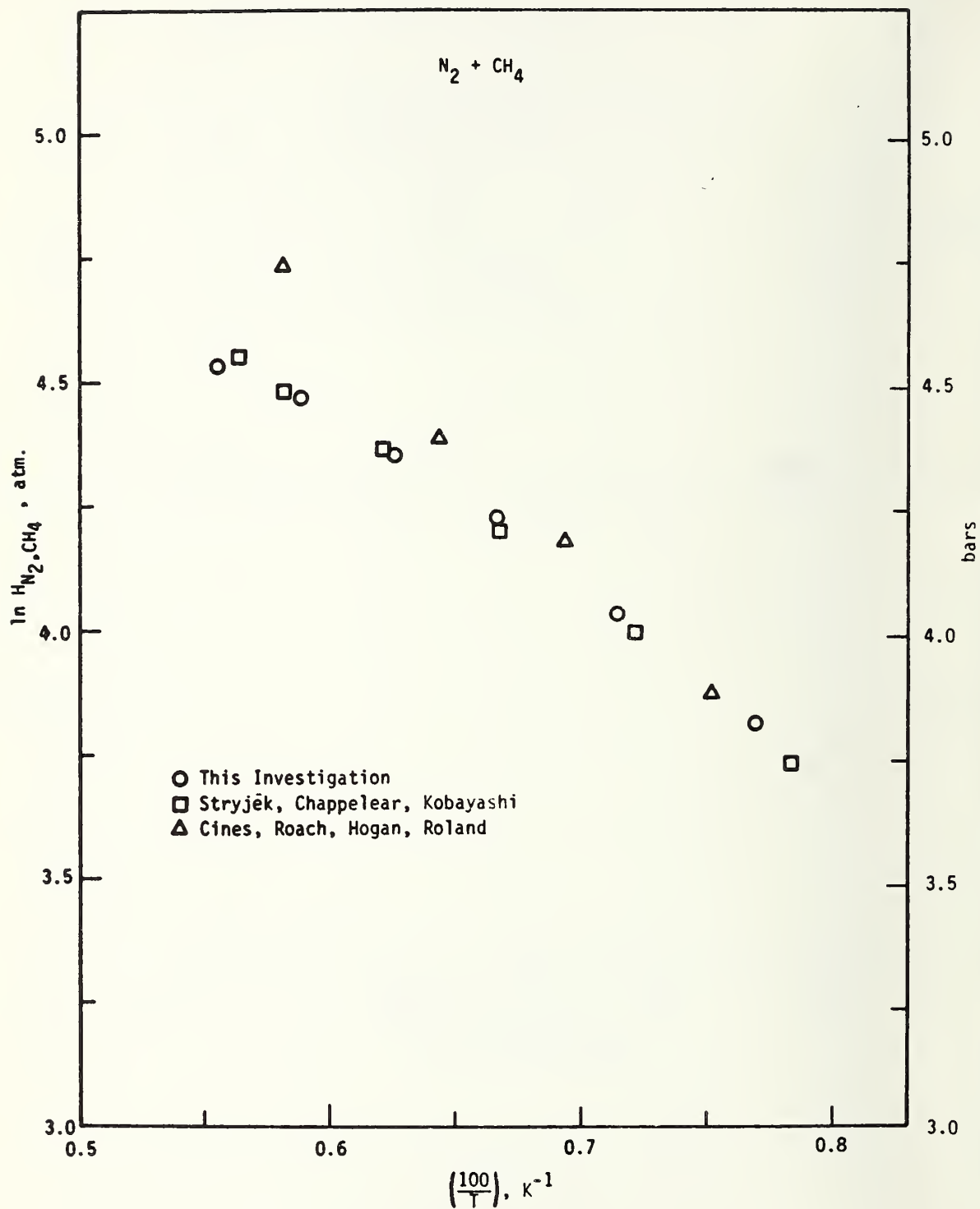


Figure 7

APPENDIX M

An equation is proposed to calculate the viscosity and thermal conductivity coefficients of methane from the dilute gas to the dense liquid. The range of validity of the equation is approximately 95–400 K for pressures up to 50 MPa (~500 atm). The reliabilities of the coefficients calculated are estimated at approximately 2% and 5% for the viscosity and thermal conductivity coefficients, respectively. The equation includes a contribution for the thermal conductivity enhancement in the critical region.

Equations for the viscosity and thermal conductivity coefficients of methane

H. J. M. Hanley, R. D. McCarty, and W. M. Haynes

This laboratory has reported results for the thermodynamic properties,¹ the equation of state,^{1,2} and the viscosity coefficient³ of methane. In this paper we extend this work by discussing briefly a correlation of the viscosity and thermal conductivity coefficient from the dilute gas to the dense liquid. Some details of the correlation are presented here but a discussion of the critical evaluation of the data with extensive tables will be published elsewhere.⁴ Interest in methane both as a pure fluid and as the major component of liquefied natural gas is extensive and it seemed worthwhile to summarize our results at this time.

In a previous paper⁵ we presented an evaluation and correlation of the transport properties of several simple fluids — argon, krypton, xenon, nitrogen and oxygen — and this work is a straightforward extension of that study to methane. Several points, in particular, were discussed in our previous publication. For example: (a) the general behaviour of the viscosity and thermal conductivity coefficients as a function of density and temperature was outlined⁶; (b) criteria for the evaluation and selection of data were established; (c) the behaviour of the thermal conductivity coefficient in the critical region was discussed; and (d) an equation was proposed to represent both viscosity and thermal conductivity data over a wide range of experimental conditions. It appears that this equation is general, that is, the form is independent of the structure of the fluid considered.

It was further emphasized in our previous paper that a proper correlation of the transport coefficients appears possible only in terms of density–temperature coordinates even though the practical variables are temperature and pressure. An accurate equation of state, therefore, is central to our programme. The equation of state used here is the BWR of McCarty, described in reference 2.

Correlating equations

We consider the viscosity coefficient, η , for methane to be given by the expression found suitable for other simple fluids,⁵

$$\eta(\rho, T) = \eta_0(T) + \eta_1(T)\rho + \Delta\eta'(\rho, T) \quad (1)$$

The authors are with the Cryogenics Division, National Bureau of Standards, Boulder, Colorado 80302, USA. HJMH is supported by the Office of Standard Reference Data (US). Received 10 March 1975.

where ρ is the density and T is the temperature. Similarly, for the thermal conductivity coefficient, λ

$$\lambda(\rho, T) = \lambda_0(T) + \lambda_1(T)\rho + \Delta\lambda'(\rho, T) + \Delta\lambda_c(\rho, T) \quad (2)$$

In these equations, η_0 and λ_0 are dilute gas coefficients; η_1 and λ_1 represent first density correction terms⁷; while $\Delta\eta'$ and $\Delta\lambda'$ are remainders. Note that (2) differs from (1) only by the inclusion of the term $\Delta\lambda_c(\rho, T)$ to take into account the known enhancement of the thermal conductivity coefficient in the region of the critical point (see Appendix C).

The dilute gas coefficients for methane were calculated from kinetic theory⁸ (Appendix B). The terms η_1 and λ_1 were represented by an empirical relation⁵

$$\eta_1(T) \text{ or } \lambda_1(T) = A + B \left(C - \log_e \frac{T}{F} \right)^2 \quad (3)$$

and $\Delta\eta$ and $\Delta\lambda$ were also represented empirically⁵

$$\Delta\eta'(\rho, T) = E \exp [j_1 + j_4/T] \left\{ \exp \left[\rho^{0.1} \left(j_2 + \frac{j_3}{T^{3/2}} \right) + \theta \rho^{0.5} \left(j_5 + \frac{j_6}{T} + \frac{j_7}{T^2} \right) \right] - 1.0 \right\} \quad (4)$$

and

$$\Delta\lambda'(\rho, T) = D \exp [k_1 + k_4/T] \left\{ \exp \left[\rho^{0.1} \left(k_2 + \frac{k_3}{T^{3/2}} \right) + \theta \rho^{0.5} \left(k_5 + \frac{k_6}{T} + \frac{k_7}{T^2} \right) \right] - 1.0 \right\} \quad (5)$$

The parameter θ is included to account specifically for the high density behaviour of the transport coefficients and is a function of the critical density, ρ_c

$$\theta = \frac{(\rho - \rho_c)}{\rho_c} \quad (6)$$

The parameters in (3)–(5) were estimated for methane by the least squares analysis procedure discussed in our previous paper, using selected data listed in Table 1. Values of the parameters determined are listed in Table 2. As noted,⁵ however, thermal conductivity data close to the critical point was excluded from the fit: rather the contribution to

the enhancement, $\Delta\lambda_c$, was obtained by the calculation outlined in Appendix C.

Comparisons and discussion

Representative comparisons between experimental data and equivalent values calculated from (1) or (2) are given in Figs 1–4.

These figures illustrate that we have been able to fit the data to within their estimated experimental accuracies. We observed only one instance where we feel our equation deviates systematically from experiment, namely the calculated viscosity coefficient appears too low close to the critical point. Although it is possible that experimental error and/or incorrect density values contribute to the deviation, it is also possible that the deviation is the result of a small enhancement in the viscosity close to the critical point¹⁹ which is not included in the correlating equation. This feature was also observed in our previous work.

Use of the equations. The equations should not be used to calculate transport coefficients beyond the range of the fitted data which is (viscosity) between 95 and 423 K for pressures up to 54 MPa and (thermal conductivity) between 99 and 725 K for pressures up to 100 MPa with the additional restriction that the density under consideration should not exceed about $2.7 \rho_c$. Within these limits, we

Table 1. Data sources

Reference	Experimental range	Estimated accuracy
<i>Viscosity</i>		
Haynes ³	Saturated liquid 95–190 K	2%
Kestin and Leidenfrost ⁹	~296 K Pressures to 15 MPa	1%
Giddings et al ¹⁰	283–410 K Pressures to 54 MPa	2%
Barua et al ¹¹	223–423 K Pressures to 17 MPa	2%
<i>Thermal conductivity</i>		
Le Neindre ¹²	298–723 K Pressures to 100 MPa	4%
Mani ¹³	139–400 K Pressures to 60 MPa	3%
Ikenberry and Rice ¹⁴	98–235 K Pressures to 50 MPa	5%

Table 2. Parameters for equations 3–5

<i>Viscosity</i>		
Equation 3	A	= 1.696985927
	B	= -0.133372346
	C	= 1.4
	F	= 168.0
Equation 4	E	= 1.0
	j_1	= -1.035060586×10^1
	j_2	= 1.7571599671×10^1
	j_3	= $-3.0193918656 \times 10^3$
	j_4	= 1.8873011594×10^2
	j_5	= $4.2903609488 \times 10^{-2}$
	j_6	= 1.4529023444×10^2
	j_7	= 6.1276818706×10^3
<i>Thermal conductivity</i>		
Equation 3	A	= -0.25276292
	B	= 0.33432859
	C	= 1.12
	F	= 168.0
Equation 5	D	= 1.0
	k_1	= -7.0403639907
	k_2	= 12.319512908
	k_3	= $-8.8525979933 \times 10^2$
	k_4	= 72.835897919
	k_5	= 0.74421462902
	k_6	= -2.9706914540
	k_7	= 2.2209758501×10^3

The units are as follows: density in g cm^{-3} , temperature in K, viscosity in $\mu\text{g cm}^{-1} \text{s}^{-1}$, thermal conductivity in $\text{MW m}^{-1} \text{K}^{-1}$

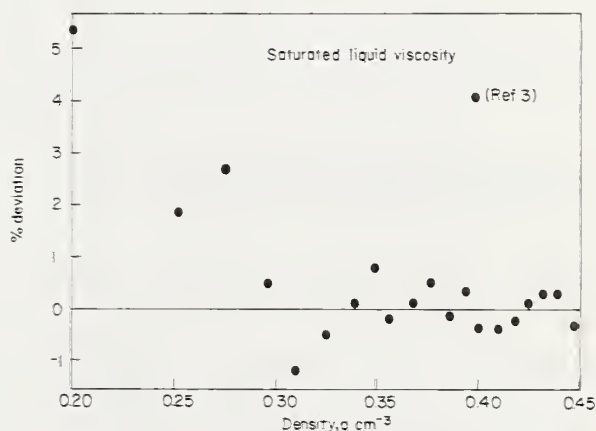


Fig.1 Deviations between calculated and experimental viscosities of the saturated liquid; data from Haynes.³ % is defined as $(\eta_{\text{exp}} - \eta_{\text{calc}}) \times 100 / \eta_{\text{exp}}$

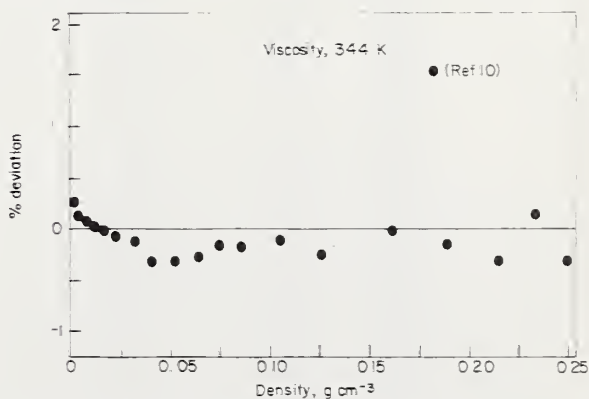


Fig.2 Deviations between calculated viscosities at 344 K and experimental values from reference 10

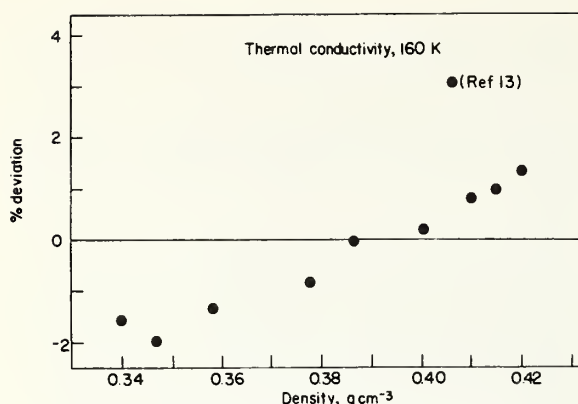


Fig.3 Deviations between calculated thermal conductivities and experimental values from reference 13 at 160 K

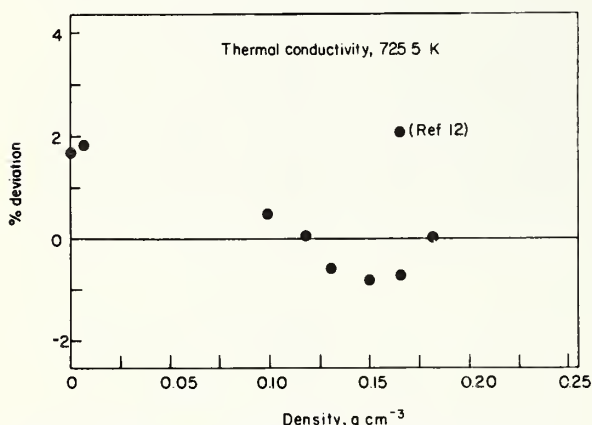


Fig.4 Deviations between calculated thermal conductivities at 725.5 K and experimental values from reference 12

Table 3. Calculated transport properties for the saturated liquid

Temperature, K	Density, mole l ⁻¹	Viscosity, $\mu\text{g cm}^{-1} \text{s}^{-1}$	Thermal conductivity, $\text{MW m}^{-1} \text{K}^{-1}$
95	27.789	1792	215
100	27.367	1563	206
105	26.934	1377	197
110	26.491	1223	189
115	26.035	1094	181
120	25.566	984	173
125	25.081	889	165
130	24.578	807	158
135	24.055	734	150
140	23.508	669	143
145	22.932	611	136
150	22.322	558	129
155	21.672	509	122
160	20.971	464	115
165	20.206	421	108
170	19.356	380	101
175	18.386	340	94
180	17.226	300	88
185	15.690	256	84
190	12.485	187	89

estimate that the calculated viscosity coefficient has an uncertainty of $\pm 2\%$ and the thermal conductivity an uncertainty of 5%, except in the critical region where the uncertainty is $\pm 20\%$.

Saturated liquid values. For convenience, we drew up Table 3 which presents calculated values at the saturated liquid boundary.

Conclusion

An equation to represent selected viscosity and thermal conductivity data of methane from the dilute gas to the dense liquid has been proposed. We note that the equation is identical in form for both transport coefficients (excluding the critical point enhancement for the thermal conductivity coefficient). We also note that the equation appears to be general in that it was used in our previous work with other simple fluids.²⁰ It is apparent that additional accurate data are required before the correlation can be improved significantly. Regions for which additional data are required include the dilute gas and vicinity of the critical point for the thermal conductivity coefficient, and the low temperature, high pressure region for the viscosity coefficient.

References

- Goodwin, R. D. NBS Tech Note No 653 (1974) and references therein; Straty, G. C. *Cryogenics* 14 (1974) 367
- McCarty, R. D. *Cryogenics* 14 (1974) 276
- Haynes, W. M. *Physica* 70 (1973) 410
- Haynes, W. M., McCarty R. D., Hanley, H. J. M. *J Phys Chem Ref Data* (in preparation); detailed tables are available from the Cryogenics Division, NBS, Boulder, Colorado
- Hanley, H. J. M., McCarty, R. D., Haynes, W. M. *J Phys Chem Ref Data* 3 (1974) 979
- Diller, D. E., Hanley, H. J. M., Roder, H. M. *Cryogenics* 4 (1970) 286
- Hanley, H. J. M., McCarty, R. D., Sengers, J. V. *J Chem Phys* 50 (1969) 858
- Hanley, H. J. M., Klein, M. *J Phys Chem* 76 (1972) 1743
- Kestin, J., Leidenfrost, W. *Thermodynamic and Transport Properties of Gases, Liquids and Solids* (ASME, McGraw-Hill, NY, (1959) 321
- Giddings, J. G., Kao, J. T. F., Kobayashi, R. *J Chem Phys* 45 (1966) 758
- Barua, A. K., Afzal, M., Flynn, G. P., Ross, J. *J Chem Phys* 41 (1964) 374
- Le Neindre, B. 'Contribution a l'etude Experimentale de la Conductivite Thermique de Quelques Fluides a Haute Temperature et a Haute Pression' Ph D Thesis, Paris (1969); Le Neindre, B., Tufeu, R., Bury, P. *Thermal Conductivity* (Proc 8th Conf, Lafayette, Ind) (Plenum Press, New York, 1969) 229
- Mani, N. 'Precise determination of the thermal conductivity of fluids using the absolute transient hot-wire technique', Ph D thesis, Univ of Calgary (1971)
- Ikenberry, L. D., Rice, S. A. *J Chem Phys* 39 (1963) 1561
- Hanley, H. J. M., McCarty, R. D., Sengers, J. V. NASA Contractor Rept NASA CR-2440 (1974)
- Vincentini-Missoni, M., Levett Sengers, J. M. H., Green, M. S. *J Res NBS* 73A (1969) 563
- Widom, B. *J Chem Phys* 43 (1965) 3898
- Sengers, J. V. NASA Contractor Rept NASA CR-2112 (1972)
- Strumpf, H. J., Collings, A. F., Pings, C. J. *J Chem Phys* 60 (1974) 3109
- Our equation for the thermal conductivity in reference 5 did not include terms proportional to θ , unlike (5) in this paper. Such a contribution appeared unnecessary since the scatter in the data used in reference 5 did not allow us to return significance in more than 3 of the k_i coefficients
- Olson, J. D. *J Chem Phys* (in press, 1975)

Appendix A

Fixed point parameters for methane^{1,2,21}

$$\begin{aligned} T_c &= 190.55 \text{ K} & \rho_c &= 10.15 \text{ mole l}^{-1} \\ P_c &= 45.387 \text{ atm (4.5988 MPa)} \\ T_t &= 90.68 \text{ K} & \rho_t &= 28.147 \text{ mole l}^{-1} \\ P_t &= 0.11590 \text{ atm (0.11744 MPa)} \\ \text{Molecular weight} &= 16.043 \end{aligned}$$

The subscripts c and t refer to the critical point and triple point respectively.

Appendix B

Dilute gas transport coefficients

The dilute gas transport coefficients were calculated using the standard kinetic theory expressions with the *m*-6-8 potential function of Hanley and Klein⁸

$$\begin{aligned} \frac{\Phi(r^*)}{\epsilon} &= \frac{1}{m-6} [6 + 2\gamma] (d/r^*)^m - \frac{1}{m-6} [m \\ &\quad - \gamma(m-8)] (d/r^*)^6 - \gamma(d/r^*)^8 \end{aligned} \quad (7)$$

where $d = r_m/\sigma$ and $r^* = r/\sigma$. The distance parameters σ and r_m , and the energy parameter, ϵ , are defined by the relationships $\Phi(r_m) = -\epsilon$ and $\Phi(\sigma) = 0$ while γ is a parameter representing inverse eighth attraction in the potential. We have previously reported⁸ that for methane

$$\begin{aligned} \frac{\epsilon}{k} &= 168.0 \text{ K}; \sigma = 3.68 \times 10^{-10} \text{ m}; \\ r_m &= 4.101 \times 10^{-10} \text{ m}; \gamma = 3.0; m = 11 \end{aligned} \quad (8)$$

where k is Boltzman's constant.

For computational convenience we fitted the calculated η_0 and λ_0 to a polynomial in temperature

$$\begin{aligned} \eta_0 &= GV(1)T^{-1} + GV(2)T^{-2/3} + GV(3)T^{-1/3} \\ &\quad + GV(4) + GV(5)T^{1/3} + GV(6)T^{2/3} + GV(7)T \\ &\quad + GV(8)T^{4/3} + GV(9)T^{5/3} \end{aligned} \quad (9)$$

and similarly for λ_0 but with coefficients $GT(i)$ ($i = 1, 9$) replacing $GV(i)$ in (9). Values of the coefficients for (9) are listed in Table 4.

Appendix C

Calculation of the thermal conductivity enhancement in the critical region

It is convenient to treat the enhancement of the thermal conductivity coefficient in the region of the critical point separately and we have written already

$$\begin{aligned} \lambda(\rho, T) &= \lambda_0(T) + \lambda_1(T)\rho + \Delta\lambda'(\rho, T) \\ &\quad + \Delta\lambda_c(\rho, T) \end{aligned} \quad (2)$$

Table 4. Dilute gas parameters

GV(1)	=	-2.090975 × 10 ⁵
GV(2)	=	2.647269 × 10 ⁵
GV(3)	=	-1.472818 × 10 ⁵
GV(4)	=	4.716740 × 10 ⁴
GV(5)	=	-9.491872 × 10 ³
GV(6)	=	1.219979 × 10 ³
GV(7)	=	-9.627993 × 10 ¹
GV(8)	=	4.274152
GV(9)	=	-8.141531 × 10 ⁻²
GT(1)	=	-2.147621 × 10 ⁵
GT(2)	=	2.190461 × 10 ⁵
GT(3)	=	-8.618097 × 10 ⁴
GT(4)	=	1.496099 × 10 ⁴
GT(5)	=	-4.730660 × 10 ²
GT(6)	=	-2.331178 × 10 ²
GT(7)	=	3.778439 × 10 ¹
GT(8)	=	-2.320481
GT(9)	=	5.311764 × 10 ⁻²

The units are: temperature in K, viscosity in $\mu\text{g cm}^{-1} \text{ s}^{-1}$, and thermal conductivity in $\text{MW m}^{-1} \text{ K}^{-1}$

where $\Delta\lambda_c(\rho, T)$ is the enhancement as a function of density and temperature. According to Hanley, McCarty, and Sengers^{5,15}

$$\begin{aligned} \Delta\lambda_c(\rho, T) &= \left(\frac{M}{\rho N k T} \right)^{1/2} \frac{k T^2}{6 \pi \eta R} \left(\frac{\partial P}{\partial T} \right)_\rho^2 \left(K_T \right)^{1/2} \\ &\quad \times \exp \left(-18.66 \tilde{\Delta T}^2 \right) \exp \left(-4.25 \tilde{\Delta \rho}^4 \right) \end{aligned} \quad (10)$$

where

$$\tilde{\Delta T} = (T - T_c)/T_c; \tilde{\Delta \rho} = (\rho - \rho_c)/\rho_c \quad (11)$$

with T_c and ρ_c the critical temperature and density, respectively. In (10), k is Boltzmann's constant, N is Avogadro's number, $K_T = \rho^{-1}(\partial \rho / \partial P)_T$ (the compressibility), and R is a length parameter (cm) given by the relation¹⁵ for methane

$$R = 1.465 \left(\frac{\rho}{T} \right)^{1/2} \times 10^{-6} \quad (12)$$

given ρ in g cm^{-3} and T in kelvin.

With the viscosity of (1) and values of $(\partial P / \partial T)_\rho^2$ and K_T from the equation of state, one could determine $\Delta\lambda_c$ but, unfortunately, the calculation would not necessarily be sufficient: it is known that an analytical equation of state, such as the equation used here, cannot accurately represent the $P\rho T$ surface very close to the critical point. It is felt, in particular, that the value of K_T from the equation of state is too small. Hanley, McCarty, and Haynes,⁵ however, proposed a procedure to partially resolve this problem: for methane $\Delta\lambda_c$ is calculated from (10) using

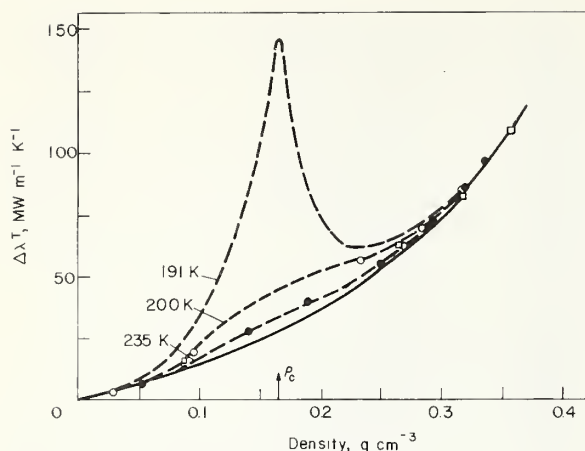


Fig.5 Plot of the thermal conductivity, less the dilute gas value, $\Delta\lambda T$, versus density for two isotherms. We define $\Delta\lambda T$ by the relation

$$\Delta\lambda T = \lambda(\rho, T) - \lambda_0(T)$$

where $\lambda(\rho, T)$ is given by (2). The critical point contribution from (2) is indicated by the dashed curves

● — reference 14 at 235 K; ○ — reference 14 at 200 K; ■ — reference 13 at 200 K

K_T values from reference 2 unless

$$\tilde{\Delta T} \leq 0.025; \tilde{\Delta \rho} \leq 0.25 \quad (13)$$

If these conditions are encountered, K_T is calculated from the scaling law equation proposed by Vicentini-Missoni, Levelt Sengers, and Green¹⁶ and by Widom.^{17, 18} Their equation is

$$[\rho^{*2} K_T^*]^{-1} = |\tilde{\Delta \rho}|^{\delta-1} \left[\delta h(x) - \frac{x}{\beta} \frac{dh(x)}{dx} \right] \quad (14)$$

where

$$\rho^* = \rho/\rho_c; X = \tilde{\Delta T}/\tilde{\Delta \rho}^{1/\beta}; K_T^* = P_c K_T \quad (15)$$

$$h(x) = E_1 \left(\frac{x+x_0}{x_0} \right) \left[1 + E_2 \left(\frac{x+x_0}{x_0} \right)^{2\beta} \right]^{(\gamma'-1)/2\beta} \quad (16)$$

and

$$\begin{aligned} \frac{dh(x)}{dx} = & \frac{E_1}{x_0} \left[1 + E_2 \left(\frac{x+x_0}{x_0} \right)^{2\beta} \right]^{(\gamma'-1)/2\beta} \\ & + \frac{\gamma'-1}{x_0} E_1 E_2 \left(\frac{x+x_0}{x_0} \right)^{2\beta} \\ & \times \left[1 + E_2 \left(\frac{x+x_0}{x_0} \right)^{2\beta} \right]^{(\gamma'-1-2\beta)/2\beta} \end{aligned} \quad (17)$$

values for T_c and P_c are listed in Appendix A. We chose (based on our work with oxygen) the following values for the other parameters of (14)–(17)

$$X_0 = 0.1892; \beta = 0.35; \delta = 4.30; E_1 = 2.058;$$

$$E_2 = 0.30; \gamma' = 1.155$$

Since data in the critical region are scarce for methane, we cannot present any extensive comparisons between experiment and calculated conductivities from (10) but the total thermal conductivity, less the corresponding dilute gas value, is plotted as a function of density for two isotherms in Fig.5. The solid curve represents the conductivity in the absence of any critical point enhancement while the dotted curves are obtained by adding the values for $\Delta\lambda_c(\rho, T)$ from (10). Data in the figure were extracted from Mani¹³ and from Ikenberry and Rice.¹⁴

Appendix D

Conversion factors

T, K	to $T, ^\circ F$: multiply by (9/5) then subtract 459.67
T, K	to $T, ^\circ C$: subtract 273.15
T, K	to $T, ^\circ R$: multiply by (9/5)
P, MPa	to $P, bars$: multiply by 10
P, MPa	to P, atm : multiply by (10/1.01325)
P, MPa	to $P, lb\ in^{-2}$: multiply by (146.9595/1.01325)
$\eta, g\ cm^{-1}\ s^{-1}$	to $\eta, Pa\ s$: multiply by 10^{-1}
$\eta, g\ cm^{-1}\ s^{-1}$	to $\eta, lb\ ft^{-1}\ s^{-1}$: multiply by 0.0671969
$\lambda, W\ m^{-1}\ K^{-1}$	to $\lambda, cal\ cm^{-1}\ s^{-1}\ K^{-1}$: multiply by 1/418.4
$\lambda, W\ m^{-1}\ K^{-1}$	to $\lambda, Btu\ ft^{-1}\ h^{-1}\ ^\circ R^{-1}$: multiply by 0.578176

APPENDIX N

EVALUATION OF CAPACITANCE DENSITOMETRY BY EXAMINATION OF THE RELATIONSHIPS
BETWEEN DENSITY, DIELECTRIC CONSTANT, PRESSURE AND TEMPERATURE FOR LNG MIXTURES

P. J. Giarratano and R. S. Collier

Cryogenics Division
Institute for Basic Standards
National Bureau of Standards
Boulder, Colorado 80302

Prepared for

The Maritime Administration
Washington, DC 20236

January 1, 1976

EVALUATION OF CAPACITANCE DENSITOMETRY BY EXAMINATION OF THE RELATIONSHIPS BETWEEN DENSITY, DIELECTRIC CONSTANT, PRESSURE AND TEMPERATURE FOR LNG MIXTURES

P. J. Giarratano and R. S. Collier

Cryogenics Division
Institute for Basic Standards
National Bureau of Standards
Boulder, Colorado 80302

ABSTRACT

Densities of typical LNG mixtures under saturation and subcooled conditions were calculated by means of the Möllerup equation of state; the corresponding density-dielectric constant relationship was determined from the Clausius-Mosotti relationship for the mixture using ideal mixing rules for the CM function. The results show that a nearly unique and linear relationship between saturation density and dielectric constant exists for both constant pressure and constant temperature conditions independent of mixture. Furthermore, it is shown that the linear relationship is not a segment of the Clausius-Mosotti function, but results from the more fundamental thermodynamic properties of the mixture. Also, the nitrogen composition of the mixture is predicted to have a pronounced effect on the saturation density versus dielectric constant, the increase in nitrogen causes an increase in saturation density for the same dielectric constant. There is also a substantial decrease in the saturation temperature with an increasing nitrogen content. For the normal range of mixtures, it is possible to determine the density to $\pm 0.3\%$ independent of a knowledge of the composition from an exact measurement of dielectric constant and temperature. Further improvements can be made if the exact composition of the mixture is known.

Key words: Clausius-Mosotti; densitometer (capacitance); density; dielectric constant; LNG; mixture(s).

1. Introduction

In response to a request from the U. S. shipbuilding industry, NBS is conducting an independent design review of the shipboard liquefied natural gas (LNG) custody transfer systems under the sponsorship of the Maritime Administration (MARAD) and in cooperation with the major U. S. shipbuilding companies.

Since the basis for sale of LNG is the total energy content of the LNG delivered, the ability for accurate determination of the total mass is of considerable importance because the specific heating value is usually measured independently. The total mass may be obtained from a measurement of density of the LNG and the volume of liquid in the storage tank, thus the need for accurate and reliable determination of these quantities.

Two possible alternatives for obtaining density are:

- (a) Prediction from measurements of temperature, pressure, and composition using an equation of state for LNG mixtures, e.g., reference [1]. Accuracies of approximately $\pm 0.1\%$ may be expected from such predictions if measurements of temperature, pressure, and composition are known exactly.[1] Inaccuracies in the measurement of temperature and composition cause increased inaccuracies in the determination of the density.
- (b) Direct measurement of a physical property such as dielectric constant or refractive index which is related to the density (e.g., the Clausius-Mosotti function or Lorentz-Lorenz function respectively).

The custody transfer system design under review incorporates a densitometer utilizing the measurement of dielectric constant and the Clausius-Mosotti relation as the primary input for determination of density. This relation is:

$$\rho_{\text{mix}} = \frac{1}{CM_{\text{mix}}} \frac{\epsilon - 1}{\epsilon + 2} \quad (2)$$

where

ϵ = dielectric constant

CM_{mix} = Clausius-Mosotti function for the mixture.

Therefore, in this report we have investigated the relationship between density and dielectric constant for a range of LNG mixtures and the resulting possible uncertainties in the density determination due to variation in composition.

At this stage we have not considered any heat transfer effects on density, any of the variables affecting the determination of total volume, nor electronic signal conditioning of the measured quantities.

2. Definitions and Range of Variables

2.1 Range of composition

In this report *normal composition range* is defined as follows:

Table 1. Normal LNG composition

<u>Component</u>	<u>Mole Fraction x_i</u>
Methane (CH_4)	0.8577 - 0.97
Ethane (C_2H_6)	0.03 - 0.09
Propane (C_3H_8)	0.0 - 0.03
Butanes ($i\text{C}_4\text{H}_{10} + n\text{C}_4\text{H}_{10}$)	0.0 - 0.01
Pentane (C_5H_{12})	0.0 - 0.0023
Nitrogen (N_2)	0.0 - 0.014

These are typical of the composition make-up found in LNG from the Algerian fields. 336 different mixtures within the range given by table 1 were calculated. The various mixtures were obtained by the following procedure.

Each component was assumed to have the possible mole fraction values of:

<u>Component</u>	<u>Mole Fraction Possible Values x_i</u>	<u>No. of Values</u>
C_2H_6	0.03, 0.04, 0.05, 0.06, 0.07, 0.08, 0.09	7
C_3H_8	0.0, 0.01, 0.02, 0.03	4
C_4H_{10}	0.0, 0.01	2
C_5H_{12}	0.0, 0.0023	2
N_2	0.0, 0.007, 0.014	3

$$\text{Then } x_{\text{CH}_4} = 1. - (x_{\text{C}_2\text{H}_6} + x_{\text{C}_3\text{H}_8} + x_{\text{C}_4\text{H}_{10}} + x_{\text{C}_5\text{H}_{12}} + x_{\text{N}_2}).$$

For $x_{\text{N}_2} = 0.0, 0.007, \text{ and } 0.014$ all possible combinations of the above were determined, (i.e., $7 \times 4 \times 2 \times 2 = 112$ different mixtures for each of $x_{\text{N}_2} = 0.0, 0.007, \text{ and } 0.014$).

The assumed limits for LNG containing more of the heavier hydrocarbons are:

Table 2. Typical Libyan LNG compositions

<u>Component</u>	<u>Mole Fraction x_i</u>
Methane (CH_4)	0.62 - 0.87
Ethane (C_2H_6)	0.08 - 0.24
Propane (C_3H_8)	0.04 - 0.10
Butanes ($i\text{C}_4\text{H}_{10} + n\text{C}_4\text{H}_{10}$)	0.01 - 0.02
Pentane (C_5H_{12})	0.0 - 0.01
Nitrogen (N_2)	0.0 - 0.01

The above limits on composition are somewhat arbitrary but typify Libyan composition LNG as given in reference [2].

Various mixtures within the Libyan composition limits were obtained by the same procedure given for the normal composition. The assumed values were:

<u>Component</u>	<u>Mole Fraction Possible Values x_i</u>	<u>No. of Values</u>
C_2H_6	0.08, 0.12, 0.16, 0.20, 0.24	5
C_3H_8	0.04, 0.06, 0.08, 0.10	4
C_4H_{10}	0.01, 0.02	2
C_5H_{12}	0.0, 0.01	2
N_2	0.0, 0.01	2

i.e., 80 different mixtures for each of $x_{\text{N}_2} = 0.0$ and $x_{\text{N}_2} = 0.01$.

2.2 Clausius-Mosotti Functions

The Clausius-Mosotti function for a mixture of LNG is given rigorously by:

$$CM_{mix} = \sum_i x_i CM_i + CM_E(x_i, T, P) \quad (3)$$

where

CM_i = Clausius-Mosotti function for each of the pure components

CM_E = Excess CM function, which is the change in CM on mixing at fixed temperature and pressure.

Diller [3] estimates CM_E to be less than $\pm 1\%$ of CM_{mix} for ordinary mixtures of LNG with high concentrations of methane. Pan, et al. [4] experimentally determined values of CM_E less than $\pm 0.1\%$ of the mixture CM values for the binary and ternary mixtures of their investigation. Therefore in this study we define

$$CM_{mix} = \sum_i x_i CM_i \quad (4)$$

with the CM_i values used given in table 3. These values were taken from Pan, et al. reference [4] and assumed to be constant since the CM_i are nearly independent of temperature and pressure [3 and 4].

Table 3. CM_i values for LNG components

<u>Component</u>	<u>CM_i (cm^3/mole)</u>
CH_4	6.548
C_2H_6	11.072
C_3H_8	16.406
$\text{C}_4\text{H}_{10}^*$	20.88
$\text{C}_5\text{H}_{12}^{**}$	25.25
N_2	4.394

* Average of $n\text{C}_4\text{H}_{10}$ and $i\text{C}_4\text{H}_{10}$

** Determined by extrapolation of the remaining hydrocarbons CM_i .

It is apparent that within the normal composition limits a maximum density exists when the maximum amount of the heavier components are present and a minimum density exists when a minimum amount of the heavier components are present. The corresponding $CM_{\text{max density}}$ and $CM_{\text{min density}}$ are (in units of m^3/kg):

$$CM_{\text{max density}} = \frac{\sum x_i CM_i}{\sum x_i MW_i}$$

where MW_i = molecular weight of component i .

$$CM_{\text{max density}} = (N_2=0\%)$$

$$\frac{(0.8677)(6.548) + (0.09)(11.072) + (0.03)(16.406) + (0.01)(20.88) + (0.0023)(25.25)}{(0.8677)(16.04) + (0.09)(30.07) + (0.03)(44.09) + (0.01)(58.12) + (0.0023)(72.15)}$$

$$= 0.398 \text{ cm}^3/\text{g} = 3.98 \times 10^{-4} \text{ m}^3/\text{kg}.$$

Similarly,

$$CM_{\text{min density}} = (N_2=0\%)$$

$$\frac{(0.97)(6.548) + (.03)(11.072)}{(.97)(16.04) + (.03)(30.07)} = 0.406 \text{ cm}^3/\text{g} = 4.06 \times 10^{-4} \text{ m}^3/\text{kg}.$$

Further, if we know only the range of N_2 composition, i.e., 0-1.4% then:

$$CM_{\text{max density}} =$$

$$\frac{(0.8534)(6.548) + (.09)(11.072) + (.03)(16.406) + (.01)(20.88) + (.0023)(25.25) + (.014)(4.394)}{(0.8537)(16.04) + (.09)(30.07) + (.03)(44.09) + (.01)(58.12) + (.0023)(72.15) + (.014)(28.01)}$$

$$= \frac{7.407}{18.8626} = 0.393 \text{ cm}^3/\text{g} = 3.93 \times 10^{-4} \text{ m}^3/\text{kg}$$

$$CM_{\text{min density}} = \frac{(.97)(6.548) + (.03)(11.072)}{(.97)(16.04) + (.03)(30.07)} = 4.06 \times 10^{-4} \text{ m}^3/\text{kg}.$$

2.3 Method used for prediction of density from equation of state

The scheme used for the prediction of density of LNG for a given composition, temperature, and pressure is that of Möllerup [1].

We have selected this method instead of the commonly used method of Klosek and McKinley [5] and other correlation methods for the following reasons:

- (1) The method of Möllerup is more versatile in its usage. Densities may be calculated for a given temperature, pressure, and composition (off the saturation surface) or saturation densities may be calculated for a given composition and pressure or a given composition and temperature. With the method of Klosek and McKinley densities may be calculated only for a specified temperature and composition. Thus, the results shown in the following sections would not have been possible using the Klosek and McKinley method.
- (2) Möllerup output includes phase equilibria data including densities of the equilibrium vapor phase of the LNG mixture.
- (3) In figures 1 and 2 we have compared the normal composition densities as calculated by Möllerup with the densities as calculated by Klosek and McKinley. For 1 atm pressure the saturation densities and saturation temperatures were determined for the various LNG mixtures by the method of Möllerup and the resulting saturation temperatures and corresponding mixture fractions were used to calculate densities by the K-M method. The relative deviations in the densities calculated by the two methods are thus plotted in figures 1 and 2 for N_2 composition of 0 and 1%, respectively.

The maximum deviation in density calculation between the two methods is 0.13% for $N_2 = 0\%$ and 0.18% for $N_2 = 1\%$. This is consistent with the claimed accuracies of $\pm 0.1\%$ for Möllerup[1] and $\pm 0.3\%$ for Klosek and McKinley[5].

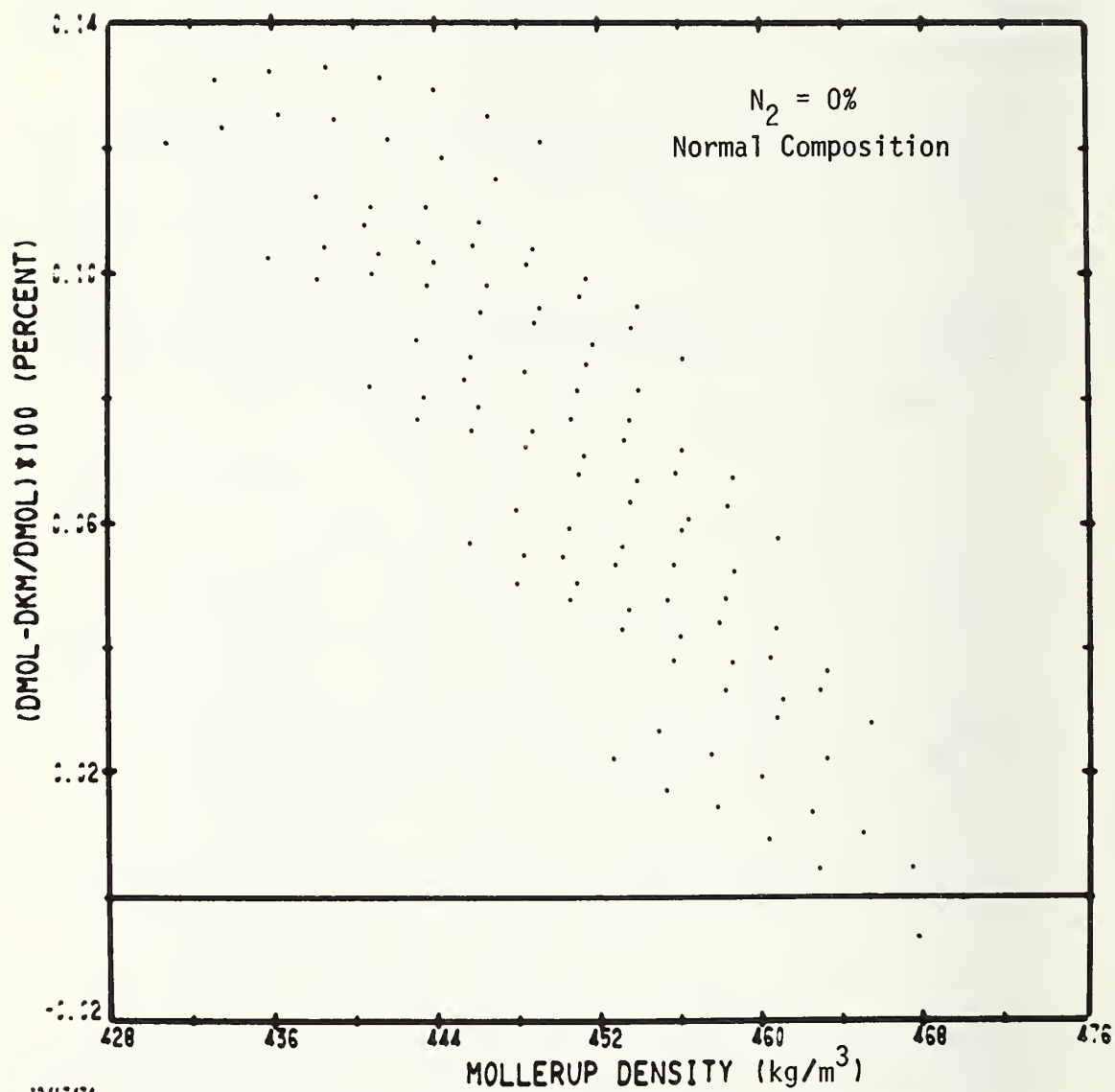
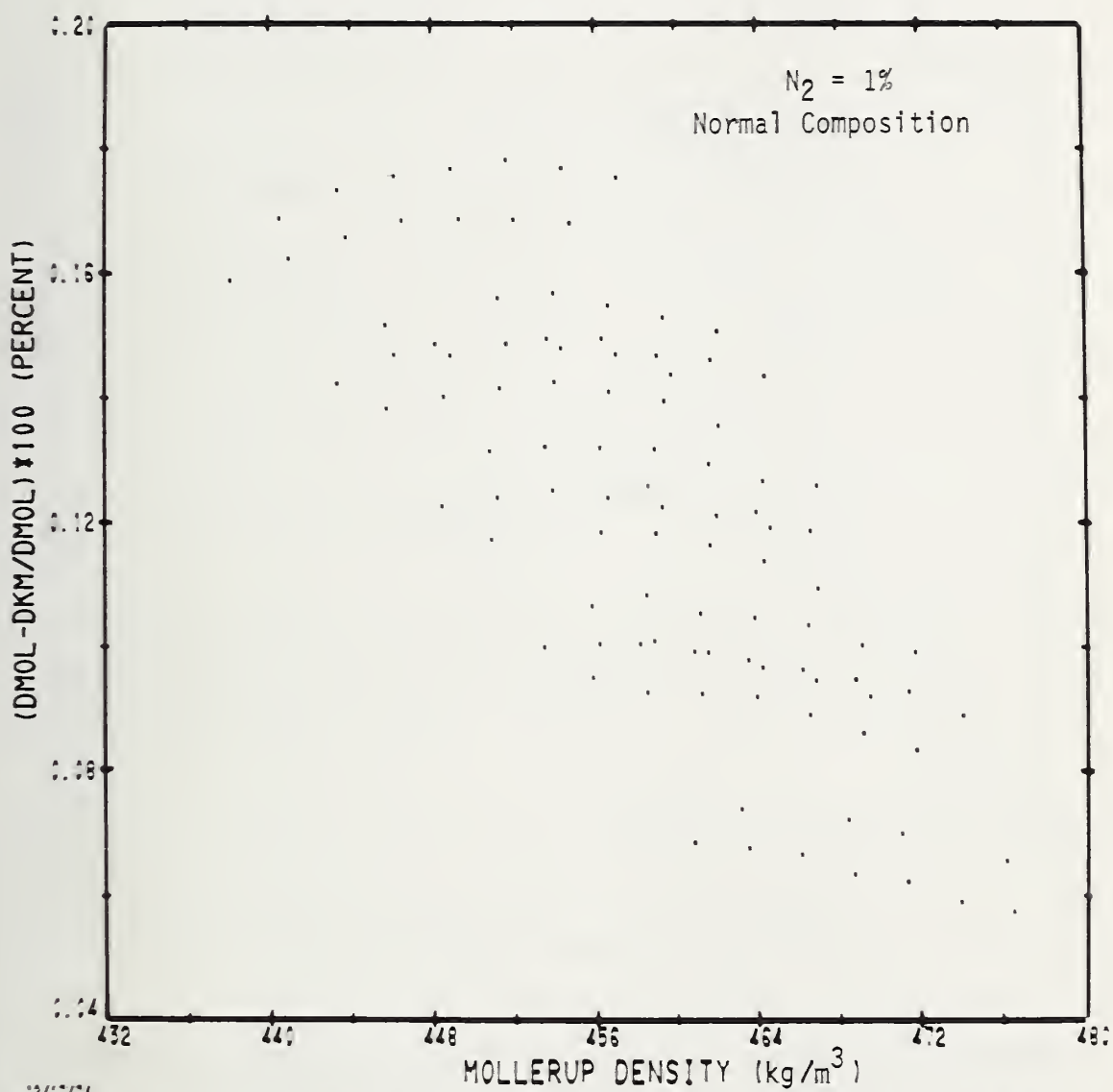


Figure 1. Comparison of density calculation methods for $N_2=0\%$



12/17/74
114 : Figure 2. Comparison of density calculation methods for N₂=1%

3. Results and Discussion

We have examined the relationship between density and dielectric constant for liquefied natural gas mixtures of normal composition via the Clausius-Mosotti relation and Möllerup's equation of state. We have also examined the improvement in density determination by measurement of temperature in addition to dielectric constant.

Four general cases or effects are considered:

Case 1 - The range of composition of the mixture is known but it is not known if the liquid is subcooled or at saturation.

Case 2 - The range of composition of the mixture is known and furthermore the fluid is known to be saturated and at constant pressure. For purposes of this study the pressure is taken to be 1 atm or 2.6 atm which is the head pressure of the bottom of a 37 meter (120 ft) deep storage container.

Case 3 - The range of the composition is known and the temperature of the fluid is uniform but the fluid is subject to varying pressure (e.g., the pressure difference between the top and bottom of a storage tank due to the weight of the liquid).

Case 4 - The range of composition of the mixture is known and furthermore the fluid is known to be saturated over a pressure range 0.5-8 atm. and at constant temperature. The range of saturation temperatures considered is 105-145 K.

Cases 1a, 2a, 3a, & 4a - As a subset of the above, the effect of nitrogen composition on the mixture density.

Case 2 is also examined for typical Libyan composition mixtures for possible evidence of deviation of results for higher density mixtures.

When applicable (cases 2 through 4) least squares fitting techniques were used to determine the probable intrinsic uncertainties in density determination (due to variation in composition) from measurement of dielectric constant only or measurement of dielectric constant and temperature. The equations are given in the Appendix. Since the equilibrium temperature of the mixture varies roughly as the inverse of the nitrogen composition (Fig. 3) and, as will be seen below, the nitrogen composition has significant influence on the density of the mixture, the effect of temperature measurement was included in the investigation. The stated intrinsic uncertainties do not include possible systematic uncertainties in the use of Möllerup's equation of state (claimed to be accurate to within

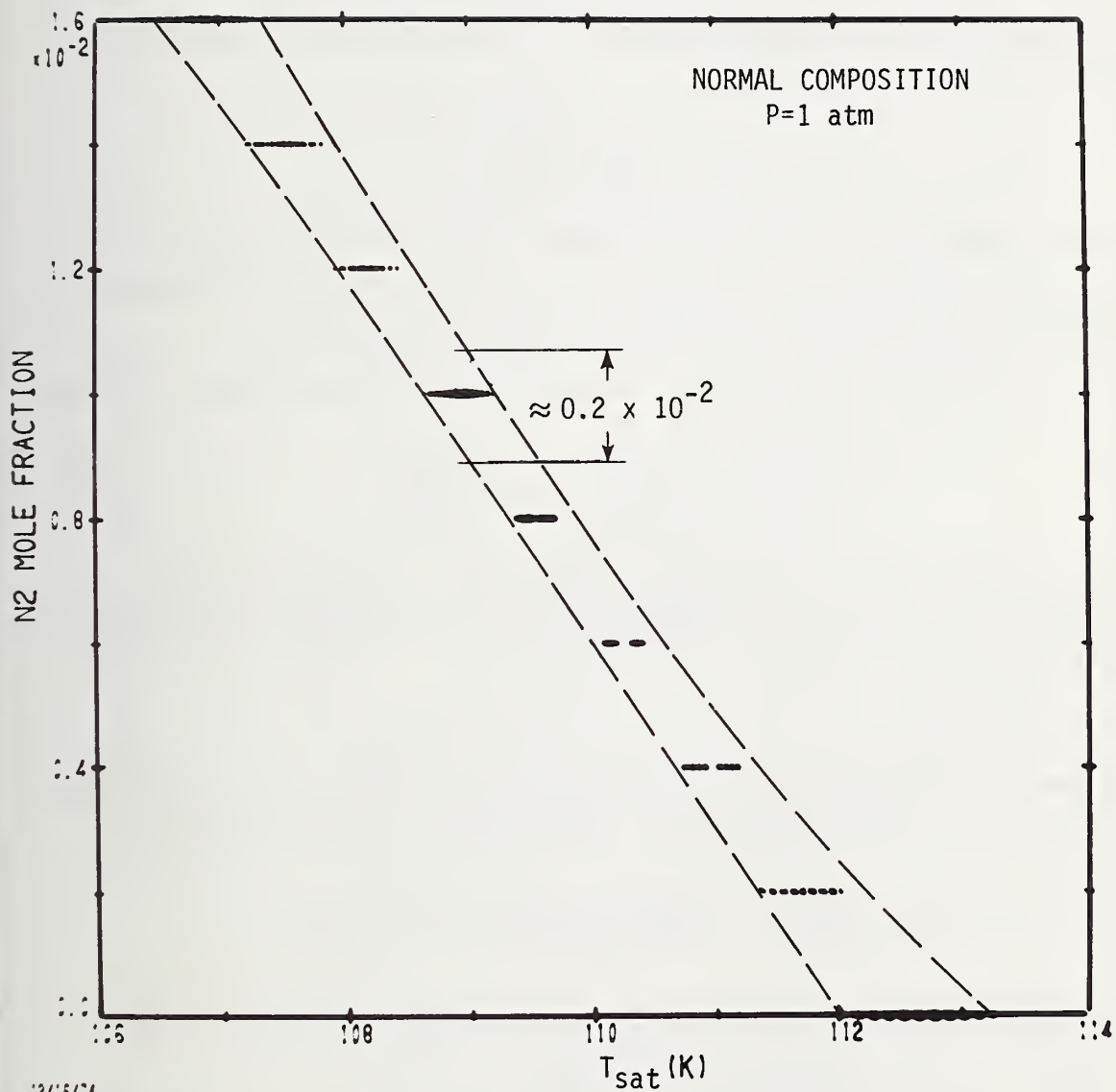


Figure 3. N₂ mole fraction vs. saturation temperature

$\pm 0.1\%$ [1]) or systematic uncertainties in the determination of dielectric constant ($\approx \pm 0.1\%$) due to neglect of CM_E . Uncertainties due to instrumentation must also be included in addition to the intrinsic and systematic uncertainties in order to obtain a total uncertainty for the system.

3.1 Case 1

As noted earlier, if a capacitance densitometer is used to measure ρ_{mix} , the defining equation is:

$$\rho_{mix} = \frac{1}{CM_{mix}} \frac{\epsilon - 1}{\epsilon + 2}.$$

This relationship is plotted in figure 4 for the range of CM_{mix} corresponding to the maximum and minimum densities possible plus three intermediate mixtures within the composition limits described in section 2.1.

The uncertainty in ρ_{mix} (due to variation in composition) may be expressed as:

$$\left| \frac{d\rho}{\rho} \right| = \left| \frac{3d\epsilon}{(\epsilon+2)(\epsilon-1)} \right| + \left| \frac{dCM_{mix}}{CM_{mix}} \right|. \quad (5)$$

Assuming no error in dielectric constant measurement, i.e., $d\epsilon = 0$, $dC_{mix} = (4.06 - 3.98)(10^{-4})$, and $C_{mix} = \frac{(4.06 + 3.98)}{2} (10^{-4})$ then $\left| \frac{d\rho}{\rho} \right| = 2.0\%$ as shown in figure 4 for $N_2 = 0\%$.

3.1.1 Case 1a

Extending the above calculation to the situation where the N_2 composition is not known but only the range of the composition (0 - 1.4%) we have:

$$\left| \frac{d\rho}{\rho} \right| = \left| \frac{dCM_{mix}}{CM_{mix}} \right| = \frac{(4.06 - 3.93) \times 10^{-4}}{\frac{4.06 + 3.93}{2} \times 10^{-4}} = 3.3\%.$$

3.2 Case 2

Using the method of Möllerup the saturation densities at 1 atm and 2.6 atm were calculated for the different mixtures described in section 2.1 and the dielectric constant for each mixture was calculated through the C-M relation (eq. 1). The corresponding ρ_{sats} vs ϵ are shown in figure 5 at $P = 1$ atm for the normal composition and $N_2 = 0\%$. It can be seen that there is a substantial improvement in $\frac{d\rho}{\rho}$ due to variation in composition if it is known that the mixture

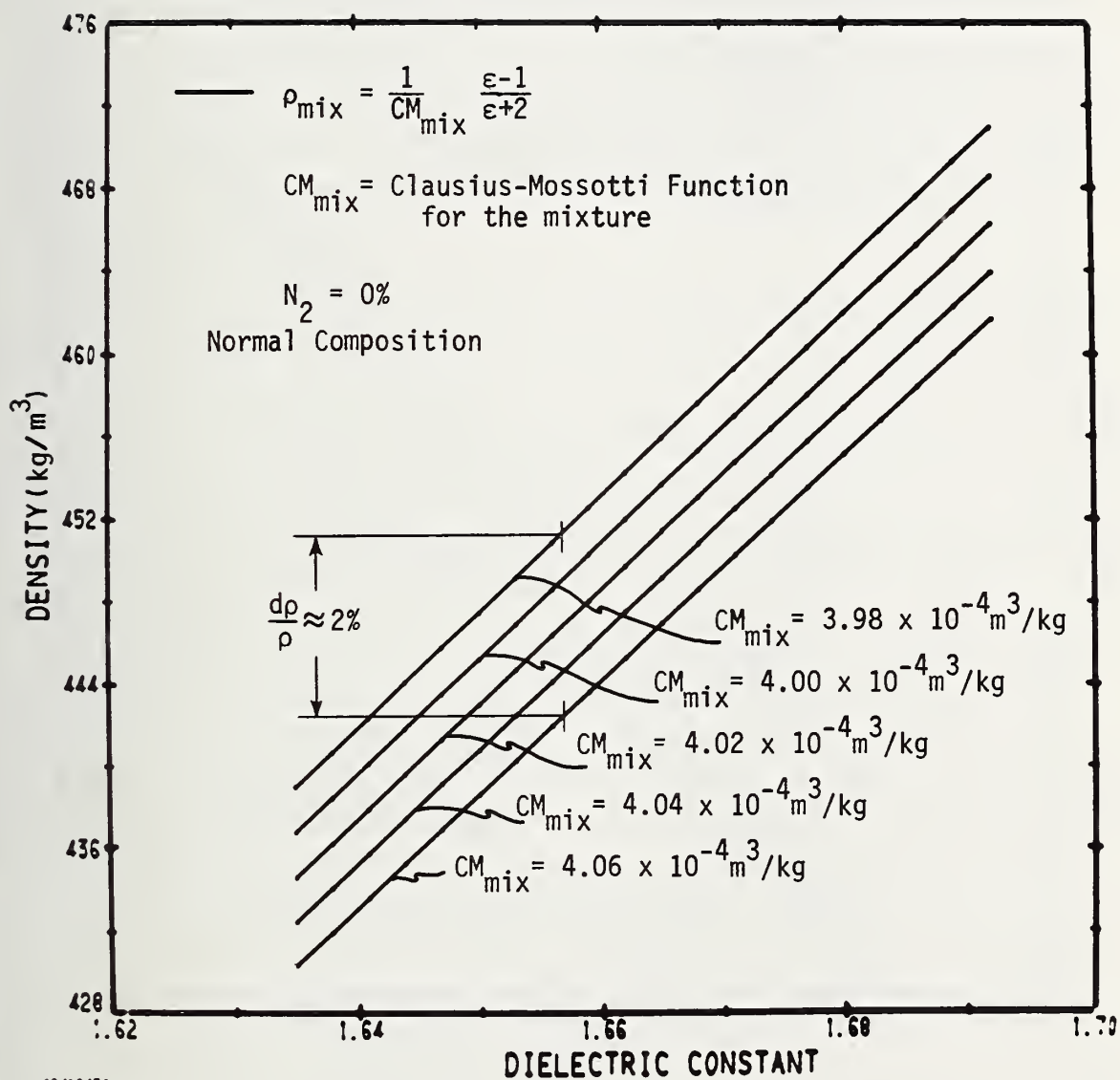
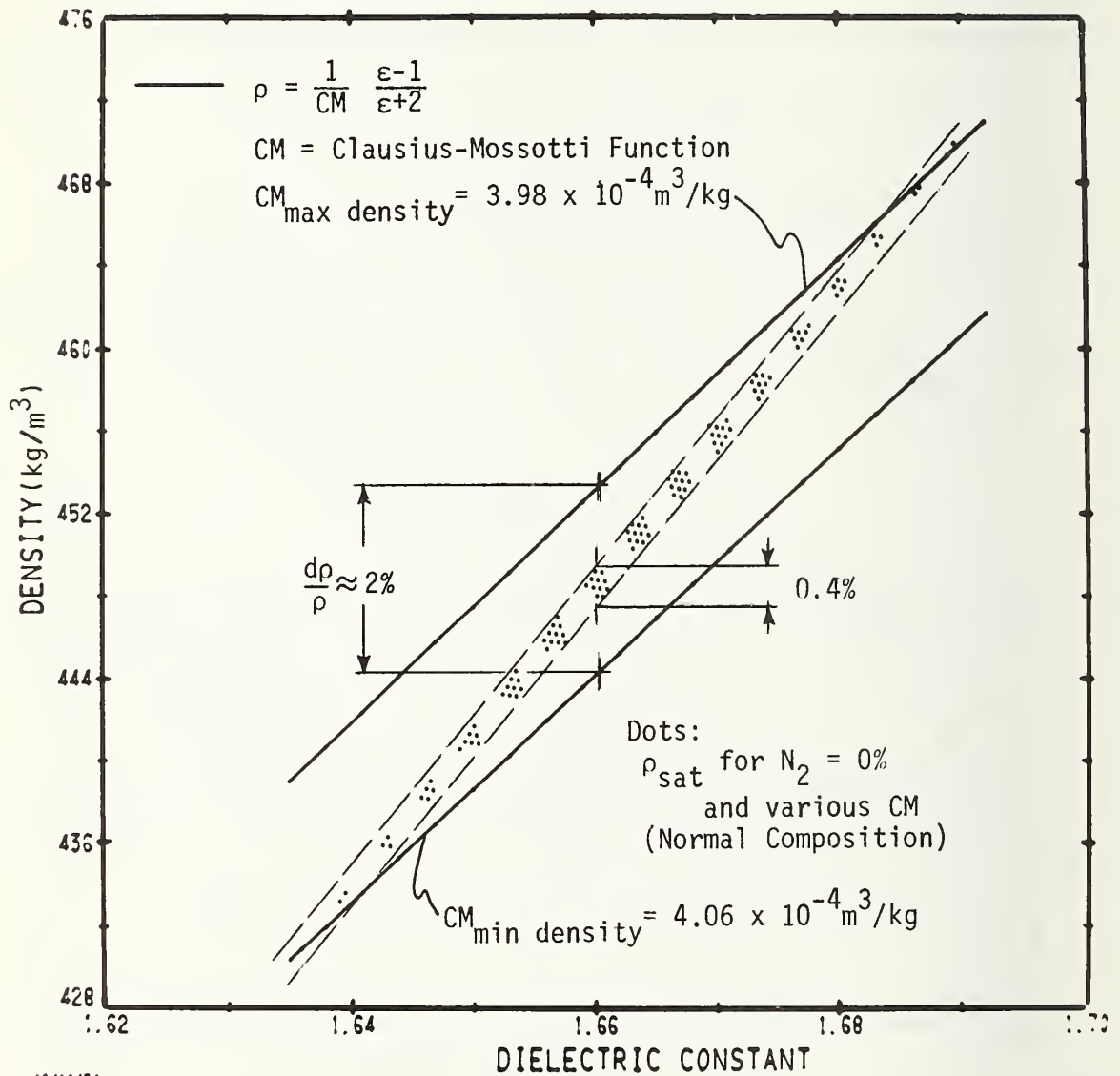


Figure 4. LNG density vs. dielectric constant with CM_{mix} as parameter



2/1/74
 PAGE 1

Figure 5. LNG saturation density vs. dielectric constant

of LNG is at saturation conditions since $\frac{d\rho}{\rho}$ is approximately 0.4% for this case compared to $\approx 2\%$ for case 1 where the thermodynamic state of the fluid was not presumed to be known. The Clausius-Mosotti relationship does not delineate the thermodynamic state of the LNG mixture but when the saturation curve is delineated through the equation of state the unique one to one relationship (within a $\pm 0.2\%$ error) between density and dielectric constant very nearly exists.

Figure 6 shows a plot of ρ_{sat} vs ϵ for three different nitrogen compositions (0%, 0.7%, and 1.4%). The three linear equations which best represent the data are given in the appendix. We note through calculation that a change in density of about 1.4% maximum results when the nitrogen composition changes from 0 to 1.4%.

3.2.1 Case 2a

Fitting all the normal composition data with one equation (range of composition known) results in a density variation of about $\pm 0.8\%$ as shown in Table 4.

We conclude that a single calibration curve for a capacitance type densitometer could not be used to predict densities to better than about $\pm 0.8\%$ for normal composition of LNG which may have a nitrogen content between 0-1.4%.

3.2.2 Measurement of temperature as well as dielectric constant for cases 2 and 2a.

For an assumed functional relationship of the form $\rho_{\text{mix}} = A + B(\epsilon - 1) + CT$, where ρ_{mix} and T were determined from the Möllerup equation of state for each mixture at the given saturation pressure, and ϵ determined through the C-M relationship, the constants A , B , and C were determined by least squares fitting techniques. As can be seen by comparison of tables 4 and 5, addition of temperature measurement when the nitrogen composition is not known exactly (only the range 0-1.4%) improves the density determination from $\pm 0.8\%$ to $\pm 0.3\%$. There is no improvement due to the additional temperature measurement for the case where the nitrogen composition and pressure are fixed.

3.3 Cases 3 and 3a

In figures 7a, 7b, and 7c we have plotted for a fixed N_2 composition, density versus dielectric constant for three different conditions:

- (1) Saturation conditions at $P = 2.6$ atm (the pressure which approximates the absolute pressure at the bottom of a 37 meter (120 ft) deep LNG storage tank).

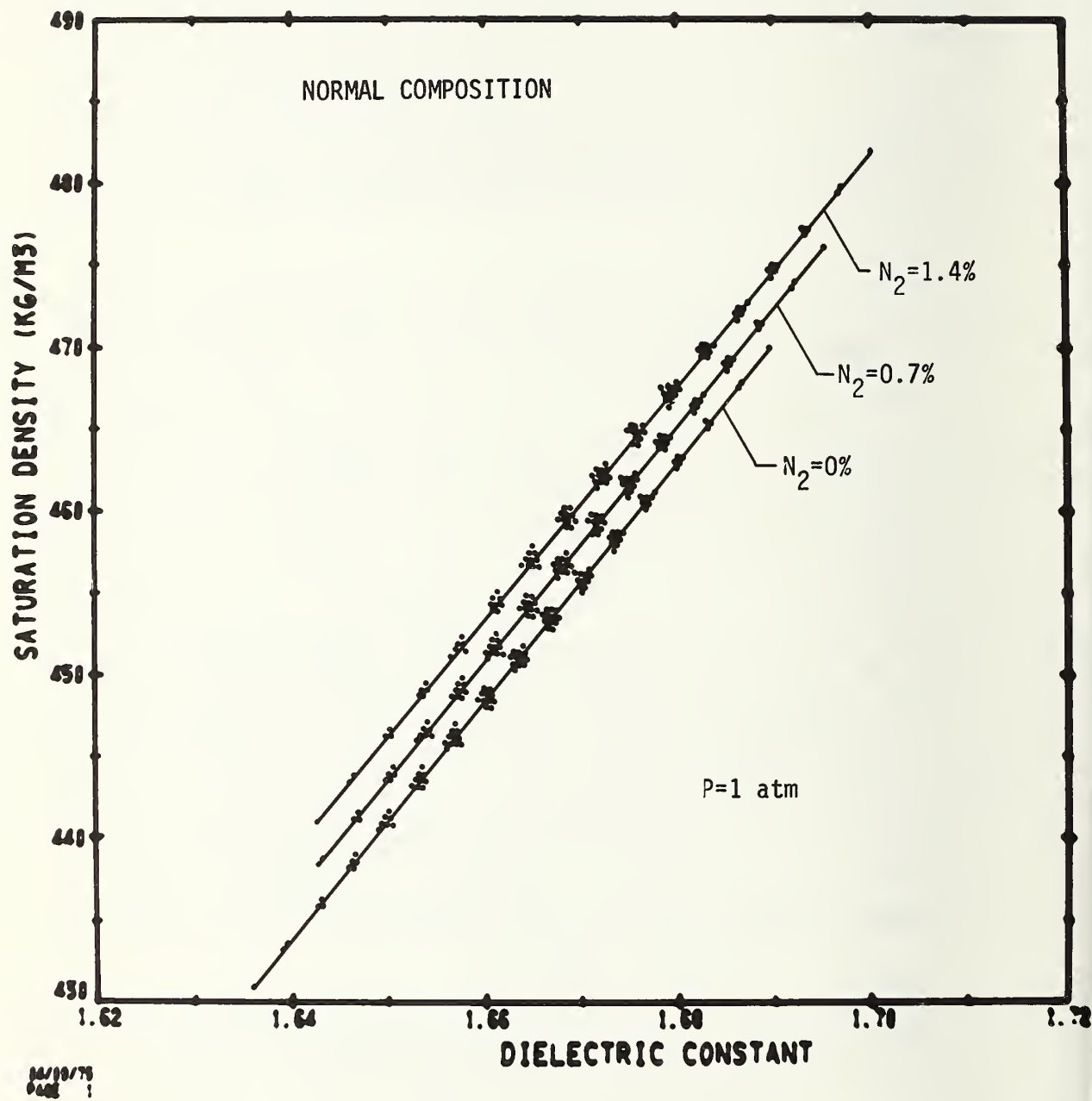


Figure 6. Effect of nitrogen composition on saturation density

Table 4. Intrinsic[†] uncertainties in density from measurement of dielectric constant only.

Thermodynamic State: Unspecified (Cases 1 and 1a)		Saturated Conditions $P_{\text{sat}} = \text{const}$ (Cases 2 and 2a)		Uniform Temperature Conditions Including Subcooled Fluid (Cases 3 and 3a)	
JJ*	KK*	JJ*	KK*	JJ*	KK*
$\pm 1.7\%^{\dagger}$	$\pm 1\%^{\dagger}$	$\pm 0.8\%^{\dagger}$	$\pm 0.2\%^{\dagger}$	$\pm 0.9\%^{\dagger}$	$\pm 0.3\%^{\dagger}$

* Headings for Table	
JJ: Only <u>range</u> of N_2 composition and <u>range</u> of hydrocarbons composition known.	
N_2 Composition Range	Hydrocarbon Composition Range
$\left. \begin{array}{c} 0-1.4\% \end{array} \right\}$	$\left. \begin{array}{c} \text{per Table 1} \end{array} \right\}$
KK: N_2 composition <u>known</u> but only <u>range</u> of hydrocarbons composition known.	
N_2 Composition	Hydrocarbon Composition Range
$\left. \begin{array}{c} \text{Fixed} \\ 0, 0.7, \text{ or } 1.4\% \end{array} \right\}$	$\left. \begin{array}{c} \text{per Table 1} \end{array} \right\}$

[†]Systematic uncertainties ($\approx \pm 0.3\%$ at present) due to inaccuracies in the Möllerup equation of state and the inaccuracies in the dielectric constant calculation procedure are not included in these numbers. Instrumentation errors that would be incurred in a measurement situation must be combined with the intrinsic and systematic uncertainties in order to obtain a total uncertainty for the measurement system.

Table 5. Intrinsic[†] uncertainties in density from measurement of dielectric constant and temperature.

Saturated Conditions $T_{\text{sat}} = \text{const}$ (105-145 K) ($P \approx 0.5-8 \text{ atm}$) (Cases 4 and 4a)		Saturated Conditions $P_{\text{sat}} = \text{const}$ (1 atm or 2.6 atm) ($T \approx 107-113^\circ$, $P = 1 \text{ atm}$) ($T \approx 121-127^\circ$, $P = 2.6 \text{ atm}$) (Cases 2 and 2a)		Uniform Temperature Conditions Including Subcooled Fluid (Cases 3 and 3a)	
JJ*	KK*	JJ*	KK*	JJ*	KK*
$\pm 0.9\%^{\dagger}$	$\pm 0.2\%^{\dagger}$	$\pm 0.3\%^{\dagger}$	$\pm 0.2\%^{\dagger}$	$\pm 0.3\%^{\dagger}$	$\pm 0.2\%^{\dagger}$

*Heading for Table

JJ: Only range of N_2 composition and range of hydrocarbons composition known.

N_2		Hydrocarbon
Composition	} 0-1.4% Range	Composition
Range		Range

per Table 1

KK: N_2 composition known but only range of hydrocarbons composition known.

N_2		Hydrocarbon
Composition	} Fixed Range	Composition
		0,0.7, or 1.4% Composition

per Table 1

[†]Systematic uncertainties ($\approx +0.3\%$ at present) due to inaccuracies in the Möllerup equation of state and the inaccuracies in the dielectric constant calculation procedure are not included in these numbers. Instrumentation errors that would be incurred in a measurement situation must be combined with the intrinsic and systematic uncertainties in order to obtain a total uncertainty for the measurement system.

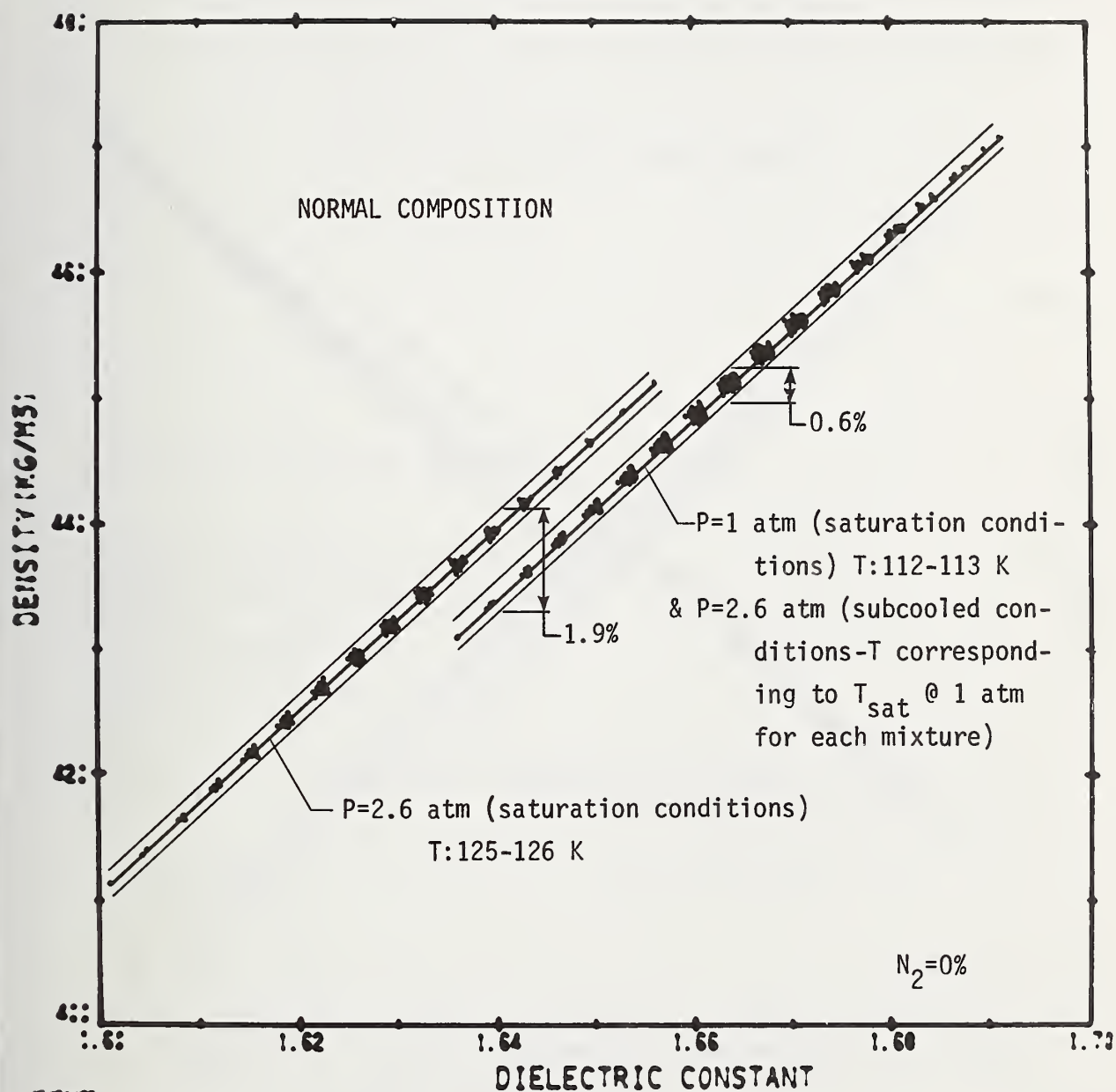


Figure 7a. Effect of pressure on LNG density vs. dielectric constant ($N_2=0\%$)

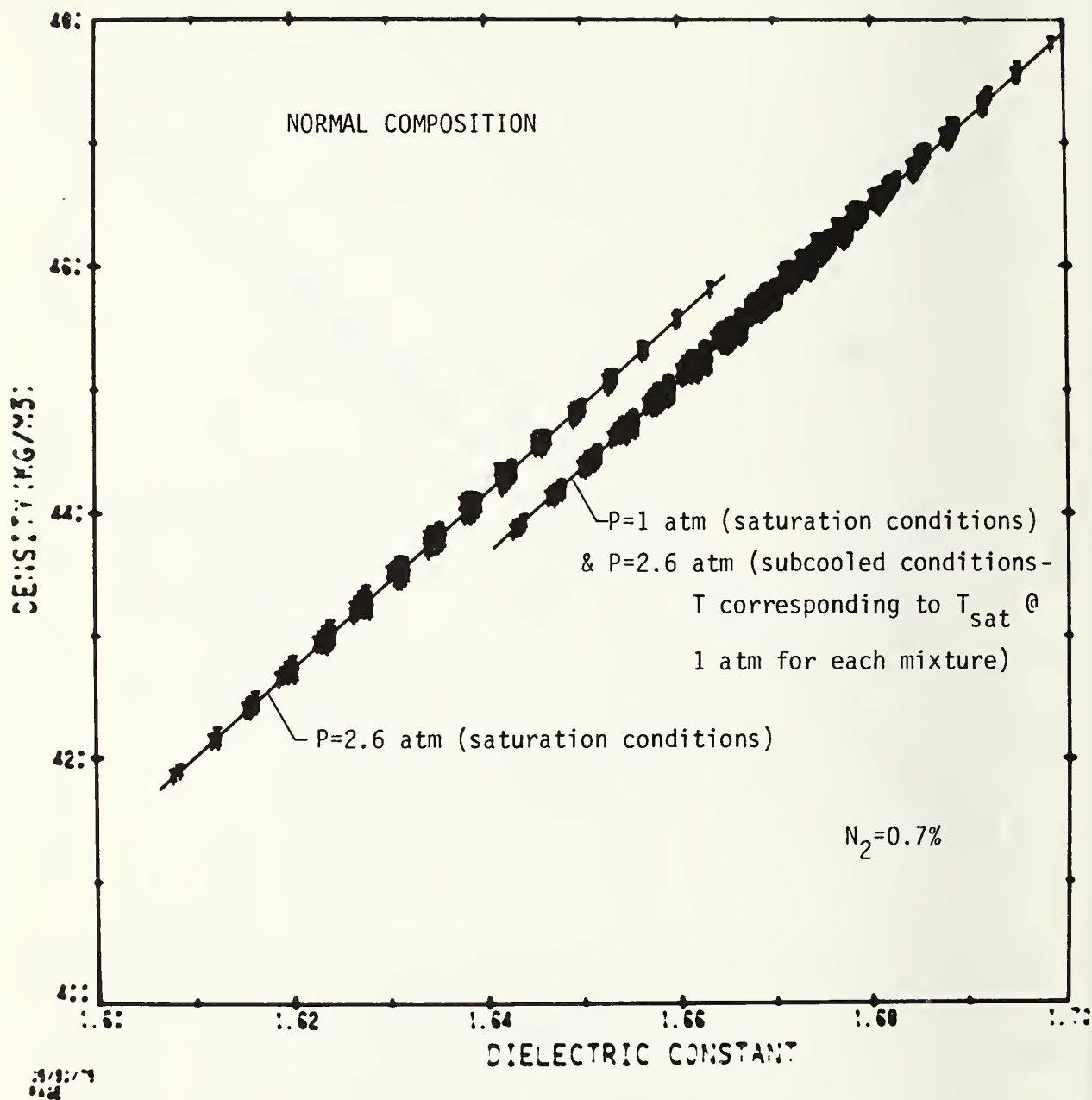


Figure 7b. Effect of pressure on LNG density vs. dielectric constant ($N_2=0.7\%$)

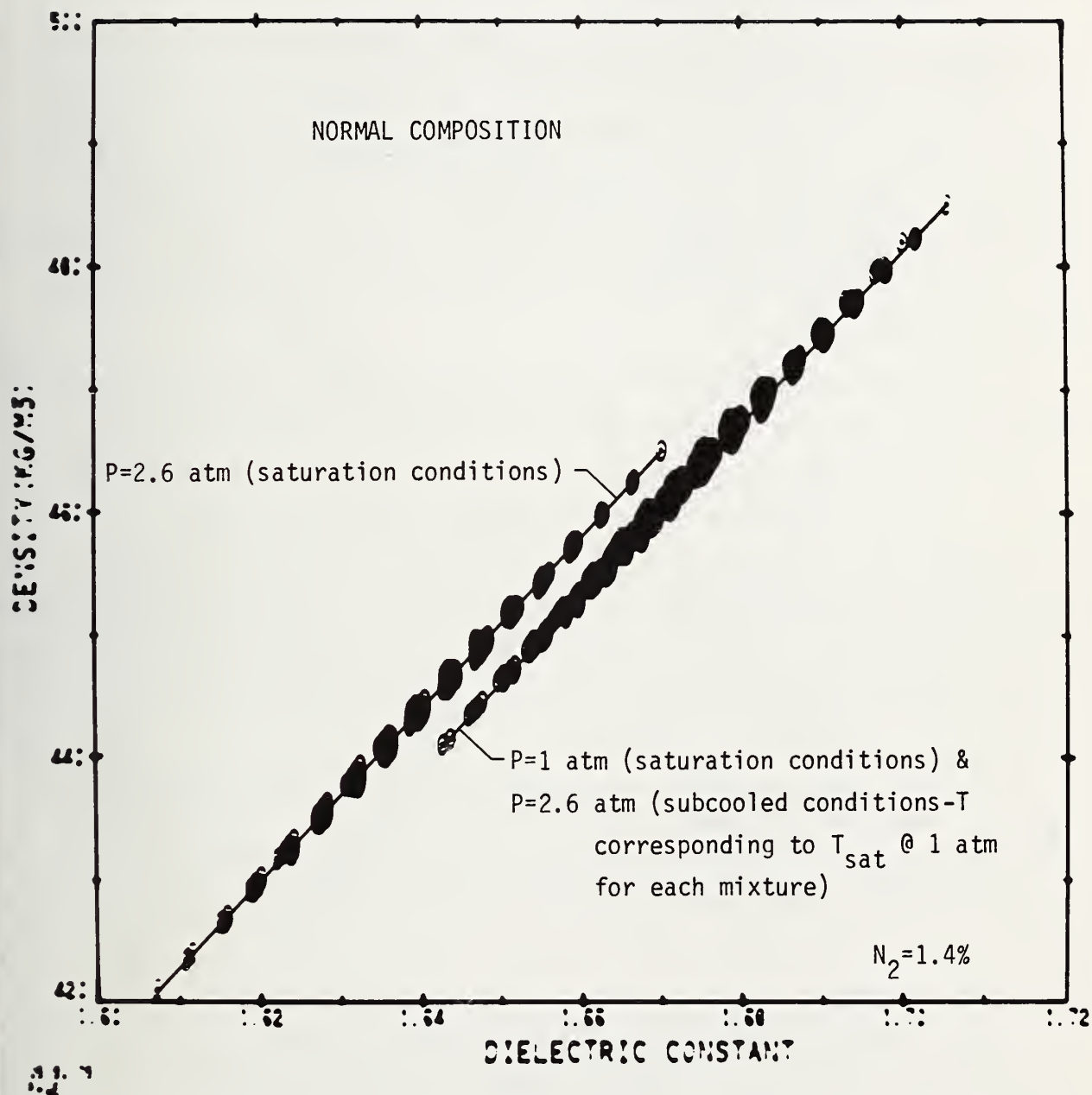


Figure 7c. Effect of pressure on LNG density vs. dielectric constant ($N_2 = 1.4\%$)

Uniform temperature conditions:

- (2) Saturation conditions at $P = 1.0$ atm.
- (3) Subcooled conditions at $P = 2.6$ atm and T corresponding to the T_{sat} at 1.0 atm for each mixture.

As shown in the graphs for fixed N_2 composition and dielectric constant and as determined by the least-squares-fitting there is not a significant change in the range of density (0.6%) when the subcooled data at 2.6 atm is included with the saturation data at 1 atm. This illustrates the predominant dependence of density on the mixture temperature as might be expected for an incompressible fluid. The range of density for a change from saturation conditions at 1 atm. to saturation conditions at 2.6 atm is approximately 1.9%, again for fixed N_2 composition and dielectric constant.

For a range of N_2 composition of 0-1.4% and the uniform temperature conditions described above the density variation is 1.8% ($\pm 0.9\%$) as shown in table 4.

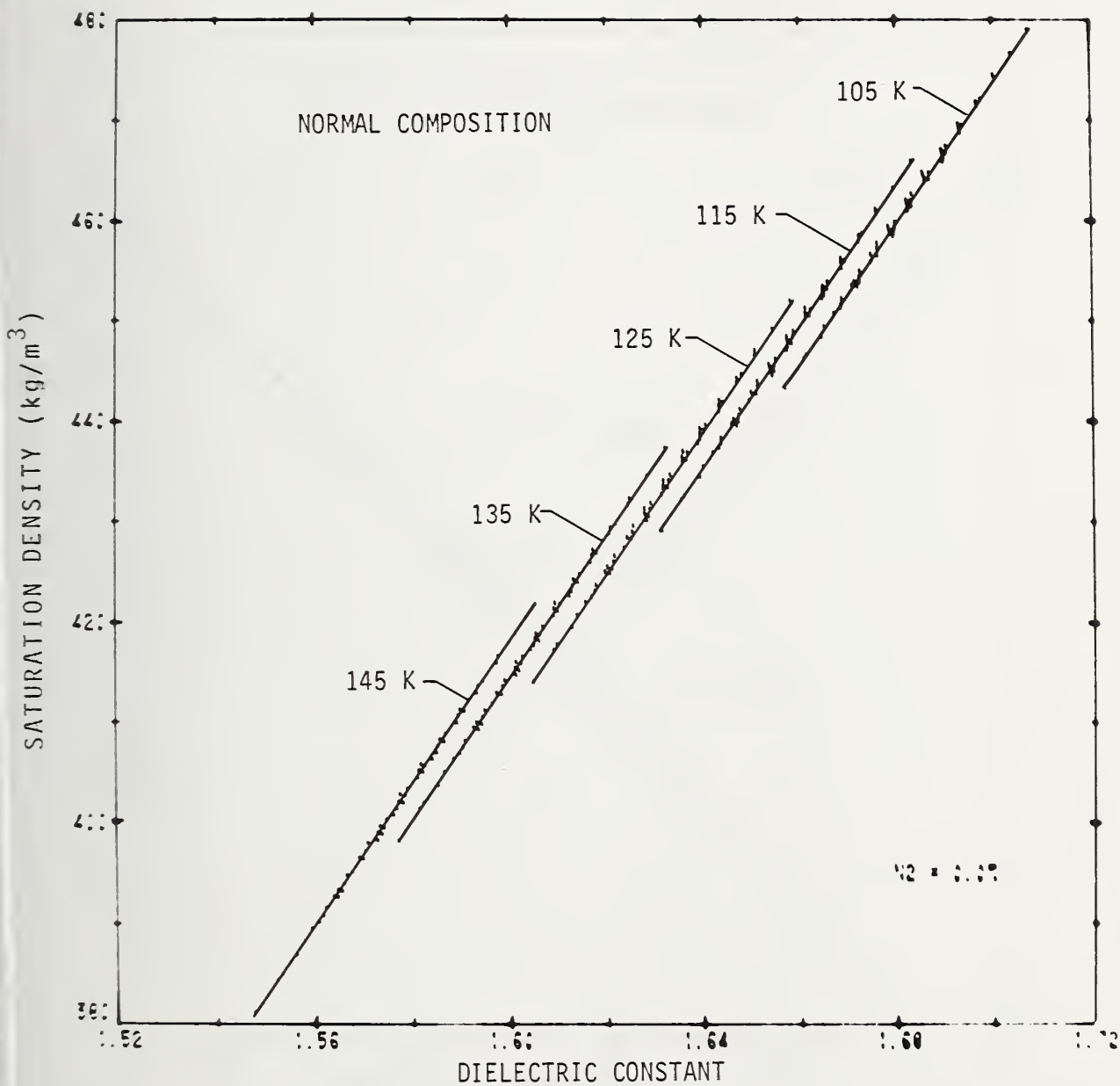
3.3.1 Measurement of temperature as well as dielectric constant for cases 3 and 3a (uniform temperature-varying pressure 1-2.6 atm).

Table 5 shows the improvement in possible error in density measurement if temperature is measured along with dielectric constant. If the nitrogen composition is not known exactly (0-1.4%) the improvement is from $\pm 0.9\%$ to $\pm 0.3\%$. For fixed nitrogen composition there is still slight improvement (from $\pm 0.3\%$ to $\pm 0.2\%$) by the additional measurement of temperature.

The above results illustrate the potential usefulness of a temperature compensated capacitance densitometer for measuring densities of LNG in a large storage tank if it's at uniform temperature but where the pressure varies from 1 atm at the top to approximately 2.6 atm at the bottom due to the weight of the liquid.

3.4 Cases 4 and 4a

A similar linear relationship between saturation density and dielectric constant exists for isotherms (P_{sat} and mixture varies along the isotherm) just as for isobars (T_{sat} and mixture varies along the isobar). This is shown in figures 8a, 8b, and 8c for saturation temperatures from 105-145 K. A bilinear relationship between density, dielectric constant and temperature is clearly



8/29/11
PAGE 2

Figure 8a. Saturation density vs. dielectric constant for various isotherms for $N_2=0\%$

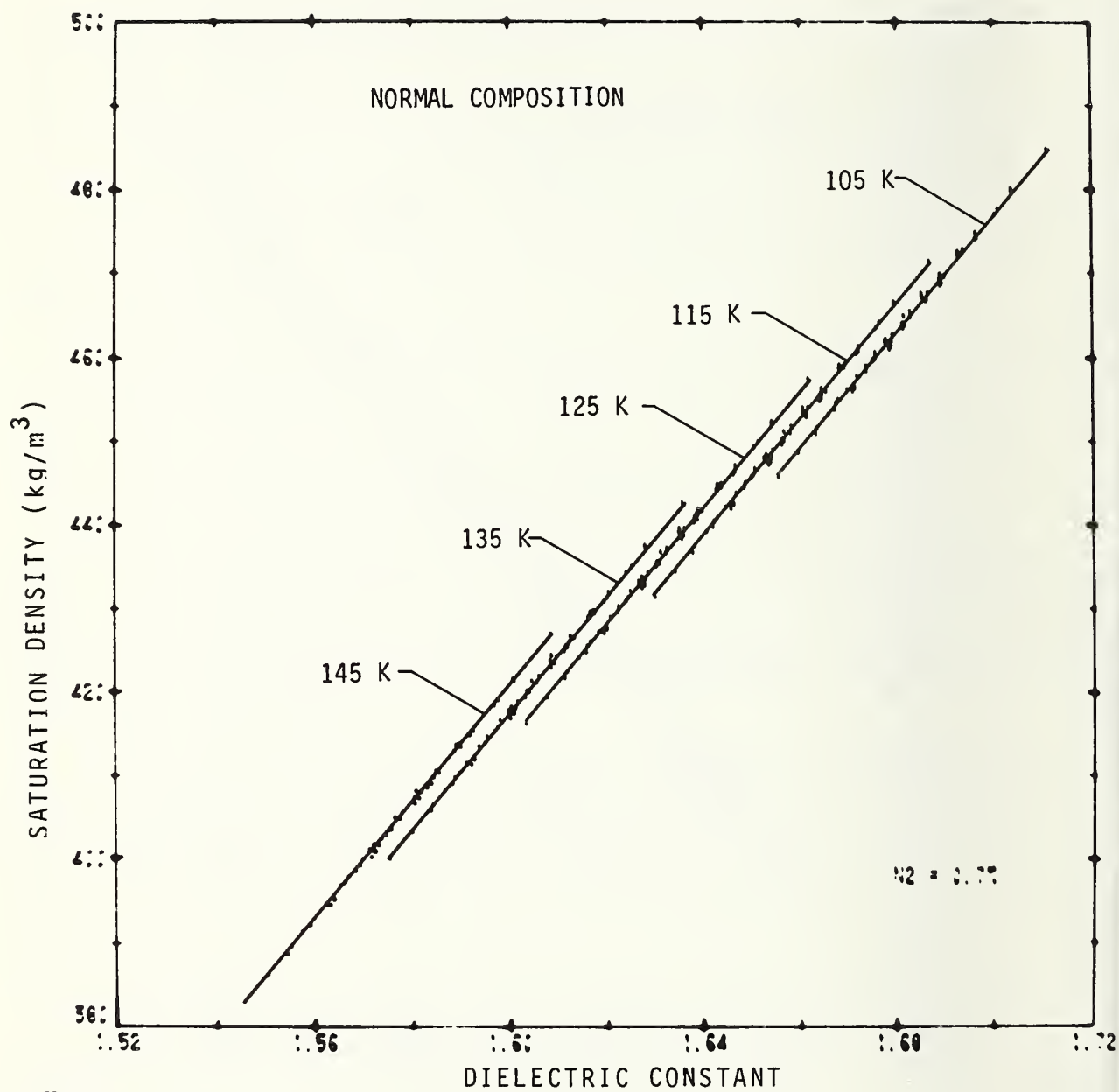


Figure 8b. Saturation density vs. dielectric constant for various isotherms for $N_2 = 0.7\%$

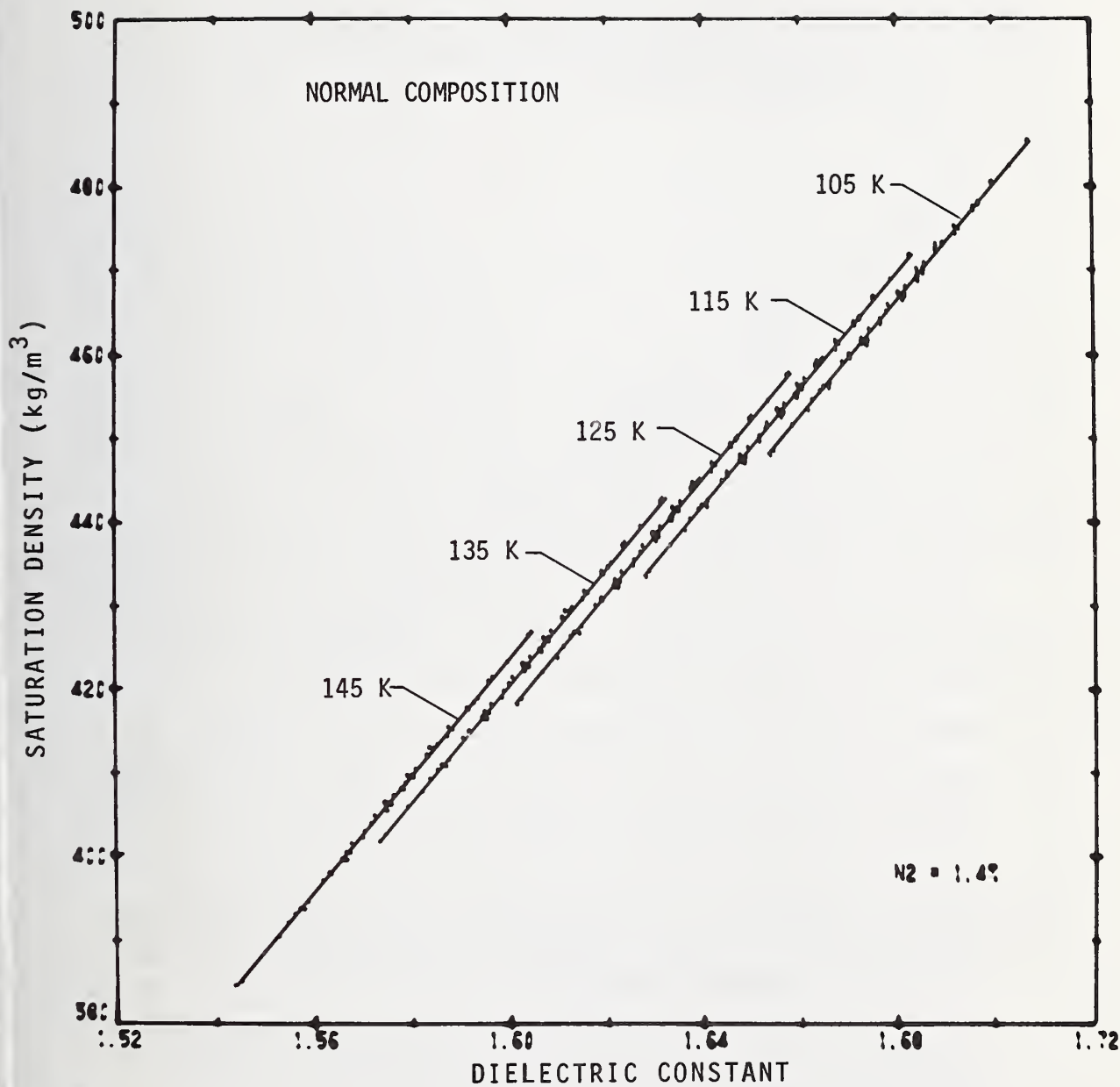


Figure 8c. Saturation density vs. dielectric constant for various isotherms for $N_2=1.4\%$

suggested by these graphs. Fitting the data for this range of temperatures resulted in a $\pm 0.2\%$ range of density for a given dielectric constant if the N_2 composition is fixed and $\pm 0.9\%$ range of density if only the range of N_2 composition (0-1.4%) is known. Thus for an anticipated use of a capacitance meter in saturated liquids which may range from 105-145 K in temperature, a single calibration may be obtained for predicting densities within the above noted limits.

3.5 Libyan Composition Results

Results similar to those noted for normal composition mixtures were obtained for Libyan composition mixtures. Figures 9 and 10 show the apparent linear relationship between ρ_{sat} and ϵ and the approximate 2.6% difference in slopes of the two curves for the two nitrogen compositions. In figure 11 it can be seen that at the higher densities the effect of nitrogen composition is qualitatively the same as for normal composition, a 1% increase in nitrogen resulting in approximately 1.3% (max) increase in density. Further even if the nitrogen composition is known the uncertainty in ρ for a given ϵ is approximately $\pm 0.4\%$ compared to $\pm 0.2\%$ for the normal composition mixtures.

We have plotted the results for all of the data (normal plus Libyan composition mixtures) in figures 12, 13 and 14. There is no significant difference in results when all data are considered together.

4. Summary of Results and Observations (see also tables 4 and 5)

- (1) The Clausius-Mosotti relationship shows a wide range of densities for a particular dielectric constant as one varies the mixture of LNG. A range of $\approx 3.3\%$ ($\pm 1.7\%$) is possible for the normal LNG mixtures of this study.
- (2) However, if the mixture is saturated then a unique linear relationship between density and dielectric constant very nearly exists for a constant pressure (or temperature) and fixed nitrogen mole fraction. For the normal range of LNG mixtures the saturation density can be determined to within approximately 0.2% at constant pressure or temperature if the nitrogen composition is known.
- (3) Nitrogen has a very pronounced effect on the density versus dielectric constant. For example, at saturation conditions and 1 atm pressure a change of nitrogen mole fraction from 0 to 1.4% of the total composition results in

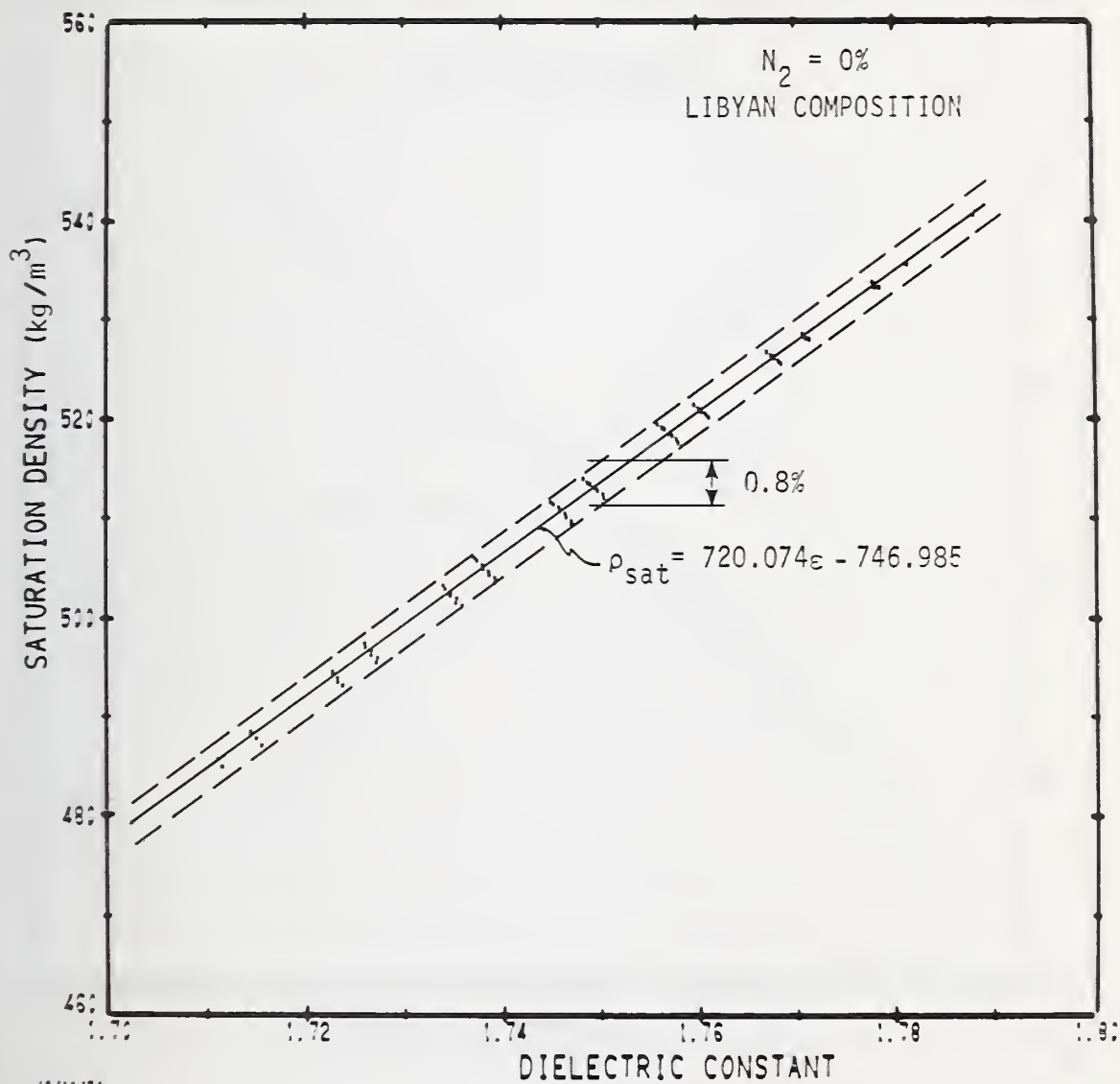


Figure 9. LNG saturation density vs. dielectric constant for Libyan composition with $N_2=0\%$

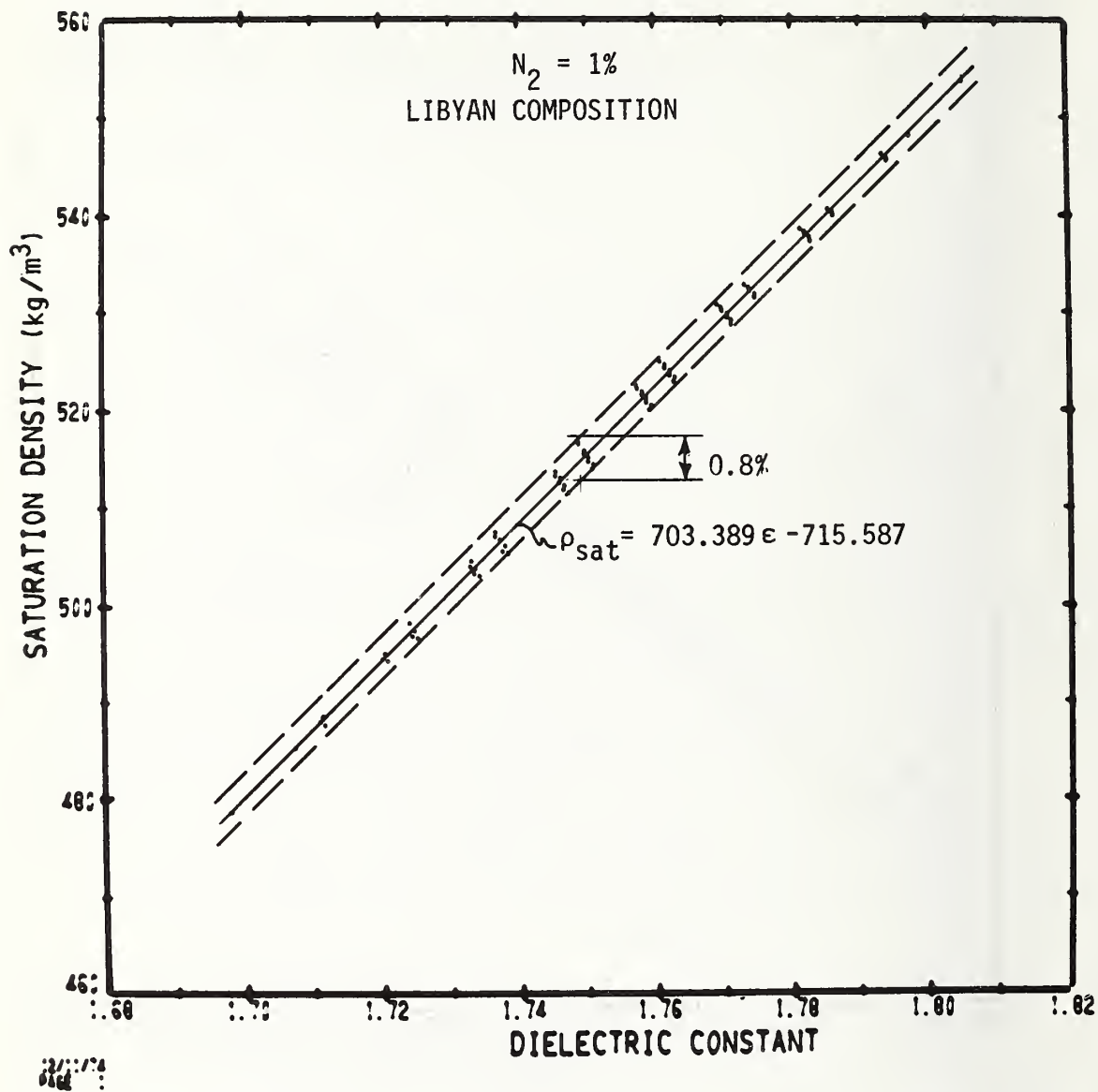


Figure 10. LNG saturation density vs. dielectric constant for Libyan composition with $N_2=1\%$

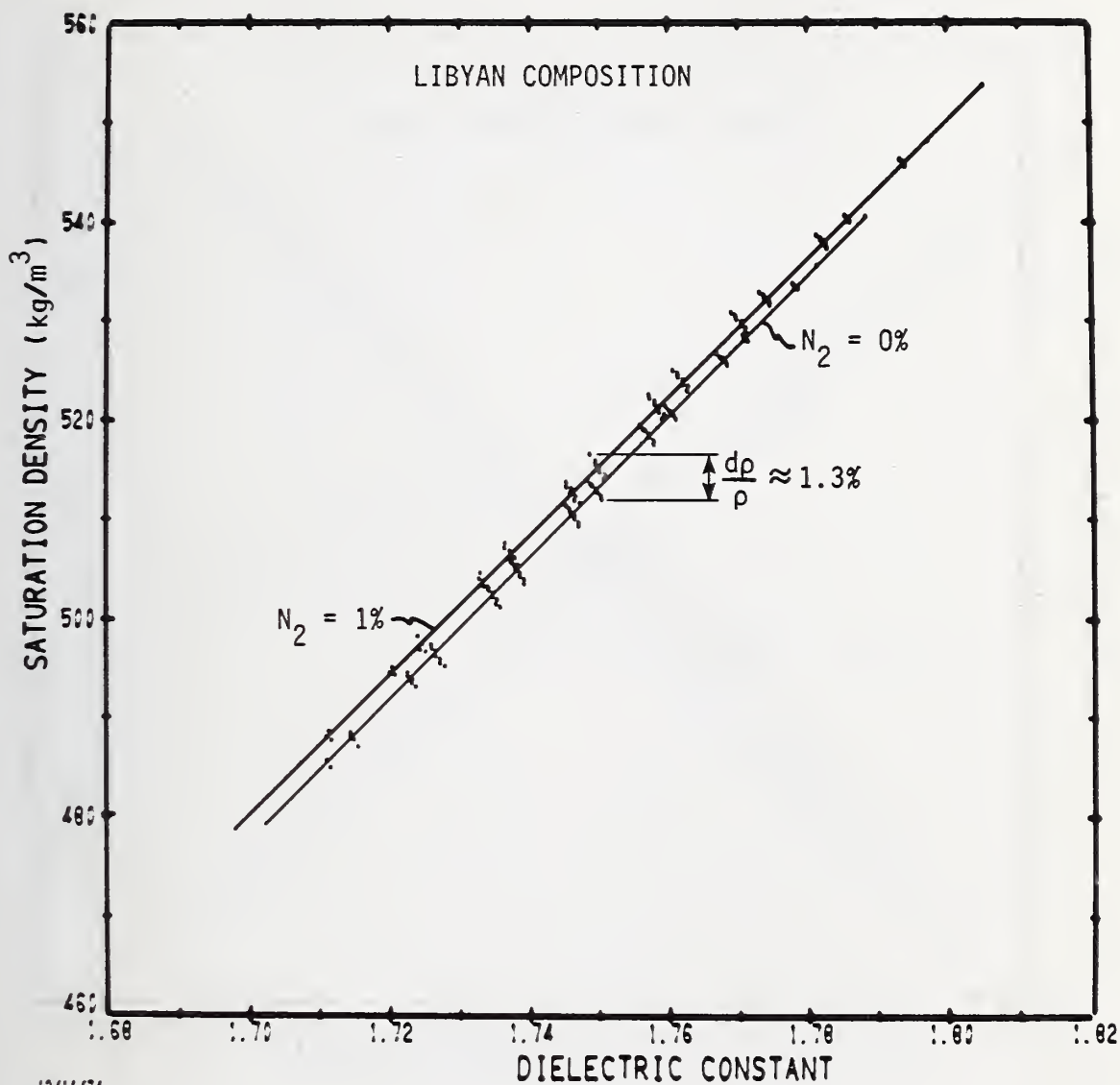


Figure 11. Effect of nitrogen composition on saturation density vs. dielectric constant for Libyan composition mixtures

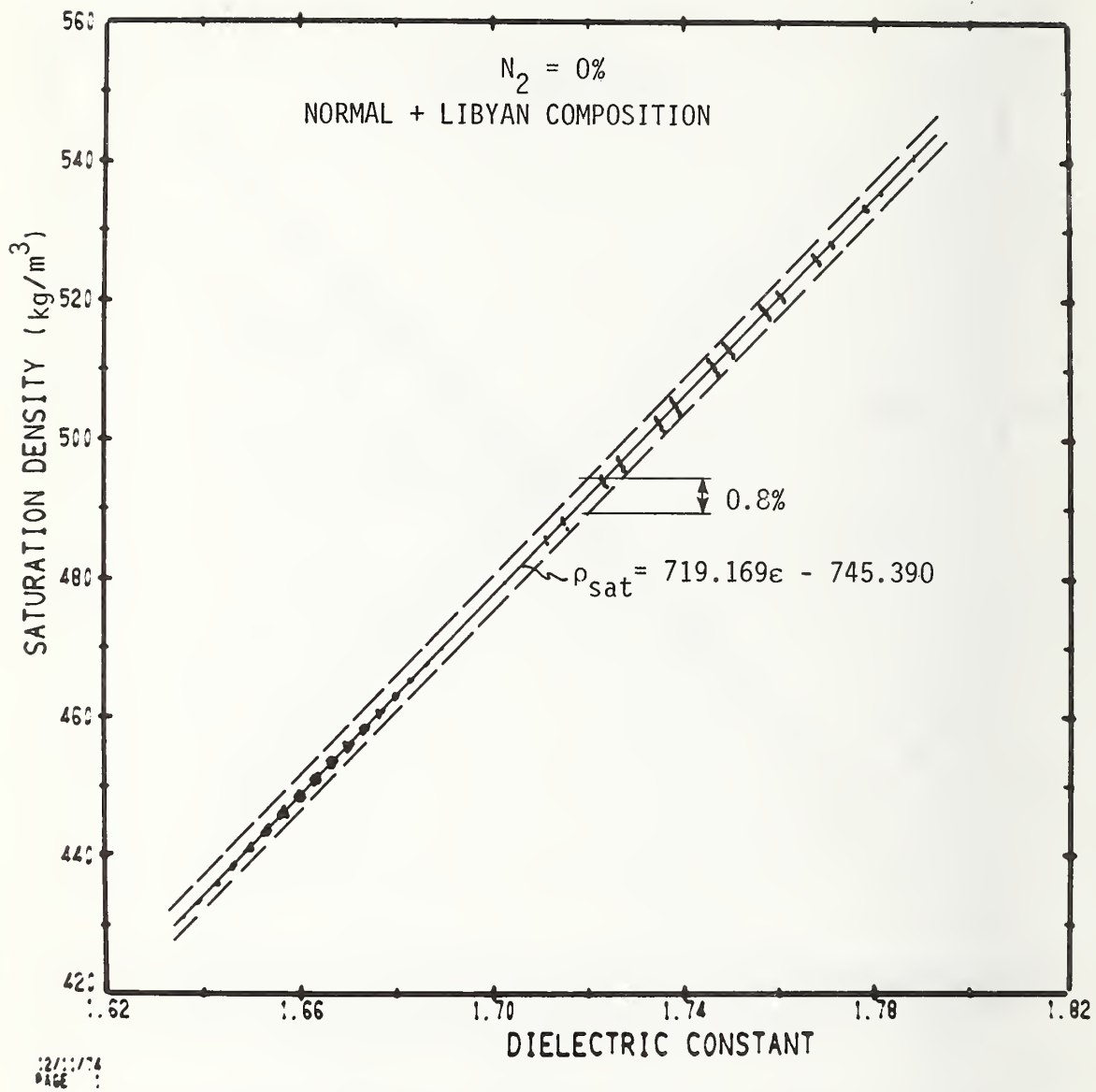


Figure 12. LNG saturation density vs. dielectric constant for normal & Libyan composition mixtures with $N_2=0\%$

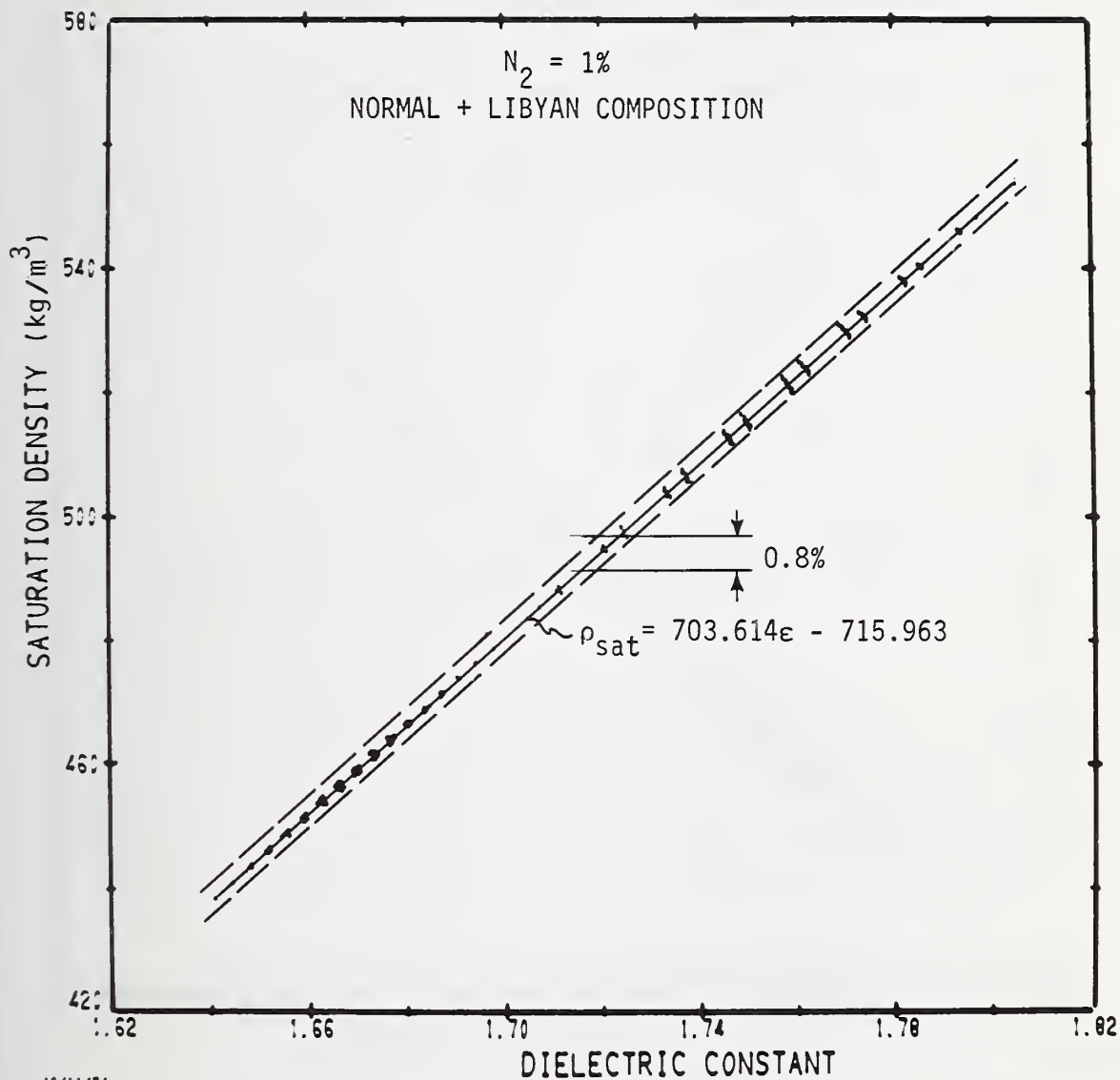


Figure 13. LNG saturation density vs. dielectric constant for normal & Libyan composition mixtures with $N_2=1\%$

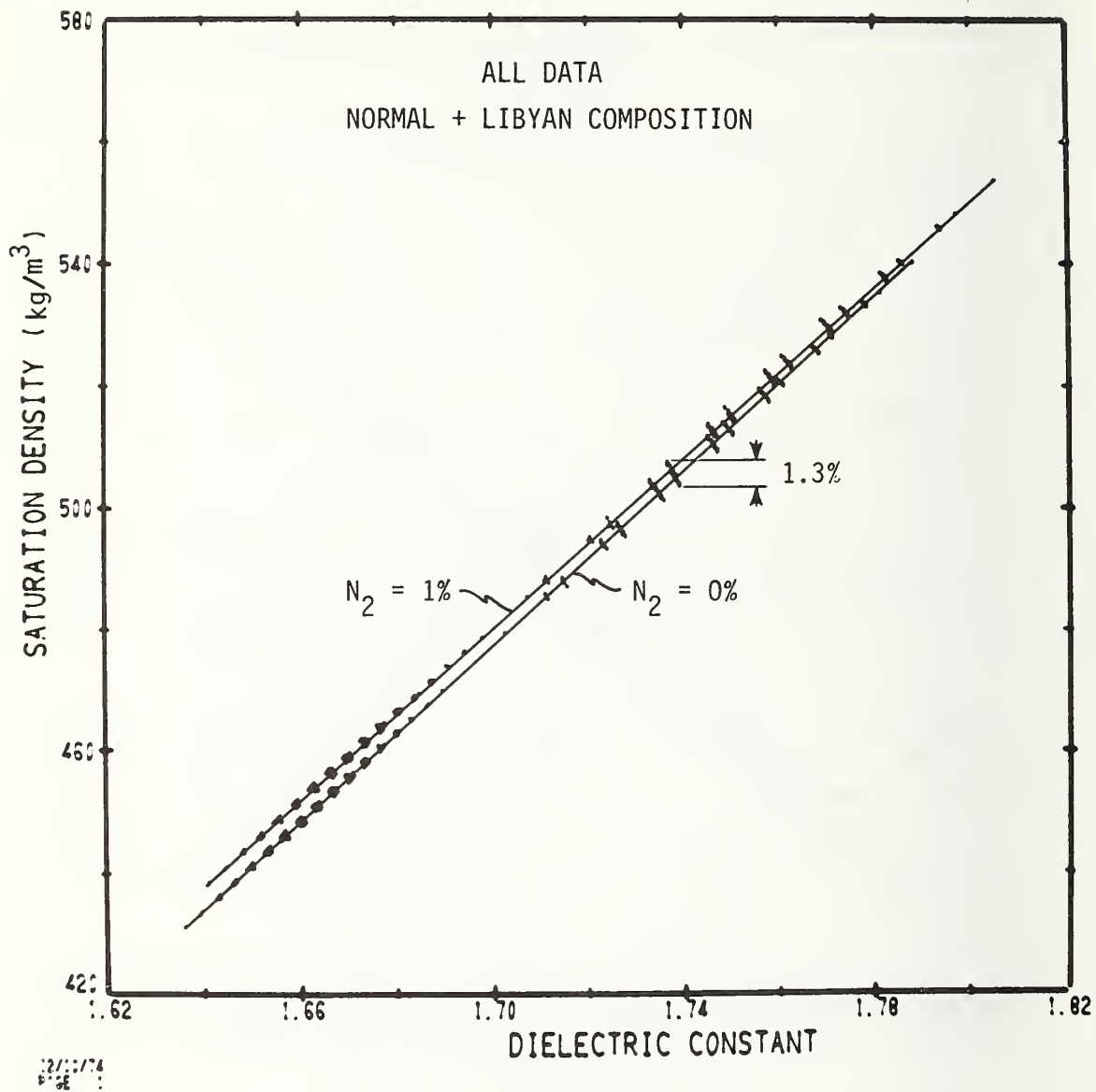


Figure 14. Effect of nitrogen composition on saturation density vs. dielectric constant for normal & Libyan composition mixtures

about a 1.4% increase in the density for the same dielectric constant. However, since the nitrogen composition significantly affects the saturation temperature it is possible to partially compensate for these changes by an independent measurement of the temperature.

- (4) For the normal range of mixtures considered the density of the mixture is predominantly dependent on the temperature. This result plus the approximate bilinear relationship between density and dielectric constant and temperature suggests a temperature compensation for a capacitance meter which allows density to be determined to $\pm 0.3\%$ over a wide range of temperatures and subcooled conditions. For all such cases considered there is substantial improvement in the density measurement when temperature as well as dielectric constant is measured. (See tables 4 and 5.)
- (5) The results of calculations for the libyan composition indicate that the intrinsic uncertainties increase as the anticipated range of composition increases.
- (6) The results of the study tend to give positive and conclusive indication of the capability of capacitance densitometry for anticipated end use onboard ship custody transfer systems.

4. Topics for Future Research

- (1) The systematic uncertainties due to state equations and the excess CM function need to be better defined and determined. This is being done currently at NBS for the state equation by a systematic acquisition of PVT data for well defined mixtures. Improvement in the excess CM function, however, will have to rely on future experimental relations between dielectric constant and density for well defined mixtures.
- (2) More work should be done explicitly on subcooled fluids although uncertainties for a given subcooled condition can be estimated from interpolations and extrapolations from the 2.6 atm results (at the corresponding 1 atm saturation temperature) given in this report.
- (3) Systematic methods need to be developed for determining intrinsic uncertainties for composition ranges other than those given in this report; Particularly to define techniques for internally calibrating the densitometer for a narrow range of mixtures or equivalently, when the approximate composition of the fluid is known.

References

1. Möllerup, J., Correlated and predicted thermodynamic properties of LNG and related mixtures in the normal and critical regions, *Advances in Cryogenic Engineering* 20 (Plenum Press, NY, 1975).
2. Sarsten, J. A., LNG stratification and rollover, *Pipeline Gas J.* 199, No. 11, 37-39 (Sept. 1972).
3. Diller, D. E., The Clausius-Mosotti functions (molar polarizabilities) of pure compressed gaseous and liquid methane, ethane, propoane, butanes, and nitrogen, *Cryogenics* 14, No. 4 (April 1974).
4. Pan, W. P., Mady, M. H., and Miller, R. C., Dielectric constants and Clausius-Mosotti functions for simple liquid mixtures: systems containing nitrogen, argon and light hydrocarbons, *AIChE Journal* 21, No. 2 (March 1975).
5. Klosek, J. and McKinley, C., Densities of liquefied natural gas and of low molecular weight hydrocarbons, *Proceedings First International Conference, IGT, Chicago, Illinois (1968)*, paper 22.

APPENDIX

Equations determined by least squares fitting techniques for the cases described in the text. (Normal Compositions)

Notation

ρ_{mix}	=	density of mixture, kg/m^3
ϵ	=	dielectric constant
T	=	temperature of mixture, K
CM_{mix}	=	Clausius-Mosotti function for the mixture, m^3/kg
CM_i	=	Clausius-Mosotti function for each component, m^3/kg .

Cases 1 and 1a (not least squares determination, see Sec. 2.2, 3.1, and 3.1.1)

$$\rho_{\text{mix}} = \frac{1}{\text{CM}_{\text{mix}}} \frac{\epsilon-1}{\epsilon+2} = \frac{1}{\sum \text{CM}_i} \frac{\epsilon-1}{\epsilon+2}$$

ρ vs $(\epsilon-1)$ equations (Table 4)

Case 2 Saturated Conditions, $P_{\text{sat}} = \text{const}$

$N_2 = 0\%$

$\rho_{\text{mix}} =$	$-29.076 + 723.5(\epsilon-1)$	$P_{\text{sat}} = 1 \text{ atm}$
$\rho_{\text{mix}} =$	$-23.602 + 723.6(\epsilon-1)$	$P_{\text{sat}} = 2.6 \text{ atm}$

$N_2 = 0.7\%$

$\rho_{\text{mix}} =$	$-20.749 + 714.6(\epsilon-1)$	$P_{\text{sat}} = 1 \text{ atm}$
$\rho_{\text{mix}} =$	$-13.419 + 710.9(\epsilon-1)$	$P_{\text{sat}} = 2.6 \text{ atm}$

$N_2 = 1.4\%$

$\rho_{\text{mix}} =$	$-13.58 + 707.68(\epsilon-1)$	$P_{\text{sat}} = 1 \text{ atm}$
$\rho_{\text{mix}} =$	$-4.726 + 700.98(\epsilon-1)$	$P_{\text{sat}} = 2.6 \text{ atm}$

Case 2a

$$\underline{N_2 = 0-1.4\%}$$

$$\rho_{mix} = -51.630 + 760.8(\epsilon-1)$$

$$P_{sat} = 1 \text{ atm}$$

$$\rho_{mix} = -42.051 + 756.1(\epsilon-1)$$

$$P_{sat} = 2.6 \text{ atm}$$

Case 3 Uniform Temperature Conditions, $P = 1-2.6 \text{ atm}$

$$\underline{N_2 = 0\%}$$

$$\rho_{mix} = -27.947 + 721.7(\epsilon-1)$$

$$\underline{N_2 = 0.7\%}$$

$$\rho_{mix} = -17.924 + 710.15(\epsilon-1)$$

$$\underline{N_2 = 1.4\%}$$

$$\rho_{mix} = -9.035 + 700.62(\epsilon-1)$$

Case 3a

$$\underline{N_2 = 0-1.4\%}$$

$$\rho_{mix} = -807.377 + 757.68(\epsilon) = -49.702 + 757.68(\epsilon-1)$$

ρ vs $\epsilon-1$, T equations (Table 5)
--

Case 2 Saturated Conditions, $P_{sat} = \text{const}$

$$\underline{N_2 = 0\%}$$

$$\rho_{mix} = -275.568 + 667.06(\epsilon-1) + 2.521(T)$$

$$\underline{N_2 = 0.7\%}$$

$$\rho_{mix} = -286.721 + 701.27(\epsilon-1) + 2.499(T)$$

$$\underline{N_2 = 1.4\%}$$

$$\rho_{mix} = -301.885 + 730.33(\epsilon-1) + 2.539(T)$$

$$P_{sat} = 1 \text{ atm}$$

$$\underline{N_2 = 0\%}$$

$$\rho_{\text{mix}} = -281.40 + 639.6(\epsilon-1) + 2.464(T)$$

$$\underline{N_2 = 0.7\%}$$

$$\rho_{\text{mix}} = -287.76 + 675.9(\epsilon-1) + 2.398(T)$$

$$\underline{N_2 = 1.4\%}$$

$$\rho_{\text{mix}} = -278.91 + 706.6(\epsilon-1) + 2.2295(T)$$

$$P_{\text{sat}} = 2.6 \text{ atm}$$

Case 2a

$$\underline{N_2 = 0-1.4\%}$$

$$\rho_{\text{mix}} = 78.71 + 720.98(\epsilon-1) - 0.9422(T)$$

$$(P_{\text{sat}} = 1 \text{ atm})$$

$$\rho_{\text{mix}} = 90.19 + 725.16(\epsilon-1) - 0.9102(T)$$

$$(P_{\text{sat}} = 2.6 \text{ atm})$$

Case 3 Uniform Temperature Conditions, $P = 1-2.6 \text{ atm}$

$$\underline{N_2 = 0\%}$$

$$\rho_{\text{mix}} = -281.18 + 664.67(\epsilon-1) + 2.5845(T)$$

$$\underline{N_2 = 0.7\%}$$

$$\rho_{\text{mix}} = -292.49 + 698.87(\epsilon-1) + 2.5768(T)$$

$$\underline{N_2 = 1.4\%}$$

$$\rho_{\text{mix}} = -269.39 + 720.10(\epsilon-1) + 2.2987(T)$$

Case 3a

$$\underline{N_2 = 0-1.4\%}$$

$$\rho_{\text{mix}} = 78.99 + 716.12(\epsilon-1) - 0.9164(T)$$

Case 4 Saturation Conditions, $T_{\text{sat}} = \text{const}$ (Range of applicability 105-145 K)

$$\underline{N_2 = 0\%}$$

$$\rho_{\text{mix}} = -62.03 + 709.4(\varepsilon-1) + 0.3747(T)$$

$$\underline{N_2 = 0.7\%}$$

$$\rho_{\text{mix}} = -52.94 + 704.5(\varepsilon-1) + 0.3518(T)$$

$$\underline{N_2 = 1.4\%}$$

$$\rho_{\text{mix}} = -46.87 + 702.8(\varepsilon-1) + 0.3369(T)$$

If N_2 mole fraction is included as parameter

$$\rho_{\text{mix}} = -56.97 + 705.4(\varepsilon-1) + 0.3543(T) + 448.3N_2.$$

Case 4a

$$\underline{N_2 = 0-1.4\%}$$

$$\rho_{\text{mix}} = -47.94 + 699.2(\varepsilon-1) + 0.3379(T).$$

U.S. DEPT. OF COMM. BIBLIOGRAPHIC DATA SHEET		1. PUBLICATION OR REPORT NO. NBSIR 76-831	2. Gov't Accession No.	3. Recipient's Accession No.
4. TITLE AND SUBTITLE Liquefied Natural Gas Research at the National Bureau of Standards			5. Publication Date 1 July-31 December, 1975	
			6. Performing Organization Code	
7. AUTHOR(S) D. B. Mann, Editor			8. Performing Organ. Report No.	
9. PERFORMING ORGANIZATION NAME AND ADDRESS NATIONAL BUREAU OF STANDARDS DEPARTMENT OF COMMERCE WASHINGTON, D.C. 20234			10. Project/Task/Work Unit No. 2750141	
			11. Contract/Grant No.	
12. Sponsoring Organization Name and Complete Address (Street, City, State, ZIP) Same as Item 9.			13. Type of Report & Period Covered Semi-annual - July 1 - December 31, 1975	
			14. Sponsoring Agency Code	
15. SUPPLEMENTARY NOTES				
16. ABSTRACT (A 200-word or less factual summary of most significant information. If document includes a significant bibliography or literature survey, mention it here.) Nineteen cost centers supported by six other agency sponsors in addition to NBS provide the basis for liquefied natural gas (LNG) research at NBS. During this six month reporting period the level of effort was at a 20 man-year level with funding expenditures of over \$600,000. This integrated progress report to be issued in January and July is designed to: 1) Provide all sponsoring agencies with a semi-annual and annual report on the activities of their individual programs. 2) Inform all sponsoring agencies on related research being conducted at the Cryogenics Division of NBS-IBS. 3) Provide a uniform reporting procedure which should maintain and improve communication while minimizing the time, effort and paperwork at the cost center level. The contents of this report will augment the quarterly progress meetings of some sponsors, but will not necessarily replace such meetings. Distribution of this document is limited and intended primarily for the supporting agencies. <u>Data or other information must be considered preliminary, subject to change and unpublished; and therefore not for citation in the open literature.</u>				
17. KEY WORDS (six to twelve entries; alphabetical order; capitalize only the first letter of the first key word unless a proper name; separated by semicolons) Cryogenic; liquefied natural gas; measurement; methane; properties; research.				
18. AVAILABILITY <input type="checkbox"/> Unlimited <input checked="" type="checkbox"/> For Official Distribution. Do Not Release to NTIS <input type="checkbox"/> Order From Sup. of Doc., U.S. Government Printing Office Washington, D.C. 20402, SD Cat. No. C13 <input type="checkbox"/> Order From National Technical Information Service (NTIS) Springfield, Virginia 22151		19. SECURITY CLASS (THIS REPORT) UNCLASSIFIED 20. SECURITY CLASS (THIS PAGE) UNCLASSIFIED		21. NO. OF PAGES 22. Price

